MreB Dependent Cell Envelope Homeostasis in *Bacillus subtilis*

Kenneth Holst Seistrup

Thesis submitted in partial fulfilment of the requirements of the regulation for the degree of Doctor of Philosophy

Newcastle University

Faculty of Medical Sciences

Institute for Cell and Molecular Biosciences

September 2018

Abstract

One of the hallmarks of cellular life is the protective membrane. The membrane not only encapsulates the nutrient rich cytoplasm, but also facilitates many important processes essential for most biological life such as the ATP producing oxidative phosphorylation, meaning that tight regulation of membrane homeostasis must be sustained. In Bacteria the membrane is also home to the final stages of peptidoglycan synthesis, thus coupling cell wall production and the membrane. The protein governing where the insertion of new peptidoglycan occurs in rod-shaped Bacteria is the actin homologue MreB (Errington, 2015). Previous studies have suggested that MreB and its homologues are involved in cell envelope homeostasis, not only through fatty acid adaptations, but through regulation of peptidoglycan degrading autolysins as well (Dominguez-Cuevas *et al.*, 2013; Strahl *et al.*, 2014).

In this thesis I aimed to describe which homeostatic changes occur within the membrane when deleting the MreB cytoskeleton, as well as describe if these changes alter the physical parameters associated with fluidity and temperature dependent growth phenotypes. Additionally, I wanted to elucidate if the deletion of *mreB* and its homologues changes the sequence of actions following disruptions to membrane homeostasis such as dissipation of membrane potential, which under normal circumstances rigidifies the membrane, delocalizes multiple membrane associated proteins, and eventually induces lysis (Strahl and Hamoen, 2010).

Through fatty acid analysis in multiple MreB cytoskeletal mutants I found that the lack of MreB and its homologues lead to altered fatty acid composition, which in turn causes membrane fluidity to be altered in a complex manner, indicating that MreB is important in maintaining a well-coordinated membrane homeostasis. Additionally, I examined membrane rigidification caused by membrane depolarization, and discovered that MreB was not involved, but rather electrostriction was the most likely candidate. Finally, through lysis assays and microscopy I examined membrane depolarization induced lysis. I found that the lysis is caused by MreB being delocalized, thus redirecting the cell wall synthesis machinery and mis-regulating autolysins essential for efficient membrane elongation, finally causing loss of communication between anabolism and catabolism of the cell wall. Together, these findings elucidate the important role MreB occupies in the membrane, not only guiding the cell elongasome, but in maintaining well-coordinated membrane homeostasis.

In dedication to you and our time apart

Acknowledgements

Firstly, I would like to direct a huge thanks to my supervisor Henrik Strahl von Schulten, whose excellent tutelage and guidance have encouraged and inspired me throughout the course of my time in Newcastle. Additional thanks goes to Richard Daniel for general advice and always having the necessary machinery ready for the odd experiment when required. I would also like to thank Kasia Mickiweicz and Marcin Dembek for help in the laboratory when working with pathogens and for advice regarding said organisms. I must also thank level 4 of CBCB for help and support when needed, especially Fran Davison for always ensuring availability of equipment and reagents.

I will give a special thanks to my friends Declan Gray, Flint Stevenson-Jones, Alexander Egan, and David Roberts for assisting me to blow off steam outside the lab both through physical exercise, but more importantly in the nerdiest way possible. May your dungeons ever be full of treasure! Additional thanks goes to David Roberts for many a political discussion, and careful and critical reading of this thesis. I would also like to thank my family and friends in Denmark for being patient and supportive, especially Klaus Christiansen and Stefan Walls with whom I will always be able to enjoy a bottle of wine, or two.

Finally, I would like to thank my beautiful fiancée, Julie Mundus Nielsen, for allowing me to leave the country for three years to pursue my dream. Without you and your support, none of this would have been possible.

Publications

Te Winkel, J. D., Gray, D. A., Seistrup, K. H., Hamoen, L. W. and Strahl, H. (2016) 'Analysis of Antimicrobial-Triggered Membrane Depolarization Using Voltage Sensitive Dyes', Front Cell Dev Biol, 4, p. 29.

Pogmore, A. R., Seistrup, K. H. and Strahl, H. (2018) 'The Gram-positive model organism Bacillus subtilis does not form microscopically detectable cardiolipin-specific lipid domains', Microbiology, 164(4), pp. 475-482.

Kepplinger, B., Morton-Laing, S., Seistrup, K. H., Marrs, E. C. L., Hopkins, A. P., Perry, J. D., Strahl, H., Hall, M. J., Errington, J. and Allenby, N. E. E. (2018) 'Mode of Action and Heterologous Expression of the Natural Product Antibiotic Vancoresmycin', ACS Chem Biol, 13(1), pp. 207-214.

Table of Figures

Table of Tables

Abbreviations

BA	Benzyl alcohol
°C	Celsius
CAA	Casamino acids
Ca^{2+}	Calcium
CCCP	Carbonyl cyanide *m*-chlorophenyl hydrazone
CFU	Colony forming unit
Da	Dalton
DGDG	Diglucosyldiacylglycerol
DOPC	1,2-Dioleoyl-sn-glycero-3-phosphocholine
DPH	1,6-Diphenyl-1,3,5-hexatriene
DSM	Difco sporulation medium
CL	Cardiolipin
EDTA	Ethylenediaminetetraacetic acid
FA	Fatty acid
FM5-95	*N*-(3-trimethylammoniumpropyl)-4-(6-(4-(Diethylamino)phenyl) hexatrienyl)Pyridinium Dibromide
g	Gram
GFP	Green fluorescent protein
GlcNAc	N-acetylglucosamine
h	Hours
H^+	Proton
H_2O	Water
HEPES	4-(2-hydroxyethyl)-1-piperazineethanesulfonic acid)
IPTG	Isopropyl β-D-1-thiogalactopyranoside
kDa	Kilodalton
K^+	Potassium
LB	Luria-Bertani medium
LTA	Lipo teichoic acid
LysPG	Lysylphosphatidylglycerol
M	Molar
mM	Millimolar

MIC	Minimal inhibitory concentration
min.	Minutes
ml	Millilitre
$MgCl_2$	Magnesium chloride
MGDG	Monoglucosyldiacylglyderol
Mg^{2+}	Magnesium
Mn^{2+}	Manganese
msfGFP	Monomeric super folded green fluorescent protein
MSM	Magnesium sucrose maleic acid supplement
MurNAc	N-acetylmuramic acid
mV	Millivolt
NA	Nutrient agar
Na^{+}	Sodium
NaCl	Sodium Chloride
NAO	Nonyl acridine orange
nm	Nanometre
OD_{600}	Optical density at 600 nm
ON	Over night
O^2	Oxygen
PBS	Phosphate buffered saline
PCR	Polymerase chain reaction
PE	Phosphatidylethanolamine
PG	Phosphatidylglycerol
PMF	Proton motive force
RFP	Red fluorescent protein
rpm	Revolutions per minute
sec	Seconds
SMM	Standard minimal medium
snp	Single nucleotide polymorphism
TCA cycle	Tricarboxylic acid cycle
TES buffer	Tris- EDTA- Sodium buffer
TGDG	Triglucosyldiacylglycerol
WTA	All teichioc acid

YFP	Yellow fluorescent protein
Å	Ångstrøm
µg	Microgram
µl	Microlitre
µm	Micrometre
µM	Micromolar
µg/ml	Microgram per mililitre
σ^{ECF}	Extracytoplasmic function sigma factor
%	Percent

Table of Content

Chapter 1 – Introduction

1.1 – General Introduction

The first defining microscopic feature discovered about biological organisms was their enclosed nature, or their cell like structure, described by Robert Hooke in 1665 (Hooke, 1665). The concept of cellular organisms was further elucidated by the discovery of moving living organisms by Anton van Leeuwenhoek in 1677 (Leewenhoeck, 1677). Since these initial pioneering studies in biology and microscopy, our understanding of cellular mechanisms and structures has developed substantially. Today we know about the three domains of life, the Bacteria, the Archaea, and the Eukaryotes. The three domains share core molecular and chemical characteristics, and large strides have been made in understanding biological heritage, protein function and evolution, and cellular life cycles. Surprisingly, one of the major structures that all three domains share, the cellular membrane, has previously been largely ignored due to a lack of efficient analysis tools, and has therefore been regarded as the mere scaffold upon which biological processes take place, as per the fluid mosaic model (Singer and Nicolson, 1972). Currently, our understanding of how the membrane is actively involved in biological processes is expanding. Although current bacterial membrane models are getting more refined, with the inclusion of domains in which certain lipids are enriched according to fatty acid characteristics as well as proteins and lipids that specifically localise based upon membrane curvature, core physical parameters such as temperature adaptation and fluid homeostasis remain poorly understood, leaving gaps in the understanding of all membrane associated processes (Strahl and Errington, 2017).

Throughout this thesis, I have been examining the bacterial membrane in the model organism, *Bacillus subtilis*. It was discovered that the bacterial lateral cytoskeleton is involved in membrane domain formation, spatial protein sorting, and autolysin secretion (Dominguez-Cuevas *et al.*, 2013; Strahl *et al.*, 2014). I aim to describe membrane homeostasis and how the cytoskeleton is involved in maintaining it, as well as what happens when the homeostasis is skewed using both temperature and membrane targeting compounds.

1.2 – *Bacillus subtilis*

Bacillus subtilis is a rod-shaped, Gram positive bacterium from the *Firmicutes* phylum, where it was first utilized as the model organism for sporulation. This is because during times of nutrient scarcity, *B. subtilis* can form a resilient endospore (herein termed

spore) protecting it almost indefinitely. More recently, the bacterium has become a model for Gram positives in general (Ryter, 1965). The spores, and thus the organism itself, has been found in wide ranging environments such as in water, soil, animal intestines (including human), associated with plants and their roots, and even freely in the atmosphere (Jaenicke, 2005; Tam *et al.*, 2006). Adapting to such varying environments regarding not only growing on solid or in liquid surroundings, but also large ranges of temperature, pH, and ion concentrations requires strict regulation of the physical properties of the membrane, keeping it within growth sustaining confines at all times. One strategy employed by the bacteria is to differentiate into biofilms, thus controlling the physical properties of the cells in the middle of the colony, while having the outer parts exposed to the environment (Branda *et al.*, 2001).

B. subtilis is naturally competent, making it extremely easy to perform genetic alterations within the chromosome, thus enabling genetic deletions of non-essential genes within a short amount of time (Michod *et al.*, 1988).

Extensive research has been undertaken in *B. subtilis*, although multiple different wild type strains have been introduced, some of which have unknown origin, making it difficult to compare results in the literature (Zeigler *et al.*, 2008). The most widespread wild type strain in European laboratories is *B. subtilis subsp. subtilis 168* that originally was created by subjecting *B. subtilis* from plant roots to X-rays, thus disrupting the tryptophan synthesis pathway, leaving all daughter strains tryptophan auxotrophs (Burkholder and Giles, 1947). *B. subtilis subsp. subtilis 168* contains a low G-C ratio genome consisting of 4.2 million base pairs that encode 4175 genes located on a single chromosome (Kunst *et al.*, 1997). As stated earlier, most *B. subtilis* strains are naturally competent, but the *168* is highly competent making it a prime candidate for genetic studies (Zenz *et al.*, 1998). Even within the subspecies 168 derivations are found, an inevitability since mutations will occur when the strain is grown in multiple different laboratories under different conditions and in a wide range of media, causing a constant slight genetic drift (Medini *et al.*, 2005).

1.3 – The Biological Cell Envelope

The cell envelope is the hallmark of the cell, and part of the very definition of the originally observed microscopic life forms. The envelope consists of different layers in each of the three Domains of life, and variations within each Domain are common. The lipid membrane is a trait all three domains share. Despite this, Archaea have evolved a slightly

different type of membrane with cross-linked isoprenoid chains, resulting in a more rigid structure that is able to withstand increased stress (Woese *et al.*, 1978). Most bacterial envelopes consist of one or two lipid bilayer membranes, a cell wall, and additional protein or carbohydrate layers (Gerbino *et al.*, 2015). For this thesis I will focus on the Gram positive cell envelope of *B. subtilis*, thus when discussing the membrane, it will concern the cytoplasmic membrane, unless stated otherwise.

1.3.1 – The biological membrane

Phospholipids are highly polar molecules with a hydrophilic head group and acyl chains of hydrophobic carbon, known as fatty acids, attached. The lipids can arrange into various structures and symmetries according to the surrounding environment and the precise lipid composition. The simplest structure phospholipids can form in an aqueous solution is the micelle, in which a single layer of lipids form a sphere with the fatty acids creating a hydrophobic interior, while the head groups create a hydrophilic exterior, or if in a hydrophobic solution the opposite configuration. The structure was first proposed in 1913 as an explanation of detergent behaviour in aqueous solutions (McBain, 1913). Larger lipid configurations are the hexagonal lipid phase, which are essentially multiple tubular micelles that are stacked onto one another (Seddon *et al.*, 1983). An additional lipid configuration is the cubic lipid phase. Unlike the previous two phases, the cubic phase is comprised of a bi-layer of lipids, in which two sheets of laterally assembled leaflets are joined by the hydrophobic interphase. A cube-like structure is subsequently folded with a hydrophilic tunnel running through the middle (Luzzati and Reiss-Husson, 1966), with multimers essentially forming a maze-like structure. All three lipid phases have been found in cells, but will not be discussed further in this thesis.

Finally, the most biologically relevant lipid structure is the lamellar bilayer, also known as the cell membrane. The cell membranes of all bacteria consist of one or two homogeneous phospholipid bilayers with proteins integrated or peripherally attached. The early model, described as the fluid mosaic model by Singer and Nicolson, defined the membrane as a two dimensional liquid acting as an inert scaffold for the attached proteins, resulting in a homogenous structure allowing for free lateral movement throughout (Singer and Nicolson, 1972). Since the description of the fluid mosaic model, significant refinements have been made as a result of the strides taken to generate a greater understanding of the

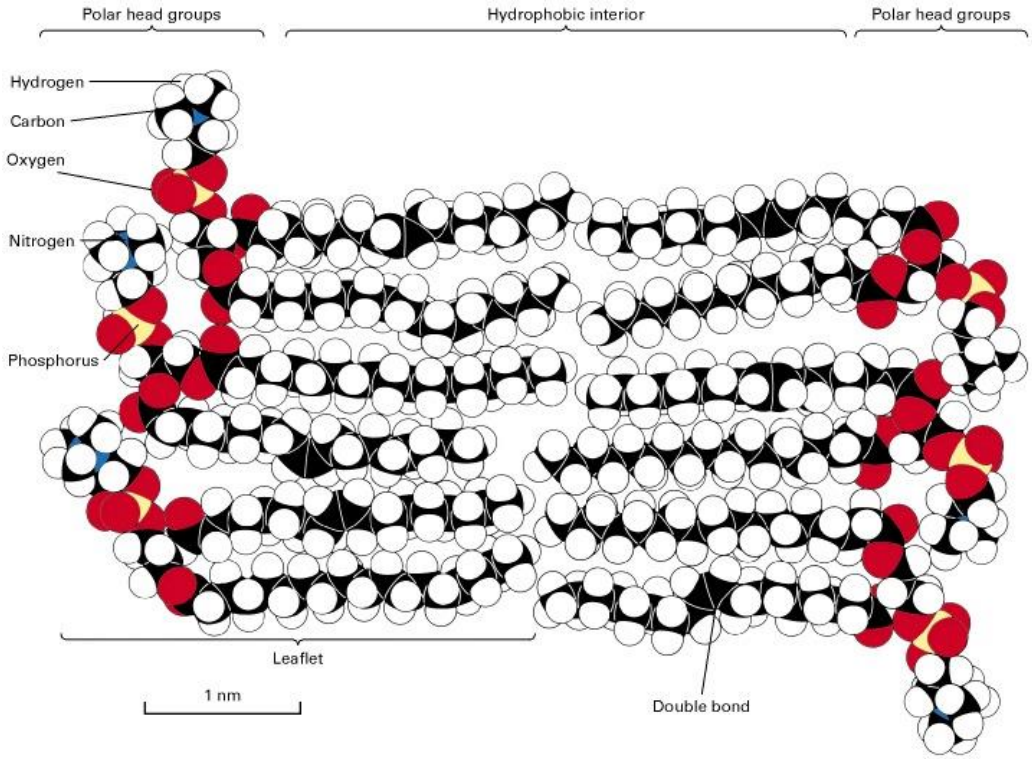

Figure 1: A space-fill model of two pairs of three phospholipids packing as imagined in a membrane. Two leaflets of phospholipids constitute the biological membrane. Each phospholipid has a polar head-group, here seen with oxygen, nitrogen, and phosphorous, and a fatty acid created from chains of 12-24 carbons long. (Lodish, 2000)

membrane, such as the inclusion of various lipid-enriched areas and the addition of a cytoskeletal structure that both lead to partial membrane compartmentalization. These will all be discussed later in this thesis.

Bacteria and Eukaryotes both have a membrane consisting of lipids, with fatty acids constituting the hydrophobic core and polar or charged head-groups making up the hydrophilic outer part of the membrane, as shown in Figure 1.

The composition of lipid types vary between bacterial species, and variations can occur within the same species when subjected to different growth conditions (Hazel and Williams, 1990). Most Bacterial phospholipid bilayers primarily consist of acyl groups of C_{12}-C_{24}, that are attached to polar head groups such as phosphatidylglycerol (PG), phosphatidylethanolamine (PE), and cardiolipin (CL). The membrane of *B. subtilis 168* is more complex than other Bacterial model organisms such as *E. coli*, having a range of different lipid species, including Glucolipids: monoglucosyldiacylglycerol (MGDG), diglucosyldiacylglycerol (DGDG), and triglucosyldiacylglycerol (TGDG); acidic phospholipids: CL, and PG; zwitterionic phospholipids: lysylphosphatidylglycerol (LysPG), and PE (C. S. Lopez *et al.*, 1998). The complex phospholipid composition might be a

consequence of the varied ecological niches *B. subtilis* inhabits. Another major and essential component of the bacterial membrane is lipid II, the precursor to cell wall biosynthesis, which will be discussed in a later section.

On average, the membrane of *B. subtilis* is about 30-40Å thick (Weber *et al.*, 2005; Andersen and Koeppe, 2007) and only allows for small molecules to pass through the hydrophobic core. Generally, gasses and smaller hydrophobic or polar molecules can diffuse through the membrane, such as O_2, CO_2, benzene, H_2O, or methanol. By contrast, charged molecules, or larger polar molecules such as glucose and ATP, are entirely unable to traverse the membrane, unless through protein pumps or channels (Cocucci *et al.*, 2017). One of the molecules unable to pass through the membrane unassisted is H^+, which is not only important for production of ATP, but also critical in upholding the electro-chemical potential across the membrane. This potential is essential for a wide range of key cellular processes, including ATP production, protein secretion, various other transport systems, motility, and membrane protein localization.

1.3.2 – Membrane fluidity & homeostasis

The lipid bilayer can exist in three distinct phases; the gel phase, the liquid ordered phase, and the liquid disordered phase, before transitioning into an overall different conformation. The gel phase occurs when the lipids are tightly packed with the fatty acids fully extended, rendering all membrane-associated processes slower or less frequent, including a loss of selective membrane permeability (Haest *et al.*, 1972), and a decrease in membrane protein activity (McKersie and Thompson, 1977). The liquid ordered phase retains the majority of fatty acids in a fully extended state, but either thermal energy or, more commonly, proteins or smaller molecules such as cholesterol in Eukaryotes are inserted in the membrane, inducing a lipid conformation allowing increased diffusion (Ipsen *et al.*, 1987). For the liquid disordered phase, either enough thermal energy is present or the membrane lipid composition favours an entirely loose configuration, where membrane associated molecules can diffuse freely and the membrane permeability is increased (Mesquita *et al.*, 2000). When transitioning between the three phases, either due to temperature shifts or insertion of compounds in the membrane, a gradual change occurs, with regions of the membrane adopting the characteristics of the new phase before a full change occurs, if ever

(Mesquita *et al.*, 2000). The two most relevant phases for this thesis are the liquid ordered and the liquid disordered, and we can thus assume that we are operating between the two.

When describing the physical properties of biological membrane, it becomes evident that the term 'fluidity' is difficult to define. In some cases membrane fluidity is described as the overall elasticity, meaning how much a membrane can stretch before breaking (Lopez-Montero *et al.*, 2008). Other studies argue that membrane fluidity is the description of liquid ordered and liquid disordered regions within the membrane, as measured through microscopy (van Ginkel *et al.*, 1989). As a consequence, there is a lack of consensus regarding the term fluidity, leaving us with vague definitions of it either being the mechanical properties of the membrane, the distribution of ordered and disordered regions or a combination thereof (Klymchenko and Kreder, 2014). In actuality, when measuring "membrane fluidity" in the lab we don't measure membrane elasticity or lipid organization directly, but rather observe the behaviour of small molecular probes inserted into the membrane (Jay and Hamilton, 2017). Two of the best characterized fluorescent molecular membrane probes are laurdan and 1,6-Diphenyl-1,3,5-hexatriene (DPH), both of which supposedly measure "membrane fluidity", although their behaviour and localization within the membrane differ substantially as seen in Figure 2. Laurdan was developed in 1981 and consists of a twelve carbon FA tail attached to the fluorescent moiety dimethylaminonaphtalene. The molecule inserts itself in the membrane where the

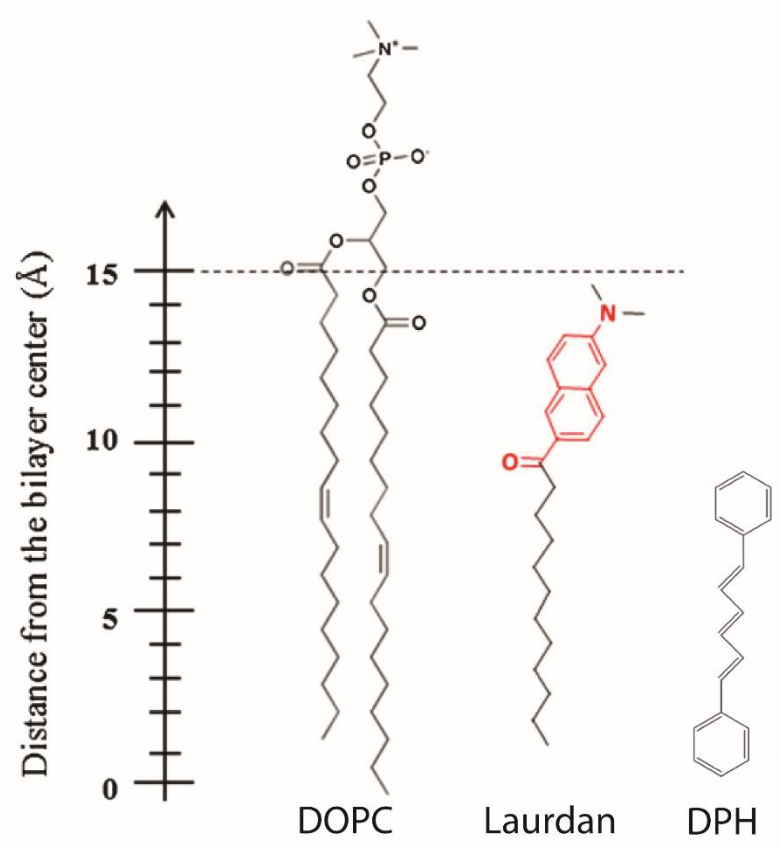

Figure 2: A scheme showing where in the membrane compounds bind. DOPC (1,2-Dioleoyl-sn-glycero-3-phosphocholine) is used as an example of a phospholipid. Laurdan binds at the hydrophobic / hydrophilic interphase, whereas DPH binds within the hydrophobic fatty acid core of the membrane. Modified from (Jay and Hamilton, 2017) with additional information from (Kaiser and London, 1998; Egan and Vollmer, 2013).

phospholipid head groups are attached to their acyl groups, in the interphase between hydrophobic and hydrophilic moieties (Macgregor and Weber, 1981). When inserted in the membrane and excited, laurdan has two emission peaks depending on which phase the surrounding lipids are arranged into, namely 440 nm from the disordered phase and 490 from the ordered phase. In reality, laurdan shifts its emission due to the amount of surrounding water molecules. Indeed, the disordered phase will have more water penetrating the outer parts of the membrane, while the ordered phase restricts the amount of water in the boundary layer. Together, these properties tightly alter the laurdan emission (Jay and Hamilton, 2017). The other compound often used for membrane fluidity measurements is DPH, a small rigid hydrophobic fluorescent molecule that packs within the membrane close to the interphase between the two leaflets in a standing configuration parallel to the fatty acid moieties as seen in Figure 2 (Kaiser and London, 1998). The fact that DPH is a rigid molecule which packs parallel to the fatty acids can be exploited using polarized light at the excitation wavelength 360 nm. The rigid structure of DPH ensures that emissions only occur on the same axis as the excitation, meaning that when light intensity is measured parallel and perpendicular to the excitation axis, we get a measure for the amount of rotation allowed within the membrane (Haugland *et al.*, 1996). Together, laurdan and DPH gives us information about phospholipid head group packing as well as fatty acid packing, each granting partial understanding of the physical properties of the membrane. However, neither provides a description of lateral membrane diffusion. What makes the term fluidity even more complicated is the fact that domains within bacterial membranes have been discovered with increased or decreased fluidities, these will be discussed later.

For this thesis, we define the term fluidity as a description of phospholipid packing, with more fluid membranes having a disordered packing pattern with increased diffusion and movement, while more rigid membranes have a tighter more ordered packing restricting movement and rotation, all occurring within the liquid disordered phase.

The chemical properties which govern membrane packing are divided into three categories: van der Waals forces of the fatty acids, hydrogen bonding between the ester groups joining the head group to the fatty acids, and electrostatics between charged head groups (Seu *et al.*, 2006). The energy of a fatty acid CH_2 van der Waals interaction is 2.1 kJ/mol, and since a typical fatty acid is 15-17 carbon long, the total energy comes to 31-36 kJ/mol. The energy of a hydrogen bond is approximately 10-40 kJ/mol. The two bonds are therefore of approximately equal strength, making both of them important for membrane

packing, and therefore fluidity (Israelachvili, 2011). The electrostatic forces of the charged head groups have been found to alter membrane fluidity only in changing concentrations of free ions in the surrounding solution. Molecular dynamics simulations have shown that these electrostatic forces seem to be more important for the binding of specific membrane-associated proteins in an amino acid-specific manner (Poyry and Vattulainen, 2016). In addition to the above chemical properties, each component of the phospholipid has additional physical characteristics that influence membrane packing. For example, the physical size of the head group can greatly influence phospholipid localization and membrane packing, where larger head groups cause local spatial disruptions, repelling similarly sized phospholipids, and possibly even forcing other lipids further into the membrane or pushing them away from the centre of the membrane, disrupting fatty acid packing (Seu *et al.*, 2006). Furthermore, lipids with comparably smaller head groups compared to the amounts of fatty acids attached, such as cardiolipin with four fatty acids, arrange themselves into a cone like shape which disrupts the local fatty acid packing and seemingly, in some organisms, forces them to localize to negatively curved membranes such as the inner leaflet of the cell pole (Mileykovskaya and Dowhan, 2000; Renner and Weibel, 2011). The final component in fluidity determination is fatty acid length, saturation and branching. As described earlier, the energy needed to break van der Waals bonding increases linearly with the length of the fatty acid, meaning that longer fatty acids increases the packing potential of the lipid. Unsaturated fatty acids in the cis-conformation, along with branched fatty acids, will decrease the packing potential of a lipid and thereby increase fluidity by introducing kinks, creating a steric hindrance within the membrane, forcing more movement by the fatty acids (Seu *et al.*, 2006).

With the membrane functioning as a scaffold and active component in multiple essential processes, it is important to regulate the fluidity of the membrane to sustain functional levels of movement for both lipids and proteins. The constant modifications and adaptations to sustain biologically relevant levels of fluidity are known as membrane homeostasis, and are essential to sustain *B. subtilis* during the transitions between environments (Ernst *et al.*, 2016). To ensure that homeostasis is upheld the organism monitors the membrane at all times. *B. subtilis* has two main mechanisms for modulating membrane fluidity; an immediate fluidization when the environment suddenly changes towards a cold shock, and a slower process that allows for adaptations over a longer period of time, and over larger ranges of environmental challenges.

The fast response to changes in membrane fluidity upon cold shock induces double bonds within already synthesised FAs. When the fluidity is lowered, proteins that induce double bonds in FAs are signalled, and the membrane fluidity is increased to maintain homeostasis. In *B. subtilis*, the membrane bound phospholipid desaturase, or Des, is responsible for *cis* double-bond formation. Upon cold shock DesK, a transmembrane dimeric histidine kinase becomes activated, switching from a phosphatase-active to a kinase-active state that stimulates auto phosphorylation (Aguilar *et al.*, 2001; Saita *et al.*, 2016). This is sensed through membrane thickness-dependent activation, where decreased temperatures cause increases to the thickness of the membrane, initiating DesK via a trans-membrane region (Cybulski *et al.*, 2010). DesK activates the transcriptional regulator of the *des* gene, DesR, driving the expression of Des. Des ensures that the membrane will remain fluid, even at low temperatures, ensuring protein diffusion, functional pumps and channels, and the flow of important metabolites across the membrane is maintained (Aguilar *et al.*, 1998). Des is responsible for the immediate adaptations to lower temperatures, as shown in the original discovery of the enzyme. When subjecting wild type *B. subtilis* or *E. coli* to sudden drops in temperature from 37°C to 20°C, a significant increase in double bonds were measured. However, when a *des* null mutant was grown at 37°C then subjected to cold shock at 20°C, the resulting lack of any increase in double bonds led to a lysis-prone phenotype. When this mutant was subjected to lowered temperatures gradually, the lytic phenotype was rescued (Aguilar *et al.*, 1998) due to the longer term fluidity adaptations (Saita *et al.*, 2016). The mechanism for turning DesK off again, thus stopping expression of Des, has yet to be fully explained. However, a feasible solution could be that the introduced double bonds either force the membrane into a thinner configuration, or reduce the pressure on the protein by the membrane (Guo *et al.*, 2002).

Additional rapid FA modifications can occur in other organisms, such as acid protection through cyclopropane FA formation in *E. coli*, and cis-trans isomerization in *Pseudomonas putida*; for a comprehensive review, see (Zhang and Rock, 2008).

The slow fluidity adaptations require *de novo* synthesis of phospholipids and the temperature-dependent regulation is unknown. The amount of newly synthesized lipids has to be tightly regulated, as unlike Eukaryotes where FAs can be stored as energy in triglycerol, Prokaryotes deposit all FAs in the membrane components (Zhang and Rock, 2008). While the *de novo* synthesis results in a slower adaptation, it does increase the range of environmental adaptations that are possible. For *B. subtilis*, the most common method of modulating the

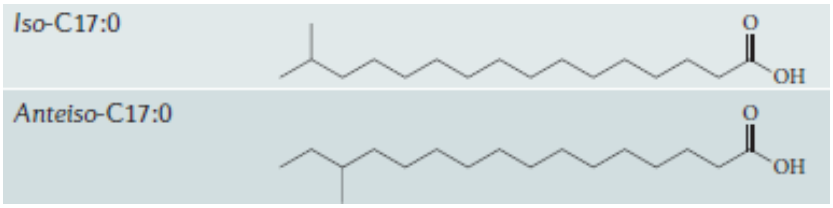

Figure 3: *Iso* and *Anteiso* fatty acids shown with 17 carbon. *Iso* fatty acids will pack more densely than *Anteiso* thus decreasing the fluidity and vice versa. Modified from (Zhang and Rock, 2008).

membrane is to synthesise *Iso* or *Anteiso* FAs to decrease or increase membrane fluidity, respectively. The structures of *Iso* and *Anteiso* FAs can be found in Figure 3. Another commonly utilized option is to synthesise FAs with varying carbon lengths according to the environmental changes. Shorter FAs allow for less ordered packing thus generating higher fluidity, whereas longer FAs have a larger packing potential, creating a more rigid membrane. Together with *Iso / Anteiso*, FA length can fine tune membrane fluidity when required.

The *de novo* synthesis of fatty acids and the subsequent attachment to the head group is achieved by a highly conserved pathway of enzymes known as the type II fatty acid biosynthesis pathway. Each of the FA synthesis proteins in the pathway is located in the cytoplasm while the acyltransferases, responsible for head group attachment, are located within the membrane; for a more comprehensive review, see (White *et al.*, 2005).

1.3.3 – Membrane domains

Until recently, it was thought that the lipid composition was homogenous throughout the membrane, but pioneering work in Eukaryotes discovered lipid domains, with individual characteristics and levels of fluidity, the best known being lipid rafts (Simons and Ikonen, 1997). From these studies three connected membrane characteristics have been described as important for lipids to segregate into domains. First, the fatty acid moieties and their differences in packing ability and relative fluidity (Vanounou *et al.*, 2002; Parsons and Rock, 2013), secondly, the total charge and physical shape of the lipid head group (Mileykovskaya and Dowhan, 2009; Frolov *et al.*, 2011), and thirdly, the lipid bilayers phase behaviour, which is the overall phase transitions within the membrane (Quinn, 2012).

Prokaryotic counterparts to the Eukaryotic rafts have since been described, such as specific phospholipid-enriched domains, and membrane domains with low fluidity and high fluidity (Strahl and Errington, 2017).

In *B. subtilis* areas of increased membrane fluidity have been observed, named Regions of Increased Fluidity (RIFs) (Strahl *et al.*, 2014). The RIFs were initially discovered using the fluorescent dye Dil-C12, which due to its relatively short (12 carbon) aliphatic tail preferably targets fluid areas of the membrane. Additionally, RIFs showed local alterations to diffusion and protein localization (Strahl *et al.*, 2014). Further studies confirmed that there were indeed links between certain RIFs and the MreB cytoskeleton, and therefore to the cell wall synthesis machinery as shown in Figure 4b. The RIFs interacting with MreB and the elongasome are additionally called cell wall synthetic fluid microdomains, but will be referred to as RIFs throughout this thesis. The authors not only showed that these regions were connected to MreB, but also that other proteins were temporally confined by these MreB-dependent micro domains (Strahl *et al.*, 2014; Oswald *et al.*, 2016). Additionally, it has been demonstrated that these cell wall connected micro domains are conserved in *E. coli*, providing strong evidence that the domains are conserved beyond *B. subtilis* and other Gram positives (Oswald *et al.*, 2016). A particular membrane component may be responsible for the induction of the RIFs. It has been suggested that this is the isoprenoid lipid carrier for cell wall precursor synthesis, lipid II. Indeed, lipid II favours fluid surroundings, and can induce lipid disorder in its vicinity both *in vitro* (Ganchev *et al.*, 2006) and *in silico* (Jia *et al.*, 2011) whilst maintaining spatial proximity to MreB due to its role in cell wall synthesis. Other fluid domains might exist, as antibiotic treatment has shown domains to form, although further characterization is needed (Oliynyk *et al.*, 2008).

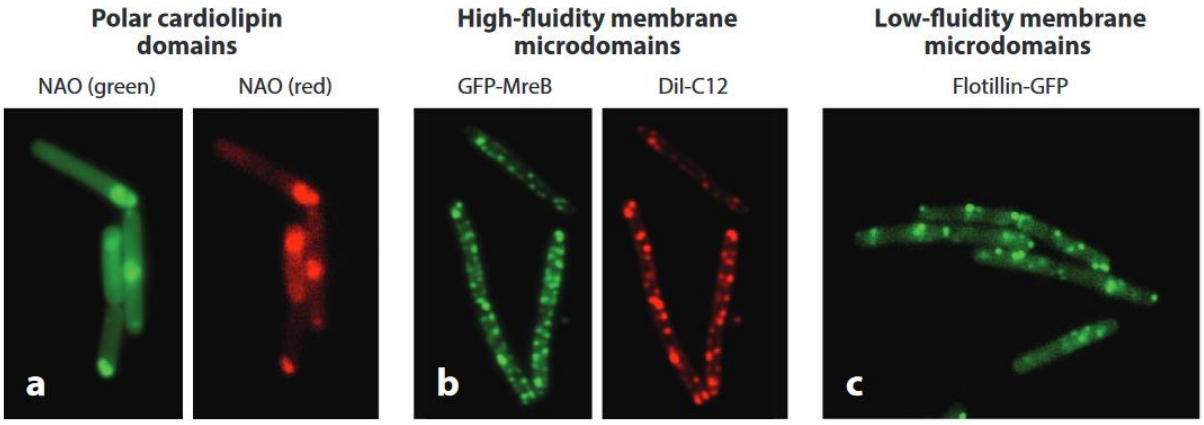

Figure 4: Examples of each of the three types of membrane domains discovered in bacteria. All images are taken in *B. subtilis*. (a) Polar lipid cardiolipin domains as shown with the dye NAO. Clear localization at the poles is visible with minor staining at the lateral part of the cell. The redshift occurs strongly at the poles. (b) High fluidity membrane micro-domains, also known as regions of increased fluidity (RIFs), as shown by the co-localization of Dil-C12 and the GFP tagged MreB. (c) Low fluidity microdomains as shown with a GFP fused to Flotillin. Discrete foci appear all along the lateral axis of the cell. (Strahl and Errington, 2017)

One of the defining factors for the formation of the Eukaryotic lipid rafts is the ability for their membranes to undergo phase separation, leading to two distinct membrane areas with different physical properties bordering each other (Simons and Ikonen, 1997). In Eukaryotes, cholesterol is used to tightly regulate the phase separation in the membrane, where it is utilized as a rigidifying agent in the bilayer, inducing lipid rafts (Lingwood and Simons, 2010). Bacteria are unable to produce cholesterol, so it was assumed that this type of rigidified phase separated membrane domain did not occur. Evidence to the contrary has emerged with the discovery of KinC, a kinase involved in regulation of *B. subtilis* biofilm differentiation, as well as KinCs activator, the farnesyl diphosphate phosphatase, YisP (D. Lopez and Kolter, 2010b). YisP produces farnesol, a compound essential in the production of the terpenoids; squalene, hopanoids, & carotenoids. All of these compounds can induce order within the bilayer, and might be the bacterial substitute for cholesterol (Gruszecki and Strzalka, 2005; Saenz *et al.*, 2012; Spanova *et al.*, 2012; Saenz *et al.*, 2015). Lipid rafts can readily be enriched and purified using detergent-resistant membrane fractioning. When this was performed on *B. subtilis*, KinC was found in a terpenoid-dependent manner along with protein homologues to the lipid raft specific flotillins, FloT and FloA. These results heavily suggest that domains of increased rigidity exist, and are biologically relevant in bacteria (D. Lopez and Kolter, 2010b). Deleting *floT* and *floA* results in a loss of KinC function, potentially proving a functional and possibly spatial connection, along with disruptions of motility, biofilm formation, competence, cell morphology, and protein secretion (Dempwolff *et al.*, 2012a; Dempwolff *et al.*, 2012b; Mielich-Suss *et al.*, 2013). Additionally, when deleting *floT* and *floA*, the observable domains disappear, with a concomitant rigidification of the membrane (Bach and Bramkamp, 2013), suggesting that the domains are important in regulating overall membrane organization and fluidity. In turn, overexpression of the flotillin homologues reduces membrane fluidity, correlating well with more rigid domains in the membrane (D. Lopez and Kolter, 2010b). These domains are visible through fluorescence microscopy, showing localization to distinct foci throughout the membrane (as seen in Figure 4c) (Donovan and Bramkamp, 2009). Since they cannot be named as lipid rafts due to a non-cholesterol formation, these domains are termed functional membrane microdomains.

The final type of lipid domain is governed by the lipid head group composition. For most of the proposed types of lipid specific domains, we have a problem detecting them due to a lack of efficient probes and purification techniques. Cardiolipin has been postulated as one of the notable exceptions to this conundrum. Nonyl acridine orange (NAO) is a

fluorescent membrane probe which has been thought to bind exclusively to cardiolipin and visualized by a redshift in cardiolipin-enriched areas. It was used to show that cardiolipin forms enriched domains at the cell poles as seen in Figure 4a (Mileykovskaya and Dowhan, 2000). Further evidence has been found to support that cardiolipin indeed does form enriched domains at the poles in *E. coli*, through minicells formed by misplaced division septa by the poles. These minicells represents almost pure polar lipids and exhibit proportionally more cardiolipin than full *E. coli* lipid extracts, suggesting that the poles are cardiolipin enriched (Koppelman *et al.*, 2001). It has been postulated that cardiolipin-enriched polar domains are found in multiple other bacterial species, such as *B. subtilis*, *Pseudomonas putida*, *Enterococcus faecalis*, and *Streptococcus pyogenes*, as shown by NAO staining (Matsumoto *et al.*, 2006; Bernal *et al.*, 2007a; Rosch *et al.*, 2007; Tran *et al.*, 2013). In *E. coli*, the domain has been associated with localization and activity of various membrane proteins including ion and metabolite transporters, and even with the selection of the cell division site (Mileykovskaya and Dowhan, 2005; Romantsov *et al.*, 2010). As discussed earlier, one of the reasons why cardiolipin is thought to localize to the pole is the cone-like structure of the lipid, combined with the negative curvature of the inner leaflet at the pole. However, this is disputed since the more cylindrical PG localizes to the cell pole in the absence of cardiolipin, pointing towards a shape-independent curvature localization mechanism that recruits anionic lipids to the poles in *E. coli* (Oliver *et al.*, 2014). It has additionally been found that NAO might stain all anionic phospholipids in the membrane rather than just cardiolipin, making it hard to determine if these domains are indeed real (Oliver *et al.*, 2014), but this will be discussed in length in Chapter 5.

1.3.4 – Membrane potential & pressure across the membrane

The membrane maintains the barrier between the interior of the cell and the surrounding environment, offering protection from unwanted compounds whilst retaining the important cellular metabolites, as well as essential macromolecules and the systems sustaining them. In order to maintain a functional cell, high intracellular concentrations of metabolites, enzyme cofactors, and essential ions have to be maintained. Many of these compounds are large, such as glucose, or charged, such as ions, leaving them unable to cross the membrane without assistance from trans-membrane protein pumps or channels. This uptake of desired metabolites and ions, and the secretion of unwanted molecules create a sharp gradient across the cytoplasmic membrane. The primary generated ion gradient is the proton motive force

(PMF), via respiration, which in turn is converted into secondary gradients. The gradients of ions create an electric potential across the membrane which is known as the membrane potential or membrane voltage (O'Shea, 2003).

The overall membrane potential in *B. subtilis* is usually at -110mV from exterior to interior (Hosoi *et al.*, 1980; Te Winkel *et al.*, 2016). The largest contributor towards the overall membrane potential is the ion species with the largest permeability across the membrane, both active and passive. In most native environments, H^+ is the ion with the highest permeability, and is thus the largest contributor for membrane potential due to its activity in oxidative phosphorylation across the membrane and upholding the proton motive force (Mitchell, 1961). Other important ions are Na^+, K^+, and in some cases Ca^{2+}, where Na^+ and Ca^{2+} usually act as secondary ions in anti-port systems responsible for H^+, K^+, or metabolite uptake into the cell (Heefner, 1982). K^+ is an important ion in osmotic stress responses, which will be discussed later.

The membrane potential is essential for a multitude of important cellular processes. The most obvious of these is oxidative phosphorylation. This is the process in which aerobic organisms generate the bulk of their ATP, as electrons are retrieved from carbon sources and transported through a selection of membrane bound complexes, known as the electron transport chain, which in turn pumps H^+ through the membrane giving rise to the majority of the proton gradient. Finally, H^+ is cycled back into the cell through the ATP synthase, producing ATP (Nath and Villadsen, 2015). Another important system requiring membrane potential is motility, as the rotation of flagella is driven by influx of H^+, similarly to the ATP synthase (Belas, 2014). Uptake of larger molecules through various transporters is often ATP driven, but others are directly linked with the proton motive force, such as uptake of lactose, peptides, xylose, etc. Many multi-drug efflux pumps are also H^+ dependent (Yan, 2013). Na^+ driven nutrient transporters are also dependent on membrane potential (Hamaide *et al.*, 1983; Togawa *et al.*, 2015), as are most protein secretion systems, which without membrane potential, either shut down entirely, or cause aberrant precursor orientation (Daniels *et al.*, 1981).

Intriguingly, membrane potential is also involved in proper localization of a series of membrane bound and associated proteins in *B. subtilis*, many of which are of particular interest for this thesis and will be discussed in detail later. MreB, Mbl, and MreBH, all members of the lateral cytoskeleton, lose their native localization upon dissipation of the

membrane potential, influencing cell wall synthesis and other downstream processes. MinD and MinC also lose their localization, influencing septal localization and cell division. Finally, components of the divisome, including FtsA, FtsZ, ZapA, EzrA, and Pbp2B, along with chromosome segregation protein Spo0J, become mis-localised upon dissipation of membrane potential, leading to improper chromosomal segregation and miss-localized division septa. All of the delocalized proteins can cause irreversible damage to the tightly regulated systems in which they are key players, halting cell division, and ultimately causing cell death and/or lysis (Strahl and Hamoen, 2010).

The many concentration gradients across the impermeable membrane are constantly attempting to regain equilibrium through a process known as osmosis. Osmosis is the phenomenon in which water travels across a membrane up a concentration gradient to reduce the concentration of a compound on the opposite side. Like Eukaryotes, Bacteria have aquaporins through which water can flow to alleviate changes in compound concentrations, allowing water to passively diffuse through the membrane. During native conditions, most bacteria experience a higher concentration of metabolites and ions in the cytoplasm compared to the external environment. As a consequence, water flows into the cytoplasm in an attempt to equilibrate concentrations thus exerting an enormous force on the membrane. The membrane is pushed against the surrounding cell wall, and the force exerted is called turgor pressure. The turgor pressure varies enormously between bacteria for unknown reasons. The Gram negative bacterium *E. coli* has a turgor pressure of about 0.3-3 atmospheres of pressure, while Gram positive *B. subtilis* has about 10 atmospheres (Rojas and Huang, 2018).

When the external compound concentrations suddenly change, either an osmotic up-shock or down-shock response is initiated. The cell has two different systems to counteract sudden changes in osmolality, both of which adjust the concentration of intracellular compounds. The first countermeasure is for osmotic up-shocks, where the concentration of a given osmolyte increases extracellularly. For this system, the cell starts *de novo* synthesis of osmolytes to retain water within the cytoplasm. Synthesizing new compounds is slow and energetically expensive, which makes it a backup system for extended periods of osmotic challenges (Cayley and Record, 2003). The system responsible for rapid osmotic regulation is dependent on transport of K^+ across the membrane. It has long been known that cells experience a K^+ influx upon osmotic up-shock (Wood, 1999; Balaji *et al.*, 2005), and since it is one of the most abundant inorganic cations, with an approximate cytoplasmic concentration of 200-300 mM, this form of osmotic regulation is able to regulate internal water levels over

enormous osmotic differences (Meury and Kepes, 1981). Through studies in *E. coli*, it has been shown that the accumulation of K^+ functions as a response to both ionic and non-ionic osmotic challenges, such as those with various salts and sugars (Meury *et al.*, 1985; Dinnbier *et al.*, 1988). The ion channels responsible for K^+ uptake in *B. subtilis* are KtrAB, and KtrCD, (Holtmann *et al.*, 2003), whose activities are regulated through two essential α-helices in an ATP/ADP-dependent manner, possibly involving di-cAMP, but the precise mechanism remains to be fully elucidated (Diskowski *et al.*, 2017). A second type of ion channel involved in K^+ uptake is KimA, which appears to be the channel responsible for upholding K^+ concentrations when at homeostatic growth, through a di-cAMP-directed manner (Gundlach *et al.*, 2018). The fact that *B. subtilis* has three separate, highly functionally redundant systems to regulate K^+ uptake and secretion underlines how important the ion is to cellular processes throughout the different environmental challenges presented to the organism.

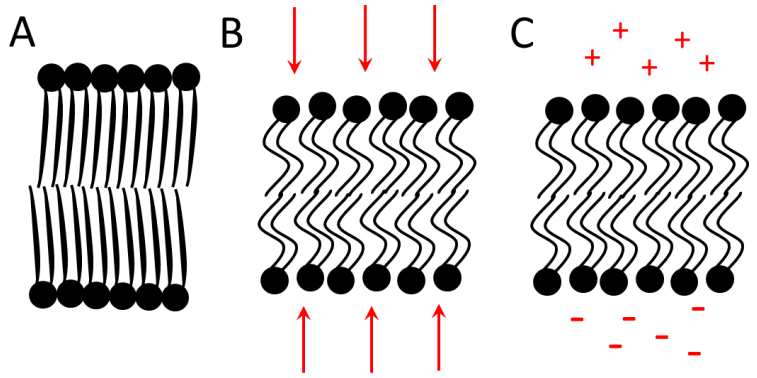

Figure 5: Electrostriction showed schematically. (A) A relaxed membrane shown with tightly packed fatty acids and head groups. (B) When forces are applied on either side of the membrane, the packing is disrupted, forcing the fatty acids into a loose conformation. (C) The forces exerted by ions on the membrane are electrical rather than physical, but the same disruption of fatty acids occur.

Besides causing turgor pressure on the membrane, ion gradients across the membrane exert a force of their own directly upon the membrane. The membrane effectively functions as an insulator between two electrically charged chambers, with the cytoplasm being one and the external surroundings the other. When there is no net charge across the membrane, the fatty acids relaxes into a configuration favoured without external forces and is thicker, more tightly packed, presumably causing a rigidification of the membrane, as shown in Figure 5a. If there were a force pushing on either side of the membrane, the fatty acids would adopt a thinner, more loosely packed state as shown in Figure 5b. Regardless of how many negatively or positively charged ions on either side of the membrane, when homeostasis is upheld and the membrane potential functioning, one side will be more positively charged, with the other having a net negative charge. Through electromagnetic forces that push on either side of the

membrane, a pressure is exerted causing the fatty acids to adopt a more fluid configuration, as shown in Figure 5c. This type of pressure is called electrostriction, and will be further discussed later (Heimburg, 2012).

1.3.5 – The cell wall

During environmental stresses such as osmotic shocks, the membrane itself can't uphold integrity since the relatively weak hydrophobic bonds holding the FAs together easily could break apart under stress, as the membrane is limited in lateral stretching capabilities. To protect the cell from cellular lysis, a peptidoglycan sacculus evolved, and is termed the cell wall. This structure is unique to the domain of Bacteria, making it the prime target for antibiotic compounds and the Eukaryotic immune system. In *B. subtilis*, the cell wall is made up of two distinct chemical structures in an approximate 4:6 – 6:4 stoichiometries: peptidoglycan (murein) and teichoic acid, respectively (Boylen and Ensign, 1968; Vollmer and Seligman, 2010). Peptidoglycan is responsible for maintaining the cell shape, it protects the cytosol against turgor pressure, and acts as a scaffold for surface proteins in Gram-positive bacteria (Dramsi *et al.*, 2008). Peptidoglycan is made up of linear glycan strands cross linked by varying types of short peptides as seen in Figure 6. Alternating sugars make up the glycan strands, *N*-acetylglucosamine (GlcNAc) and *N*-acetylmuramic acid (MurNAc), which are linked to one another. The peptide cross links vary across species, but the most predominant structure includes an unusual amino acid and is L-Ala-γ-D-Glu-(*meso*-A_2pm or L-Lys)-D-Ala-D-Ala, where the last D-Ala residue is lost during the cross-linking process (*B. subtilis* has the *meso*-A_2pm residue) (Vollmer *et al.*, 2008). Two distinct types of anionic teichoic acids are

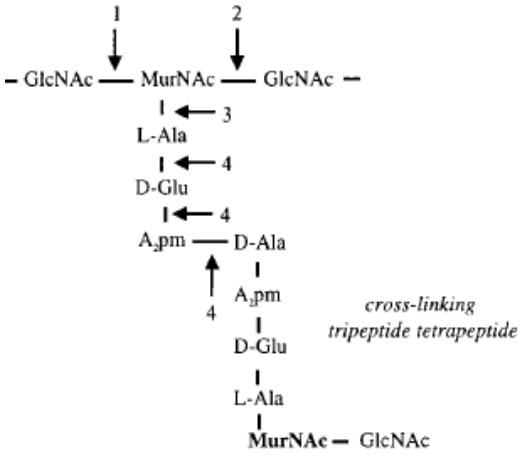

Figure 6: Chains of alternating GlcNAc and MurNAc make up the bulk part of the peptidoglycan, while the strands of sugar are held together with peptides spanning the gaps. In *B. subtilis* 35 different autolysins target 4 different types of chemical bonds within the peptidoglycan to ensure insertion of new cell wall material. (1) & (2) The GlcNAc-MurNAc bond is broken by exo-transglycosylases. (3) The bond between MurNAc and the first L-Ala residue is digested by MurNAc-L-alanine amidases. (4) The internal bonds within the peptide cross-links are carried out by DD-endopeptidases. Modified from (Smith *et al.*, 2000; Egan and Vollmer, 2013).

used in Gram-positive cell wall architecture: the wall teichoic acid (WTA), which is linked directly to the peptidoglycan, and the lipoteichoic acid (LTA), which is attached to a lipid anchor and imbedded in the membrane (Neuhaus and Baddiley, 2003). In *B. subtilis*, two forms of WTA occur, the major form is made from glycerol phosphate repeats, whilst the minor form is made from glucosyl-*N*-acetylgalactosamine-1-phosphate repeats (Schaffer and Messner, 2005). It has been shown that abolishing WTA production impaired cell growth and resulted in swollen cells that formed clumps, while removal of LTA resulted in twisted cells that grew in chains (D'Elia *et al.*, 2006; Schirner *et al.*, 2009). These phenotypes can be explained by the fact that the WTA and LTA has been found to steer important autolysins in their lysis of peptidoglycan, resulting in aberrant cell wall breakdown upon depletion of either component (Kasahara *et al.*, 2016). It is possible for Bacteria to grow without a cell wall under specific circumstances. When the surrounding environment has high concentrations of osmolytes such as sucrose, the turgor pressure is effectively negated, allowing for removal of the otherwise essential cell wall synthesis enzymes, thus losing the protective peptidoglycan. The resulting organism has a less regular morphology and grows slowly; with division resulting from an overproduction of membrane followed by blebbing, rather than the well-regulated cytokinesis seen in walled bacteria. These organisms are known as L-forms, and a more comprehensive review can be found here (Errington, 2017).

De novo synthesis of peptidoglycan occurs via two distinct processes in *B. subtilis*, namely at cell division, and during cell elongation. The initial steps of peptidoglycan synthesis are common to both, only differing in the subcellular synthesis location and the precise enzyme that is responsible for the insertion. The proteins responsible for the synthesis of peptidoglycan and cell division are encoded by the *mur*-operon (Ikeda *et al.*, 1991). The operon encodes the peptidoglycan precursor synthesis enzymes, the enzymes responsible for incorporation of new cell wall material known as penicillin-binding proteins (PBP), and several of the cell division proteins, such as FtsA and FtsZ (Ikeda *et al.*, 1991). The initial steps in synthesizing the peptidoglycan precursor occurs in the cytoplasm, and is performed by MurA and MurB, where the two sugars MurNAc and GlcNAc are activated by UTP, creating the UDP bound derivatives. The subsequent reactions are carried out by MurC, MurD, MurE, and MurF, ligating L-Ala, D-Glu, *m*-Dap, and D-Ala-D-Ala to UDP-MurNAc (Barreteau *et al.*, 2008). The first cell wall / cell membrane interaction is the synthesis of the intermediate, lipid I, which incorporates UDP-MurNAc-pentapeptide into the lipid pool by a step known as the transfer reaction (Anderson *et al.*, 1965). The reaction is catalysed by

MraY, which is encoded in the *mur*-operon, and attaches UDP-MurNAc-pentapeptide to the lipid undecaprenyl phosphate (C_{55}-P) (Higashi *et al.*, 1967). Although this intermediate is important for proper cell wall synthesis, it was found that *E. coli* only contains about 700 molecules of lipid I (van Heijenoort *et al.*, 1992). The low number of lipid I emphasises its function as an intermediate, heavily pushing the reaction equilibrium towards continuous production when producing cell wall, and quickly halting production as growth comes to a rest. The next and final step in the synthesis of the cell wall precursor lipid II is carried out by MurG, and transfers GlcNAc from UDP-GlcNAc to the free C4 hydroxyl group on lipid I resulting in the disaccharide-pentapeptide (lipid II) (Bouhss *et al.*, 2008). Lipid II is subsequently flipped to the outer leaflet of the membrane by a flippase; either MurJ, FtsW, or RodA, a subject which is still highly controversial (Mohammadi *et al.*, 2011; Emami *et al.*, 2017). Lipid II clusters with the elongasome during growth and with the divisome when the cell division septum forms (Lages *et al.*, 2013). Lipid II has, as previously stated, been linked with increased membrane fluidity and interaction with the actin homologue MreB. Upon cell elongation or division, penicillin binding proteins, or Pbps, catalyse the glycosyltransferase reaction, which inserts the precursor into the existing peptidoglycan structure, releasing undecaprenol for another round of precursor biosynthesis (Barrett *et al.*, 2007). Finally, the glycan strands are cross-linked by transpeptidase reactions, also performed by Pbps, producing the peptidoglycan mesh encapsulating the entire cell (Sauvage *et al.*, 2008).

To ensure growth, the bacterial cell needs to incorporate newly synthesized peptidoglycan into the already existing cell wall in a manner where the cellular integrity is not compromised. This incorporation involves breakdown of the existing crosslinks in order to present a free peptide strand for safe insertion of newly synthesized peptidoglycan sheets. A tight control of the breakdown is necessary to avoid the catastrophic event of cellular lysis, while still maintaining steady growth. The insertion of new cell wall only takes place at the membrane due to the Pbps being membrane bound, while hydrolysis occurs throughout the cell wall mesh, necessitating a constant cell wall turnover. *B. subtilis* has developed an impressive array of 35 autolysins divided amongst 11 different protein families, targeting four different types of chemical bonds in the peptidoglycan as shown in Figure 6, with an additional cleavage type when including the initial glycosyl-transferase reaction for novel peptidoglycan insertion (Smith *et al.*, 2000; Egan and Vollmer, 2013). All of the 35 enzymes exhibit redundancy, and the entire complement has yet to be fully characterized, although the most important members during vegetative growth in liquid media have been discovered

(Smith *et al.*, 2000). Three main types of autolytic enzymes exist, within which all 11 protein families occupy. The first types of enzyme are the transglycosylases and glucosaminidases, which cleave the bond between MurNAc and GlcNAc as shown in Figure 6(1) & (2). A noteworthy member of this group of enzymes in *B. subtilis* is LytD, which is a major autolysin during vegetative growth (Rashid *et al.*, 1995). The next group of enzymes are the amidases, which degrade the MurNAc-L-Ala bond as shown in Figure 6(3), with a noteworthy member in *B. subtilis*, LytC that is important for cell separation as well as other maintenance tasks (Kuroda and Sekiguchi, 1991). The final and largest main type of autolysins is the endopeptidases. These enzymes cleave the bonds within the peptide cross-links as seen in Figure 6(4). Noteworthy members include LytE, which is responsible for cell separation and elongation during vegetative growth (Margot *et al.*, 1998); LytF which is important in cell separation during vegetative growth as well (Margot *et al.*, 1999), and CwlO which is important in cell elongation during vegetative growth (Yamaguchi *et al.*, 2004). I will describe the significant autolysins in depth later in this chapter.

In addition to regulating the lysis and insertion of new peptidoglycan, the cells need to regulate elongation speed through cytoplasmic membrane expansion and cell wall growth, ensuring they expand at the same velocity. This regulation is maintained by the MreB-directed elongasome, which I will describe in detail later in this chapter. Another important point of membrane-wall regulation is during cell division. Here, a multi-protein complex, the divisome, regulates the insertion of new peptidoglycan, the relevant details of which will be described later in this chapter.

1.4 – Relevant Envelope-Associated Proteins

Throughout this thesis, multiple proteins from the systems described previously in this chapter were used. Most notably are the actin homologues MreB, Mbl, and MreBH. As these are the main focus of the thesis, they are described in detail in the following sections, as well as autolytic enzymes, stress response proteins, and division machinery proteins that have been utilized in this work.

1.4.1 – Actin homologues in B. subtilis and the elongasome

The actin homologues in bacteria were first discovered to be important in cell shape determination in *E. coli* in 1988, but later studies found that *B. subtilis* also carries the homologue (Doi *et al.*, 1988; Abhayawardhane and Stewart, 1995). Since then it has been revealed that almost all rod-shaped bacteria encode one or more actin homologues, with the only exceptions being organisms exclusively growing from the cell poles, such as *Actinomycetes*. *B. subtilis* carries three paralogue genes encoding three highly similar variants of the actin homologue: *mreB, mbl* and *mreBH*. The three proteins have been found to be part of the lateral cytoskeleton, responsible for guiding insertion of newly synthesized peptidoglycan. *B. subtilis* MreB is a 337 amino acid long protein with a molecular weight of 36.000 Da, and is expressed as part of an operon, along with other members of the elongasome, such as MreC and MreD (Levin *et al.*, 1992). In *B. subtilis*, MreB is loosely peripherally attached to the membrane, whereas in *E. coli* the protein is attached via an amphipathic helix (Salje *et al.*, 2011). MreB-like protein, or Mbl, is a 333 amino acid long protein weighing 35.700 Da, which as its name suggests is highly similar to MreB, but the gene is not part of an operon, nor is it in close proximity to any other elongasome component (Abhayawardhane and Stewart, 1995). MreB homologous protein, or MreBH, is a 335 amino acid protein weighing 35.500 Da, and is similar to MreB. It is expressed as a standalone protein and is the least studied of the three actin homologues (Carballido-Lopez *et al.*, 2006). Experiments have shown that the three proteins are mutually redundant, each of them being able to guide peptidoglycan insertion upon deletion of the others (Schirner and Errington, 2009a). MreB and Mbl are both expressed at a constant level of between 1000-5000 molecules per cell, while MreBH expression is off during vegetative growth, only being expressed during heat shock response or in the absence of the two other homologues (Nicolas *et al.*, 2012; W. Z. Huang *et al.*, 2013; Trip *et al.*, 2013). When deleting each of the homologues, the cell morphology changes slightly, suggesting that they are important in maintaining the tightly regulated cell wall synthesis. When deleting MreB, the cell becomes thicker and occasionally bulges from the cell poles. Deletion of Mbl causes slightly shorter undulated cells, while deletion of MreBH doesn't appear to change cell morphology during vegetative growth (Y. Kawai *et al.*, 2009). It is possible to delete all three homologues, if the repressor of σ^I, *rsgI*, is deleted as well. When all four genes are deleted, the cells lose their rod-shape morphing into cocci-like structures, emphasising that MreB and its homologues are important in lateral cell wall synthesis (Schirner and Errington, 2009b). Furthermore, a high

concentration of Mg^{2+} is required in the growth media when deleting any of the cytoskeletal proteins for unknown reasons (Schirner and Errington, 2009b).

MreB has been found to localize as short antiparallel helical filaments on the cytosolic side of the cell membrane (van den Ent *et al.*, 2014). The antiparallel nature of the MreB filaments ensures that both polymeric structures can attach to the membrane without any steric hindrance. Filament assembly by MreB is ATP/GTP-dependent, and as such has the same characteristics as actin, meaning that MreB polymers are constantly formed and degraded during cellular growth (van den Ent *et al.*, 2014). It was discovered, through fluorescence imaging, that MreB moves perpendicular to the cell axis along the longitudinal axis of the bacteria, and that MreB interacts with the entire cell wall synthesis machinery through the mediating proteins MreC and MreD as shown in Figure 7(Typas *et al.*, 2012). Together, MreB and the cell wall machinery are known as the elongasome. The elongasome is a large multi-protein complex with the overarching function of maintaining cell wall growth and integrity across the lateral cell axis. *B. subtilis'* cell wall is complex as described earlier, with multiple components and regulatory mechanisms ensuring safe growth of the cell, which is why the elongasome has been proposed to have at least 25 individual components, with possible multimers of select proteins (Errington and Wu, 2017). Multiple Pbps, and their regulatory proteins, has been either confirmed or speculated to be part of the elongasome, with Pbp1, Pbp2A, and PpbH being the confirmed major components (Errington and Wu, 2017). Teichoic acid synthesis is also a core function of the elongasome, with at least six of the synthesis enzymes

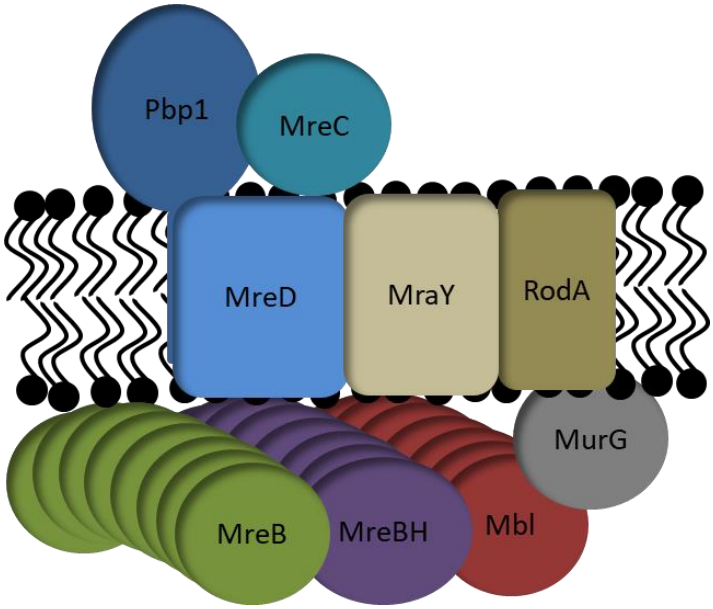

Figure 7: A stylized drawing of the current understanding of the elongasome with emphasise on proteins important for this thesis. MreB, MreBH, and Mbl are all able to, and might indeed intermix, form the helical filaments upon which the elongasome slides. The elongasome is attached to the MreB cytoskeleton via MreC and MreD, which in turn acts as a scaffold for the core parts of the elongasome. Pbp1 is the main Pbp in the elongasome. MraY synthesizes lipid I, MurG synthesizes Lipid II, and RodA is important for maintaining rod-shape, as it might indeed be the flippase as discussed earlier.

associated thereto (Formstone *et al.*, 2008). Multiple peptidoglycan synthesis proteins are located at the elongasome as well, such as the GTase and possible flippase RodA (Emami *et al.*, 2017). Finally, all the autolysins responsible for opening the peptidoglycan strands for novel insertion of peptidoglycan are members of the elongasome as well, but these will be discussed later in this chapter. A few of the proteins used from the elongasome in this thesis, along with the major Pbp, has been emphasized in Figure 7.

The movement of MreB is perpendicular to the lateral axis of the cell and is peptidoglycan synthesis-dependent, meaning that without active Pbps, MreB filaments come to a stop (Dominguez-Escobar *et al.*, 2011; Garner *et al.*, 2011). The importance of MreB polymerization is less understood, but it appears to play a role in curvature-dependent localization of the MreB cytoskeleton, which is essential for maintaining rod shape (Ursell *et al.*, 2014)

Apart from being involved in cell shape determination and direction of cell wall synthesis, the three actin homologues appear to direct specific autolysins to ensure a tight regulation of cell wall breakdown, as will be discussed in detail later (Dominguez-Cuevas *et al.*, 2013). In addition to regulating certain autolysins, MreB has been postulated to aid in spatially distributing other membrane-associated proteins in both *B. subtilis* and *E. coli* properly through temporally partitioning the cell with its discrete filaments (Strahl *et al.*, 2014; Oswald *et al.*, 2016). As stated earlier, it was recently discovered that MreB and its paralogues, along with the cell wall machinery, co-localise with RIFs. During the investigations it was found that not only did MreB and RIFs co-localise, the RIFs are dependent on the presence of MreB or one of its paralogues. Furthermore, it was found that when dissipating the membrane potential, MreB delocalises into specific foci along with the RIFs. This delocalization was accompanied by a general loss of fluidity in the membrane, eventually resulting in cell lysis (Strahl *et al.*, 2014). The mechanism responsible for MreB delocalisation upon membrane potential dissipation is thus far unknown; as is the concomitant cell lysis.

1.4.2 – Autolytic enzymes

Previously, I described how peptidoglycan is synthesized, as well as how important regulated breakdown is to bacterial growth. *B. subtilis* has developed an impressive array of 35 autolysins, mostly exhibiting redundancy and different conditions under which they are

expressed. The autolytic enzymes described in this section will cover the five most important to the cellular processes of elongation, division, and separation during vegetative growth (Smith *et al.*, 2000).

LytC is a 52.500 Da *N*-acetylmuramoyl-*L*-alanine amidase, which cleaves the MurNAc-L-ala bond as shown in Figure 4. LytC is expressed in an operon along with two other proteins, LytA, and LytB, under σ^A and σ^D promoters, but further regulated by SlrR, a repressor of the operon when sporulation is initiated (Lazarevic *et al.*, 1992). LytA is a protein which solely drives the secretion of LytC into the extracellular surroundings (Lazarevic *et al.*, 1992). LytB is the regulator of autolysin LytC, and is anchored on the extracellular side of the membrane. When the two proteins interact, the activity of LytC is increased up to about three-fold, thus ensuring high autolytic activity close to the membrane with decreasing activity further away, protecting the peptidoglycan mesh stability (Lazarevic *et al.*, 1992). LytC is localized across the entire outer surface of the membrane and does not exhibit diffusion to a large extent (H. Yamamoto *et al.*, 2003). LytC is a general hydrolase that is highly expressed from early logarithmic growth phase until stationary phase. Due to its localization to the entire outer surface of the membrane, the amidase is somewhat involved with general cell wall turnover, cell separation, competence, and digestion of the mother cell during sporulation. However, most importantly, it appears to be the major autolysin for synthesis and insertion of new flagella, and their subsequent stability (Chen *et al.*, 2009).

LytD is a 95.400 Da peptidoglycan *N*-acetylglucosaminidase, which cleaves the GlcNAc-MurNAc bonds within the peptidoglycan as shown in Figure 4. It is expressed as a standalone protein under the σ^D promoter and is secreted to the extracellular surroundings through an unknown mechanism (Margot *et al.*, 1994). The localization of LytD has yet to be examined, but its activity as a major cell separation autolysin suggests that it would localize to the division site. As *B. subtilis* has many autolysins targeting cell separation, the specific role and post-translational regulation for LytD is unclear (Chen *et al.*, 2009).

LytE is a 37.100 Da *D*,*L*-endopeptidase that cleaves the amino acid bonds in the peptide crosslinks as shown in Figure 4, which is expressed as a standalone enzyme under three different sigma-factors, σ^A, σ^H, and σ^I (Ishikawa *et al.*, 1998; Tseng *et al.*, 2011). LytE is secreted to the extracellular surroundings through an MreB- and MreBH-mediated or regulated system as shown in Figure 8, although this is not fully elucidated (Dominguez-Cuevas *et al.*, 2013). Surprisingly, the localization of LytE is mostly at cell division sites, and

to a lesser extent, across the lateral axis of the cell (H. Yamamoto *et al.*, 2003). LytE is important in cell separation as suggested by its septal localization, but additional evidence shows that LytE also functions as one of two major cell elongation autolysins (Smith *et al.*, 2000). The two mutually redundant cell elongation autolysins are LytE and CwlO, and without at least one of the two the cells are unable to elongate and die (Bisicchia *et al.*, 2007). When LytE is deleted, the cells appear to lose their diameter control, widening compared to wild type cells. The same phenotype is visible when deleting the two LytE secretion directing actin homologues, MreB and MreBH, suggesting that the cytoskeleton is intimately involved in the regulation of peptidoglycan insertion and remodelling (Dominguez-Cuevas *et al.*, 2013).

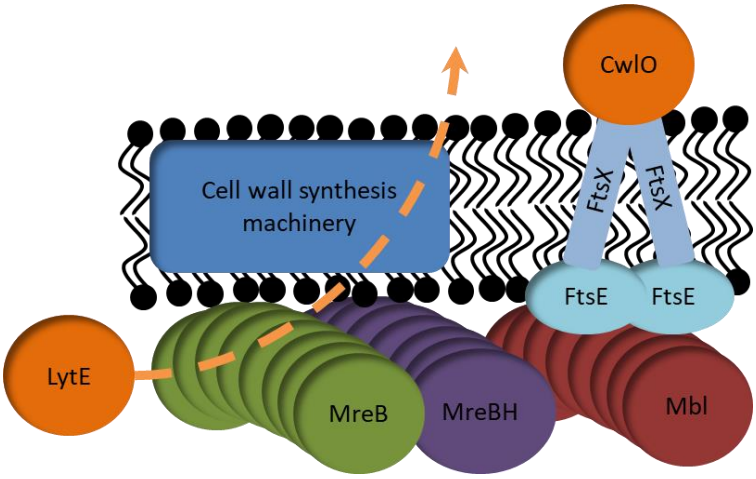

Figure 8: A stylized drawing of the regulation of LytE secretion and CwlO regulation through the actin homologues. LytE is secreted through an until now un-elucidated MreB and MreBH dependent mechanism. CwlO is secreted and subsequently sequestered and regulated by the proteins FtsE and FtsX via Mbl in an ATP hydrolysis dependent manner. LytE and CwlO are mutually redundant.

CwlO is a 50.900 Da *D*,*L*-endopeptidase which, just as LytE, cleaves the amino acid bonds in the peptide crosslinks as shown in Figure 4. CwlO is expressed as a single enzyme and is controlled by the σ^A promoter, but is further regulated by the WalRK two-component system (Noone *et al.*, 2014). CwlO is mutually redundant with LytE, and is a major autolysin in cell elongation. CwlO is secreted and regulated by the two proteins, FtsE and FtsX, via an Mbl mediated system as shown in Figure 8. The differential regulation of CwlO by Mbl and LytE by MreB is the only current functional difference known between the two actin homologues. Once secreted, CwlO is retained by an interaction with the trans-membrane protein FtsX. The suggested mechanism is that if the cell is lacking nutrients and ATP is scarce, CwlO is inactive, but when nutrients are plentiful, ATP is hydrolysed by FtsE and a signal is mediated through FtsX, activating CwlO that allows cell wall digestion and elongation (Dominguez-Cuevas *et al.*, 2013). CwlO is responsible for longitudinal control of cell wall breakdown, and if deleted the cell length is disrupted and division becomes uneven between bacteria. The same phenotype is visible if deleting Mbl, again emphasizing that the

cytoskeleton is more than a rail for the cell wall synthesis machinery (Dominguez-Cuevas *et al.*, 2013).

LytF is a 51.200 Da γ-*D*-glutamate-meso-diaminopimelate muropeptidase, which cleaves at the unusual amino acid in the peptide crosslink in peptidoglycan as shown in Figure 4. LytF is expressed alone under the control of the σ^D promoter, but is further regulated by SlrR similarly to LytC (Ohnishi *et al.*, 1999). Localization of LytF is exclusive to the cell division site where its exact regulation is unknown, although it appears that LTA might influence its activity and localization (H. Yamamoto *et al.*, 2003; Kiriyama *et al.*, 2014). The function of LytF is as a major cell division autolysin, as the localization pattern suggests. This activity was further established by the observation that it is down-regulated in stationary phase, when the cells have stopped dividing (Chen *et al.*, 2009).

1.4.3 – Homeostasis regulating proteins

Bacterial gene expression is largely governed by sigma factors and their regulating components. Two overarching types of classical sigma-factors exist in Bacteria, σ^{54} and σ^{70}. The σ^{54} type sigma factor is mostly involved in the metabolism of nitrogen and is considered rare (Gruber and Gross, 2003), and will not be discussed further. Most Bacteria have four different classifications of σ^{70}, which are all length variations of the same core domains. Sigma factors are made from up to four sub-regions; sub-region 1 is responsible for inhibiting non RNA-polymerase-bound sigma factors from binding the DNA, and to accelerate initiation at certain promoters. Sub-region 2 is involved in creating the transcription bubble that is required for recognition of the -10 promoter element. Sub-region 3 is responsible for recognition of extended -10 promoter elements, and sub-region 4 is responsible for interacting with additional transcription activators and repressors as well as the -35 promoter element interaction (Souza *et al.*, 2014). Group 1 sigma factors are the longest consisting of all four sub-regions and are considered the primary sigma factors, where their main task is to control transcription of house-keeping enzymes and are essential for survival (Paget and Helmann, 2003). σ^A, the main sigma factor in bacteria is part of group 1. Group 2, or the "primary-like sigma factors", have sub-regions 2, 3, and 4, but only parts of 1, and are not essential for survival under optimal conditions. Group 2 sigma factors are responsible for general stress response in a limited number of bacteria, not including *B. subtilis* (Gruber and Gross, 2003). Group 3 sigma factors consist of sub-regions 2, 3, and 4, and are typically involved in heat

shock responses, flagella synthesis, and sporulation. σ^I is a member of group 3, and is involved in heat shock adaptations (Zuber *et al.*, 2001), and will be discussed further below. Finally, group 4 sigma factors only have sub-regions 2 and 4 and are known as "extracytoplasmic function sigma factors" (σ^{ECF}), and are the functionally most diverse group. The σ^{ECF} are usually initiated by extracellular signals and are responsible for such varied processes as changes in osmolality, changes in pressure, nutrient limitation, oxidative stress, and other envelope stresses (Souza *et al.*, 2014). The combined stresses involving the cell wall and membrane are recognized as envelope stress, the protection towards which σ^{ECF}s are highly involved.

The sigma factors are mainly controlled by anti-sigma factors, which specifically bind the sigma factor, rendering it unable to associate with the RNA polymerase, inhibiting transcription. Anti-sigma factors are usually encoded in operons along with the sigma factor to facilitate immediate regulation. In the case of σ^{ECF}, the anti-sigma factor is inserted into the membrane, where it retains the sigma factor. When the appropriate stress signal is induced, whether being increased concentrations of certain molecules, pressure, or membrane alterations, a protease cleaves the anti-sigma factor, releasing the sigma factor into the cytoplasm, allowing RNA polymerase interaction and transcription. The stress response genes usually include the sigma factor itself along with the anti-sigma factor, for termination of the signal. (Ho and Ellermeier, 2012)

In *B. subtilis*, 7 σ^{ECF} exists, 4-5 of which are involved with envelope stress and homeostasis. The sigma factors involved in envelope stress are σ^M, σ^V, σ^W, σ^X, and σ^Z, where σ^Z is of unknown function, but could regulate certain envelope stresses (Asai *et al.*, 2003). σ^M is involved in response to cell wall-targeting antibiotics, osmotic changes, ethanol, acid, and heat shock. All of the responses are envelope related, with ethanol, acid and heat shock directly influencing the membrane fluidity, possibly explaining how the stress response is conveyed. σ^M has a rather large regulon, including alternative *pbp*s, the *mur*-operon, *rodA* and the *mreB*-operon, all seemingly for renewing the essential elongasome components (Thackray and Moir, 2003).

σ^V is released upon cell wall stress in the form of lytic digestion from enzymes such as lysozyme, and given time, confers resistance to enzymatic digestion of the cell wall. The regulon of SigV includes the *mreB*-operon, alternative *pbps*, teichoic acid synthesis enzymes,

and finally, sporulation initiation enzymes. The regulon suggests that the conferred resistance towards lytic cell wall digest might be induced by sporulation initiation (Ho *et al.*, 2011).

σ^W is involved in the response towards compounds which interfere with the synthesis and proper assembly of the cell wall, such as vancomycin or D-cycloserine, along with detoxification of the cell. The σ^W regulon is large and contains many proteins of unknown function, but the known genes consist of fatty acid synthesis, efflux pumps, inorganic metal uptake, *floA* and *floT*, and the phage shock gene *pspA*. Many of the components of this regulon are involved in membrane re-modulation (Cao *et al.*, 2002) and in the case of *floA* and *floT*, domain formation. σ^W is known to reduce membrane fluidity in an effort to reduce the diffusion of compounds across the membrane (Kingston *et al.*, 2011).

σ^X is part of the heat shock response, as well as controlling cell envelope modifications, biofilm architecture, and conferring resistance towards cationic antimicrobial peptides. The σ^X regulon is small compared to the previously discussed sigma factors, but includes teichoic acid synthesis components, iron uptake systems, heat shock proteins, lipid metabolism and modification enzymes, and alternative *pbps* (X. Huang and Helmann, 1998). As a consequence of the additional insertion of the cationic teichoic acids after initiation of the σ^X regulon, one would expect positively charged molecules would have a harder time reaching the surface of the membrane, corresponding well with the conferred resistance towards cationic antimicrobial peptides.

σ^I is a group 3 sigma factor induced by heat shock. σ^I is spatially regulated by its membrane-anchored regulatory protein RsgI, which upon heat stress changes conformation revealing a DnaK cleavage site. This allows the protein to be cleaved, releasing σ^I into the cytoplasm where it associates with RNA polymerase, initiating the transcription of its (Asai *et al.*, 2007) small regulon, which consists of 16 genes, half of which are involved in iron metabolism (Ramaniuk *et al.*, 2018). The remaining regulon consists of *ykpC*, a protein with an unknown function, *bcrC*, encoding the enzyme responsible for producing undecaprenyl phosphate, *gsiB*, a general stress response protein, protecting other proteins during thermal shock, *lytE*, an autolysin important for cell elongation as described previously, and *mreBH*, the third member of the MreB cytoskeleton (Tseng and Shaw, 2008). Expression of *sigI* has furthermore been shown to be essential upon deletion of the MreB cytoskeleton (Schirner and Errington, 2009a), perhaps because of the up-regulation of *bcrC* which in turn causes increased levels of precursor for lipid II allowing for more cell wall production.

To further add to the complexity regarding the regulation of σ^I expression, it has been shown that the two component system WalRK is not only involved in the sigma factor regulation, but also in the regulation of mutually redundant autolysins CwlO and LytE as shown in Figure 9. During vegetative growth, RsgI retains σ^I rendering it inactive, but at the same time, WalR is phosphorylated by WalK, keeping the expression of both CwlO and LytE at sufficient levels for cell elongation, with CwlO at highest expression. Meanwhile, *sigI* and *rsgI* transcription is kept at a background level through a σ^A promoter, while the more potent σ^I promoter is inhibited. When heat shock occurs, WalR phosphorylation is decreased, ending the high expression of CwlO. The heat shock releases σ^I from the membrane allowing it to stimulate its own up-regulation and the up-regulation of LytE expression, causing an abundance of LytE compared to CwlO (Salzberg *et al.*, 2013). This shift in autolysin expression from CwlO in vegetative growth to LytE during heat shock corresponds well with the fact that MreBH, the protein primarily responsible for the LytE secretion and regulation, is

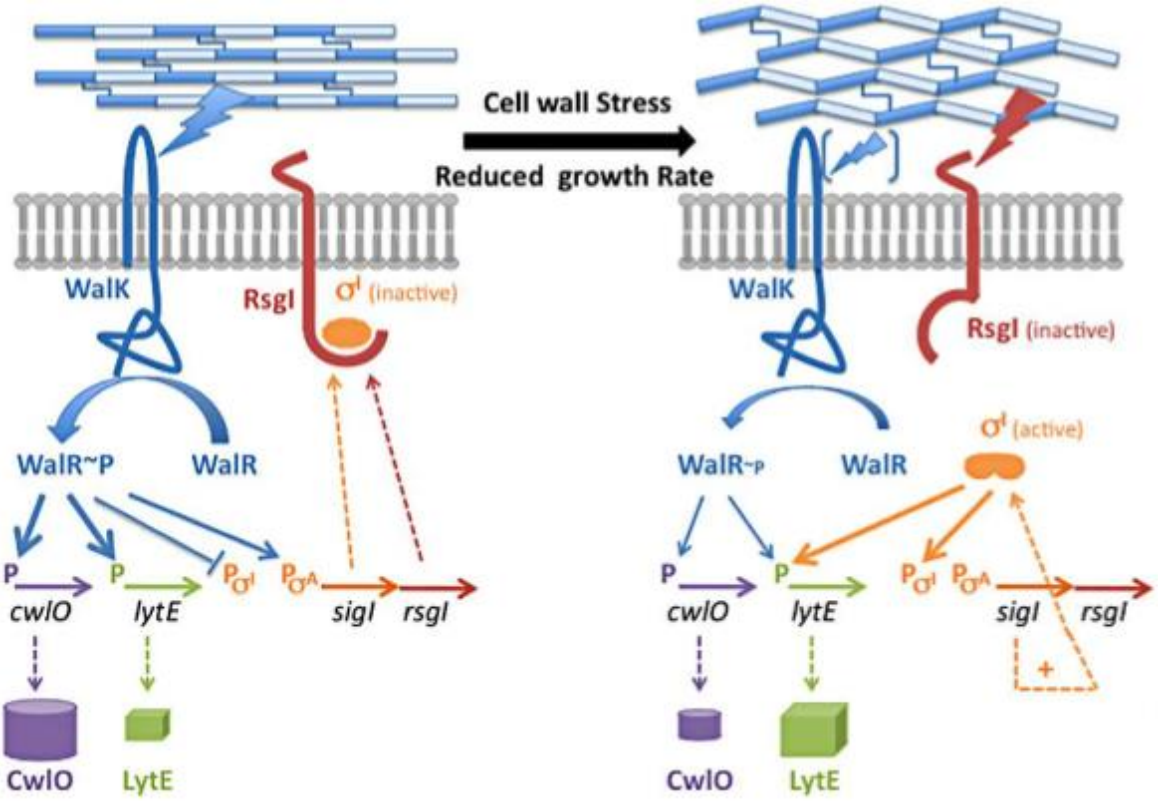

Figure 9: A schematic drawing of how WalRK and SigI regulate the two mutually redundant autolysins CwlO and LytE. Arrows from WalR and SigI signify transcription and their intensity how much transcript is produced, while a bracket signifies down-regulation. Broken lines represent protein translation. In vegetative growth, WalR is phosphorylated, which causes up-regulation of both autolysins, and a low level of *sigI* and *rsgI* transcription through a σ^A promoter. When heat shock is induced, WalR phosphorylation is reduced, lowering the transcription of both autolysins, and altogether stopping the inhibition of the more intense σ^I self-induction. σ^I highly increases its own transcription, and up-regulates the expression of LytE. (Salzberg *et al.*, 2013)

only expressed at high levels during heat shock, making the combined WalRK and σ^I regulation of the cytoskeletal components and autolysins temporal, reducing wasteful protein expression (W. Z. Huang *et al.*, 2013).

1.4.4 – The Min-system and division sites

Symmetrical cell division is the main type of proliferation in vegetatively growing *B. subtilis* in nutrient-rich media. In order for the organism to determine where cell division occurs, a tightly regulated system has been developed. Different species of bacteria have developed varying systems to ensure reliant division with *B. subtilis* and *E. coli* being the most well-studied. *B. subtilis* has two systems in place to ensure efficient division site placement, one of which is nucleoid exclusion, which ensures that the division site doesn't form around still replicating DNA, but rather where the DNA has separated (Harry *et al.*, 1999). To prevent multiple division sites forming where the nucleoid has condensed, a second system, termed the Min-system, is in place that involves, but is not limited to, the proteins DivIVA, MinD and MinC. DivIVA is a membrane-associated protein which localizes to the base of the first formed septum at mid-cell (Edwards and Errington, 1997) in a negative curvature-dependent manner (Lenarcic *et al.*, 2009; Ramamurthi and Losick, 2009). The protein MinD is subsequently recruited by DivIVA, along with the protein MinC through an interaction with MinJ, inhibiting the formation of additional division sites or breaking up rogue FtsZ rings (Bramkamp *et al.*, 2008; Gregory *et al.*, 2008). As division is finalized, the septum turns into a cell pole, where the DivIVA-MinD-MinC complexes are retained, inhibiting polar division site formation. The protein complexes are stationary and present at both cell poles and at septum with single proteins able to oscillate between sites in *B. subtilis* (Bach *et al.*, 2014), while the entire complex oscillates from pole to pole in *E. coli.* For a more comprehensive review on division site determination in various bacteria, see (Monahan *et al.*, 2014).

Interestingly, it appears that the localization of MinD is dependent on membrane potential. It was discovered that upon dissipation of membrane potential, the distinct polar and septal localization was lost entirely, delocalizing the protein to the cytoplasm. This was due to a loss of affinity to the membrane by the amphipathic helix responsible for membrane attachment (Strahl and Hamoen, 2010).

1.4.5 – Division and the Z-ring

When the cell division site has been selected, the divisome is responsible for cell division, initiating the formation of the septum. The divisome consists of more than 30 different proteins, including PBPs for cell wall synthesis, autolysins for cell wall degradation, scaffolding proteins, and the cytoplasmic components known as the Z-ring (Egan and Vollmer, 2013). The ring part of the Z-ring is made up of the tubulin homologue FtsZ, which functions as a treadmilling polymer upon which the rest of the divisome is assembling for cell division (Bisson-Filho *et al.*, 2017). As division starts, FtsZ localizes to the division site, polymerizes, and forms bundles that are subsequently recruited and attached to the membrane via either FtsA or SepF, forming the proto-ring (Duman *et al.*, 2013). Other than functioning as a membrane anchor for FtsZ, SepF forms large ring-like structures *in vitro* and is known to confer the bundling effect on FtsZ polymers (Gundogdu *et al.*, 2011), possibly aiding the constriction of the Z-ring. FtsA, an ATPase, is part of the internal components, and is one of the first divisome components to assemble, where it is known to form multimers (Sanchez *et al.*, 1994). FtsA localizes to the division septa in a clear ring-like structure (Errington *et al.*, 2003), and is attached to the membrane via an amphipathic helix (Rico *et al.*, 2013). Once the Z-ring is formed, the rest of the divisome is assembled on top of it, initiating septum formation and Z-ring constriction. This constriction is essential for cell division, but the method by which the constriction occurs has so far eluded discovery. For a more comprehensive review on divisome assembly and function, see (den Blaauwen *et al.*, 2017) and for a more comprehensive review on possible Z-ring constriction hypotheses see (Osawa and Erickson, 2018).

Upon membrane potential dissipation, FtsA, just as MinD, loses membrane association and is released to the cytoplasm. The mechanisms appear to be similar, as both proteins are associated with the membrane via an amphipathic helix (Strahl and Hamoen, 2010). The mechanism through which both MinD and FtsA lose membrane association is not well understood and needs further elucidation.

1.5 – Membrane-Targeting Antibiotics

Multiple targets exist for antimicrobials in Bacteria, most of which are specific to inhibiting certain proteins or larger ribozymes. Usually, the mode of action of these antimicrobials is to bind the target in an active site or in specific binding pockets. Common

between them is that a single mutation within the target enzyme or the regulatory components of the targeted enzyme renders the compound useless. These alterations to the genome are of course hereditary, causing lasting resistance towards the compound for generations. (Martinez, 2014)

Compounds targeting the bacterial membrane are more difficult to generate resistance towards, as no single protein makes up the membrane, but rather many millions of non-genetically encoded phospholipids. That is not to say that resistance cannot evolve towards membrane targeting compounds, as examples already exist, with bacteria changing polarity of the phospholipids from anionic to cationic, or overproducing charged lipids or teichoic acid to inhibit insertion of charged molecules (Epand *et al.*, 2016). These modifications usually come with a large cost to fitness and are thus less sustainable than point mutations.

The compounds discussed in this section are all important for this study, as they target the membrane in different ways to dissipate membrane potential, granting various conditions to study.

1.5.1 – CCCP

Carbonyl cyanide *m*-chlorophenyl hydrazone, or CCCP, was one of many cyanide derivatives developed and examined in 1962. It was found that their mode of action was to drive H^+ gradient uncoupling in mitochondria, and therefore also of aerobic Bacteria (Heytler and Prichard, 1962). CCCP is a small molecule, which when in a protonated state, is able to penetrate and traverse the membrane. When entering the membrane in its anionic form, CCCP takes up a proton from the extracellular environment, allowing it to diffuse across the membrane. Once in the cytoplasm, CCCP releases the proton, effectively collapsing the electrochemical proton gradient. Once the proton is released, CCCP returns to its anionic form, still being membrane permeable returning CCCP to the extracellular environment, possibly uncoupling more protons, thus fully depolarizing the cell (Cunarro and Weiner, 1975). CCCP is difficult to develop resistance against, but resistance does occur. Resistance experiments were undertaken in *B. subtilis*. The mutants were isolated in the days before full genome sequencing, but it was evident that the changes had occurred in the membrane. They found that the resistant strains all had reduced amounts of C16 monounsaturated fatty acids, but elevated iso-C15 fatty acids (Guffanti *et al.*, 1987). This might be a direct effect, stopping CCCP from traveling across the membrane, but is more likely a down-stream knock-off

effect, as CCCP functions at all biologically relevant temperatures, where one would expect various fatty acid compositions, including the shift in the mutant strains.

1.5.2 – Valinomycin

Valinomycin is a natural dodecadepsipeptide antibiotic weighing about 1100 Da. Valinomycin consists of three repetitions of D- and L-valine residues, L-lactic acid, and D-alpha-hydroxyvalerate acid, joined by alternating amide and ester bonds (Kroten *et al.*, 2010). Valinomycin was originally found in the bacterial family of *Streptomyces*, but is now produced in *B. subtilis* and *Streptomyces tsusimaensis* (Cheng, 2006). Valinomycin functions as a monomeric K^+-specific chelating agent, allowing for it to freely travel down the gradient across the membrane, out of the cell (Duax *et al.*, 1996). The compound works in both prokaryotes and eukaryotes, thus making valinomycin unfit for clinical use, but highly useful in studies of membrane potential, as the K^+ specificity can be used to accurately calibrate the membrane potential (Mitchell, 1961).

1.5.3 – Ion channels

Ion channels are trans-membrane proteins, typically facilitating transport for a single or few ion species. The natively encoded ion channels are tightly regulated proteins, which control membrane permeability of ions and are key components in upholding membrane potential and homeostasis. As described previously, membrane potential is important for proper membrane function, protein localization, and essentially cellular life. The scarcity of nutrients in some natural environments has thus forced bacteria to weaponize ion channels. One such ion channel is gramicidin, which has been used extensively throughout this thesis.

Gramicidins are highly hydrophobic linear pentadecapeptide antibiotics weighing about 1900 Da. Gramicidins are produced from alternating L- and D-amino acids, and are created by the soil dwelling bacterium *Bacillus brevis* (Sarges and Witkop, 1965). The channel that is formed is strictly monovalent cation-specific, with a conductance of about 10^7 ions per second, making it an extremely efficient ion de-coupler (Hladky and Haydon, 1972). Three variants of gramicidin occurs naturally, denoted A, B, and C, with A being about 80% of the mixture, and B and C making up the remaining 20%. The difference between the three variants is a single amino acid residue at position 11, which in A is tryptophan, B is

phenylalanine, and C is tyrosine. As all are aromatic structures, only slight changes to ion specificity occur between the 3 variants (Kelkar and Chattopadhyay, 2007). The gramicidin channel is formed by dimers, one monomer inserted in the inner leaflet and one in the outer, meeting in the middle to form the channel. The size of the channel is about 4 Å, which allows for the monovalent cations to pass freely, including the highly important K^+, effectively incapacitating the bacterium's ability to uphold membrane potential and K^+ homeostasis (Urry *et al.*, 1971).

1.5.4 – Membrane pores

Membrane pores, unlike ion channels, are large structures inserted into the membrane, which allow for large cytoplasmic components to leak out of the cell. Pores come in many shapes and sizes, but most stable pores are made up of multiple proteins, often in a symmetrical conformation. While many ion channels are used to combat opponents in nutrient acquisition in soil or other environments, membrane pores are often developed to kill as either virulence factors by pathogenic organisms, or as defence mechanisms by the host (Ros and Garcia-Saez, 2015). Later in this thesis, two relatively small membrane pores, LL-37, a human defensin, and Nisin, a lantibiotic, were used to determine lysis through pore formation.

LL-37, which is part of the innate immune response, consists of 37 amino acids and has a molecular weight of 4.500 Da. It is classified as a cathelicidin, which are lytic molecules stored in cytoplasmic granules within neutrophil leucocytes, and released upon activation. Upon activation, LL-37 adopts an α-helix conformation that effectively functions as an amphipathic helix (Gudmundsson *et al.*, 1996). LL-37 is active against both Gram positive and negative bacteria, since it can traverse both outer and inner membranes in a similar manner. The peptide, with the adopted α-helix conformation, attaches to the membrane of the bacteria via its amphipathic helix-like structure. When multiple LL-37 molecules have attached themselves to the membrane, they start attaching to each other, forming a carpet like structure on the outside of the membrane. This causes local perturbations in the membrane, in which monomeric LL-37 molecules penetrate and essentially disintegrates the membrane, allowing for multiple other molecules to flow through, transiently forming a non-selective toroidal lipid pore (Oren *et al.*, 1999). Toroidal lipid pores are formed when the outer and inner leaflet of the membrane fuses along the outer confines of the pore, allowing not only rapid loss of cytoplasmic components, but exchange of lipids between the two leaflets,

disrupting any built up asymmetry within the membrane (Gilbert *et al.*, 2014). Upon formation of the pore, larger cytosolic components leak out causing cellular lysis.

Nisin is an antimicrobial peptide naturally isolated from *Lactococcus lactis* (Mattick and Hirsch, 1947). It is classified as a lantibiotic type A that consists of 34 amino acids, and is highly active against Gram positive bacteria, whilst having low toxicity against eukaryotes (Severina *et al.*, 1998). Nisin has affinity for anionic phospholipids, especially lipid II. Nisin recruits lipid II and polymerizes. The multimerization of the nisin-lipid II complexes allows the unbound end of nisin to flip across the membrane, forming the pore. The pores are formed by 6-8 molecules and generate a 20-40 Å large gap through which ATP, amino acids, and all ions are allowed through (Breukink *et al.*, 2003; Tong *et al.*, 2014). The release of the cytoplasmic components will cause membrane depolarization and eventually lysis.

1.5.5 – Daptomycin

Daptomycin is a lipopeptide antibiotic originally found produced in the Gram positive soil dwelling bacterium *Streptomyces roseosporus* (Debono *et al.*, 1987). It is created from a macrolactone core built from 10 amino acids and three exocyclic amino acids linked to a decanoyl fatty acid tail (Huber *et al.*, 1988). Daptomycin has an overall negative charge, which is negated by the presence of Ca^{2+}, which also stimulates the oligomerization. When bound to Ca^{2+}, daptomycin has an increased affinity for negatively charged phospholipids (Jung *et al.*, 2004).

The mode of action for daptomycin is still fiercely debated, and various avenues have been examined. Early studies suggested that the peptidoglycan synthesis pathway was the target for daptomycin (Allen *et al.*, 1987). However, more recent studies have found that daptomycin induces membrane deformations that recruit the division protein DivIVA, which has increased affinity for negatively curved membranes (Lenarcic *et al.*, 2009; Ramamurthi and Losick, 2009). This recruitment could result in general aberrant membrane protein localization leading to cell envelope defects and eventually lysis (Pogliano *et al.*, 2012). An additional effect of daptomycin is membrane depolarization, which isn't explained by the previous hypothesis. Depolarization could be explained by a recent study where it was found that daptomycin causes lysis by insertion into the membrane by the short fatty acid tail that is covalently bound to daptomycin. Here, a two-step Ca^{2+}-stimulated oligomerization occurs. First a single Ca^{2+} ion binds daptomycin, causing light aggregation, followed by insertion by

ornithine-6, which leads to a second Ca^{2+} ion binding daptomycin tightly aggregating the molecules. The aggregation causes the large cyclic head group of daptomycin to submerge into the bilayer, which leads to distortions within the membrane. The short tail section of daptomycin, and the distortions caused by the head group, force packing in more fluid areas of the membrane, resulting in clustering with RIFs, which ultimately cause inhibition of cell wall synthesis due to the elongasome being co-localized with RIFs (Muller *et al.*, 2016). The sequestering of RIFs has been hypothesized to disturb the membrane integrity in the now sharp interphase between ordered and less ordered domains of the membrane, causing leakage of essential molecules and ions leading to membrane depolarization (Muller *et al.*, 2016).

More work is needed to find the actual mode of action for daptomycin, or to determine if the compound is working due to a plethora of effects, all crippling the target cells.

1.5.6 – Aim of study

In this thesis I aimed to describe which homeostatic changes occur within the membrane when deleting the MreB cytoskeleton, as well as describe if these changes alter the physical parameters associated with fluidity and temperature dependent growth phenotypes. Additionally, I wanted to elucidate if the deletion of *mreB* and its homologues changes the sequence of actions following disruptions to membrane homeostasis such as dissipation of membrane potential.

Chapter 2 – Materials and Methods

2.1 – Bacterial Strains and Growth Conditions

The strains used, their names, genotypes, and origins can be found in Table 1. All strains were grown at 37°C in LB medium unless stated otherwise. The WT *B. subtilis* 168, and all derivatives hereof, are tryptophan auxotrophs, and tryptophan is thus needed as a supplement in minimal media.

Name	Strain	Species	Strain genotype	Origin
KS1	168CA	*B. subtilis*	*trpC2*	WT
GP146	-	*B. subtilis*	*sigL::spec*	(Commichau *et al.*, 2007)
KS2	168CA	*B. subtilis*	*sigL::spec*	This study
PB344	-	*B. subtilis*	*sigBΔ2::cam*	(Boylan *et al.*, 1991)
KS3	168CA	*B. subtilis*	*sigB::cam*	This study
BKE06180	-	*B. subtilis*	*pspA::ery*	(Koo *et al.*, 2017)
KS4	168CA	*B. subtilis*	*pspA::ery*	This study
BKE33120	-	*B. subtilis*	*liaH::ery*	(Koo *et al.*, 2017)
KS5	168CA	*B. subtilis*	*liaH::ery*	This study
BP079	-	*B. subtilis*	*cwlO::spec*	(Bisicchia *et al.*, 2007)
KS6	168CA	*B. subtilis*	*cwlO::spec*	This study
1A792	-	*B. subtilis*	*lytABC::kan, lytD::tet, lytF::spec, lytE::cam*	(Margot *et al.*, 1999)
KS7	168CA	*B. subtilis*	*lytF::spec*	This study
KS8	168CA	*B. subtilis*	*lytE::tet*	This study
KS9	168CA	*B. subtilis*	*lytD::tet*	This study
KS10	168CA	*B. subtilis*	*lytABC::kan*	This study
KS19	168CA	*B. subtilis*	*lytABC::kan, lytD::tet, lytF::spec, lytE::cam*	This study
HB5134	-	*B. subtilis*	*des::spec*	(Hachmann *et al.*, 2009)
KS20	168CA	*B. subtilis*	*des::spec*	This study
4264	168ED	*B. subtilis*	*Ω(neo::spec) rsgI*	(Schirner and Errington, 2009b)
KS35	168CA	*B. subtilis*	*Ω(neo::spec) rsgI*	This study
3728	168ED	*B. subtilis*	*Ωneo3427 ΔmreB*	(Schirner and Errington, 2009b)
KS36	168CA	*B. subtilis*	*Ωneo3427 ΔmreB*	This study

4261	168ED	*B. subtilis*	*mbl::cam*	(Schirner and Errington, 2009b)
KS37	168CA	*B. subtilis*	*mbl::cam*	This study
4262	168ED	*B. subtilis*	*mreBH::erm*	(Schirner and Errington, 2009b)
KS38	168CA	*B. subtilis*	*mreBH::erm*	This study
HB10216	-	*B. subtilis*	*sigM::kan*	(Luo and Helmann, 2012)
KS41	168CA	*B. subtilis*	*sigM::kan*	This study
HB7007	-	*B. subtilis*	*pheA1, sigX::spec*	(X. Huang *et al.*, 1997)
KS42	168CA	*B. subtilis*	*sigX::spec*	This study
1A905	-	*B. subtilis*	*trpC2 sigW::mls attSPbeta*	(Cao *et al.*, 2001)
KS43	168CA	*B. subtilis*	*sigW::erm*	This study
1A909	-	*B. subtilis*	*trpC2 sigY::mls attSPbeta*	(Cao *et al.*, 2003)
KS44	168CA	*B. subtilis*	*sigY::erm*	This study
HB0028	-	*B. subtilis*	*sigV::kan attSPbeta*	(Cao *et al.*, 2005)
KS48	168CA	*B. subtilis*	*sigV::kan*	This study
HB0032	-	*B. subtilis*	*sigZ::kan attSPbeta*	(Cao *et al.*, 2005)
KS49	168CA	*B. subtilis*	*sigZ::kan*	This study
LC5	-	*B. subtilis*	*pheA1, des::kan*	(Aguilar *et al.*, 2001)
KS50	168CA	*B. subtilis*	*des::kan*	This study
3481	168ED	*B. subtilis*	Ω*neo3427 mreC*	(Leaver and Errington, 2005)
KS55	168CA	*B. subtilis*	Ω*neo3427 mreC*	This study
4277	168ED	*B. subtilis*	Ω*neo3427 ΔmreB, mbl::cam, mreBH::erm,* Ω*(neo::spec) rsgI*	(Schirner and Errington, 2009b)
KS60	168CA	*B. subtilis*	Ω*neo3427 ΔmreB, mbl::cam, mreBH::erm,* Ω*(neo::spec) rsgI*	This study, (Pogmore *et al.*, 2018)
KS60 III	168CA	*B. subtilis*	Ω*neo3427 ΔmreB, mbl::cam, mreBH::erm,* Ω*(neo::spec) rsgI*	This study
KS60 V	168CA	*B. subtilis*	Ω*neo3427 ΔmreB, mbl::cam, mreBH::erm,* Ω*(neo::spec) rsgI*	This study
KS60 VI	168CA	*B. subtilis*	Ω*neo3427 ΔmreB, mbl::cam, mreBH::erm,* Ω*(neo::spec) rsgI*	This study
TNVS229	-	*B. subtilis*	*amyE::spec Pxyl-murG-mcherry*	Gift from Terrance Saaki
KS62	168CA	*B. subtilis*	*amyE::spec Pxyl-murG-mcherry*	This study
1981	168ED	*B. subtilis*	*erm spc minD::ermC,*	(Marston *et al.*, 1998)

			amyE::Pxyl-gfp-minD	
KS64	168CA	*B. subtilis*	*amyE::spec Pxyl-GFP-MinD*	(Te Winkel *et al.*, 2016) This study
JS27	DH5a	*E. coli*	*pJS105 amyE::spec Pxyl-msfGFP-MreB*	Janina Stautz (Unpublished)
KS69	168CA	*B. subtilis*	*amyE::spec Pxyl-msfGFP-MreB*	This study
JS28	DH5a	*E. coli*	*pJS106 amyE::spec Pxyl-msfGFP-Mbl*	Janina Stautz (Unpublished)
KS70	168CA	*B. subtilis*	*amyE::spec Pxyl-msfGFP-Mbl*	This study
LB243	-	*B. subtilis*	*amyE::spec Pxyl mGFP-minD*	Laura Bohorquez (Unpublished)
KS75	168CA	*B. subtilis*	*amyE::spec Pxyl mGFP-minD*	This study
3750	-	*B. subtilis*	*amyE::spec Pxyl-YFP-mreBH*	(Carballido-Lopez *et al.*, 2006)
KS80	168CA	*B. subtilis*	*amyE::spec Pxyl-YFP-mreBH*	This study
EP99	168ED	*B. subtilis*	*pMutin4:cwlO::ery*	Emily Perry (Unpublished)
KS81	168CA	*B. subtilis*	*lytABC::kan, lytF::spec, lytD::tet, cwlO::ery*	This study
3427	168ED	*B. subtilis*	Ω*neo3427*	(Leaver and Errington, 2005)
KS91	168CA	*B. subtilis*	Ω*neo3427*	This study
YK206	-	*B. subtilis*	*purA16 metB5 hisA3 guaB, ftsA::erm Pspac-ftsZ*	(Ishikawa *et al.*, 2006)
KS97	168CA	*B. subtilis*	*ftsA::ery*	This study
RD159	-	*B. subtilis*	*neo rodA::Pspac-rodA*	(Strahl *et al.*, 2014)
KS99	168CA	*B. subtilis*	*neo rodA::Pspac-rodA*	This study
KS100	168CA	*B. subtilis*	Ω*neo3427 mreC, amyE::spec Pxyl-msfGFP-mreB*	This study
KS101	168CA	*B. subtilis*	*(Pspac-rodA, KmR), amyE::spec Pxyl-msfGFP-mreB*	This study
799	-	*B. subtilis*	*ftsL::Pspac-pbp2B, kan*	(Daniel *et al.*, 1996)
KS108	168CA	*B. subtilis*	*ftsL::Pspac-pbp2B, kan*	This study
1801	-	*B. subtilis*	*Pspac-ftsZ, Phl*	(Beall and Lutkenhaus, 1991)
KS109	168CA	*B. subtilis*	*Pspac-ftsZ, Phl*	This study

BKE04320	-	*B. subtilis*	*kimA::ery*	BGSC strain
JS52	168CA	*B. subtilis*	*ktrAB::kan, ktrC::spec, ktrD::tet, kimA::ery*	Janina Stautz (Unpublished)
HB5343	-	*B. subtilis*	*psd::ery*	(Salzberg and Helmann, 2008)
KS119	168CA	*B. subtilis*	*psd::ery*	This study
PG62	-	*B. subtilis*	*spc aprE::Pspac-yfp-ftsA*	(Gamba *et al.*, 2009)
KS120	168CA	*B. subtilis*	*spc aprE::Pspac-yfp-ftsA*	This study
4265	168ED	*B. subtilis*	*trpC2 ΔsigI rsgI::neo*	(Schirner and Errington, 2009a)
KS121	168CA	*B. subtilis*	*ΔsigI, rsgI::neo*	This study
SDB206	-	*B. subtilis*	*clsA(ywnE)::ery, clsB(ywjE)::spc, ywiE::neo*	(F. Kawai *et al.*, 2004)
HB5347	-	*B. subtilis*	*clsA(ywnE)::tet*	(Salzberg and Helmann, 2008)
ARK3	168CA	*B. subtilis*	*clsA(ywnE)::tet, clsB(ywjE)::spc, ywiE::neo*	(Pogmore *et al.*, 2018) & this study
Δ6	168	*B. subtilis*	*ΔSPβ; sublancin 168-sensitive; Δskin; ΔPBSX; Δprophage 1; pks::Cm; Δprophage 3; Cm^r*	(Westers *et al.*, 2003)

Table 1: Strains used throughout this thesis.

The compositions of the various liquid media used are shown in Table 2. When necessary for selection or induction, antibiotics or other supplements were added at relevant concentrations, as described in Table 3.

Media/Component	**Composition**
DSM media	8 g Nutrient broth 1 g Potassium chloride 0.25 g Magnesium sulphate 1 mM Calcium nitrate 10 µM Manganese dichloride 1 µM Iron sulphate

	pH adjusted to 7 and made to 1 L
Solution E	40 % (w/v) glucose
Solution F	1 M $MgSO_4.7H_2O$
SMM salts	0.2 % (w/v) ammonium sulphate 1.4 % (w/v) dipotassium phosphate 0.6 % (w/v) potassium dihydrogen phosphate 0.1 % sodium citrate dehydrate 0.02 % (w/v) magnesium sulphate
SMM media	10 ml SMM salts 120 µl Solution E 100 µl Tryptophan (40%) 60 µl Solution F 10 µl Casamino acids (20%) 5 µl ferric ammonium citrate (2.2 mg/ml)
LB media	10 g Tryptone 5 g Yeast Extract (Difco) 10 g NaCl Adjust to pH 7.0 and make up to 1 L
Valinomycin media	10 g Tryptone 5 g Yeast extract 300mM KCl Adjust to pH 7.0 and make up to 1 L
BHIS media	5 g beef heart infusion 12.5 g calf brain infusion 2.5 g disodium hydrogen phosphate 2 g glucose 10 g peptone 65 g sodium chloride Adjusted to pH 7.4 and made up to 1 L
LB 20% for time lapse	2 g Tryptone 1 g Yeast Extract (Difco) 10 g NaCl Adjust to pH 7.0 and make up to 1 L

BHI	5 g beef heart infusion 12.5 g calf brain infusion 2.5 g disodium hydrogen phosphate 2 g glucose 10 g peptone Adjusted to pH 7.4 and made up to 1 L
MSM supplement	20mM $MgCl_2$ 20mM maleic acid 0.5M sucrose Adjusted to pH 7.0

Table 2: All liquid media used throughout this thesis.

Compound	**Concentration**
Chloramphenicol	5 µg/ml
Erythromycin	1 µg/ml
IPTG	0.1-1 mM
Kanamycin	2 µg/ml 5 µg/ml when with 20 mM Mg^{2+}
Phleomycin	1 µg/ml
Spectinomycin	50 µg/ml
Tetracycline	6 µg/ml
Xylose	0.1-0.5 %

Table 3: Concentration of all antibiotics and inducers used throughout this thesis. The concentration of the inducers are in ranges as they changed between strains and experiments. For strains with poor expression or poor fluorescence higher concentrations were used. Additionally, kanamycins function is reduced when with high concentrations of Mg^{2+}, and is thus used at higher concentrations.

2.2 – General Methods

The following methods were used in creation of most of the strains used in this thesis. During the early stages of this work we decided to move strain background to 168CA to unify the various genotypes in a single WT strain. Furthermore, many of the strains previously created in the laboratory were in the background strain 168ED, which has a mutation rendering the WalRK two component system constitutively active. The WalRK two component system initiates a cell envelope stress response which would most likely interfere

with the experiments in this thesis (Dubrac and Msadek, 2008). Thus, almost all strains used are transferred genotypes from the old strain background to the new or indeed from other strain backgrounds. The data regarding the creation of the strains will not be shown nor discussed as the phenotypes have been discussed in previous publications as seen in Table 1. The list of the buffers used, and their components, are shown in Table 4.

Buffer name	Components
TES	10mM Tris-HCl pH 8 1mM EDTA 100mM NaCl
PBS	137 mM NaCl 2.7 mM KCl 10 mM Na_2HPO_4 1.8 mM KH_2PO_4
PBS – Sodium based	140 mM NaCl 11.8 mM Na_2HPO_4
TAE	40 mM Tris-acetate pH 8.5 1 mM EDTA

Table 4: List of buffers used throughout this thesis.

2.2.1 – Phenol/chloroform extraction of chromosomal DNA

Overnight (ON) cultures of the desired strains were grown in LB medium at 30°C with addition of 0.2% glucose to prevent spore formation. Deletion strains *ΔmreC*, *ΔmreB*, *ΔmreBH*, *Δmbl*, and combinations thereof, were additionally grown with 20mM Mg_2SO_4. 2ml culture was centrifuged at 14,000 g and washed in TES buffer. The pelleted cells were resuspended in 750 µl TES buffer. 25 µl Lysozyme (10 mg/ml) was added and the samples left to incubate for 10 min. at 37°C. Following this, 50 µl Pronase (10 mg/ml) and 30 µl Sarkosyl (30%) was added and the samples vortexed and left to incubate for 30 min. at 37°C. Next, 250 µl phenol (pH 7) and 250 µl chloroform was added and the samples were vigorously shaken followed by 4 min. centrifugation at 14,000g. The aqueous phase was transferred to a new tube and 500 µl chloroform was added. The sample was vigorously shaken and centrifuged at 14,000g for 4 min. The aqueous phase was again transferred to a new tube and 1.5x volume isopropanol was added. The sample was gently inverted until a clear precipitate appeared. The precipitate was transferred to a new tube and dried for 5 min.

at room temperature. The DNA was resuspended in 100µl TES buffer. The sample was gently heated to 37°C for 30 min. until the DNA was entirely resuspended, followed by immediate use or storage at -20°C.

2.2.2 – Transformation of B. subtilis

For each standard transformation, where a single gene was knocked out, the strain *B. subtilis* 168 was used. Selected single knock out strains were further manipulated whereby additional genes were either deleted or inducible genes inserted. 10 ml SMM was inoculated with bacteria from a fresh ON plate, resulting in an OD_{600} ~ 0.2. The inoculum was subsequently incubated for 3 hours at 37°C while shaking. 10 ml SMM salts (120 µl solution E, and 60 µl solution F; Table 2) was added and the samples were left to incubate for a further 2 hours at 37°C while shaking. 400 µl culture was transferred to a fresh tube and 2 µl chromosomal DNA was added. The sample incubated for 1 hour at 37°C while shaking. Plates with the relevant antibiotic were prepared and 100 µl sample was plated and incubated at 37°C overnight. When constructing the quadruple knockout strain (*ΔrsgI*, *ΔmreBH*, *Δmbl*, *ΔmreB*) and *ΔmreC*, the plates were infused with the supplement known as MSM, as described in (Leaver *et al.*, 2009), to protect against osmotic stress. For depletion strains with inducible genes lethal if missing, the inducer was also added to the selection plates. Following selection, single colonies were clean streaked onto plates with the relevant antibiotic and grown overnight. A single colony was grown over night in liquid media with the relevant antibiotic. Bacterial stock solutions were prepared from the final overnight culture with a final glycerol concentration of 25%.

2.2.3 – amyE starch assay

For strains with the classic *amyE* insertion of fluorescent fusion proteins, a starch assay was performed following transformation. *amyE* is involved in starch catalysis, and therefore if insertions are introduced in this gene, starch degradation would seize. NA plates were prepared with 2 mg/ml starch. A single colony from a transformation plate was transferred to a tube containing 100 µl LB medium. 5µl cell suspension was transferred to the starch plate and to a plate containing the selection antibiotic, along with a positive and negative control. The plates were left to incubate ON at 37C°. The following morning several iodine crystals were added to the lid of the starch plate and left to incubate for approximately

15 min. Since iodine only stains the starch, any starch-less halos would be visible (indicative of amylase activity) around colonies with intact *amyE* genes, whereas continuous staining would be observed around *amyE* insertion mutants. The plates were evaluated visually.

2.2.4 – Polymerase chain reaction to evaluate mutants

PCR was used to determine if the final MreB cytoskeletal mutant was indeed created properly. Colonies with the correct phenotype were selected and cultured and DNA was extracted according to the previous extraction protocol. The DNA concentration was measured and diluted accordingly. For each PCR a forward and reverse primer is needed. The primers were designed such that there were two reverse primers, one internally in the gene and one external. Each primer pairs expected length was calculated with the WT genes, any deviation from those lengths would signify a deletion / insertion into the gene. If the internal reverse primer reaction yielded no product compared to the WT, it would signify a deletion. The primers used, along with their melting temperatures, and their product lengths are shown in Table 5. The reagents needed for each PCR is recorded in Table 6.

Name	Sequence	Melting temp (°C)	Description	Product length
KS1	GCTTTAAGAAAGGAAGATACAT	51.92	forward *ΔmreB*	-
KS2	TCGACAATTGTAGATACAGT	51.37	internal reverse *ΔmreB* KO	811bp
KS3	TTAAATCTGTAAGGTCAGCC	52.59	external reverse *ΔmreB* KO	1881bp
KS4	AAATTAGGATAGAGATTGGGT	51.23	forward *ΔmreBH*	-
KS5	TGGCTCTTCGATTAAATGAA	52.59	internal reverse *ΔmreBH*	432bp
KS6	TCCATTTCCCACAATATGAA	52.06	external reverse*ΔmreBH*	1114bp
KS7	GGATATTTACTGTGAAACAGAT	51.65	forward *Δmbl*	-
KS8	AGAAGAGGAGGTGACAATAT	52.70	internal reverse *Δmbl*	565bp
KS9	CCTATTATCGTCATTTAACATCT	51.94	external reverse *Δmbl*	1127bp
KS10	TTGCGAATCCCTATCAAAT	51.89	external forward *ΔrsgI*	2008bp
KS11	TGTATTATCATTACGGGTGATT	52.77	internal forward *ΔrsgI*	1261bp
KS12	GGTACAGCAAGCACAAT	52.10	reverse *ΔrsgI*	-

Table 5: Primers used in the PCR assay to examine the final MreB cytoskeletal mutants genetic composition

Component	Final Concentration
5x GoTaq Reaction Buffer	1x
dNTP Mix	0.2 mM each dNTP
Forward Primer	1 µM
Reverse Primer	1 µM
Chromosomal DNA	<200 ng
GoTaq DNA Polymerase (Promega)	1.25 u
Nuclease Free Water to	20 µl

Table 6: Reagents needed for GoTaq PCR

The PCR reactions were carried out on a Thermal Cycler Techne FTGene-2D using the program shown in Table 7. The PCR products were run on a 1x TAE agarose gel and visualized using 1x SYBR Gold (Thermo Fisher).

Step	Temperature (°C)	Time	Cycles
Initial Denaturation	95°C	2 min.	1x
Denaturation	95°C	30 sec.	35x
Annealing	See Table 5	30 sec.	
Extension	72°C	60 sec.	
Final Extension	72°C	5 min.	1x
Final Hold	16°C	Infinite	1x

Table 7: Program for all PCRs. Annealing temperatures are shown in Table 5.

2.3 – Bacterial Growth and Lysis Assessments

2.3.1 – Minimal inhibitory concentration (MIC) determination

This assay was performed to determine working concentrations for the lysis assay for the antibiotics CCCP, gramicidin, daptomycin and LL-37, since certain mutant strains could induce increased resistance that might explain the various observations regarding strain survival or rescued lysis. ON cultures were prepared with the relevant antibiotic. An ON culture was diluted 1:100 with no selection and grown to mid-log phase. The cells were then diluted to a concentration of 20.000 cells / ml and transferred to a pre-heated microtiter plate. The plate was prepared with an initial high concentration of the desired antimicrobial compound and a 1:2 dilution series was performed throughout the plate. The cells were added to the plate for a final concentration of 10.000 cells / ml, along with the inclusion of any inducers needed to support the growth of selected mutants. The plate was incubated at 37°C for 16 hours while shaking. Results were generated optically using a BMG FLUOstar OPTIMA plate reader. The highest concentration without growth would determine the MIC.

2.3.2 – Lysis assay

This assay was performed on strains grown to mid logarithmic phase unless stated otherwise. The strains were grown to an OD_{600} ~ 0.6 and transferred to a microtiter plate in triplicates, to a final volume of 200 µl in each well. The compound in question would be added and OD_{600} measurements was conducted every 5 min ON to determine a lysis curve. The experiment was conducted with shaking when there were no measurements taken in order to optimise oxygenation. The different compounds used and their final concentrations are found in Table 8. The plate was placed in a plate reader (FLUOstar OPTIMA from BMG LABTECH) and grown while shaking at 37°C unless stated otherwise. For all the MreB cytoskeletal mutants 20 mM Mg_2SO_4 was supplemented.

Compound	Function	Concentration
CCCP	Proton decoupler	100 µM
Vancomycin	Cell wall inhibitor	10 µg/ml
Valinomycin	Ion channel	5 µM
Gramicidin	Ion channel	10 µg/ml
Daptomycin	Membrane active	10 µg/ml
Chloramphenicol	Ribosome inhibitor	100 µg/ml
LL-37	Membrane pore	40 µg/ml
Nisin	Membrane pore	10 µM

Table 8: Standard concentrations of commonly used compounds in the assays performed throughout this thesis.

2.3.3 – Killing beyond lysis assay

When determining whether the cells died throughout the lysis experiment, samples were taken every hour and diluted 1000 times in LB without compound, followed by a further 1:10 dilution series. 5 µl of each dilution was transferred to a nutrient agar plate (containing 20 mM Mg_2SO_4 for MreB cytoskeletal mutants) and grown ON at 30°C to prevent excessive growth. The treated cells were compared to non-treated controls, showing whether the cell count was decreased, thus showing dying cells, or if the cell count grew or stabilized, suggesting bacteriostatic properties or no impact on the cells. The plates were evaluated visually.

2.4 – Microscopy

2.4.1 – General epifluorescence microscopy

For standard fluorescence microscopy, the slides were prepared with 1.2% agarose in H_2O on teflon coated glass slides. Unless stated otherwise, cells were grown to mid-logarithmic phase with any inducers needed for fluorescent protein expression, and 200 µl culture was then transferred to a 2ml round bottomed Eppendorf tube with a perforated lid. The samples were incubated with vigorous shaking at 37°C unless stated otherwise. The cells were then treated with either antibiotics or dyes at the relevant concentrations, according to Table 8 and Table 9 respectively for standard concentrations, or at concentrations that were specified for the individual experiments. After treatment, a droplet of the sample was transferred to the prepared slide and the liquid evaporated by blowing warm air over the slide. The slide was immediately taken to the microscope for imaging. The excitation and emission wavelengths used for each fluorophore is located in Table 9. Since the proper localization of the proteins and or dyes used throughout the experiments were membrane potential dependent, imaging was carried out as quickly as possible with as few samples on each slide as possible to ensure continuous membrane potential. Microscopy was carried out with a Nikon Eclipse Ti (Nikon Plan Apo1.40 Oil Ph3 objective) and a Sutter Instrument Company Lambda LS xenon arc light source, and the images were acquired with a Prime 4.2 sCMOS camera (Photometrics) and Metamorph 7 (Molecular Devices).

Fluorophore	Function	Concentration	Ex/Em filters (nm)
Nile Red	Membrane dye	0,5 µg/ml	560-40/630-75
FM5-95	Membrane dye Time lapse microscopy	150 µg/ml	560-40/630-75
$DiSC_3(5)$	Membrane potential dye	10 µM	628-40/692-40
Laurdan	Membrane fluidity dye	10 µM	350-10/430-10 350-10/500-10
DPH	Membrane fluidity dye	10 µM	360-10/450-10
NAO	Membrane dye	100 nM standard See Chapter 5	470-40/525-50 470-40/630-75
GFP	Fluorescent protein	-	470-40/525-50
mCherry	Fluorescent protein	-	560-40/630-75
YFP	Fluorescent protein	-	500-20/535-30

Table 9: Fluorophores, their function, final concentrations, and excitation and emission wavelengths used throughout this thesis.

2.4.2 – Time lapse microscopy

The desired strain of bacteria was grown overnight in LB media infused with the relevant antibiotic. The following day the overnight culture was diluted 1:100 in LB without antibiotic but in the presence of inducer, when necessary, and grown to mid-logarithmic phase. Along with the low concentration LB, a 2x High-resolution low-melting agar solution was prepared. The microscopy slide was prepared approximately 30 min. before sample preparation to ensure the agar was properly set. A Gene frame (Thermo Fisher) was placed on a clean slide. To avoid osmotic up-shock, a lower concentration of LB was added to the agar as evaporation and sample preparation would concentrate the nutrients; 1 volume of LB (20%) and 1 volume of 2x agar was mixed (any dye or compound was included in this step). 600 µl LB-agar mix was transferred to the gene frame and a new slide was placed on top and gently pressed against the gene frame. The slide was left to solidify for 30 min. at 4°C. The top slide was removed and a sliver cut in the solidified agar to allow for oxygen within the closed gene frame. The culture was diluted to OD_{600} of either 0.015 (if growth was examined) or OD_{600} 0.2 (if lysis was examined) and 1.5µl added to the sliver of agar. Once the excess water was evaporated, a cover glass was placed on the gene frame. The slide was placed in a pre-heated microscope at 37°C unless stated otherwise and left to incubate for 1 hour, before starting the capture.

2.4.3 – Analysis & quantification of microscopy images

The microscopy images were all analysed using the Fiji plugin to ImageJ (Schindelin *et al.*, 2012). For fluorescent intensity quantification Fiji was also used. A line the width of a *B. subtilis* cell was manually drawn for all cells in an entire field of view using the ROI tool. Average intensities were measured for each cell, and standard deviations calculated. For specific statistical analysis, details will be provided in the relevant Chapter.

2.5 – Membrane Fluidity and Potential Assays

2.5.1 – Laurdan generalized polarization based fluidity measurements

6-Dodecanoyl-2-Dimethylaminonaphthalene, or Laurdan, is a fluorescent membrane probe that inserts into the top layer of the membrane since it has a hydrophobic end and a hydrophilic end. The emission of the fluorophore undergoes a redshift when water is in

abundance, thus making it possible to probe membrane head group stacking as a measure for membrane fluidity. Higher fluidity gives rise to a redshift in emission due to water having easier access to the outer most layer of the membrane. The following protocol is to be performed in the dark where possible due to the photo- sensitivity of the Laurdan dye. Cells were grown to the desired OD_{600} in LB medium supplemented with 0.1% glucose at the desired temperature. 1 ml cell suspension was transferred to a 2 ml Eppendorph tube and Laurdan (Thermo Fisher) was added to a final concentration of 10 µM. The cells were incubated for 5 min. while shaking at the desired temperature. The cells were washed four times with 2 ml pre-warmed PBS + 0.1 % glucose supplemented and centrifuged at 15,000 rpm for 1 min. The final pellet was resuspended in 1 ml PBS + 0.1% glucose. 500 µl was transferred to a new tube and centrifuged. The supernatant was carefully harvested as it would serve as background fluorescence for the measurements. 150 µl of cell suspension was added to each well in a pre-warmed flat bottomed black 96-well microtiter plate. 150 µl supernatant was added to separate wells for background determination and later subtraction. Excitation filter used: 350-10nm, emission filters used: 430-10nm & 500-10nm. For slow acting antibiotics, preincubation was performed before starting any measurements to ensure that the cells were not damaged by ROS, generated by the continued light exposure, before any important data gathering time points. For fast acting antimicrobials, measurements were initiated immediately after addition. For kinetic experiments, measurements were taken every minute. Benzyl alcohol was used as a fluidizing control at a concentration of 50 µM. The generalized polarization (GP) was determined using the formula below, with values ranging from -1 to 1 and physiological fluidity typically at about 0.25, where lower numbers describe a more fluid membrane, while higher numbers describes increased membrane rigidity.

$$GP = \frac{\lambda_{430} - \lambda_{500}}{\lambda_{430} + \lambda_{500}}$$

2.5.2 – DPH polarization based fluidity measurements

1,6-Diphenyl-1,3,5-hexatriene, or DPH, is a fluorescent membrane probe which inserts within the hydrophobic core of the membrane. DPH is an entirely rigid molecule with only a few flexible bonds. When using DPH we take advantage of the rigid structure of the molecule, as a rigid membrane will restrict the rotation of the compound, while a more fluid membrane allows for more rotation. If measuring the emission at parallel and perpendicular

angles to the excitation, we directly measure the amount of molecules allowed to rotate within the timeframe.

Cells were grown to approximately OD_{600} ~ 0.5 at the desired temperature. 1 mL was subsequently transferred to a 2 mL Eppendorf tube followed by the addition of DPH to a final concentration of 10 µM. The cells were then incubated at the desired temperature while shaking for 5 min., followed by centrifugation at 14.000g for 2 min. The supernatant was discarded and the cells were resuspended in pre-warmed PBS supplemented with 0.1% glucose, to keep the cells energized. If the measurements were to be followed for more than 30 min., 100 µg/ml of chloramphenicol was also added to restrict growth while not interfering with the membrane potential. 150 µl of the resuspended cells was transferred to a black flat-bottomed microtiter plate in triplicates. Measurements were undertaken using a CLARIOstar plate reader from BMG every minute with shaking in between measurements. The excitation wavelength used was 360-10nm, while the emission was measured at angles parallel and perpendicular at 450-10nm. The fluidity of DPH can be represented by either fluorescence anisotropy or milli-polarization. The two are measured as follows:

milli-Polarization: $$mP = \frac{\| - ٢}{\| + ٢} \cdot 1000$$

Fluorescence anisotropy: $$r = \frac{\| - ٢}{\| + (2 \cdot ٢)}$$

All results will be shown in mP, since this measurement shows the direct correlation between the intensities of the two angles.

2.5.3 – $DiSC_3(5)$ fluorometric membrane potential measurements

The desired *B. subtilis* strain was grown to the OD_{600} of choice at 37°C unless stated otherwise. The culture was diluted to an OD_{600} of 0.2 in pre-warmed LB medium supplemented with 0.5 mg/ml BSA, and 135 µl of diluted culture was added to a pre-warmed black flat-bottomed microtiter plate. Excitation filter used: 610nm. Emission filter used: 660nm. The plate was placed in the plate reader and measurements performed for 5 min. to determine a fluorescence baseline for the cells and the medium. The $DiSC_3(5)$ was added to a final concentration of 1 µM and DMSO at 1% and measurements were undertaken for approximately 5 min. to allow initial quenching of the fluorophore. After the measurements had stabilized, the compound of interest was added and measurements undertaken every

minute for up to 60 min. 1 µM gramicidin was used as complete depolarization control compound as CCCP interferes with the fluorophore. To prevent cell growth from interfering with the results, all samples were treated with 50 µg/ml chloramphenicol.

2.5.4 – Resazurin cell viability assay

Active cellular respiration was assayed using the commercial kit AlamarBlue from Thermo Fisher. Living polarized cells maintain a constant reducing environment within the cytoplasm through the process of oxidative phosphorylation by the electron transport chain. It is possible to measure the reductive capabilities of the cell by measuring the redox dependent conversion of the compound resazurin into the fluorescent resorufin.

WT *B. subtilis* was grown to OD_{600} 0.2 at 37°C in LB while shaking. 100 µl cell culture was transferred to a microtiter plate along with 5 µl AlamarBlue and left to incubate for 1h, followed by fluorescence measurements using a BMG Clariostar plate reader. Excitation wavelength was 550±5nm and emission wavelength at 595±5nm. Larger reducing potential would correlate directly with a higher fluorescent signal as more resazurin would be converted into the fluorescent resorufin. To prevent cell growth from interfering with the results, all samples were treated with 50 µg/ml chloramphenicol.

2.6 – Sample Preparations for Outsourced Analysis

2.6.1 – Fatty acid composition determination

The cells were grown at 37°C in 500 ml LB medium. When OD_{600} reached 0.5 (0.25 for strains with increased biomass pr. Volume) the cells were harvested and washed in cold 0.5 M NaCl. The cells were resuspended in 50 ml 0.5M NaCl and transferred to a falcon tube for an additional spin down. The cell pellet was resuspended in 2 ml 0.5M NaCl and spun down a final time. The supernatant was removed and the cell pellet was snap frozen using liquid nitrogen and stored at -80°C until required. The numerous washings of the cells ensure that the final pellet only contained cells, thus granting a result reflecting the lipid composition of the membrane, rather than including any secreted compounds. The samples were lyophilized and sent for analysis at Deutsche Sammlung von Mikroorganismen und Zellkulturen GmbH (DSMZ), where they perform fatty acid extraction and liquid chromatography. The data received was given as a percentage of each fatty acid species. We

set a cut-off value of <0.5 %, as these species are at low levels, either being close to the detection limit, invalidating the data points, or being biologically irrelevant.

2.6.2 – Thin-layer chromatography

Cells were grown in LB at 37°C to an OD_{600} of 1, followed by centrifugation. The cells were washed in 100 mM NaCl, followed by centrifugation. The supernatant was removed and the cell pellets were snap-frozen in liquid nitrogen. The frozen pellets were lyophilized ON and the samples were sent to Deutsche Sammlung von Mikroorganismen und Zellkulturen GmbH (DSMZ), where they carry out two-dimensional silica gel thin layer chromatography using the Bligh and Dyer extraction method (Bligh and Dyer, 1959). The plates were stained with molybdatophosphoric acid and the individual lipid species were identified using specific staining reagents as described in (Tindall *et al.*, 2007).

2.6.3 – Full genome sequencing

We had our full genome sequencing performed by MicrobesNG at Birmingham University. Tubes with a saline solution were supplied along with beads to protect the cells for travel. An entire petri dish of cells were grown ON at 37°C and harvested with a pipette tip and transferred to the provided tube. The prepared samples were sent away and sequencing was performed by Illumina sequencing. Contig assembly was performed by MicrobesNG, followed by our comparative analysis of the various constructs with the *B. subtilis* laboratory WT, which was performed using CLC Genomics from QIAGEN. For SNP detection, a threshold of >50% occurrences in the genomic reads was set.

Chapter 3 – The Role of MreB-Dependant Cell Wall Synthesis in *B. subtilis* Lipid Homeostasis

3.1 – Introduction

Membrane lipid homeostasis, as previously established, is highly important for proper functioning membrane proteins and, consequently, for cellular growth. Recently, the cell wall synthesis regulator MreB and its homologs were shown to be somehow involved in the adaptation of membrane lipid composition and fluidity in *B. subtilis (Strahl et al., 2014).* Furthermore, as discussed in Chapter 1, at least one of the MreB-homologs is transcriptionally regulated upon thermal shock, further highlighting a poorly understood role of the MreB-cytoskeleton in membrane fluidity homeostasis.

In order to examine the role of MreB, Mbl, and MreBH in membrane fluidity homeostasis, single gene deletion mutants of each actin homologue were needed, along with a full deletion strain of all three. These deletion mutants already existed in the *B. subtilis* strain *168ED*-background, as listed in Chapter 2, Table 1. The recent genome sequencing of *168ED* revealed a point mutation rendering the major cell envelope regulatory two component system WalRK constitutively active (Dominguez-Cuevas *et al.*, 2012). As discussed in Chapter 1.4.3, WalRK is a heat shock response system, and is therefore a major regulator of envelope homeostasis as well as an important regulator of actin homologue MreBH, the autolytic enzymes CwlO and LytE, and sigma factor σ^I. Previous results were therefore obtained in a strain background with potentially non-wild type envelope state and composition (Strahl *et al.*, 2014). For these reasons, we opted to transfer the deletions of the relevant genes into the background *168CA,* followed by repeated genome sequencing to identify the presence or absence of suppressor mutations that might influence envelope homeostasis.

In the original construction of the full MreB cytoskeleton deletion strain, it was confirmed that *rsgI* also had to be deleted, but it was never examined if further suppressor mutations were essential (Schirner and Errington, 2009a). Furthermore, the original construction was performed in the *168ED* strain background. To determine if deleting all three mreB-homologs (*mreB, mbl, mreBH*) required suppressor mutations or active WalRK for viability, the deletion strains were genome sequenced and analysed. The same strains were then used to determine if the membrane fatty acid composition had changed compared to wild type, and to determine if the normal temperature-dependent adaptation of membrane fatty acid composition was affected by the absence of MreB-cytoskeleton. To further elucidate the

effect of deleting the lateral cytoskeleton, membrane fluidity measurements were performed at different temperatures. Finally, I examined the growth phenotype and rates of the mutants to determine if any altered fatty acid composition might correlate with growth defects.

3.2 – Results

3.2.1 – Genomic changes in the mreB, mbl, mreBH cytoskeleton knockout mutants

In order to examine how MreB influences membrane homeostasis we needed to recreate the full lateral cytoskeleton deletion strain. I did this by transferring the deletions, which were associated with selectable resistance markers, from the already existing deletion strains into our new strain background, *168CA*. Before the transfer of the deletions, I sequenced our new wild type to ensure that the strain was in consensus with the reference genome (Barbe *et al.*, 2009). Upon analysing the genome, we found three single nucleotide polymorphisms (snps), all within the same gene *uvrX*. UvrX is a non-essential UV damage repair enzyme, with multiple redundancies (Au *et al.*, 2005). We deemed that these "potential" snps are very unlikely to influence our results.

Next, we recreated the full lateral cytoskeletal mutant. When creating a full *mreB, mbl, mreBH* deletion, you additionally need to delete *rsgI*, the regulator of σ^I, rendering the sigma factor constitutively active (Schirner and Errington, 2009a). Deleting the three cell shape determining proteins would induce an incredible stress upon the cells since they would lose their rod-shape. As a result, we expected suppressor mutations to occur frequently. The order in which the deletions were transferred was *mreBH, rsgI, mbl, mreB,* which was chosen due to the increasing severity of associated phenotypes. The final deletion, which removes the final component of the lateral cytoskeleton, forces a loss of rod-shape, changing the organism to a coccoid morphology. I performed two separate constructions of this strain, isolating two individual strains from each batch, giving us four different isolates of the potentially same organism. The two first isolates are from now on called KS60 and isolate III, while those from the second batch are isolate V and isolate VI. Each of the four isolates was sent for Illumina genome sequencing. We analysed the genomes and found all the deviations from our own wild type (168CA) strain. The results of the genome sequencing are summarized in Table 10.

The first four snps listed in Table 10 are found in all four isolates, and are all localised in close proximity of the deleted genes. Consequently, these are most likely to represent scars

of the deletion construction rather than suppressor mutations required for the viability of the *mreB* triple deletion strains. Two of the snps are found in in the immediate neighbourhood of the anti-sigma factor *rsgI*-deletion, and map to its sigma factor pair *sigI*. The first 90 A>G mutation is silent, thus causing no change in amino acid sequence, while the 472 A>G mutation causes an amino acid change of lysine to glutamate at position 158 of SigI, which could potentially alter the function of the protein. The mutation has occurred outside of the RNA polymerase binding site located at amino acids 61-74, and is therefore unlikely to affect the interaction directly. Furthermore, as the deletion of *rsgI,* or the overexpression of SigI, is necessary for strain viability (Schirner and Errington, 2009a), it is unlikely that the released protein would lose its function.

Gene	Protein function	Nucleotide	Amino acid	Mutation type	Strain occurrence
sigI	Sigma factor I	90 (A>G)	30	Silent	KS60, III, V, VI
sigI	Sigma factor I	472 (A>G)	158 (K>E)	Miss sense	KS60, III, V, VI
ykrK	Membrane protein quality control	15 (A>G)	5	Silent	KS60, III, V, VI
flhO	Flagella component	-	-	Gene deletion	KS60, III, V, VI
yfmO	Copper efflux pump	145 (C>T)	49 (H>Y)	Miss sense	KS60
exuT	Hexuronate transporter	913 (G>A)	305 (V>I)	Miss sense	KS60
rapD	Response regulator aspartate phosphatase	818 (C>T)	273 (A>V)	Miss sense	KS60
flhB	Flagella component	791 (G>A)	264 (E>K)	Miss sense	KS60
ywoH	Transcription factor	139 (G>A)	47 (G>R)	Miss sense	KS60
yvzC	Transcription regulator	223 (A>G)	75 (K>E)	Miss sense	III
gltT	Proton/sodium-glutamate symporter	688 (T>C)	230 (Y>H)	Miss sense	VI
spoVD* -> *pyrP	All proteins in between	-	-	Duplication	KS60
yknZ* -> *pyrP	All proteins in between	-	-	Duplication	III

Table 10: All snps found in the four isolated MreB-cytoskeleton deletion strains. The first four snps occur in genes flanking the purposefully deleted genes, and are thus scars from the construction. The rest of the mutations are only found in a single isolate, thus ruling out any necessity for them as essential mutations for strain survival. The only strain without any non-scar snps is isolate V.

The *ykrK* gene, which encodes a transcription repressor located next to *rsgI,* carries a snp in its coding sequence that is also present in all the *mreB* triple deletion strains. The corresponding 15 A>G mutation is silent, and as such, likely to be inconsequential. Surprisingly, it turned out that *flhO* is deleted in its entirety in all four isolates. The *flhO* coding sequence is located immediately next to *mbl*, and encodes one of the flagella basal-

body components essential for the initial hook formation (Courtney *et al.*, 2012). Consequently, the loss of this gene will abolish the motility of the cells. As with the other mutations in the immediate neighbourhood of *mreB*, *mbl*, *mreBH* and *rsgI*, this deletion is also likely to have emerged during the construction of *Δmbl* strain and probably does not represent a suppressor mutation required for the viability of the *mreB* triple deletion strain.

The next five mutations listed in Table 10 all occurred solely in strain KS60. The *yfmO* gene encodes a trans-membrane copper efflux pump, and has a single snp located at amino acid 145 C>T, resulting in a histidine to tyrosine switch at amino acid 49, both large aromatic amino acids. The mutation is located in the first extracellular loop of the pump, and might have an effect on the pump affinity for copper or the pumping action itself, as histidines are often involved in the catalytic activities of enzymes ('Structural chemistry,' 1990). The *exuT* gene encodes a hexuronate transporter, and is thus involved with the uptake and metabolism of extracellular galacturonate (Mekjian *et al.*, 1999). The mutation is a 913 G>A causing a valine to isoleucine exchange at amino acid 305 in the 8th trans-membrane helix. Both valine and isoleucine are branched aliphatic amino acids which, when exchanged, are unlikely to cause a major difference in protein function, especially when located within a trans-membrane helix. The *rapD* gene encodes an aspartate phosphatase which regulates ComA activity. ComA is responsible for cell population density measurements and the following cell differentiation between quorum sensing or competence initiation (D. Lopez and Kolter, 2010a). The mutation occurred at nucleotide 818 C>T, causing an amino acid 273 alanine to valine exchange. Valine is slightly larger than alanine and could thus affect protein function, although a more likely scenario is that the mutation has no significant effect. Additionally, the mutation occurs outside the proteins six known protein-protein interaction sites, further reducing the likelihood of a strong phenotype. The *flhB* gene encodes another component of the flagella synthesis machinery; one of the transporters responsible for secretion of extracellular components. The mutation occurs at nucleotide 791 G>A, conferring a glutamate to lysine exchange at amino acid 264. The mutation sits on the intracellular side of the transporter, and might have an influence on the function of the protein, for example by inhibiting export of essential flagella components. Even if FlhB is inactive due to the mutation, the effect would be minimal as one of the essential basal components of the flagella (FlgO) is already missing in the strain. The *ywoH* gene encodes a transcription regulator with an unknown regulon. The mutation is located at nucleotide 139 G>A, and confers an exchange of glycine to arginine at amino acid 47. This mutation is a

major shift from the smallest possible amino acid to a large charged residue. Furthermore, position 47 is located close to the DNA-binding domain positioned at amino acids 51-74. It is difficult to predict the effects of the mutation due to the unknown function of the protein.

The two final snps observed occur in two individual isolates. The *yvzC* gene is another uncharacterized transcriptional regulator. The mutation occurred only in isolate III, and happened at nucleotide 223 T>C, conferring a lysine to glutamate shift at position 75. Once more, this amino acid shift changes the charge of the residue and although the mutation occurred outside the DNA interaction domain in the C-terminus of the protein, a significant phenotype cannot be ruled out. It is again difficult to predict the effects if the protein is altered, as the regulon is currently unknown. The *gltT* gene encodes a Na^+ dependent glutamate / aspartate symporter. The mutation occurs in isolate VI at nucleotide 688 T>C and confers a tyrosine to histidine change at position 230. Position 230 is located within a trans-membrane helix, possibly on the interior channel side of the helix, as the polar nature of the residue could aid in the transport of the substrates. The change from a polar aromatic residue to a potentially charged residue could significantly change the activity of the transporter. Glutamate is an important osmolyte within *B. subtilis*, and is known to aid in upholding osmotic protection upon stress (Zaprasis *et al.*, 2015). The mutation in *gltT* could potentially mitigate osmotic stresses isolate VI encounters during the transformation or indeed during vegetative growth.

Two additional differences were discovered in isolates KS60 and III. It appeared that large sections of their genomes have been duplicated. The number of reads in these areas was twice as abundant as the rest of the genome, as shown in Figure 10A and B. In both strains, the duplicated region ends at *pyrP*, but starts at different loci, thus indicating two independent duplication events. The KS60 duplication initiates at *spoVD*, granting an almost 40.000 nucleotide duplication including, but not limited to, the Mur-operon (*murE-murB*), FtsAZ-operon, the Ylm-operon (*ylmA-divIVA*), sigma factors *sigE* and *sigG*, bacillopeptidase *bpr*, and isoleucine-tRNA synthetase *ileS*. Most of the duplicated genes are involved in peptidoglycan synthesis and cell division, suggesting that this strain has potentially obtained the ability to grow and divide faster. Similar results were observed in *E. coli*, where upon deletion of *mreB*, although not viable, overexpression of FtsAZ restores viability (Bendezu and de Boer, 2008). The duplication in isolate III starts at *yknZ* and as well as the above mentioned enzymes and operons, this duplication also included non-sporulating cell toxin transporters, sugar uptake transporters, citric acid cycle components, *ftsW*, co-factor synthesis

enzymes, cytochrome C synthesis enzymes, *pbpB*, and many more. Isolate III has duplicated a large genomic region encoding genes involved in both core and auxiliary metabolism, making predictions almost impossible to foresee. The duplications in KS60 and to a greater extent isolate III will have an enormous number of pleiotropic effects due to the sheer amount of repeated DNA, but the duplication in KS60 does appear more logical and coherent, whereas isolate III has duplicated enzymes involved in almost all cellular systems.

Interestingly, when looking at Table 10, isolate V does not appear to have any genome alterations, besides the ones obtained as scars in the transfer of the genotypes from the old strain. This suggested that it is likely that no suppressor mutations are absolutely essential to provide viability to the *mreB* triple deletion strain, suggesting that the suppressors in the other isolates are more likely to be related to restoring higher growth speed rather than overall

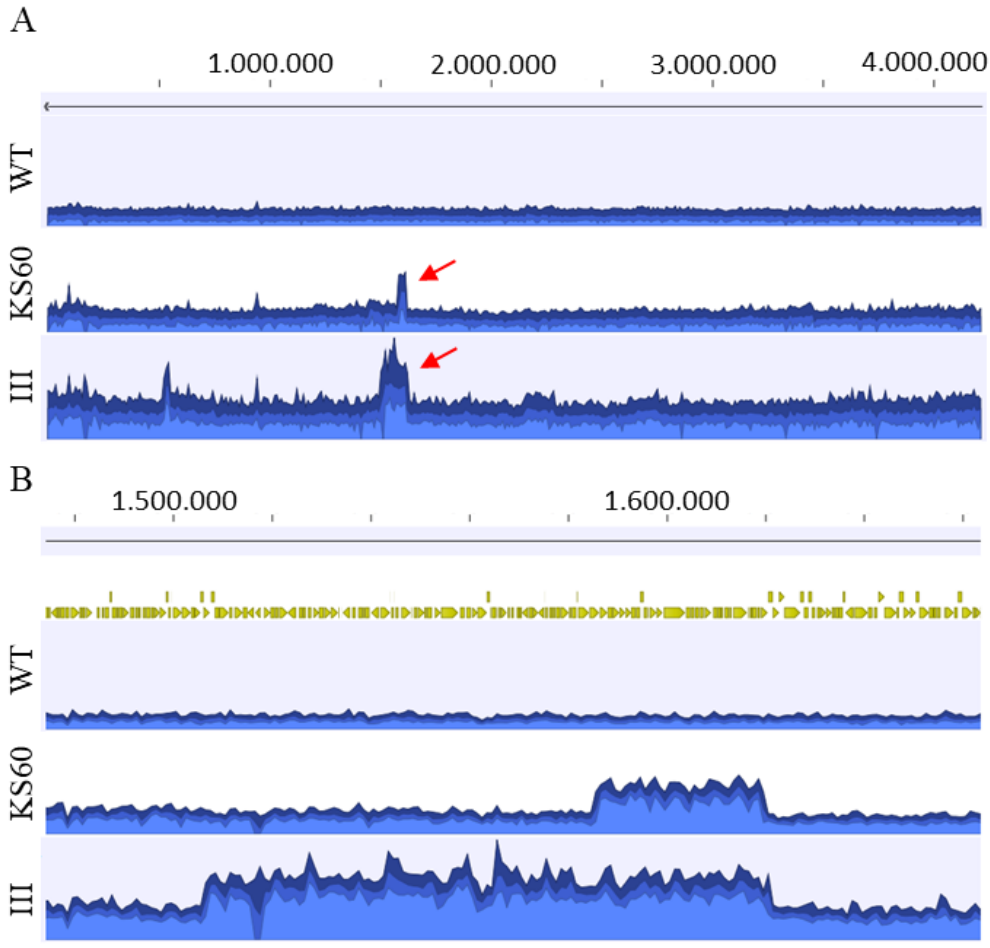

Figure 10: Screenshots of the sequence analysis software showing comparisons of reads between WT, KS60, and isolate III. The scales are measured in nucleotides and represent the entire genome. (A) The entire genome of the three strains as shown in the amount of reads. The y-axis is in similar scales. The red arrows point towards the duplications. (B) Zoomed in view of the duplicated area. The reads are twice as abundant in this area for both KS60 and isolate III. Isolate III exhibits almost three times as many genes duplicated as KS60. Genes are shown as yellow arrows above the reads.

survival. Additionally, isolate V was found to easily restore a faster growth speed when left to grow on plates or planktonically in liquid, suggesting that the strain easily gained growth associated suppressor mutations, supporting the hypothesis that the observed snps are involved in growth rate rather than survival. Finally, none of the snps found in this study were found in the original strain in the *168ED* background (Schirner and Errington, 2009a), further confirming that the mutations are not essential for strain viability.

To further investigate if MreB and its homologues are involved in membrane homeostasis, two strains were chosen to examine growth phenotypes as well as membrane fluidity. The two strains were, KS60 to investigate the strain with most snps and a somewhat logical duplication, and isolate V as it only carries snps that are unlikely to have emerged as suppressors for the *mreB* triple deletion.

3.2.2 – The Fatty acid composition is altered upon lateral cytoskeleton deletion

Initially, I wanted to examine if the constitutive activation of σ^I caused by the required deletion of the anti-sigma factor *rsgI* would alter the membrane fatty acid composition, as it is part of the cellular heat shock response which also involves adaptation of membrane fatty acid composition and fluidity. Additionally, we wanted to examine if each individual actin homologue in *B. subtilis* would influence the fatty acid composition upon deletion. To determine if any of these single deletion strains altered fatty acid composition, I grew the cells at 37°C prior to harvesting them for fatty acid analysis. The fatty acid composition is found in Table 11. When discussing fatty acid length, we have denoted carbons of 15 or shorter to be relatively shorter and from 16 or longer denoted as longer.

For the wild type strain, it is seen that the bulk of fatty acids are 15 and 17 carbon long with more iso compared to anteiso fatty acid species. When examining *ΔrsgI*, we see no significant differences compared to wild type, except for the loss of very long fatty acids of >17C, which were scarce in wild type as well. Consequently, I conclude that the *rsgI* deletion does not alter fatty acid composition significantly, and the SigI regulon is not involved in regulation of membrane fatty acid composition. Comparably, the *Δmbl* strain did not appear to exhibit any major differences either, although a small shift towards shorter fatty acids is visible through a lower level of 17:0 and a slight increased level of 14:0 and 15:0. The *ΔmreBH* strain also did not show any differences compared to wild type, which is not necessarily surprising as *mreBH* is usually up-regulated during thermal shock or envelope

stress, as inferred by its regulator WalRK (W. Z. Huang *et al.*, 2013), and therefore wouldn't majorly impact homeostatic growth at 37°C. The *ΔmreB* strain was interesting since two major shifts were observed in the fatty acid composition. Compared to wild type, *ΔmreB* was characterised by a 5 % decrease in 15:0 iso, and a comparable increase in 17:0 anteiso fatty acids. This change creates a rather large shift towards longer fatty acids in the anteiso branching configuration. This is interesting, as longer fatty acids will result in a more rigid membrane, whereas the anteiso configuration would result in a more fluid membrane. These results suggest that MreB is involved in the fatty acid homeostasis.

FA	*168*		*ΔrsgI*		*Δmbl*		*ΔmreB*		*ΔmreBH*	
<14:0	-	-	-	-	-	-	-	-	-	-
14:0 ISO	1.31	± 0.11	1.39	± 0.04	1.41	± 0.60	0.77	± 0.26	1.61	± 0.05
14:0	-	-	-	-	0.17	± 0.10	-	-	-	-
15:0 ISO	21.44	± 0.94	20.25	± 2.72	21.46	± 1.87	16.65	± 3.18	21.14	± 0.85
15:0 ANTEISO	39.65	± 1.04	40.14	± 0.05	40.30	± 1.24	40.62	± 0.44	39.37	± 0.18
16:0 ISO	4.56	± 0.33	4.64	± 0.30	4.60	± 1.62	3.24	± 0.80	5.35	± 0.01
16:0	3.50	± 0.37	3.26	± 0.23	3.80	± 0.50	4.04	± 0.86	3.58	± 0.23
17:0 ISO	13.29	± 0.35	13.14	± 0.30	12.07	± 0.37	13.83	± 0.07	12.86	± 0.48
17:0 ANTEISO	15.05	± 0.56	15.24	± 1.45	14.50	± 1.98	19.13	± 3.00	14.36	± 0.37
18:1 w9c	-	-	-	-	-	-	-	-	-	-
18:0	0.45	± 0.31	-	-	0.68	± 0.15	0.83	± 0.26	0.76	± 0.01
>18:0	-	-	-	-	-	-	-	-	-	-
SUM	99.21	± 1.13	98.04	± 0.52	98.99	± 0.28	99.12	± 0.35	99.02	± 0.56

Table 11: Fatty acid composition determination of MreB cytoskeletal single deletion strains at 37°C. The data is given in % of the entire amount of phospholipids in the extract. *ΔrsgI* does not appear to alter its fatty acid composition compared to wild type. *Δmbl* exhibits a slight change to fatty acid composition in the form of a minute shift towards shorter fatty acids. *ΔmreBH* does not appear to alter the fatty acid composition. *ΔmreB* show a relatively large alteration of the fatty acid composition with a reduction in shorter chains and an increase in longer chains. Furthermore, it appears that a shift towards more anteiso has occurred. ± values represents standard deviation. 168 n=2, *ΔrsgI* n=2, *Δmbl* n=3, *ΔmreB* n=3, *ΔmreBH* n=2.

Following these encouraging results, it was decided to examine the fatty acid profiles of the strains KS60 and isolate V. As these two strains have lost their rod-shape, we decided to include a rod to cocci control in the form of *ΔmreC*. When MreC is missing from the elongasome, MreB and the lateral cytoskeleton lose association to the extracellular cell wall synthetic machinery (Defeu Soufo and Graumann, 2005), resulting in a failure to insert peptidoglycan laterally leading to a coccoid cell shape. When sequenced, the *ΔmreC* strain had a single silent mutation in *mreD*, thus it was deemed unimportant. The results for the mreB triple deletion strains and *ΔmreC* are shown in Table 12. The *ΔmreC* strain exhibited a

clear shift towards longer fatty acids, with a 7 % decrease in 15:0, and a 5 % increase in 17:0, along with minor increases in very long fatty acids. Interestingly, the iso / anteiso ratio was relatively stable, with only a minor shift towards observed anteiso. Isolate V also showed an increased fatty acid length with a major loss of 15:0 type fatty acids of 20 %, redistributed across longer fatty acid species. Interestingly, 16:0 was enriched significantly, along with the 18:0 species, suggesting that not only the fatty acid length but also the regulatory mechanism determining the degree and type of fatty acid branching was affected in this strain. Non-branched fatty acids make up 16 % of the fatty acids in isolate V, whereas they only make up about 5 % in the wild type. Additionally, isolate V exhibited a shift towards the more fluid anteiso configuration in the fatty acids that do undergo branching. Isolate KS60 also exhibited an overall increase in fatty acid chain length, similar to "suppressor-free" isolate V and Δ*mreC*, with a decrease in 15:0 of approximately 7 % distributed across longer fatty acids, including unsaturated acids. An interesting observation was that KS60 has an increased amount of both very long and very short fatty acids suggesting that the gained suppressor mutations clearly influence the membrane fatty acid composition and, thus, could act by trying to restore a fatty acid profile more optimal for growth. Additionally, isolate KS60 had an increased amount of anteiso, thus showing similar but not as severe results as isolate V.

FA	168		*ΔmreC*		KS60		V	
<14:0	-	-	-	-	0.56	± 0.32	-	-
14:0 ISO	1.31	± 0.11	0.88	± 0.08	1.04	± 0.32	0.77	± 0.06
14:0	-	-	-	-	-	-	0.57	± 0.06
15:0 ISO	21.44	± 0.94	16.32	± 3.23	17.37	± 2.46	13.42	± 0.86
15:0 ANTEISO	39.65	± 1.04	37.18	± 1.89	39.36	± 1.39	36.20	± 0.08
16:0 ISO	4.56	± 0.33	3.98	± 0.35	3.99	± 0.32	3.41	± 0.20
16:0	3.50	± 0.37	4.89	± 2.40	4.80	± 2.50	8.59	± 0.88
17:0 ISO	13.29	± 0.35	15.88	± 0.86	13.83	± 0.62	14.67	± 0.91
17:0 ANTEISO	15.05	± 0.56	17.85	± 1.47	16.87	± 1.75	17.13	± 0.18
18:1 w9c	-	-	-	-	0.23	± 0.40	-	-
18:0	0.45	± 0.31	1.60	± 1.20	1.01	± 1.05	3.44	± 0.36
>18:0	-	-	0.29	± 0.17	0.17	± 0.30	0.64	± 0.04
SUM	99.21	± 1.13	98.87	± 0.43	99.11	± 0.66	98.82	± 0.23

Table 12: Fatty acid compositions of wild type along with the cocci-like strains *ΔmreC*, KS60 and isolate V at 37°C. *ΔmreC* exhibits a clear shift towards longer fatty acids, while the iso / anteiso ratio remains the same. KS60 exhibits a general shift towards longer fatty acids, but with very short fatty acids occurring as well, while the iso / anteiso ratio shifts slightly towards more anteiso. isolate V shows overall longer fatty acids, with a major shift towards 16:0. . ± values represents standard deviation. 168 n=2, *ΔmreC* n=3, KS60 n=3, isolate V n=2.

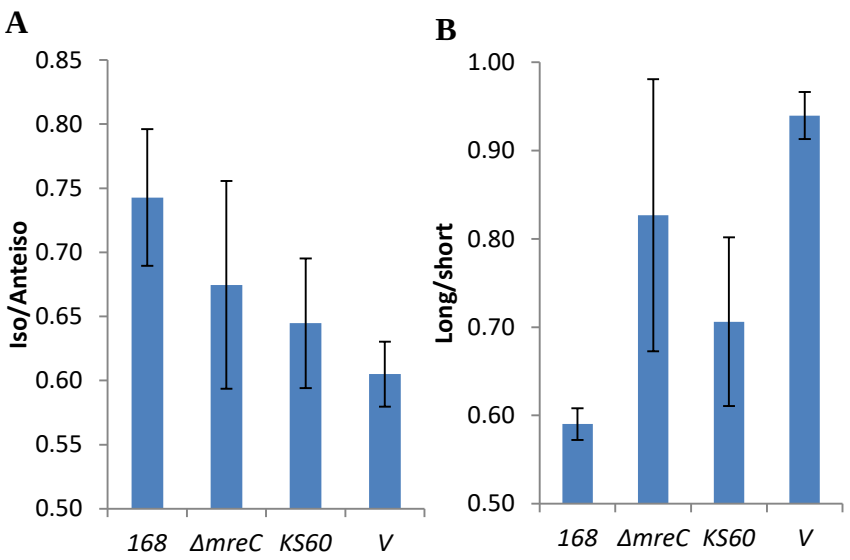

Figure 11: Iso / anteiso and Long / short ratios of fatty acids for 168, *ΔmreC*, KS60, and isolate V at 37°C. (A) Iso / anteiso ratios. All the mutant strains have an increased amount of anteiso fatty acids, with isolate V having the most severe phenotype. (B) Long / short ratio. All the mutant strains are exhibiting longer fatty acids, with isolate V exhibiting the extreme. Error bars represent standard deviation.

Another way of visualizing the fatty acid changes within the membrane is to plot the ratio between long and short fatty acids, as well as the ratio between iso and anteiso species (Figure 11). In wild type we observed the normal iso / anteiso ratio of approximately 0.75, whereas all mutant strains exhibited an increased amount of anteiso fatty acid species. Isolate V, which has not yet gained additional suppressor mutations, exhibited the most extreme shift compared to the wild type profile. In contrast, isolate KS60 had, presumably due to the accumulated suppressor mutations, acquired intermediate levels of iso fatty acids compared to isolate V, thereby shifting the iso / anteiso ratio closer to that found in the wild type.

The long / short ratios exhibit largely the same trends as the iso / anteiso ratios. All three coccoid mutants have longer fatty acids, which could suggest that the coccoid morphology was the driving force, although the single *ΔmreB* strain exhibited similar compositions making this conclusion unlikely. This rather suggests that the loss of MreB, or the loss of connection between MreB and the rest of the elongasome, caused the fatty acid change towards longer fatty acids. Isolate V exhibited the largest shift towards long fatty acids while isolate KS60 appeared to has a fatty acid length profile more comparable to the wild type. These results suggest that a dysfunctional MreB cytoskeleton and the disassociated elongasome had severe consequences for the membrane fatty acid composition, implying that the MreB-cytoskeleton is indeed important for the steady-state fatty acid homeostasis.

During the construction of the *mre* deletion mutants, temperatures ranging from 30°C to 37°C are required, which could be due to faulty membrane homeostasis regulation during the deletion process. To further understand the influence of temperature on the membrane and the possible faulty regulation in the MreB cytoskeletal mutant, we decided to investigate the fatty acids at 30°C. Unfortunately, the *ΔmreC* mutant was not included due to an extremely sick phenotype at 30°C, which did not allow for stable growth to the ODs required for sample extraction, and a population which unfortunately collapsed early after inoculation when grown in large flasks. The fatty acid compositions of wild type, KS60 and isolate V at 30°C are shown in Table 13. When comparing the fatty acid profile of the wild type strain grown at 30°C to the one at 37°C, it is immediately evident that the fatty acid composition had shifted sharply towards shorter chains with an enrichment of the anteiso conformation. Additionally, a small amount of unsaturated fatty acids were now present, all confirming that the homeoviscous adaptations towards cold environments have taken place, modulating the membrane in a more fluid direction to counteract the loss of thermal energy. Having shown that the wild type indeed does conform to homeoviscous adaptation, isolate V and KS60 were examined next to explore if the deletion of the MreB cytoskeleton impairs cold adaptation. Isolate V again exhibited a shift towards longer fatty acids, with approximately 20 % decrease in 15:0 compared to wild type that was distributed across longer fatty acids. Again, un-branched fatty acids were significantly increased from 3 % in wild type to 13 % in isolate V. The adaptations exhibited by isolate V are almost identical to the wild type, although were skewed towards longer unbranched fatty acids, comparable to 37°C. KS60 had once again adapted differently than isolate V. When compared to wild type, KS60 exhibited a 7 % decrease of 15:0, shifted to an

FA	168	KS60	V
14:0 ISO	1.04	-	0.55
14:0	-	-	0.61
15:0 ISO	20.78	13.48	11.78
15:0 ANTEISO	43.46	43.59	39.35
16:0 ISO	3.43	2.57	2.58
16:1 w11c	0.70	3.92	0.64
16:0	2.48	0.58	9.44
ISO 17:1 w10c	1.22	-	-
17:0 ISO	9.46	10.53	11.43
17:0 ANTEISO	14.76	22.27	17.96
18:0	0.63	1.34	2.98
>18:0	-	-	0.99
SUM	97.96	98.28	98.99

Table 13: The fatty acid composition of wild type, KS60 and isolate V at 30°C. The numbers are in % of the entire fatty acid extract. Wild type has shorter fatty acids with the anteiso conformation than at 37°C. Additionally, unsaturated fatty acids are occurring in wild type. KS60 has an increased amount of long anteiso fatty acids. isolate V has decreased iso and generally longer fatty acids. 168 n=1, KS60 n=1, isolate V n=2.

approximate 8 % increase of 17:0. Furthermore, the amount of anteiso had also increased. The changes between KS60 and wild type are similar to the ones at 37°C, suggesting that the regulatory systems responsible for the temperature-dependent membrane fatty acid homeostasis are still operating, albeit aiming for a different composition. Alternatively, the observed changes could be the result of two overlaid adaptations, the first being the wild type homeoviscous adaptations, and the second being the influence of losing MreB.

We can again show the results as ratios, granting a more visual representation of the changes in fatty acid composition (Figure 12). The data clearly shows that the wild type had synthesized more anteiso fatty acids in response to the colder growth temperatures. Furthermore, we observed that KS60 and isolate V both exhibited a further shift towards anteiso, but unlike at 37°C, KS60 has the most extreme composition, suggesting that the iso / anteiso regulation might have been impeded even further by the suppressor mutations at 30°C. The wild type has also increased the amount of shorter fatty acids to reflect the requirements for colder growth temperatures. Interestingly, both KS60 and isolate V have barely altered the length composition compared to 37°C, suggesting that the cytoskeleton is more intricately involved in the length adaptation. Additionally, we observed that KS60 had adapted better, most likely due to the suppressor mutations. Together these results suggest that iso / anteiso adaptations still occur upon deletion of the MreB cytoskeleton, but that fatty acid length

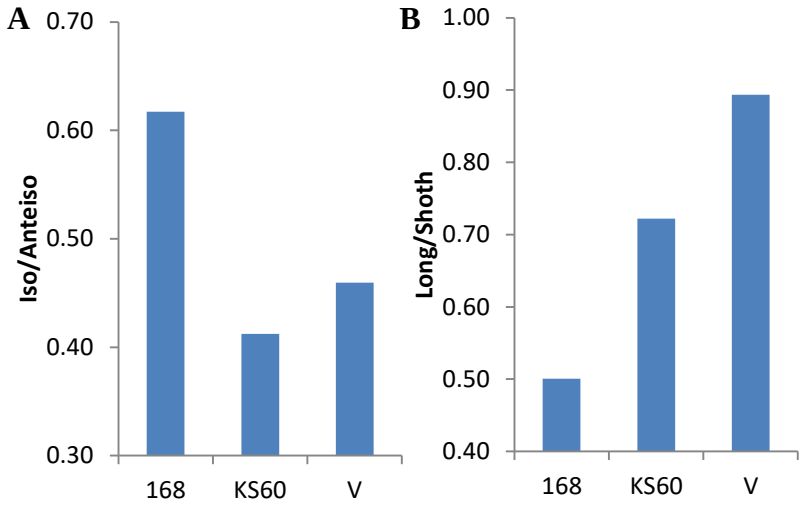

Figure 12: Iso / anteiso and long / short ratios of fatty acids in 168, KS60, and isolate V at 30°C. (A) Iso / anteiso ratio. The MreB cytoskeletal mutants both exhibit more anteiso fatty acids, with isolate V showing the most extreme phenotype. (B) Long / short ratio. The cytoskeletal mutant both exhibit longer fatty acids with isolate V again showing the greatest change from 168.

adaptations appear much weaker, or indeed are repressed all together.

Due to how similar the changes in the MreB cytoskeleton deletion strains were at 37°C and 30°C, we wanted to examine if the observed changes were consistent across a larger temperature range. We therefore decided to examine wild type, *ΔmreC*, KS60, and isolate V at 45°C. The fatty acid composition is summarized in Table 14. Wild type grown at 45°C exhibited an increase in long fatty acids, divided between multiple species. Additionally, a large shift from anteiso to iso has occurred. The longer fatty acids, with emphasis on iso, is what we would expect from higher growth temperatures, as the membrane needs an increase in more rigid lipids to maintain its stability and appropriate state at the higher temperatures. Surprisingly, *ΔmreC* has a composition that was almost identical to that of wild type, suggesting that the shift from rod-shaped to cocci-like does not need an altered fatty acid composition at higher growth temperatures. Isolate V had once again longer fatty acids than wild type, although the length composition doesn't change much between temperatures for this isolate. An increase in iso fatty acids and decrease in anteiso both of about 3 % was observed, which is to be expected at higher temperatures. When compared to the directions of adaptations occurring in the wild type, isolate V changed in a similar direction, although not to the same extent. KS60 continued with its consistently longer fatty acids in the anteiso composition as compared to wild type. KS60 additionally had about 5% less 15:0 iso, shifted towards both 15:0 anteiso and 17:0 anteiso as compared to wild type. KS60 adapts in similar directions as the wild type as well, although not reaching similar values.

Again, we can visualize the fatty acid compositional changes at 45°C graphically, as shown in Figure 13. Immediately, we notice that wild type has adapted for higher temperatures with both more iso configured and longer fatty acids. Surprisingly, *ΔmreC* appears to have retained wild type adaptations at 45°C for both branching and length. KS60 has adapted similarly to the previously examined temperatures, with more anteiso and longer fatty acids. Isolate V still exhibited longer fatty acids than KS60, suggesting that the suppressor mutations are decreasing fatty acid length. However, isolate V does not follow the previously exhibited adaptations when examining the iso / anteiso ratio. Strikingly, isolate V has shifted dramatically towards a more iso-rich membrane rather than anteiso.

FA	168		*ΔmreC*		KS60		V	
<14:0	0.69	± 0.06	0.77	± 0.05	0.27	± 0.37	0.54	± 0.03
14:0 ISO	2.18	± 0.01	1.36	± 0.86	1.72	± 0.06	1.71	± 0.03
14:0	1.28	± 0.02	1.34	± 0.06	0.91	± 0.16	0.81	± 0.02
15:0 ISO	23.09	± 0.49	23.63	± 0.16	18.27	± 0.75	23.59	± 0.12
15:0 ANTEISO	29.49	± 0.13	30.02	± 0.30	32.50	± 0.21	26.91	± 0.25
16:0 ISO	5.17	± 0.18	4.39	± 0.42	5.00	± 0.51	4.66	± 0.04
16:0	7.88	± 0.65	8.87	± 1.13	8.00	± 0.97	8.73	± 0.01
17:0 ISO	14.90	± 0.91	14.66	± 1.79	15.55	± 1.18	19.07	± 0.29
17:0 ANTEISO	8.73	± 0.46	8.77	± 0.25	12.03	± 0.95	8.81	± 0.08
18:1 w9c	2.75	± 0.42	2.43	± 0.01	1.26	± 0.59	0.67	± 0.06
18:1 w6c	0.37	± 0.52	0.72	± 1.02	0.31	± 0.44	-	-
18:0	1.78	± 0.01	1.80	± 0.43	2.37	± 0.06	3.36	± 0.03
>18:0	0.70	± 0.02	0.46	± 0.64	0.75	± 0.13	0.62	± 0.01
SUM	98.97	± 0.34	99.18	± 0.70	98.91	± 0.30	99.45	± 0.05

Table 14: Fatty acid compositions at 45°C for wild type, *ΔmreC*, KS60, and isolate V. On average, wild type exhibits longer fatty acids predominantly in iso conformation. *ΔmreC* has an almost identical composition as wild type. KS60 exhibits a shift towards longer fatty acids in the anteiso conformation. isolate V exhibits longer fatty acids, while changing the composition towards iso rather than anteiso. ± values represents standard deviation. n=2

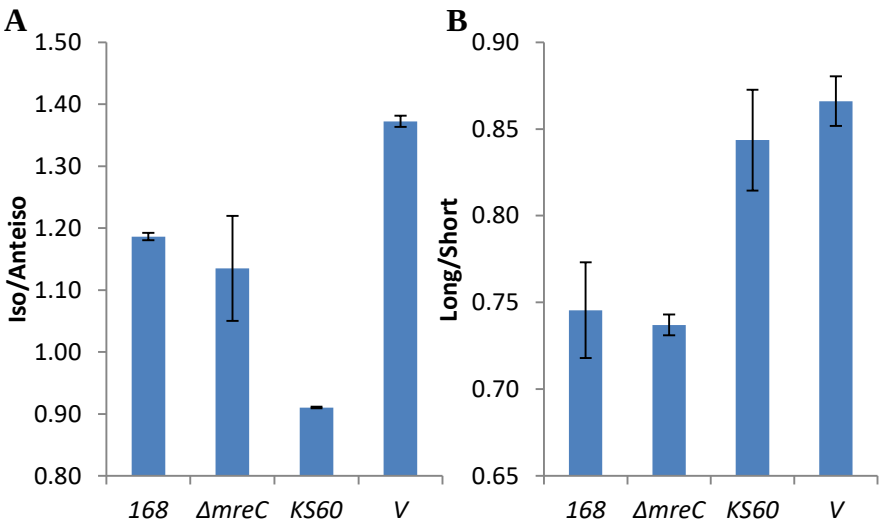

Figure 13: Iso / anteiso and long / short ratios of fatty acids in 168, *ΔmreC*, KS60, and isolate V at 45°C. (A) Iso / anteiso ratio. *ΔmreC* has adapted similarly to 168. KS60 exhibit more anteiso fatty acids, while isolate V, has adapted towards the iso configuration. (B) Long / short ratio. *ΔmreC* has adapted similarly to 168. The cytoskeletal mutants both exhibit longer fatty acids with isolate V again showing the greatest change from 168. Error bars represent standard deviation.

The fatty acid composition in our wild type strain is clearly following the theory of homeoviscous adaptation, by increasing the fatty acid length and shifting to iso type of fatty acid branching at higher temperatures, and modulating in the opposite direction at lower temperatures. At 37°C and 30°, isolate V exhibited more anteiso compared to wild type, but drastically increased amounts of iso at 45°C. Regarding length adaptations, Isolate V remained at a long/short ratio of about 0.9 throughout all three temperatures, whereas wild type modulated the composition between 0.5 and 0.75, suggesting that less length adaptations were performed without an MreB cytoskeleton. KS60 exhibited consistently lowered iso/ anteiso ratios and increased long/short ratios throughout the temperature ranges, adapting in similar directions to wild type, although not to the same extent. These results suggest that the suppressor mutations increased the adaptive capabilities of KS60 regarding both branching and length. Together, all of these results suggest that MreB and its homologues are involved in maintaining homeoviscous homeostasis, and that suppressors are able to make up for the loss of the MreB cytoskeleton.

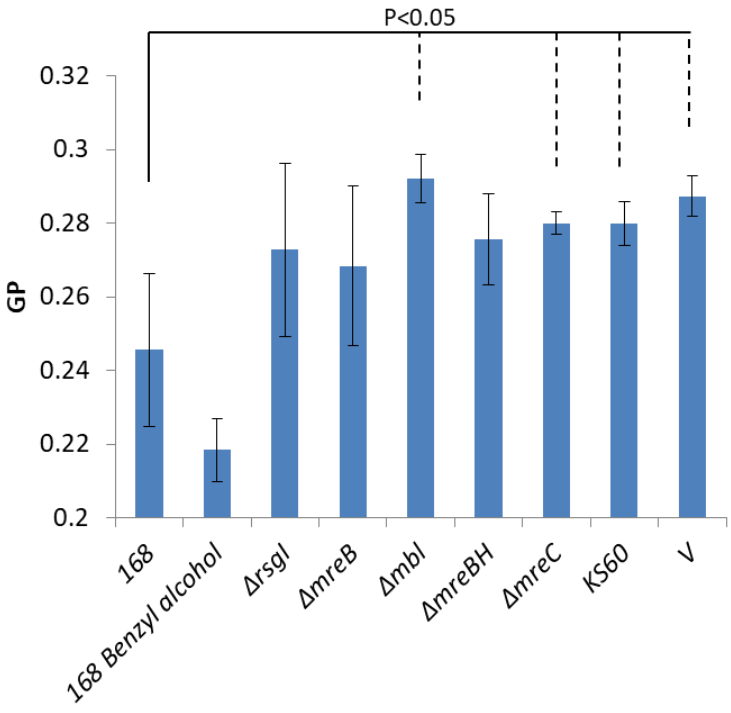

Figure 14: Laurdan fluidity of the cytoskeletal single and full mutants as well as controls at 37°C. 168 is at about 0.25 with a rather large standard deviation. The fluidizing agent benzyl alcohol is added as a control, decreasing the general polarization (GP). *ΔrsgI, ΔmreB,* and *ΔmreBH* all exhibit increased average GP, but not statistically significant. *Δmbl, ΔmreC,* KS60, and isolate V all exhibit statistically significant increased GP. Statistical analysis was Students t-test. Error bars represent standard deviation. n=3

Next we wanted to examine if the temperature-dependent changes observed in wild type resulted in the same fluidity at the different growth temperatures (as predicted by the homeoviscous adaptation model), and explore any consequences of the mixed changes (both length and iso/anteiso changes) of the fatty acid profile observed in the *mre* mutants for the membrane fluidity of these strains.

3.2.3 – MreB, Mbl, & MreBH are linked to membrane fluidity

To determine membrane fluidity, we use two dyes, laurdan and DPH. The mechanism of the two dyes has been discussed earlier in Chapter 1. Initially we wanted to utilize laurdan, as it is the best described of the two compounds. We started by measuring the fluidity of the single cytoskeletal component deletions as well as the full cytoskeletal deletion strains to ensure that the homeostatic fluidity reflects the fatty acid composition at 37°C. The results are shown in Figure 14. Wild type was measured at a general polarization (GP) of about 0.25, with a rather large standard deviation. To ensure that the assay is measuring membrane fluidity, we added the known membrane fluidizer, benzyl alcohol (Reyes and Latorre, 1979). As expected, benzyl alcohol treated wild type cells had a decreased GP, indicative of increased fluidity. We then tested each of the single lateral cytoskeletal deletions, *ΔmreB, Δmbl, ΔmreBH,* and *ΔrsgI*. All four mutants exhibited increased average GP, translating to more rigid membranes, but with rather large standard deviations. Only *Δmbl* was significantly different from wild type. These results are surprising, as the fatty acid composition data suggested *ΔmreB* as the only strain deviating from wild type. To further examine if laurdan reflects our fatty acid data we subjected *ΔmreC*, KS60 and isolate V to the assay. The three strains exhibited approximately similar increases in GP, all of them being statistically significant from wild type. This corresponds well with the observed data of longer fatty acids for all three strains, suggesting that this parameter is influencing the fluidity to a greater extent than the iso / anteiso changes.

When doing laurdan measurements, it quickly becomes evident that sufficient reproducibility is difficult to obtain due to the multiple washing steps required to remove unbound laurdan. Therefore, a more reliable and robust measure for membrane fluidity was required.

To further examine the membrane fluidity, we tested the strains using DPH. As described earlier, DPH only fluoresces once inserted into the membrane, drastically reducing signal to noise. As a result, the measurements are more reliable, while having less washing steps compared to laurdan and similarly increasing the signal-to-noise ratio. Additionally, the output from a DPH measurement is unique to the instrument used, and we thus need to create a baseline from which we measure. The baseline measurement was created by growing wild type at 30°C, 37°C**,** and 45°C. I then prepared a plate with interchangeable strips of wells, at each of the three temperatures, and filled all unused wells with H_2O at the same temperature to sustain the desired temperature for as long as possible. The treated cells were added and immediately measured in a plate reader set at 37°C. I calibrated the measurements for our 37°C sample to be as close to 100 mP as possible and received the data shown in Figure 15. The basic assumption of homeviscous adaptation model is that the temperature-dependent changes observed in the fatty acid profiles in different growth temperatures aim at, and are sufficient to maintain effectively the same levels of membrane fluidity in the different growth temperatures. Surprisingly, we see clear differences in the steady state membrane fluidity for the wild type cells grown in the different temperatures. Furthermore, one would expect that the membrane at lower temperatures would exhibit less fluid characteristics, and vice versa,

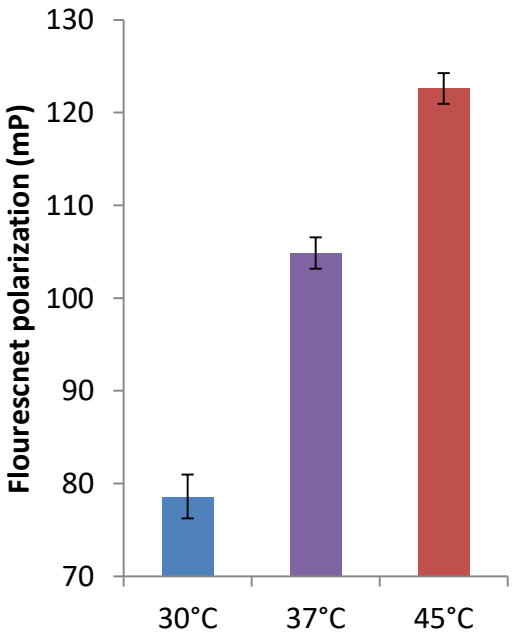

Figure 15: Calibration of DPH values with 37°C set to 100 mP. Our calibrated values are 30°C=79, 37°C=104, 45°C=123. Higher values signifies more rigid membranes, while lower values signifies more fluid membranes. Error bars represent standard deviation. n=3

but what we see is the exact opposite. We observe that the membrane at 30°C has a lower mP and thus a higher fluidity, while the membrane at 45°C exhibits higher mP, and therefore a more rigid membrane. Perhaps the bacteria are wired to over-compensate their membrane fluidity in the opposite direction to the thermal stress, or perhaps DPH measures the physical characteristics of the membrane directly without the thermal input to the membrane, although this is unlikely.

Next, we measured the DPH fluidity for all of the single cytoskeletal deletions strains as well as *ΔmreC*, KS60, and isolate V at 37°C, all of which are shown in Figure 16. Wild type was within the calibrated value, validating the rest of the measurements. Interestingly, the DPH mP values were all quite different compared to the laurdan GP values, when comparing wild type to the rest of the strains. Where all the deletion strains had higher GP values compared to wild type, most of them have similar or lower mP values. When observing the single cytoskeletal deletion mutants, they all had similar values to wild type, showing a good correlation with the corresponding fatty acid data, except for *ΔmreB* which had longer fatty acids compared to wild type. When examining the *ΔrsgI* mutant, it exhibited a significantly lower mP value and therefore a higher fluidity, indicating that something

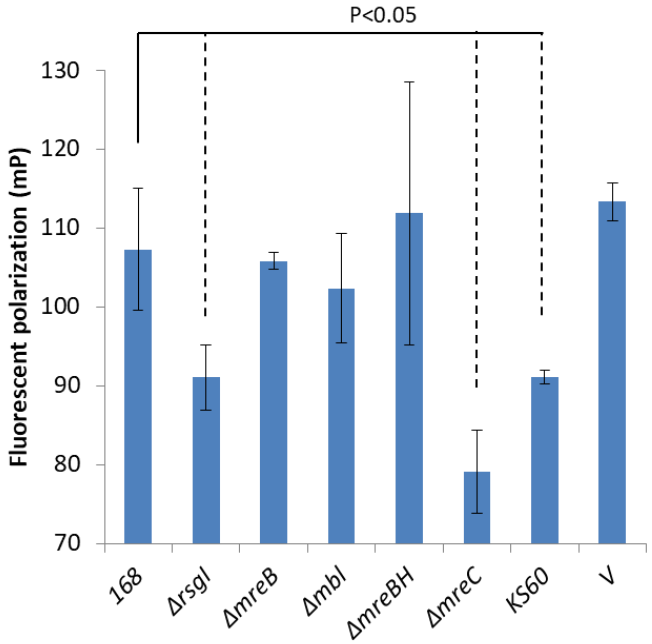

Figure 16: DPH fluidity of the cytoskeletal single and full mutants at 37°C. 168 is close to the calibrated 104. *ΔmreB, Δmbl, ΔmreBH* and isolate V all have fluidities within a standard deviation of 168, although visually it appears that *ΔmreBH* and isolate V both on average have slightly higher mP. *ΔrsgI, ΔmreC,* and KS60 all have significantly lower mP. Statistical analysis was Students t-test. Error bars represent standard deviation. n=3

downstream of SigI induction is likely to influence fluidity but not fatty acid composition. The *ΔmreC* and KS60 strains also both showed significantly decreased mP values, again signifying higher fluidity within the membrane. For KS60, this increased fluidity could be explained by the shift from iso to anteiso, but might be counteracted by the lengthening of the carbon chains. The results are even more astonishing when comparing the increased fluidity in *ΔmreC* with the fact that there is not the same iso to anteiso shift, but the lengthening of carbon chains was retained. Surprisingly, isolate V was measured to a statistically similar fluidity as wild type.

The complex data shown above suggested that membrane fluidity, as measured by DPH, was clearly determined by factors that go beyond the fatty acid profile alone.

To further elucidate our understanding of membrane fluidity without the lateral cytoskeleton at varying temperatures, and to examine if their adaptive response is functional, I performed homeostatic measurements of wild type, *ΔmreC*, KS60 and isolate V at 30°C and 45°C as well. We chose to perform the measurements using DPH due to the high signal to noise ratio, the fact that the cells remain in their native growth environments closer to the time

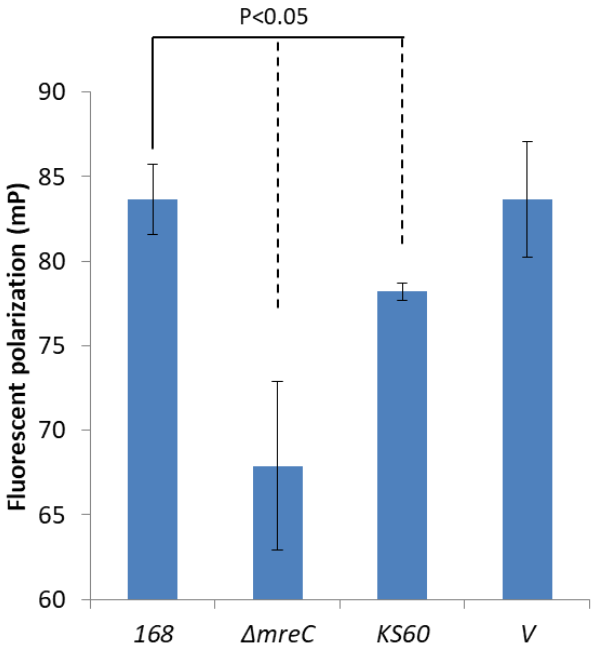

Figure 17: DPH fluidity measurements of 168, *ΔmreC*, KS60, and isolate V at 30°C. 168 conforms to the calibrated value of about 80 mP. *ΔmreC* is almost 20 mP lower than 168 which is significantly lower. KS60 is significantly lower as well, although only with about 7 mP. Isolate V does not exhibit any changed fluidity compared to 168. Statistical analysis was Students t-test. Error bars represent standard deviation. n=3

of measurement, and because of the relative low loss of cells throughout the procedure, as some of our mutants are difficult to pellet and wash.

At 30°C, wild type conformed to our calibrated value of about 80 mP (Figure 17). The *ΔmreC* and KS60 strains both exhibited statistically significant lowered mP values, with *ΔmreC* being more extreme. These results meant that both have higher fluidity compared to wild type. In contrast, and even more surprising, was the fact that the full cytoskeletal deletion mutant without any suppressors, isolate V, had exactly the same fluidity as wild type, while KS60, which has many suppressors, had altered fluidity, especially at lower temperatures.

Finally, we wanted to examine the fluidity of the full cytoskeletal deletion strains at higher temperatures. At 45°C, wild type was measured to be slightly above the calibrated value of 123 mP, but was within a standard deviation of one another, making the measurements valid. The DPH measurements obtained at 45°C are shown in Figure 18. The *ΔmreC* strain once again exhibited a lower polarization than wild type. About 20-25 mP seems to be the discrepancy between the two strains regardless of temperature, which corresponds to the difference between wild type at 30°C and 37°C. KS60 appears to have similar fluidity as wild

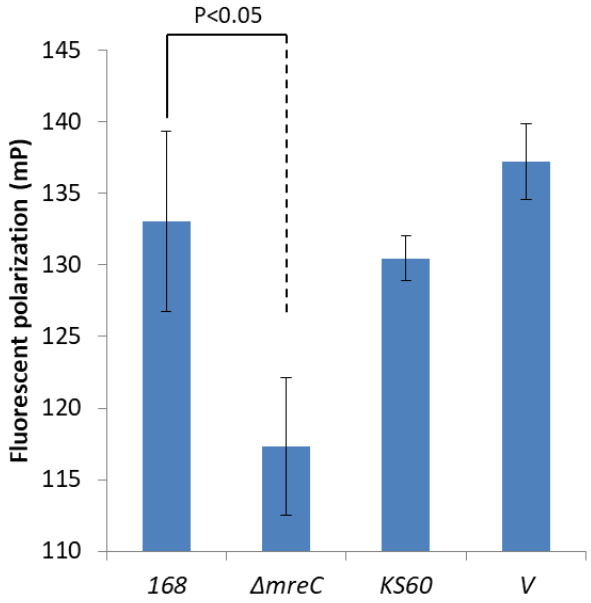

Figure 18: DPH fluidity measurements of 168, *ΔmreC*, KS60, and isolate V at 45°C. 168 is measured at 133 mP, which is slightly above the expected 123. *ΔmreC* has a lower mP at 117, while KS60 is similar to 168. Isolate V has a slightly higher polarization at 138, but it is not significantly higher than 168. Statistical analysis was Students t-test. Error bars represent standard deviation. n=3

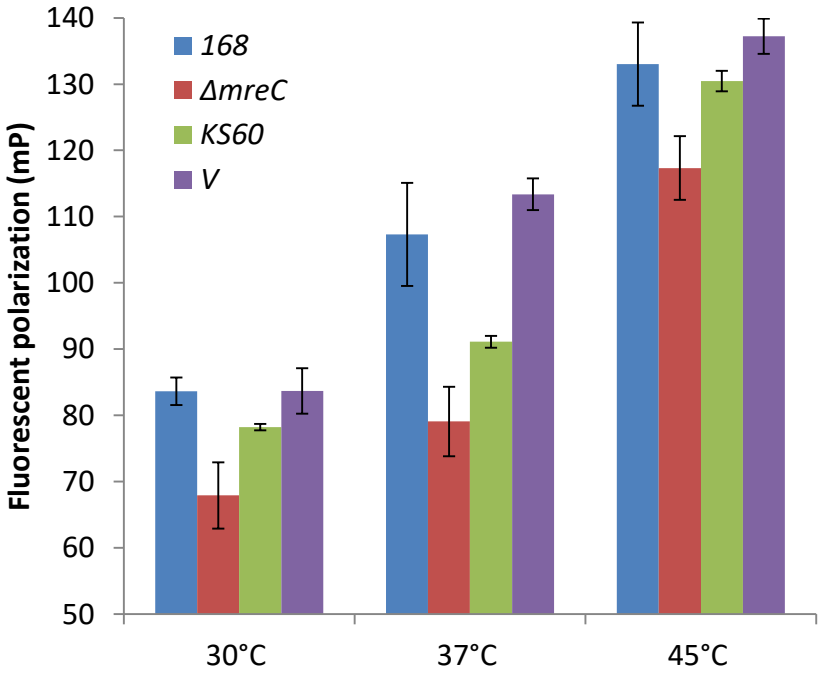

Figure 19: Summary of DPH fluidity measurements for each of the three temperatures 30°C, 37°C, and 45°C. The data is the same as previously discussed in this chapter. Error bars represent standard deviation.

type at 45°C, which is interesting, as they exhibited clear differences at lower temperatures, with 18 mP at 37°C and 7 mP at 30°C. Interestingly, this was the inverse correlation with the differences in fatty acids, as the two strains were more similar at 37°C than at 30°C or 45°C. Isolate V had a similar polarization as wild type, which as with KS60 was surprising since the fatty acid profiles were dissimilar at all temperatures. These results highly suggest that more factors are needed in upholding membrane fluidity than just fatty acid composition. Surprisingly, the fluidity pattern of the four strains looks entirely similar to the pattern at 37°C, again suggesting that the fluidity homeostatic regulation of the membrane has been shifted, rather than lost entirely (Figure 19).

Having measured the fluidities and the fatty acid profiles of the cytoskeletal deletion mutants at different temperatures, I next wanted to examine if the observed changes and potential miss-balances, both in terms of fatty acid composition and fluidity, influence the growth behaviour of the cells.

3.2.4 – Growth of the mreB, mbl, mreBH cytoskeleton deletion mutants

In order to examine how the aberrant fatty acid profiles and membrane fluidity states influence the temperature-dependent growth behaviour, I compared the growth curves of wild type cells and chosen cytoskeletal mutants grown in a plate reader under continuous agitation at different growth temperatures (30°C, 37°C, and 45°C). From the obtained growth curves (Figure 20A-C), doubling times were calculated (Figure 20D). Under these experimental conditions, the wild type strain has a doubling time of approximately 30 min, with only a slightly lower and higher doubling times in 45°C and 30°C, respectively. In contrast, *ΔmreC* grows extremely slowly compared to the wild type, with doubling times of approximately 150 min. at 30°C, 130 min. at 37°C, and 90 min. at 45°C. It is tempting to speculate that the severe growth defect observed in this strain is due to the very high membrane fluidity. Consistent with this notion, both *mreB*-triple deletion mutants, which also lack lateral cell wall synthesis but do not exhibit comparably high fluidity values, grew significantly faster. Nevertheless, the *mreB* triple deletion strain carrying suppressor mutations (KS60) had, with doubling times of approximately 52 min at 30°C and 37°C, longer doubling times than the wild type strain as well. Interestingly, at 45°C this strain was capable of growing with doubling times almost comparable to that observed for the wild type cells. This behaviour also showed a strong correlation with the measured membrane fluidity values under the corresponding conditions, with the difference in fluidity between the mutant and wild type being more pronounced in 30°C and 37°C. Additionally, KS60 clearly grows much faster than isolate V, showing that the suppressor mutations are increasing growth speed.

In contrast to the suppressor carrying strain KS60, isolate V exhibited an interesting growth phenotype in that it had equal initial doubling times at 30°C and 45°C at about 67 min. while the doubling time at 37°C is slightly higher at about 85 min. In isolate V the doubling times were not directly comparable to membrane fluidity, as isolate V had similar fluidity as wild type at all three temperatures examined.

The doubling times in the previous section were calculated from the early logarithmic growth phase. The reason for this is because, as we examined the data, we discovered that both KS60 and isolate V exhibited a clear and surprisingly diauxic shift in growth at all three temperatures. Diauxic growth is expected to occur when a metabolic shift occurs between two mutually exclusive carbon sources. A common metabolic shift is that between glycolysis and gluconeogenesis (Lehninger *et al.*, 2013). In order to test if the diauxic growth was caused by

the shift from glycolysis to gluconeogenesis additional glucose was added. The growth curve with and without added glucose at 37°C can be found in Figure 21A. In wild type cells the metabolic shift from glycolysis to gluconeogenesis usually occurs at relatively high ODs. In

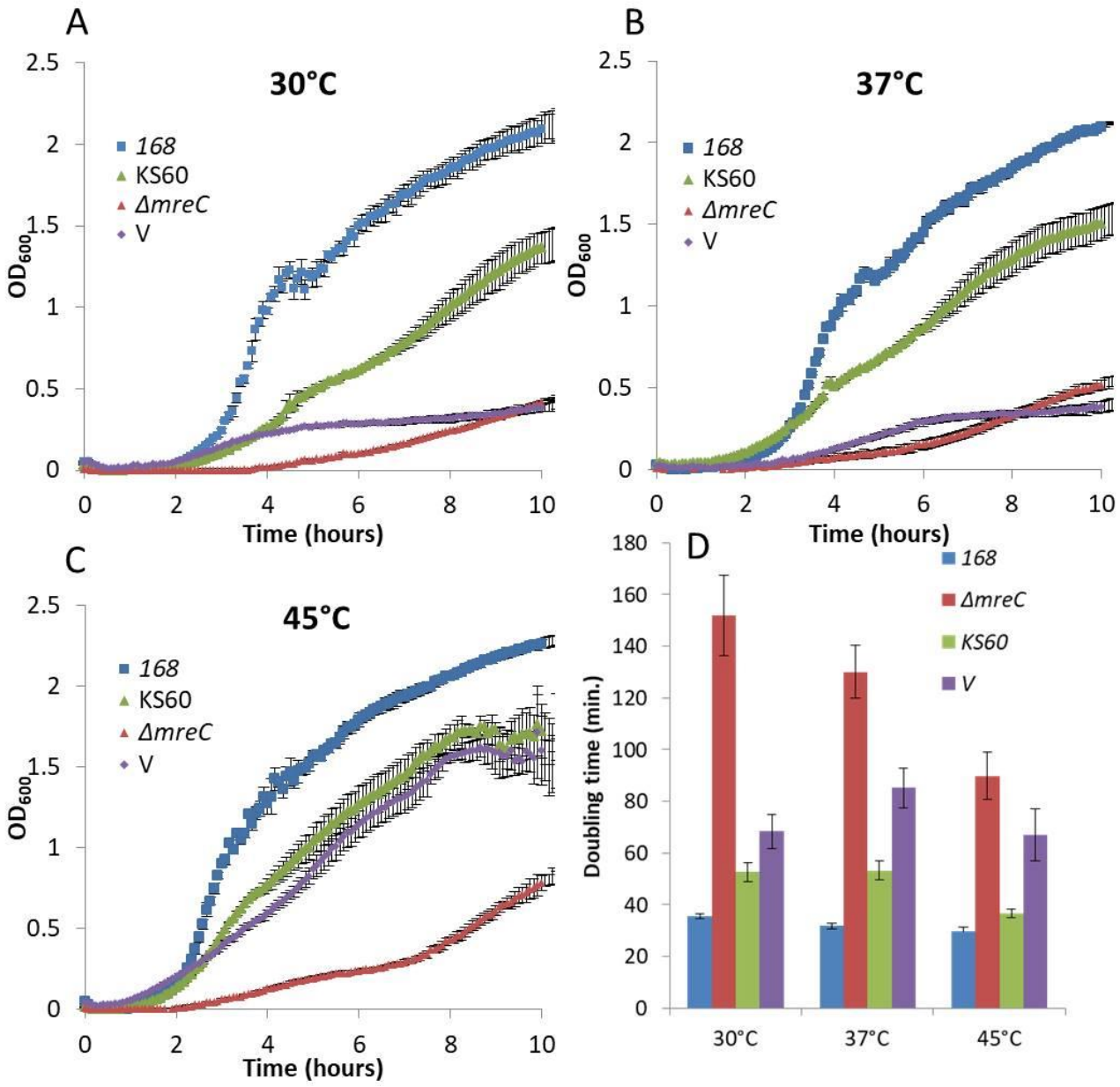

Figure 20: (A-C) Growth curves for 168, KS60, *ΔmreC*, and isolate V at 30°C, 37°C, and 45°C. (D) Initial doubling times for 168, *ΔmreC*, KS60, and isolate V. The four strains exhibit similar patterns across all three temperatures. 168 (wild type) has a steady doubling time at about 30 min. at 37°C, only slightly increasing and decreasing at lower and higher temperatures. *ΔmreC* is growing at a slow pace, which gradually increases as the temperature increases. KS60 grows slow at both 30°C and 37°C, with almost WT growth speed at 45°C. Isolate V exhibits an odd growth phenotype, with 37°C, being the slowest growth temperature. Error bars represent standard deviation. n=3

our plate reader settings this is observed at OD_{600} values of approximately 1.2 (Figure 21A). When supplementing the growth media with 0.1% glucose, we observed a slightly increased initial growth speed along with a longer glycolytic growth phase, followed by shift to gluconeogenesis-dependent growth at OD_{600} of approximately 1.6. In contrast, strain KS60 changed to gluconeogenesis prematurely, at OD_{600} of approximately 0.5. When grown in the presence of 0.1% glucose, the initial growth speed again increased slightly, and the diauxic shift was again only reached at a higher OD_{600} of 1.2. A similar growth phenotype was also seen for isolate V, although the diauxic growth occurred even earlier at OD_{600} 0.3 without added glucose, whereas when glucose is supplemented it occurred at 0.6. At 37°C *ΔmreC* exhibited a slight variation of the growth phenotype. Without supplemented glucose the diauxic growth occurs at OD_{600} 0.6, and can be shifted to about 0.9 with supplemented glucose. Interestingly, it appeared that the addition of glucose induced a population density beyond what the strain can uphold when the extra nutrients are consumed, resulting in cellular lysis immediately after exhaustion of glucose.

The finding that the cytoskeleton is involved with sugar metabolism is interesting, and should be examined further. Perhaps the mutants somehow consume energy at a much higher rate, either through a process which is so far unknown or through a faulty nutrient to energy conversion, possibly through a suboptimal electron transport chain or ATP synthesis since these are membrane bound. Alternatively, the elevated need for nutrients could stem from lack of intake of glycolytic amino acids, through dysfunctional transporters, also inhibited by the changes in the membrane. Further studies are needed to elucidate the cause and effect.

Having found that the two full MreB cytoskeletal deletion strains, KS60 and isolate V, behave differently during growth, I wanted to inspect their growth microscopically as well. In order to visually examine the growth behaviour we set up a time lapse experiment, in which we took images every 5 min. The experiment was performed at 37°C, and with membrane dye present. The results for KS60 and isolate V can be found in Figure 22A and B respectively. Both of the full MreB cytoskeletal deletion strains grow as a large cluster of cells with coccoid morphology. When examining the location of septum formation, KS60 forms the division sites symmetrically when in low population density, giving rise to two identical non-separated daughter cells, as seen highlighted by the arrows. At subsequent higher density, divisions appear increasingly random, occasionally being symmetrical, although oddly placed divisions are common, often resulting in 4-leaf clover-like structures. Surprisingly, KS60 exhibited almost no cellular lysis, which is impressive due to the unnatural coccoid growth of

the mutant. Isolate V on the other hand, formed almost exclusively asymmetrical division sites throughout growth. The daughter cells appear to grow much slower, which correlates well with the slower growth observed in the growth curves. Rarely, a few cells lyse, which could contribute to the slow growth rate, although unlikely as the lysis usually occurs after periods of sustained growth. The oddly placed division sites in isolate V usually results in three cells being stuck together, growing for a while before initiating division again, as observed in the last couple of frames of Figure 22B. It is difficult to determine average sizes

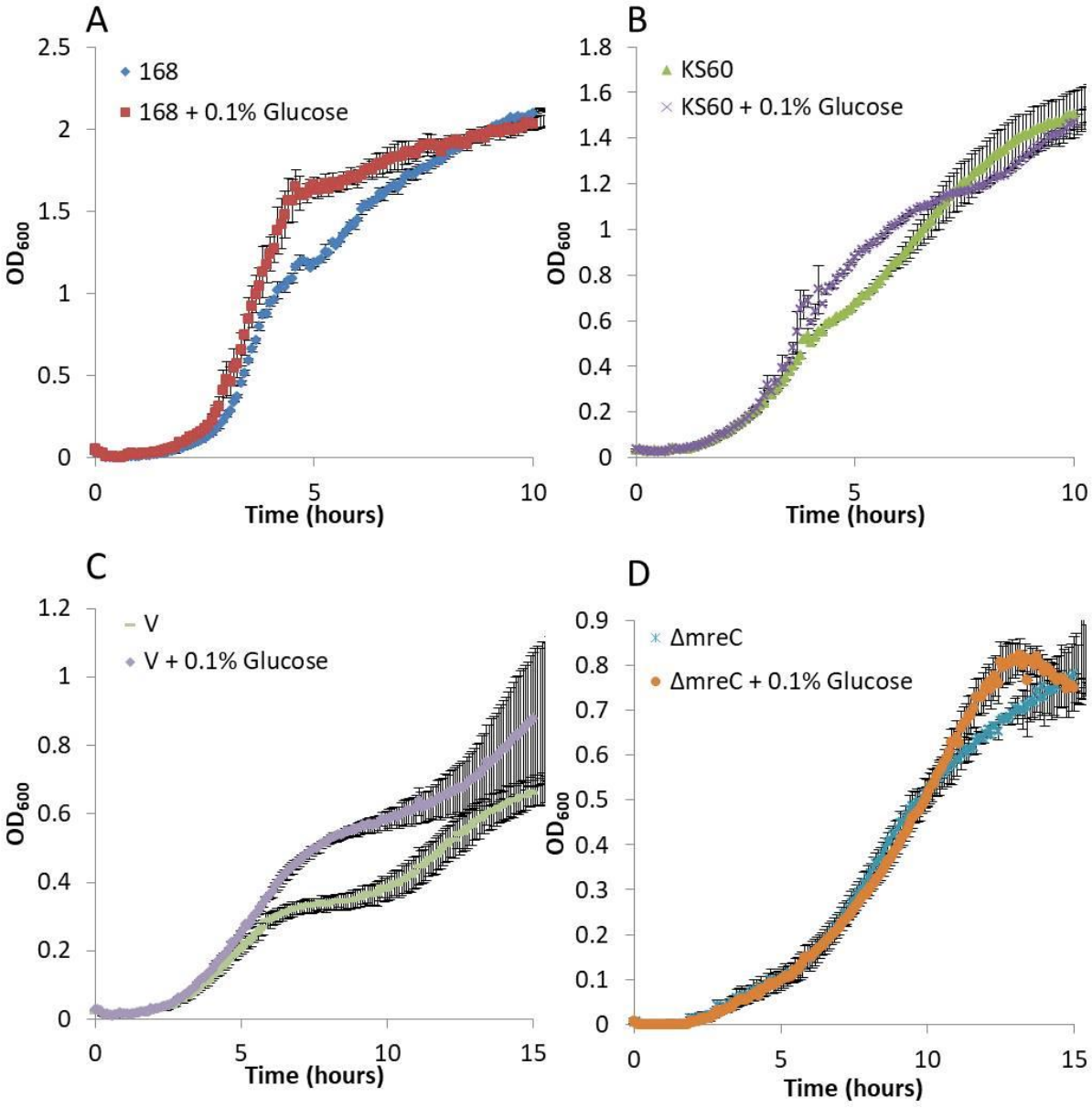

Figure 21: Growth curves for 168 (A), KS60 (B), *ΔmreC* (D), and isolate V (C) at 37°C. The same diauxic growth pattern is seen for all strains, although at different OD_{600}. The shift to the second growth phase can be alleviated by addition of glucose in all strains, indicating that it is indeed a metabolic shift. Additionally, only 168 and KS60 grows beyond OD_{600} of 1. Error bars represent standard deviation. n=3

for the cells, as they are irregular, but it appears that the KS60 cells on average are larger than the isolate V cells, which could be explained by many suppressor mutations present in KS60. The volume differences of the two strains should be examined further.

3.3 – Discussion

As indicated by the data presented above, when the lateral cytoskeleton, or its attachment to the elongasome is interrupted, not only the lateral cell wall synthesis but also the membrane lipid homeostasis is disturbed, resulting in reduced growth speed.

The changes in membrane fatty acid composition in KS60 and isolate V are large compared to wild type, with a constant shift towards longer fatty acid species. The *ΔmreC* strain has a fatty acid composition with longer fatty acids at lower temperatures, but wild type-like length composition at higher temperatures, revealing that *B. subtilis*doesn't need the longer fatty acids as a general adaptation for cocci-like growth. Alternatively, cocci-like cells at higher temperatures might need similar adaptations as wild type cells at 37°C. Perhaps, when the MreB cytoskeleton is deleted, the RIFs are dispersed throughout the membrane, possibly causing fluidisation, which is counteracted by longer fatty acids. Another possibility is that the system responsible for length adapting fatty acids are miss-regulated or disturbed, as isolate V continuously adapts for a long / short ratio of about 0.9, whereas the wild type operates within ratios of 0.5-0.75. Interestingly, KS60 exhibits slightly decreased fatty acid length compared to isolate V, indicating that the suppressor mutations present in KS60 are restoring the fatty acid composition towards the wild type situation. It would be interesting to examine which of the suppressors are responsible for the membrane adaptations, or if the suppressors result in pleotropic consequences. When examining the iso / anteiso composition, it once more became evident that a shift towards either configuration was not especially needed for cocci-like growth, as *ΔmreC* had close to wild type compositions at both of the conditions examined. At 30°C and 37°C we observed that KS60 and isolate V both have a drastic shift towards the anteiso conformation, possibly fluidizing the membrane. Once again, the suppressor mutations in KS60 appear to correct the mis-regulated fatty acid biosynthesis. Surprisingly, at 45°C, isolate V has drastically shifted towards the iso conformation, having clearly elevated levels compared to wild type. Currently, we have no explanation for the sudden shift towards iso at higher temperatures. Furthermore, at 45°C KS60 still exhibited a significantly anteiso

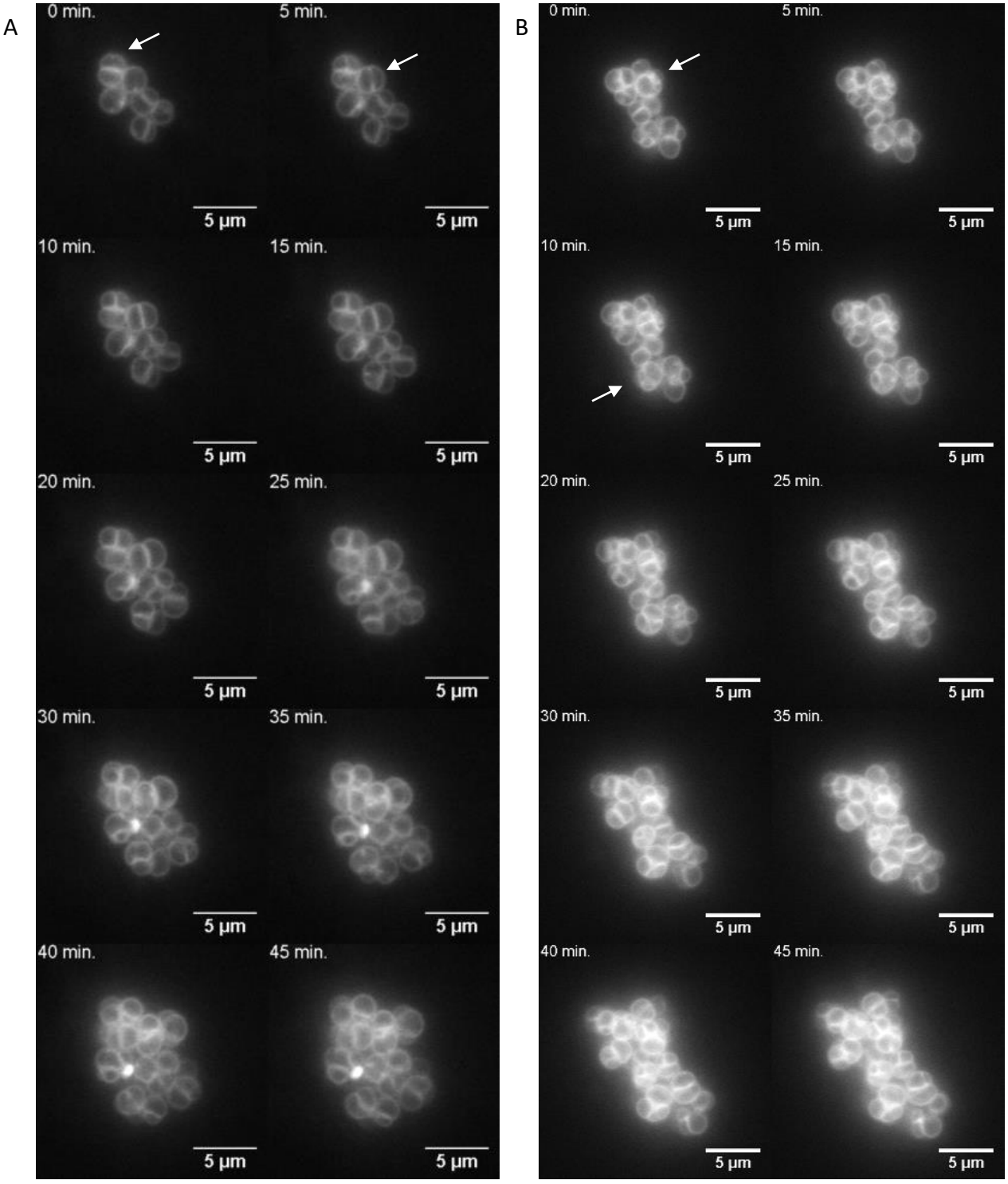

Figure 22: Time lapse images of KS60 and isolate V at 37°C, with FM5-95 membrane dye. Arrows signify initiation of a few interesting division sites. (A) KS60 growth for 45 min. If following the division of the cells highlighted by the arrows, one will find that most of the divisions are occurring in conjunction with yet to be finished divisions. KS60 usually has 2-4 cells attached, either unable to finish the division or the segregation. The cells are in average rather large. (B) Isolate V growth for 45 min. When following the division of the highlighted cells, one will find that usually 2 divisions are occurring at the same mother cell, creating a 3-leafed clover-like structure. The cells appear to be smaller at later stages of division.

enriched membrane compared to wild type. When comparing KS60 iso / anteiso and long / short ratios at the three different conditions it does appear as if the point mutations have partially suppressed the length increase phenotype, but is having problems correcting the branching alterations. Finally, when comparing the current results to previous publications we find that the changes are similar (Strahl *et al.*, 2014), but that in our study isolate V exhibits clearer phenotypes, suggesting that the 168ED strain used in previous studies had suppressors of its own, possibly beyond the already known constitutive activation of the WalRK two component system.

When looking at the fluidity of the various strains, what is immediately evident is that DPH and laurdan does not measure exactly the same parameters of the membrane. When measuring the fluidity using laurdan, all the strains had a tendency to exhibit a decreased fluidity, compared to the wild type. This doesn't agree with previous publications that used strains with unknown suppressors and a constitutively active WalRK (Strahl *et al.*, 2014), where the authors found the equivalent of KS60 to have higher fluidity than wild type. Unfortunately, it is difficult to compare these studies, as the wild type was different. The previous study used the old 168ED based strain with the constitutively active WalRK heat shock response, whereas in this study we use the apparently clean 168CA strain. This was an additional reason to recreate the strains in the same strain background without constitutively active envelope stress responses. The discrepancy between the two studies was partially why we changed fluidity probe to DPH, as we needed a more reproducible probe with a higher signal to noise ratio and where we lost fewer cells in the initial preparations. The different results between laurdan and DPH could also inform us about the differences in head group and fatty acid changes when deleting the cytoskeleton. It is feasible that the changes seen in laurdan represent actual changes in the head group composition of the cells, and it would thus be interesting to analyse those as well to get a full picture of the membrane.

The DPH results are puzzling on their own when comparing KS60 and isolate V. It would be expected that the strain without any suppressor mutations, isolate V, would have the largest differences compared to the wild type, while the strain with multiple suppressors and large genomic duplications would exhibit fewer changes, since this mutant would attempt to regain wild type fluidity. Alternatively, the coccoid cells no longer attempt to adapt to wild type compositions, if indeed a different composition is needed when spherical. What was observed is that the alterations in the membrane in isolate V barely changed the fluidity, while in KS60 a drastical change in the fluidity was seen. One explanation might be due to

membrane domains and lipid II. As discussed in Chapter 1, RIFs co-localize with MreB and its homologues. When deleting the actin homologues, the RIFs, which normally recruits lipid II are dissolved, allowing for lipid II to more freely diffuse in the membrane. This could increase fluidity throughout the membrane, which when taken together with the on average longer fatty acids could explain why the fluidity in isolate V is similar to wild type. KS60 obtained a duplication of the entire Mur-operon, possibly creating increased amounts of lipid II, which could increase the fluidity, as lipid II favours fluid surroundings and can induce lipid disorder in its vicinity both *in vitro* (Ganchev *et al.*, 2006) and *in silico* (Jia *et al.*, 2011). This supports the notion that it is the suppressor mutations that actually cause the increased membrane fluidity in the strain lacking MreB homologs. It also reveals that in order to sustain fast growth without the MreB cytoskeleton, the strain needs increased fluidity. MreB directly interacts with members of the *mur*-operon MraY and MurG (Favini-Stabile *et al.*, 2013). The loss of this interaction could influence the synthesis rate of lipid II, thus locally changing the fluidity in the membrane. The suppressor mutations could occur in an attempt to negate any negative effect on the membrane from the possibly altered lipid II synthesis. This hypothesis also fits with why *ΔmreC* is exhibiting higher fluidity overall. In *ΔmreC*, the lipid II rich RIFs are still present, but no longer co-localizing with the cell wall synthesis machinery. In contrast, they possibly accumulate due to the disconnection between the MreB cytoskeleton and cell wall synthesis machinery. This disconnection could result in a build-up of lipid II and, consequently, in increased fluidity. Finally, and perhaps most importantly, from what we observe, it appears that the fatty acid composition alone does not determine membrane fluidity, as we see no clear correlation between the fatty acid changes observed in the cytoskeletal mutants and the measured fluidities. Perhaps membrane bound proteins, or components yet to be elucidated, contribute significantly to membrane fluidity.

The strains *ΔmreC*, KS60, and isolate V all lost their rod-shape turning to a cocci-like growth. When measuring growth speed, *ΔmreC* showed the longest overall doubling time, which is surprising as until now MreC was thought to be the adapter protein between the MreB cytoskeleton and the rest of the elongasome, thus should not exhibit a different phenotype to isolate V. We find that *ΔmreC* exhibited both a different fatty acid composition along with a slower growth rate. These findings suggest that the MreB homologues have additional secondary functions that are still to be discovered. The growth speeds of KS60 and isolate V are quite different, and from the OD measurements it appears that the mutations in KS60 are obtained to increase doubling times, but when we examine the microscopy images,

another conclusion can be drawn. KS60 starts off with approximately 9 cells in the cluster increasing to about 22 after 45 min., while isolate V initiates with 14 cells increasing to approximately 34 cells after 45 min. This gives them both doubling times of about 35 min. at 37°C on solid agar. The difference in OD might thus be attributed, not to the amount of cells, but the difference in volume between the two cells. The suppressors in KS60 might not drive faster division, but could increase the surface/volume ratio, perhaps to protect itself better from osmotic stresses. A CFU experiment along with a measurement of dry weight at various growth stages could show if the numbers of cells actually differ, or if the volume of those cells account for the difference in OD.

A further interesting observation is the apparent connection between the deletion of the MreB cytoskeleton and sugar metabolism. It appears that KS60 and isolate V either have trouble taking up the nutrients from the surroundings, or the mutants require much larger amounts of energy to grow and divide. One could envisage that these cells now have a large amount of waste processes occurring, both directly due to the deletion, such as upholding the entire system for lateral growth although it is now unnecessary, and indirectly due to downstream effects, which could include initiation of stress responses through which unnecessary proteins would be synthesized, or even the loss of spatial segregation of certain proteins, which now are allowed to diffuse and cause unwanted effects throughout the cell. Additionally, the gluconeogenic factor YvcK in *B. subtilis* has been linked to loss of rod-shape and was also linked to the expression of the WalRK two components system (Sperber and Herman, 2017). The precise function of YvcK is unknown, but it appears to be involved in regulation of lateral cell growth during the shift from glycolysis and gluconeogenesis. Since the cytoskeletal mutants appear to have an altered transition from glycolytic to gluconeogenic growth, a potential miss-regulated and poorly understood regulatory system involving rod shape, WalRK and YvcK could contribute to the underlying reason for the metabolic problems observed in the *mre*-mutants.

Another possibility why the shift from glycolysis to gluconeogenesis occurs faster in the mutants could be due to a faulty respiratory chain. If respiration was uncoupled somehow, the need for more energy would be substantial, thereby forcing the cells into using the nutrients faster. This would in turn cause the shift from glycolysis to gluconeogenesis to occur at an earlier growth stage. Further studies will be needed regarding lateral cell wall synthesis and metabolism to conclude a certain cause and effect.

The prevailing model of membrane homeostasis, the homeoviscous adaptation, has concentrated on the core hypothesis that the biological membrane stays within a relatively narrow fluidity range in order to optimally support cellular functions, and that this is achieved by carefully adapting the membrane lipid composition, and that living *B. subtilis* cells maintain similar membrane fluidity levels at different growth temperatures. Our findings somewhat disagree with this. Rather, *B. subtilis* cells are able to grow with remarkably different levels of membrane fluidity. Instead, we found that the membrane fluidity is significantly higher at lower temperatures and lower at higher temperatures, respectively.

Chapter 4 – Interplay Between Membrane Potential and Membrane Fluidity

4.1 – Introduction

As discussed in Chapter 1, membrane potential is essential for a variety of biological processes, including ATP production, nutrient transport across the membrane, motility, protein secretion, etc. It has also been found to be important for membrane association and correct localization of proteins involved in both elongation and division. Upon dissipation of membrane potential, numerous peripheral membrane proteins, such as MinD and FtsA, lose their membrane association and are released to the cytoplasm (Strahl and Hamoen, 2010) where they are unable to perform their function (Figure 23). Additionally, upon membrane depolarization MreB loses its native localization and clusters in a few specific foci within the cell membrane, or is released from the membrane entirely (Strahl and Hamoen, 2010; Strahl *et al.*, 2014). Furthermore, MreB is associated with fluid lipid domains (RIFs) that delocalise alongside MreB (Strahl *et al.*, 2014). Membrane binding of amphipathic helices, and thus the membrane binding of MinD and FtsA, has been shown to be dependent on multiple factors, including the ionic composition and strength of the surrounding environment, the local lipid composition (anionic phospholipids such as PG or cardiolipin increase the helices' affinity for the membrane) (Mileykovskaya *et al.*, 2003; Mileykovskaya and Dowhan, 2005), and membrane fluidity, as a tighter packing of the lipids decreases the insertion of non-lipid entities (Bigay and Antonny, 2012). One such fluidity dependent binding is exemplified by

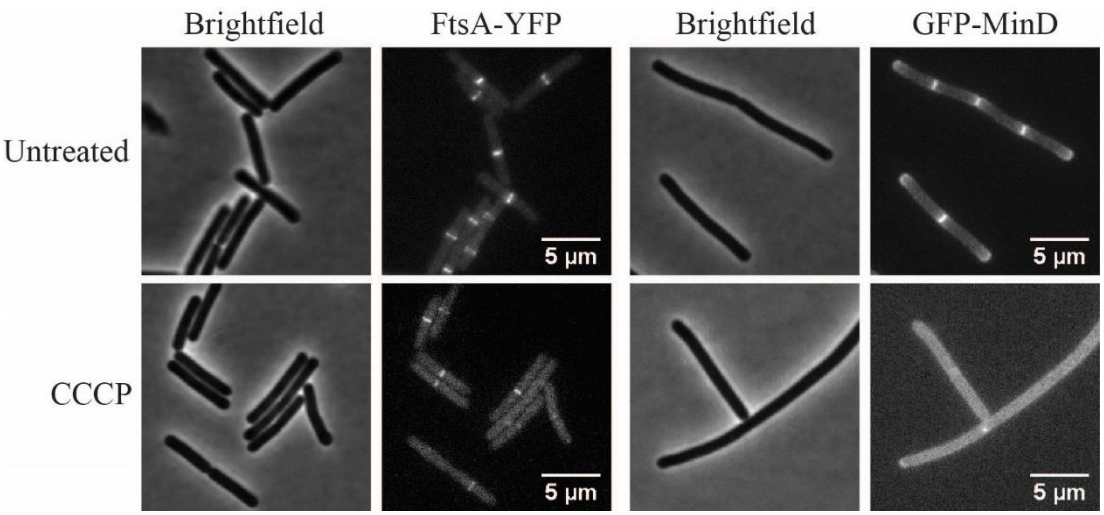

Figure 23: Microscopy images of FtsA-YFP and GFP-MinD untreated and with CCCP. FtsA localizes to mid-cell when untreated. Upon CCCP treatment, FtsA localization shifts towards a cytoplasm localization with slightly weaker septal foci. MinD localizes to septum and cell poles when untreated. When treated with CCCP, MinD detaches entirely from the membrane going into the cytoplasm.

MinD in *E. coli*, which changes the lipid packing upon insertion into the membrane (Mazor *et al.*, 2008).

In an effort to understand why proteins attached to the membrane via amphipathic helices lose native localization upon dissipation of membrane potential, I developed three hypotheses to possibly explaining this phenomenon. The first hypothesis was that the cardiolipin specific membrane domains, which have been postulated to be enriched both at cell poles and cell division sites of *B. subtilis* (F. Kawai *et al.*, 2004), which coincide with the native localisation pattern of both MinD and FtsA, could be redistributed or even dissolved upon membrane depolarisation, thereby triggering delocalisation of MinD and FtsA. The second hypothesis was that the dissipation of membrane potential, which causes MreB and the associated fluid lipid domain to delocalize and cluster (Strahl and Hamoen, 2010), could cause rigidification of the membrane thereby indirectly inhibiting the membrane binding of amphipathic helices. The third and final hypothesis was that upon dissipation of membrane potential, a fluidity promoting electrostrictive force exerted by the transmembrane electric field is also dissipated (Heimburg, 2012), thereby triggering membrane rigidification and, consequently, the dissociation of amphipathic helices from the membrane. Electrostriction is caused by having an insulator, in this case the membrane, and two differently charged chambers on either side (the cytoplasm and the extracellular space). The difference in charge across the insulator forms an electrical field pushing from either side onto the insulator, exerting a constrictive force. (Heimburg, 2012)

In order to test the three hypotheses, I started by examining the cardiolipin domains in the membrane of *B. subtilis*, and found that the experimental tools used to support the very existence of cardiolipin domains are unreliable, and the observation of cardiolipin-specific domains in *B. subtilis* is not reproducible in our hands. I therefore discarded the first hypothesis and the analysis of the cardiolipin domains will be discussed separately in Chapter 5. Hypotheses two and three both involved detecting changing fluidities upon membrane depolarization, which I followed using the fluidity probes laurdan and DPH, which were already introduced in Chapter 3. Additionally, to test if the delocalisation of MreB is involved in the process, I used the full *mreB* deletion mutant (Δ*mreB* Δ*mreBH* Δ*mbl*) from previous chapters to examine changes in fluidity upon dissipation of membrane potential in the absence of MreB homologs. It is worth mentioning that due to the order in which strains were made, these experiments were carried out with strain KS60 that carries both genomic duplications and snps as described in Chapter 3. Furthermore, I decided to test alterations in membrane

fluidity upon changes in turgor pressure, as both electrostriction and turgor exert forces that theoretically favour the thinner, more fluid membrane configuration. Consequently, dissipation of both forces could potentially result in comparable rigidification of the membrane. Finally, I used MinD and FtsA as probes to determine if their dissociation from the membrane upon depolarization can be rescued by supressing the membrane potential-sensitivity of MreB, or if their dissociation can also be triggered by changes in turgor pressure.

4.2 – Results

4.2.1 – Membrane depolarization induces membrane rigidification

Initially, I wanted to show that the compounds I used indeed dissipated membrane potential. To measure membrane polarization, I used the fluorescent dye $DiSC_3(5)$ that accumulates in the cell in a voltage-dependent manner. Upon accumulation, the fluorescence is quenched, thereby lowering the overall fluorescent signal measured from the cell suspension. When the membranes are depolarized, the dye is released from the cytoplasm into the surrounding media. The associated de-quenching can be observed as increased fluorescence of the cell suspension. Before performing the experiment with cells, I wanted to determine if our compounds were compatible with $DiSC_3(5)$. I therefore carried out the $DiSC_3(5)$ assay in the absence of cells, but with the addition of our compounds CCCP and

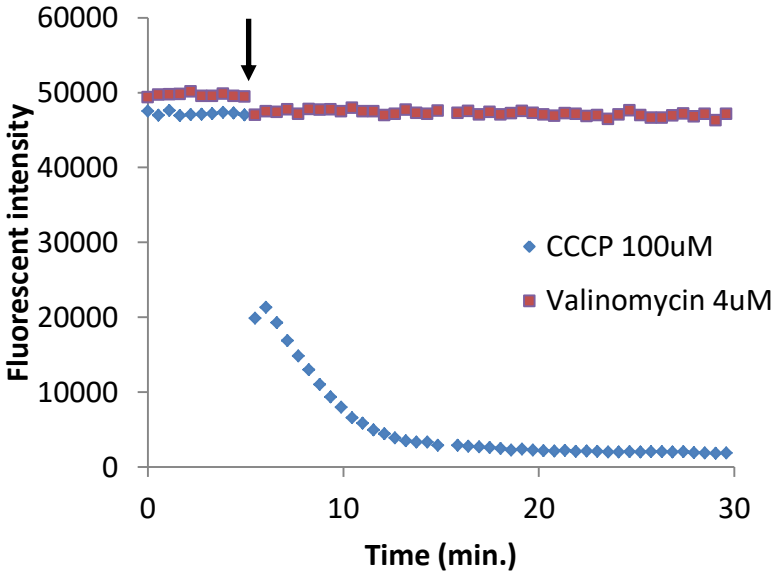

Figure 24: Graph showing the influence on $DiSC_3(5)$ fluorescence by CCCP and valinomycin. The black arrow shows the point when the compound was added. CCCP suppresses the fluorescence almost completely, while valinomycin only modulates the signal slightly.

valinomycin. As seen in Figure 24, the addition valinomycin only altered the $DiSC_3(5)$ fluorescence to a small degree whereas CCCP entirely suppressed the signal. This result demonstrated that CCCP cannot be used in combination with $DiSC_3(5)$, although reports from the literature detail that CCCP does indeed collapse membrane potential (Heytler and Prichard, 1962). Since it is compatible with all of the three main assays in this chapter (depolarisation, membrane fluidity, and protein localisation analyses), I chose to use valinomycin as the means to trigger membrane dissipation in this Chapter.

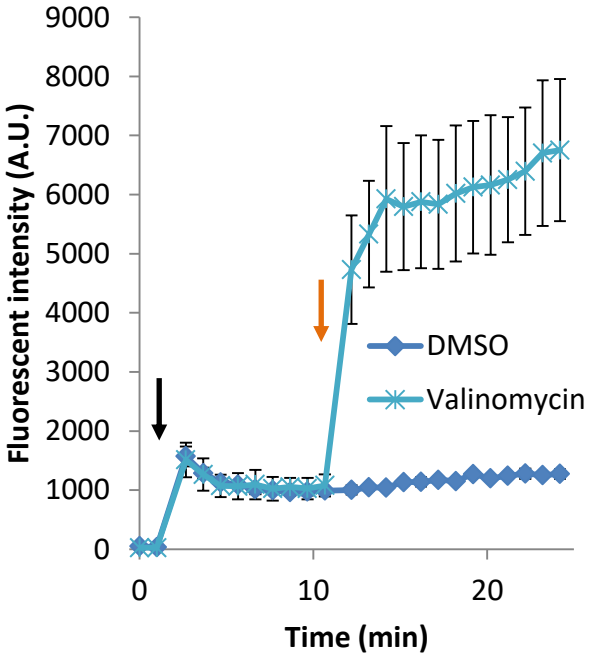

Figure 25: $DiSC_3(5)$ assay using wild type. The black arrow indicates when $DiSC_3(5)$ is added and the orange arrow indicates where the compounds DMSO and valinomycin are added. DMSO does not alter the polarization of the cell, while valinomycin potential dissipates membrane potential. Error bars represent standard deviation. n=3

To verify that valinomycin does indeed depolarize the cells, the $DiSC_3(5)$ assay was conducted with wild type cells. The course of the experiment is shown in Figure 25. Initially, I measured the cells without any dye in order to monitor the relatively insignificant cellular auto-fluorescence at $DiSC_3(5)$ emission wavelengths. Following this, $DiSC_3(5)$ was added (as indicated by the black arrow). After about 10 min. of incubation, during which time the dye is internalised and reaches equilibrium with the cellular trans-membrane potential, either valinomycin or DMSO (the solvent used to dissolve valinomycin) was added, as indicated by the orange arrow. A rapid increase in fluorescence intensity was immediately observed in the

valinomycin treated cells, whereas the DMSO-treated sample remained unaffected. This clearly showed that valinomycin rapidly depolarizes *B. subtilis* cells.

Having demonstrated that valinomycin dissipates membrane potential under our experimental conditions, I next wanted to examine whether membrane depolarisation also affected membrane fluidity. For this aim I used the two membrane fluidity sensitive fluorescent dyes, laurdan and DPH. As described in Chapter 1, laurdan is inserted at the fatty acid / head group interphase while DPH is inserted deep within the aliphatic core of the membrane. The results of the time resolved assays are found in Figure 26. The first four measurements were taken before treatment with valinomycin and all fluctuated, demonstrating the difficulty in generating stable signal to noise ratios for laurdan. Nevertheless, following the addition of valinomycin, a sharp increase in GP was observed, signifying strongly reduced membrane fluidity. This clearly indicates a connection between membrane potential and fluidity. Even after the treatment, the values measured for the

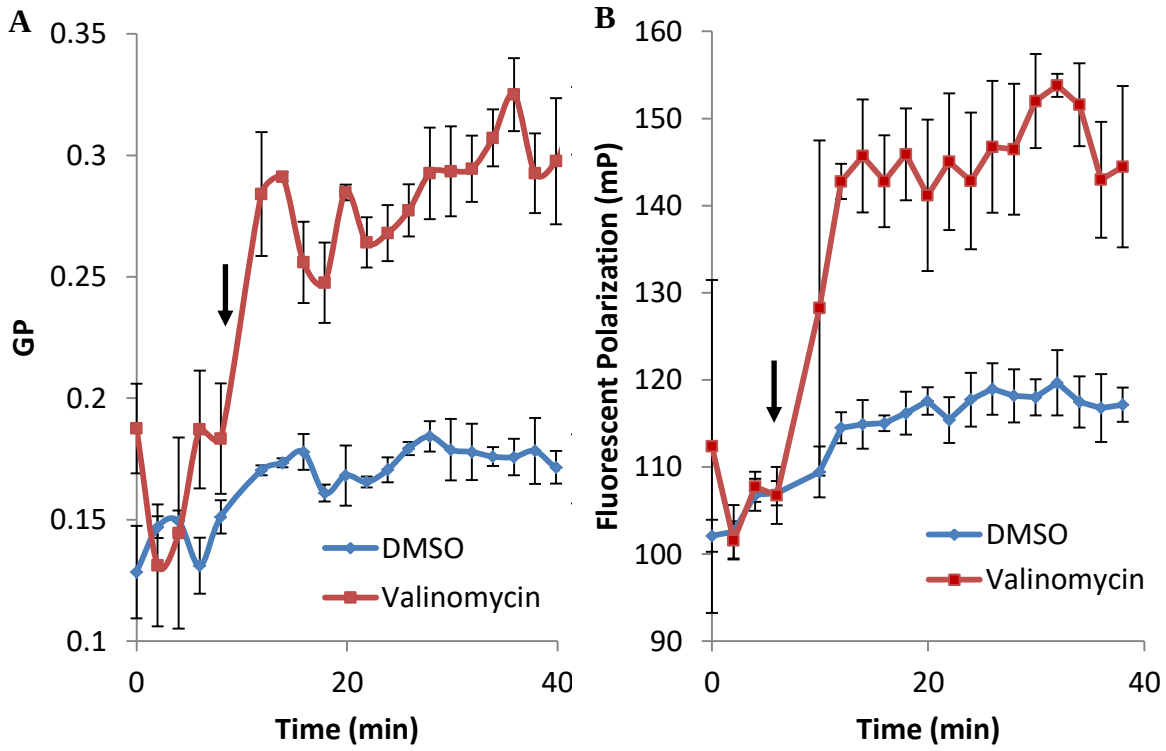

Figure 26: Fluidity measurements of wild type upon treatment with cation chelating agent valinomycin using the two fluorescent membrane fluidity probes laurdan and DPH. The black arrows indicate the time point when the compounds are added. (A) Laurdan fluidity measurements of wild type upon treatment with valinomycin. A clear increase in GP is seen upon treatment with valinomycin indicating a decrease in fluidity of the membrane. (B) DPH fluidity measurements of wild type upon treatment with valinomycin. Upon treatment with valinomycin, an immediate increase in mP is seen, revealing a rigidification of the membrane. Error bars represent standard deviation. n=3

samples still fluctuated, indicating that the signal to noise ratio is relatively low, although still reliable as the standard deviations show. The DMSO treated sample exhibited a slightly elevated GP, which could be due the fact that the plate reader was open during the compound addition, thereby potentially cooling the sample slightly and thus giving rise to a more rigid membrane. I would expect that DMSO, if it was actively influencing membrane fluidity, could fluidize the membrane slightly since it is an organic fluidizer (Gurtovenko and Anwar, 2007). In the DPH measurements an increased stability of the measured values were observed, as compared to laurdan. Again, a slight increase in mP occurred in the DMSO treated sample, while the valinomycin treated sample exhibited highly elevated values that signified a significantly rigidified membrane. As both membrane fluidity probes reported decreased membrane fluidity, we were confident that the membrane was more rigid at both head group fatty acid interphase and deep within the aliphatic core. Consequently, membrane depolarization appeared to correlate with strong membrane rigidification, thereby strengthening the hypothesis that changes in membrane fluidity could underlie the membrane potential-dependent membrane binding of MinD and FtsA.

4.2.2 – Fluidity changes of the membrane upon depolarization without the MreB cytoskeleton

The rapid rigidification of the membrane upon membrane depolarization could be caused by the delocalization or dissipation of RIFs upon MreB delocalization or membrane disassociation. In order to examine if the delocalization of the MreB cytoskeleton is involved in membrane rigidification, I used the strains (*ΔmreB, Δmbl, ΔmreBH*) (KS60) and *ΔmreC*. The (*ΔmreB, Δmbl, ΔmreBH*) strain has all three actin homologues deleted, and the RIFs normally associated with the MreB filaments appear qualitatively dissolved. By contrast, RIFs are still present in *ΔmreC* mutants, but MreB does not delocalize upon membrane depolarization (Strahl *et al.*, 2014). I can thus use (*ΔmreB, Δmbl, ΔmreBH*) to determine if MreB is involved in changes in fluidity upon dissipation of membrane potential, while *ΔmreC* is used to determine if MinD and FtsA still delocalize upon membrane depolarization in a strain in which MreB does not. The two strains were subjected to both the laurdan and DPH assay during valinomycin-mediated depolarisation.

The results from the two time resolved assays are found in Figure 27. In the laurdan assay, once more a slight DMSO-dependent GP-increase in the wild type was observed, while

the valinomycin treated cells exhibit strong membrane rigidification with GP-values fluctuating at around 0.3. As shown in the previous chapter, (*ΔmreB, Δmbl, ΔmreBH*) has a decreased membrane fluidity in the uninhibited state. When treated with valinomycin, the strain deficient for MreB-homologs also exhibited a clear membrane rigidification.

To verify the findings observed with Laurdan, the membrane fluidity measurements were repeated by using DPH polarisation. The DPH data (Figure 27B) further confirmed that wild type treated with DMSO slightly increased in mP, while the valinomycin treated wild type sample exhibited a rapid and significant increase in mP. Upon valinomycin treatment (*ΔmreB, Δmbl, ΔmreBH*) undergoes rapid membrane rigidification, immediately reaching membrane fluidity values even lower than those observed for the wild type cells. These results suggest that although the MreB cytoskeletal deletion strain exhibits increased rigidification compared to the wild type, MreB is not responsible for the overall phenomenon of membrane fluidity alterations upon dissipation of membrane potential.

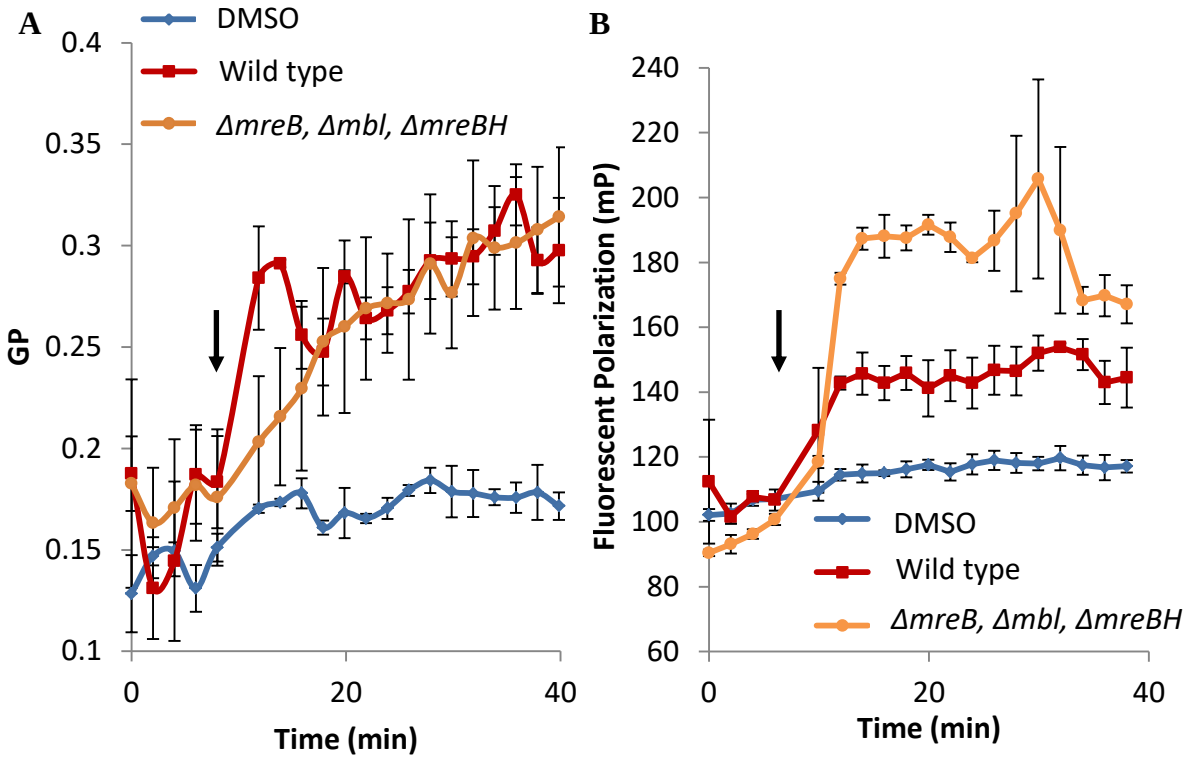

Figure 27: Fluidity measurements upon treatment with valinomycin of wild type and the full cytoskeletal deletion strain (*ΔmreB, Δmbl, ΔmreBH*). The black arrows indicate when the compounds were added. (A) Laurdan fluidity measurements for wild type and (*ΔmreB, Δmbl, ΔmreBH*) treated with valinomycin. As observed in previous chapter, (*ΔmreB, Δmbl, ΔmreBH*) measures at higher GP than wild type. After treatment of valinomycin wild type rapidly rigidifies, whereas (*ΔmreB, Δmbl, ΔmreBH*) slowly rigidifies, finding a plateau at the same level of wild type. (B) DPH fluidity measurements of wild type and (*ΔmreB, Δmbl, ΔmreBH*) treated with valinomycin. As described in previous chapter, (*ΔmreB, Δmbl, ΔmreBH*) exhibits lower mP compared to wild type. After valinomycin treatment, wild type rapidly rigidifies, interestingly, (*ΔmreB, Δmbl, ΔmreBH*) rigidifies at an increased rate and finds a plateau at much higher mP values, indicating more rigid membranes. Error bars represent standard deviation. n=3

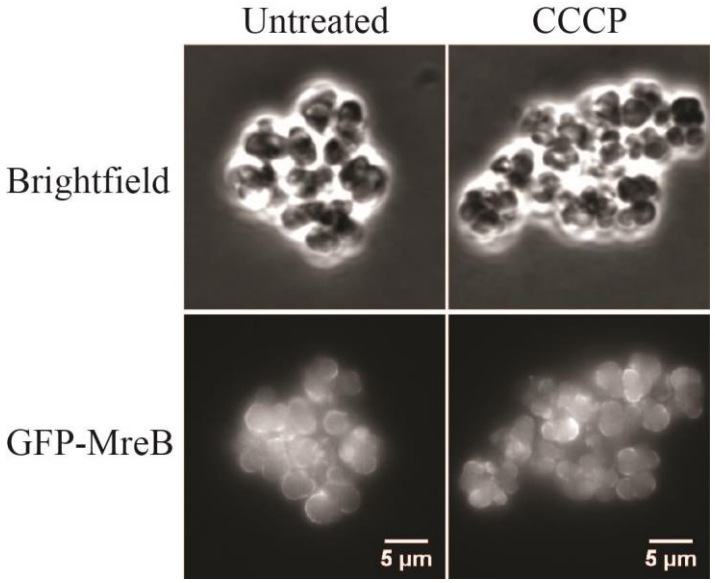

Figure 28: MreB localization upon dissipation of membrane potential in *ΔmreC*. MreB localizes to the entire membrane, except division sites it appears. CCCP treated MreB does not delocalize.

To further investigate the hypothesis that MreB is responsible for delocalization of MinD and FtsA, a strain harbouring *ΔmreC* was utilized. From previous experiments in our group, it was discovered that MreB doesn't delocalize upon membrane potential dissipation in a *ΔmreC* background. I recreated these results clearly showing that untreated cells exhibit MreB localization in specific membrane foci along the entire cell periphery, and that upon treatment with CCCP, the localization remains the same (Figure 28). Next, I used this phenomenon to examine if MinD and FtsA delocalization is MreB-localization dependent.

In the *ΔmreC* background, FtsA localizes to septa similarly to wild type, as indicated by arrows (Figure 29). When treated with CCCP, an almost complete detachment from the membrane was observed, much like the detachment seen when wild type cells are treated with CCCP. Surprisingly, MinD localizes almost uniformly throughout the membrane in the *ΔmreC* background. When treated with CCCP, again an almost complete detachment from the membrane was observed. This localization pattern is similar to not only the FtsA data in *ΔmreC*, but to the wild type MinD delocalization upon CCCP treatment. The fact that both MinD and FtsA delocalize upon membrane potential dissipation in the *ΔmreC* strain, in which MreB remains natively localized, suggest that their delocalization is MreB independent.

In conclusion, based on measured changes both in Laurdan GP and DPH polarisation, the delocalisation of MreB and the associated fluid lipid domains do not appear to be the root cause for either the membrane rigidification observed upon membrane depolarisation, or for the delocalisation of MinD and FtsA observed under the same conditions. Consequently, I also discard hypothesis two.

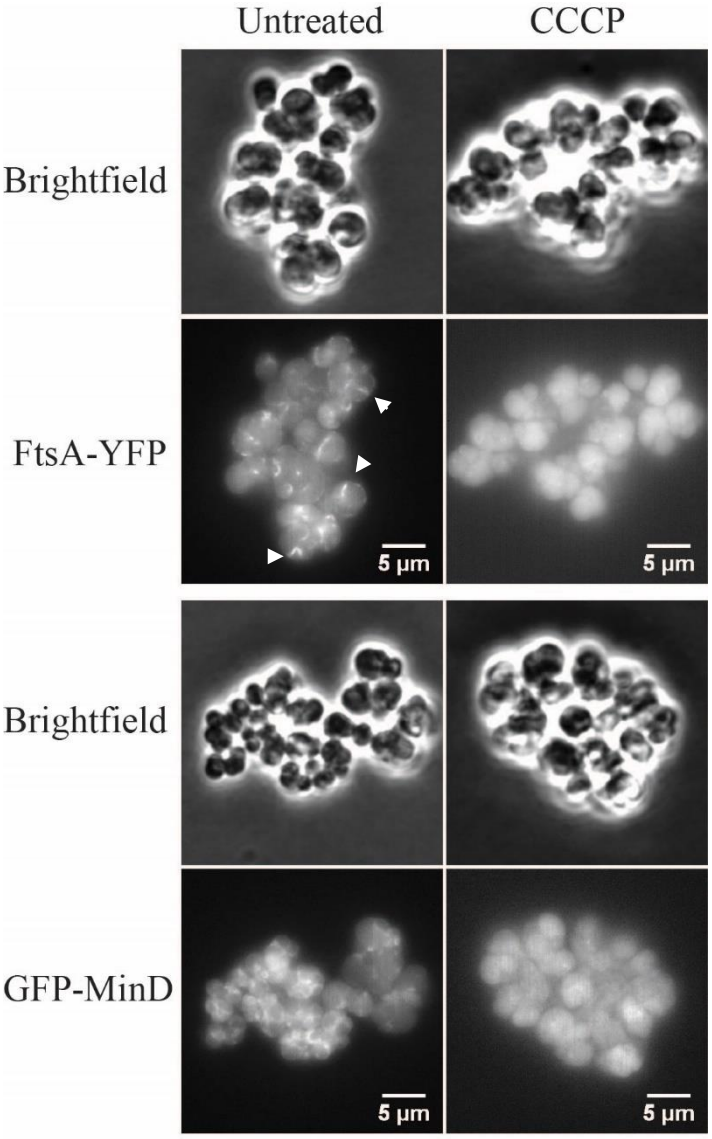

Figure 29: FtsA and MinD localization in the *ΔmreC* mutant. FtsA localizes to septum, as shown with arrows. CCCP treated FtsA detaches from the membrane. MinD localizes throughout the entire membrane. CCCP treated MinD detaches from the membrane.

4.2.3 – Membrane fluidity changes upon changes in pressure across the membrane

I next wanted to test hypothesis three, that electrostriction is the root cause for membrane fluidity changes and MinD / FtsA delocalization upon potential dissipation. Electrostriction is, as was described earlier, what happens when two differentially charged chambers apply bilateral pressure on the insulator that keeps them apart. The extent of electrostrictive force depends on the strength of the electric field across the membrane, and the thickness and relative permittivity of the membrane (Heimburg, 2012). The exact forces involved, and the relevance of this force on the bilayer structure in biological systems, remains poorly understood. However, theoretical considerations and calculations do support the hypothesis that electrostriction can influence membrane fluidity to a significant degree, especially in bilayers close to transition temperatures (Heimburg, 2012). While the verification of this hypothesis requires experiments such as Molecular Dynamics simulations that are beyond the scope of this thesis, consequences of a comparable lateral force acting on lipid bilayers, the force exerted by turgor, on membrane fluidity and protein localisation was analysed. Turgor pressure is formed when compound concentrations vary on either side of a semi-permeable membrane. In Bacteria, the concentration of nutrients is larger than in the surrounding media. To equilibrate the concentrations of compound, water seeks to pass through the membrane into the cells, diluting the cytoplasm. This in turn expands the cell volume pushing the membrane against the cell wall, exerting the turgor pressure.

When the concentration of medium solutes is increased by addition of NaCl or sucrose, the cells experience an osmotic up-shock that results in water leaving the cells. Consequently, the cells lose turgor and the pressure upon the membrane should be relieved. Upon loss of turgor, cells rapidly accumulate K^+ in an attempt to restore turgor (Meury and Kepes, 1981; Wood, 1999). To prevent rapid restoration of turgor, a strain deficient for the higher affinity K^+ transporters, KtrAB and KimA, was chosen for the experiments analysing the changes of membrane fluidity upon osmotic up shock. The deletion mutant will be denoted as *ΔktrAB, ΔkimA* throughout this sub-section. Additionally, the buffer (PBS + 0.2 % glucose) in which the cells were washed was made exclusively from Na-ions (void of K^+) thereby supressing the activity of the remaining low-affinity transporter KtrCD.

The changes in membrane fluidity upon osmotic up-shock can be found in Figure 30. The experiment was carried out by growing the cells under standard conditions, in LB at 37°C. Regardless of staining protocol, whether laurdan or DPH, the final wash step was performed using buffer with the addition of 1 M NaCl or sucrose, followed immediately by

the measurements. In the laurdan measurements, the untreated sample in PBS was at a reasonable GP when compared to the other experiments in the thesis. When osmotic up shock was applied with 1M sucrose, the measured membrane fluidity does not change significantly. In contrast, when osmotic up shock was applied with 1M NaCl, the cells exhibited a significant change in membrane fluidity towards a more rigid state. This change was similar to what was seen when dissipating membrane potential. The untreated sample in the DPH experiment had a somewhat high polarization as compared to other experiments, although this can be explained by yearly fluctuations of temperature in the laboratory. When treated with sucrose, the sample did not exhibit any significant change. When treated with NaCl, I measured a significant rigidification of the membrane, although to a lesser extent than when dissipating membrane potential.

Thus, it appears that sucrose and NaCl do not induce similar changes in fluidity, despite the fact that both compounds should elicit a comparable loss of turgor. This prompted me to investigate whether both shock-treatments are inducing an osmotic up-shock, reducing the size of the cells. Additionally, since NaCl is a salt and sucrose a sugar, I wanted to examine if the up shock applied with NaCl could interfere with the membrane potential, thereby explaining the observed reduction of membrane fluidity.

I performed the cell size and membrane potential assay in the same microscopy experiment. For this, the cells were grown in LB medium, followed by centrifugation and

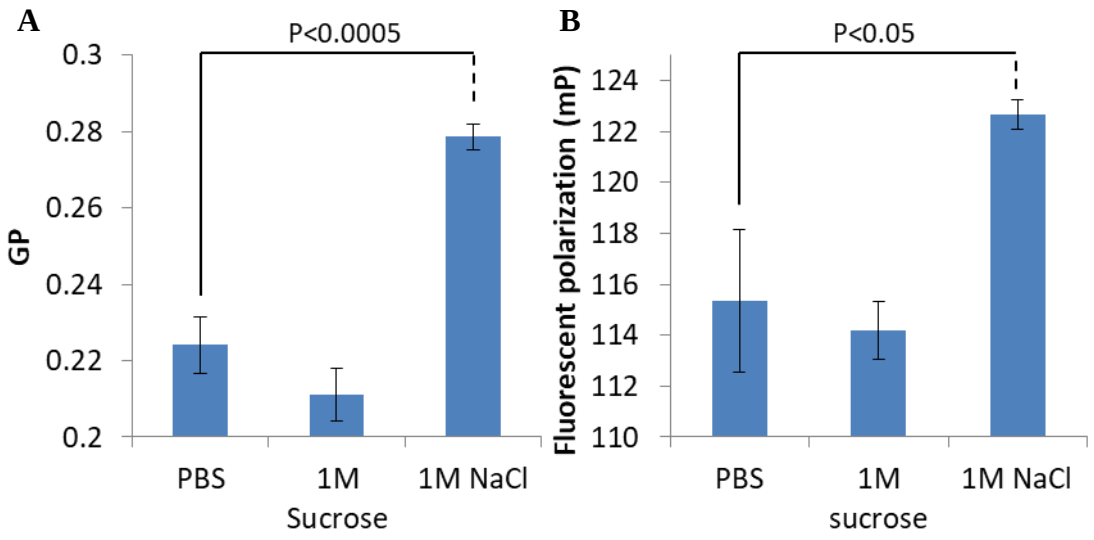

Figure 30: Fluidity changes upon osmotic up-shock by sucrose and NaCl as measured by laurdan and DPH. (A) Laurdan fluidity measurement. Sucrose does not alter membrane fluidity, while NaCl significantly rigidifies the membrane. (B) DPH fluidity measurements. Sucrose does not alter membrane fluidity, while NaCl significantly rigidifies the membrane. strain used: *ΔktrAB, ΔkimA*. Statistical analysis was Students t-test. Error bars represent standard deviation. n=3

resuspension in Na^+ based PBS to inhibit osmotic shock adaptations. The agarose slides were created with supplemented 1M NaCl or sucrose, respectively. The excitation and emission spectrum of $DiSC_3(5)$ partially overlaps with commonly used red fluorescent membrane dyes nile red and FM 5-95. For this reason, phase contrast images, as opposed to membrane stain fluorescent images, were used to approximate the changes in the width of the cells upon osmotic up shock. Consequently, the values should not be interpreted as measurement for the absolute cell width. For comparison to a wild type cell, I normally measure width through membrane stains at 0.750 ± 0.05 µm. The osmotic up-shock width measurement results are found in Figure 31. Untreated cells exhibit an average apparent width of about 1.8 µm, whereas sucrose and NaCl shocked cells were narrower at about 1.68 µm and 1.65 µm, respectively. While both compounds are statistically significant compared to the untreated cells, they remain within statistically similar values when compared to each other. These results demonstrate that the up shock applied with both of the two compounds does indeed induce loss of turgor, reducing the width of the cells. Consequently, the observed differences in the change in fluidity must be due to an unrelated reason, such as collapse of membrane potential.

The microscopy data discussed in the context of the apparent cell width measurements was carried out with cells stained with the voltage-sensitive dye $DiSC_3(5)$, thus allowing the

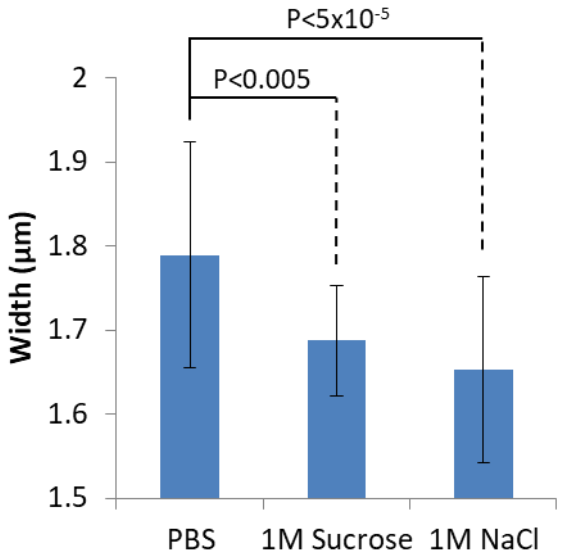

Figure 31: Width changes of the *ΔktrAB, ΔkimA* strain upon osmotic up-shock with sucrose and NaCl. Statisticly significant reductions in cell width are observed for both conditions, with a more substantial change using NaCl. Statistical analysis was Students t-test. Error bars represent standard deviation. n=28 randomly selected cells for each condition.

analysis of how the applied shocks influence membrane potential. When using $DiSC_3(5)$ in microscopy, more intense cellular fluorescence signals indicate a more polarized membrane and thus more energised cells. This is in contrast to the population-based fluorometric plate reader assay where the dye is accumulated in the cell and indirectly detected via the associated fluorescent quenching. Following capture of the images, cells were manually measured for fluorescence intensity as described in materials and methods, Chapter 2.4.3. Sample images from the experiment are found in Figure 32A. The quantification of cellular $DiSC_3(5)$ fluorescence revealed that the sucrose-shocked cells have slightly reduced membrane potential as compared to the untreated cells. In strong contrast, the NaCl-shocked cells show extensive membrane depolarisation with only a small population present with remaining slight membrane polarisation. To ensure that the high salt concentration does not interfere with the microscopic $DiSC_3(5)$ assay, the experiment was repeated with cells that were pre-adapted to grow in the presence of 1M NaCl, thereby removing the applied shock. As seen in Figure 32B, cells grown at 1M NaCl are well stained with $DiSC_3(5)$, ruling out dye-interference as the reason for the observed low $DiSC_3(5)$ signals upon NaCl up shock. It is also worth mentioning that with an apparent cell width of 1.82 ± 0.13 µm, the pre-adapted cells did not show a reduction of apparent cell width, verifying the experimental setup even further.

Together, these results suggest that the fluidity changes that occur when treating with NaCl are indeed due to reduced membrane potential rather than a reduction in the pressure acting on the membrane. We can even rule out that turgor pressure is a significant influencer on membrane fluidity, since the sucrose treated cells reduce their apparent cell width, indicating loss of turgor, but retain their membrane fluidity in a range comparable to cells with turgor. Unfortunately, the results cannot explain why the membrane fluidity is reduced upon membrane depolarization.

Finally I tested if changes in turgor pressure from sucrose osmotic up-shock would influence the localization of FtsA and MinD. NaCl was included to determine if the combination of dissipation of membrane potential and removal of turgor pressure would result in different outcomes. The results are found in Figure 33.

When untreated, FtsA localized to the septum as previously shown. Upon osmotic up-shock using NaCl, the localization was largely the same, although single foci were occasionally observed along the cell membrane. When treated with sucrose, FtsA behaved

similarly to when treated with NaCl, in that single foci occasionally appeared, although to a lesser extent. These findings are not surprising since treatment with CCCP gave similar results. Untreated MinD localized to the septum and cell poles as previously shown. When treated with NaCl, MinD completely delocalizes into sporadic foci across the cell axis. However, when treated with sucrose, MinD exhibited a more heterogeneous localization from cell to cell. In some cells the localization remained the same, with only the occasional foci, whereas other cells had similar localization pattern as seen when treated with NaCl. These results suggested that the pressure exerted on the membrane might be involved with MinD localization.

Together, the results show that our method of attempting to replicate loss of electrostriction across the membrane, via osmotic up-shock-induced loss of turgor using 1M sucrose, does not alter the membrane fluidity. Additionally, NaCl-driven osmotic up-shock

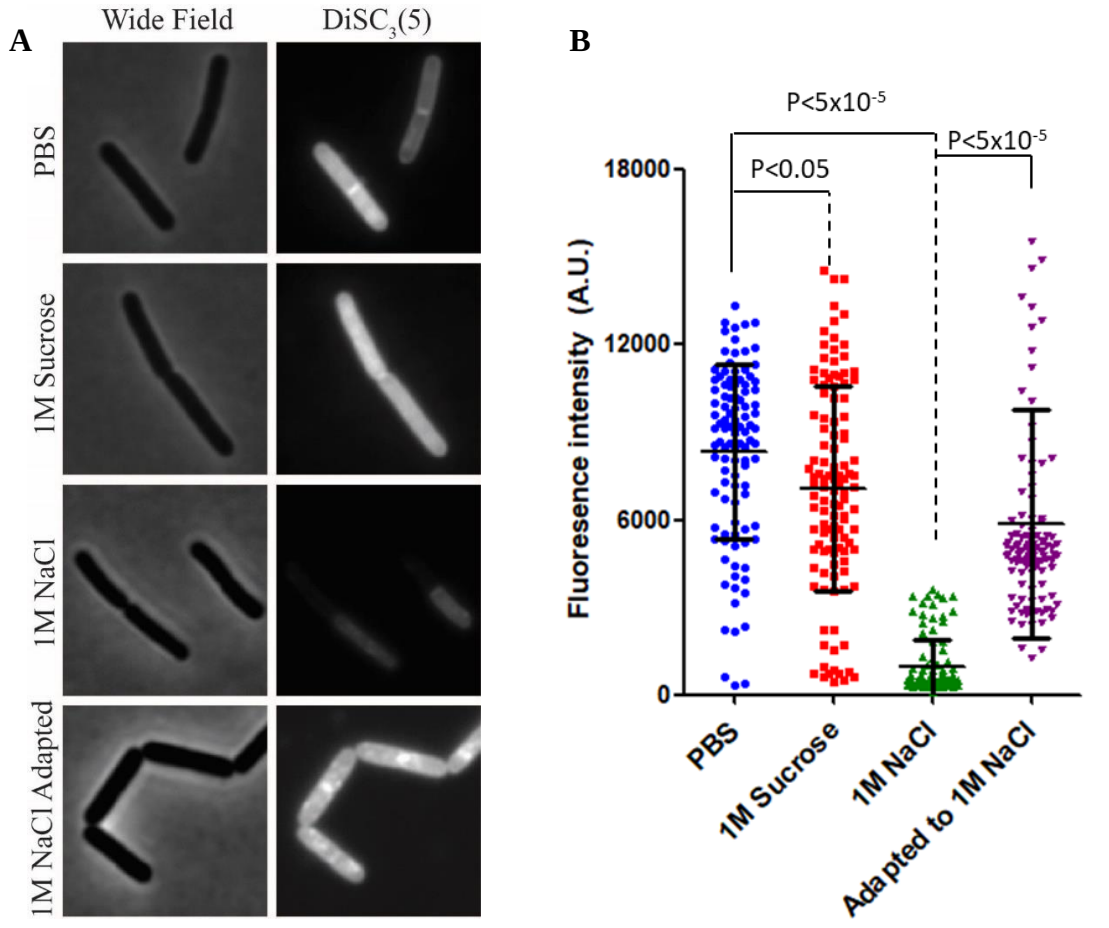

Figure 32: Sucrose and NaCl's influence on membrane potential. (A) Example microscopy images used for quantification of membrane polarization. All images are set to same scale. (B) Quantification of sucrose and NaCl's influence on membrane potential. Untreated cells and sucrose behave comparably similar, while NaCl treated cells are almost completely depolarized. Statistical analysis was Students t-test. Error bars represent standard deviation. PBS n = 105, Sucrose n=116, NaCl n=105, NaCl adapted n=112

causes loss of membrane potential, and is thus not suitable for use as a turgor dissipation inducer. MinD delocalization was induced using 1M sucrose, suggesting that the dissipation of turgor pressure, and therefore of electrostriction when dissipating membrane potential, is involved in the protein's localization. FtsA only delocalized upon NaCl-induced osmotic up-shock, accompanied by membrane depolarization, suggesting that another mechanism could cause the observed localization pattern for this protein.

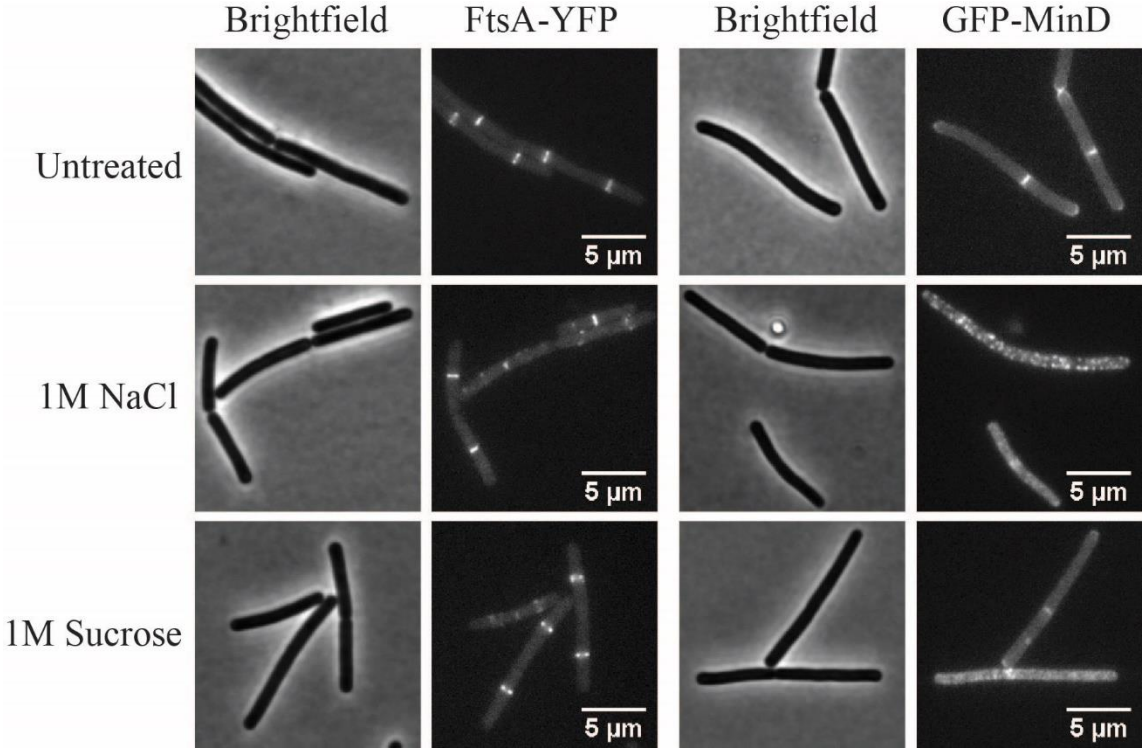

Figure 33: FtsA and MinD localization upon osmotic up-shock. Untreated FtsA localizes to the septum. NaCl and sucrose treated FtsA localizes normally to the septum with sporadic foci appearing. Untreated MinD localizes to septum and cell poles. NaCl treated MinD delocalizes into foci all along the longitudinal axis of the cell. Sucrose treated MinD localizes heterogeneously throughout the cells, with some localizing normally, but weaker than untreated, while other cells exhibit foci generation.

4.3 – Discussion

The aim of the research described in this Chapter was to test several hypotheses related to the delocalisation of peripheral membrane proteins including MinD and FtsA upon membrane depolarisation. The first hypothesis concerned polar cardiolipin domains, which coincidentally co-localized with our two proteins of interest, and how these domains might change the proteins localization upon membrane depolarization. When I tested the first hypothesis, I discovered that the tools utilized for cardiolipin domain staining were less reliable in my hands than claimed in the literature, prompting a further examination of the

domains and the staining tools. The results of the examination of cardiolipin domains are found in Chapter 5, and caused me to discard the first hypothesis entirely.

In the second hypothesis, MreB and its delocalization upon membrane depolarization was theorized to be responsible for the subsequent membrane rigidification, and for the delocalization of other membrane associated proteins such as MinD and FtsA. The full MreB cytoskeletal deletion mutant did not abolish the rigidification, but rather increased the differences between treated and untreated samples. Indeed, this result supports the previous Chapter where I showed that membrane homeostasis regulation was influenced by the cytoskeleton. It is feasible that the membrane is more sensitive to external forces when MreB is missing, as it is an important protein responsible for spatial regulation of certain critical proteins and processes since it guides the elongasome around the cell periphery (Strahl *et al.*, 2014). The results do make sense when comparing to the fatty acid length increases observed in the previous chapter. It is feasible that an increased length of fatty acids would, when packed tightly, induce an increased rigidifying effect. To further test this hypothesis, the experiments could be repeated at different temperatures with altered fatty acid compositions. Additionally, a strain was recently created in our group in which the initial stages of the fatty acid synthesis pathway has been deleted (fatty acid auxotroph), making it possible to fine tune fatty acid composition through the addition of specific fatty acid precursor molecules. This strain could be used to manually alter the fatty acid composition in the cells, thus directly examining how fatty acid length influences membrane rigidification upon depolarization. Additionally, analysing the phospholipid head group profiles in the MreB cytoskeletal deletion mutants would grant an increased insight into any possible composition changes that could influence fluidity. Phospholipid head group composition has previously been shown to greatly modulate membrane fluidities (Fajardo *et al.*, 2011), possibly changing the cellular reaction to external stimuli as well.

I additionally performed MinD and FtsA localization experiments in a *ΔmreC* background, in which MreB remains properly localized upon depolarization. Both MinD and FtsA detached from the membrane upon depolarization, clearly showing that the process of delocalization of these two proteins is MreB independent. Together these results clearly demonstrate that the membrane potential dissipation induced membrane rigidification and the subsequent delocalization of MinD and FtsA occurs in a MreB / RIF-independent manner. These results could explain why MinD and FtsA both delocalize upon membrane potential dissipation in *E. coli* while MreB does not, emphasizing the disconnection between the

delocalization of the three proteins (Strahl and Hamoen, 2010). I therefore discard hypothesis two.

The third hypothesis was based on the concept of electrostriction, and how the loss of electrical potential across the membrane upon membrane potential dissipation would result in membrane rigidification through a relaxation of the fatty acids, which could trigger the delocalization of MinD and FtsA (possibly other proteins as well). I initially decided to use turgor pressure as a proxy for the electrical pressure exerted on the membrane by the electric potential across the bilayer. I used both sucrose and NaCl to exert osmotic up-shocks, and discovered that only NaCl changed the membrane fluidity. Upon closer inspection, it became evident that the measured rigidification was due to membrane depolarization rather than changes in turgor pressure. When examining cells during osmotic up-shock using sucrose, we discovered that loss of turgor was induced without dissipating membrane potential. From our data, it can be concluded that the osmotic up-shock using 1 M sucrose is not enough to significantly influence the membrane fluidity, nor does it influence FtsA localization. Surprisingly, the sucrose-induced osmotic up-shock did alter the localization of MinD, although for unknown reasons. Furthermore, it is largely unknown how much force is exerted on the membrane by electrostriction, making it difficult to compare to turgor. Although I have no direct experimental evidence to suggest that electrostriction is involved in depolarization-induced membrane rigidification, previous studies have shown that the cytoskeleton can reduce the effects that electrical pressure exerts on a membrane (Brooks, 2014). A reduction in the observed effect by electrostriction when an active cytoskeleton is in place could explain why I see a significantly more rigid membrane after depolarization in (*ΔmreB, Δmbl, ΔmreBH*), as it could have lost its protective ability as the cells became spherical, thus exhibiting more rigid membrane upon depolarization. The data gathered does not confirm nor disprove hypothesis three, although there were indications supporting the notion that pressure across the membrane does influence the localization of certain proteins, such as MinD. Further studies are required to further elucidate the mechanism behind membrane potential dissipation induced fluidity changes and protein delocalization. One such study has already been planned with Dr. Ulrich Zachariae (Dundee University), in which molecular dynamics will be utilized in an attempt to create a model examining the physical properties of the membrane during potential dissipation.

Additionally, we know that electrostriction and membrane potential are intrinsically connected, making it impossible to dissipate membrane potential without relieving

electrostriction as well. This does indeed make sense, as when dissipating membrane potential, we allow ions to pass down the electro-chemical gradient, until the electric potential across the membrane has disappeared entirely. As the two phenomena are linked, I can assume that the rigidification is due to a relaxation of the membrane regardless. As this is the case, perhaps measuring the changes in fluidity upon osmotic up-shock should be performed in already depolarized cells. Having removed the apparently larger of the two pressures across the membrane, it might then be possible to measure any remaining changes exerted by the turgor pressure.

To further investigate FtsA and MinDs localization upon fluidity changes of the membrane, additional experiments have to be performed. Using the fatty acid auxotroph strain in combination with fluorescent FtsA and MinD, it should be possible to image their localization pattern across multiple fluidity stages, once and for all determining if their localization is sensitive towards changes in membrane fluidity. I could additionally tune the fatty acid composition to be similar to those of the MreB cytoskeleton deletion strain. Through this, I could examine if the increased rigidification upon potential dissipation is due to the altered fatty acid composition or the loss of MreB.

Finally, I can conclude that the first two hypotheses I examined, cardiolipin dependency and MreB delocalization dependency were not involved in membrane potential dissipation induced membrane rigidification and MinD and FtsA delocalization. Additionally, we did not confirm that electrostriction is the main mechanism governing the rigidity or the protein delocalization. Despite this, we have ascertained certain indications that pressure across the membrane does indeed influence protein localization, as seen with MinD, and that turgor pressure alone is not enough to alter membrane fluidity.

Chapter 5 – Cardiolipin does not form detectable membrane domains in *Bacillus subtilis*

5.1 – Introduction

Cardiolipin is a major phospholipid component of the cytoplasmic membrane in most bacteria, including *B. subtilis* (C. S. Lopez *et al.*, 1998). Rather than being uniformly distributed, it has been postulated that cardiolipin forms specific clusters, or domains, that localise to the poles and cell division sites in a large number of studied bacteria including *E. coli* (Mileykovskaya and Dowhan, 2000), *B. subtilis* (F. Kawai *et al.*, 2004), *Pseudomonas putida* (Bernal *et al.*, 2007a), *Streptococcus pyogenes* (Rosch et al., 2007), *Haloquadratum walsbui* (Lobasso et al., 2009), *Mycobacterium smegmatis* (Maloney et al., 2011), *Enterococcus feacalis* (Tran et al., 2013), and *Pseudomonas aeruginosa* (El Khoury et al., 2017). Due to its molecular structure with four fatty acid moieties attached, cardiolipin adopts an atypical cone-shape that favours curved membrane areas (Renner and Weibel, 2011) which has been postulated as a potential explanation for the preferential localization to cell poles and cell division sites (Mileykovskaya and Dowhan, 2009). The main means to visualise cardiolipin, and therefore to strongly promote the concept of cardiolipin-specific lipid domains, has been the use of the cationic membrane dye N-nonyl acridine orange (NAO). Due to its positive charge, NAO preferentially stains membranes containing anionic phospholipids. Furthermore, it was postulated based on studies conducted in *E. coli* that, upon specific interaction with cardiolipin, NAO exhibits a strong emission red-shift. Consequently, red fluorescence emitted by NAO has been used as a specific cellular reporter for cardiolipin (Mileykovskaya and Dowhan, 2000). However, the idea that NAO is cardiolipin specific has been questioned in *E. coli* (Oliver *et al.*, 2014), which has questioned if it can be used as a cardiolipin determinant at all.

Initially we hypothesised that changes in the domain formation of cardiolipin could be responsible for the membrane potential dissipation-induced delocalisation of cell division proteins MinD and FtsA, which both bind anionic membranes by means of a membrane targeting cationic amphipathic helix. However, since membrane depolarization also induces clusters of fluid lipid domains due to delocalisation of MreB (Strahl *et al.*, 2014), we first needed to verify the specificity of NAO in order to distinguish these two parallel processes from each other.

By carefully re-analysing the staining procedure used to visualise cardiolipin domains, and by analysing the staining specificity of NAO using strains with modified lipid composition, including those deficient for cardiolipin, we reached the conclusion that the previously observed domains are likely an artefact of the staining protocol used, and that NAO shows no specificity towards cardiolipin in *B. subtilis* membranes. As a consequence, we also abandoned the hypothesis that induced changes in cardiolipin domain organisation underlie the membrane potential-sensitivity of MinD and FtsA. These studies were carried out as a close collaboration between Alex Pogmore, a BSc-student in our lab, my supervisor Henrik Strahl, and myself, and the results of the chapter have been published with me as co-first author (Pogmore *et al.*, 2018).

5.2 – Results

5.2.1 – Staining conditions and the promotion of lipid domain formation

When we initially started working with NAO, we were surprised to find that in our standard growth conditions (LB medium and 37 °C) and when stained with the routine membrane staining protocol we use, which consists of staining logarithmic growth phase cells at the growth temperature while keeping the cells thoroughly aerated, no NAO-stained domains were observed. By contrast, we observed an entirely smooth membrane stain in both the green range (500-550 nm) and at the postulated to be cardiolipin-specific red range (593-667 nm), as seen in the left panel of Figure 34a. Only at very low frequency were occasional foci observed (see Table 15). However, instead of using LB medium (the standard growth medium in our group), the original paper describing cardiolipin domains in *B. subtilis* used DSM medium (F. Kawai *et al.*, 2004). We therefore also applied our standard staining conditions for cells grown in DSM. Surprisingly, we still observed an entirely smooth membrane stain at both wavelengths, as shown in the right panel of Figure 34a. The only elevated fluorescent signal was detected at septum, which indeed was interpreted by Kawai *et al* as cardiolipin enrichment (Kouji Matsumoto, personal communication). However, the complication in the interpretation of

Number of foci / cell	LB medium	DSM medium
0	96 % (n=180)	94 % (n=256)
1	2 % (n=3)	4 % (n=11)
>2	2 % (n=4)	2 % (n=5)

Table 15: Number of foci observed in NAO-stained cells. Cells grown in both LB and DSM medium at 37°C have very few foci when stained at the growth temperature. Data gathered in collaboration with Henrik Strahl.

septal fluorescence signals are the two membrane layers present at the septum, resulting in expected fluorescent signal levels that are twice those found in other membrane areas. Consequently, if the NAO fluorescence signal found at septum exceeds twice of that found on lateral membrane, we can assume that there is indeed an enrichment of NAO-stained lipids, and if the red wavelength range shows even further increase, we can assume that these lipid are likely to be cardiolipin. The lines used for measuring the fluorescence intensities in the cells are shown in Figure 34c. When quantified, we found that the lateral fluorescent signal levels at 525 nm were approximately 2000 (a.u) while the septal signal was approximately 3200 (a.u) (Figure 34d).

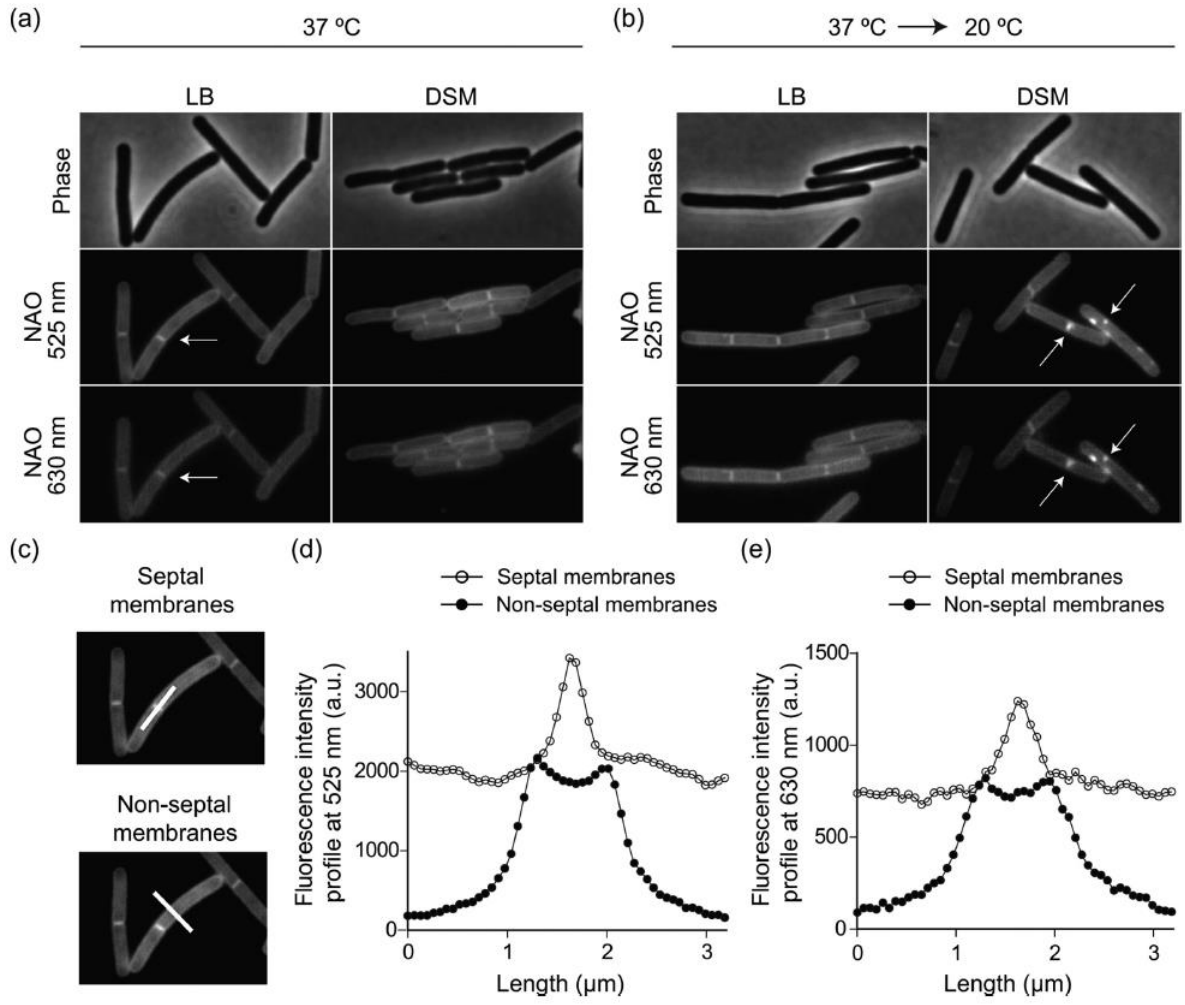

Figure 34: (a) Phase contrast and fluorescent images of NAO-stained *B. subtilis* wild type cells grown in LB and DSM media at 37 °C. The cells were stained for 20 minutes at 37°C. The arrow indicates a cell division site. (b) Phase contrast and fluorescent images of NAO-stained *B. subtilis* wild type grown in LB and DSM media at 37 °C but stained at 20 °C for 20 minutes. The emerging domains are indicated by an arrow. (c) Fluorescent micrographs of NAO stained cells. The lines indicate the sections used for the quantification of fluorescent intensities shown in panel (d) and (e). (d) NAO fluorescence line scans measured across septal and non-septal membranes at 525 nm for cells grown in LB medium and stained for 20 min at 37°C. (e) The corresponding NAO fluorescence line scans measured across septal and non-septal membranes at 630 nm. Data generated in collaboration with Henrik Strahl and Alex Pogmore. (Pogmore *et al.*, 2018)

The signal was, thus, even lower than the values expected from two parallel membrane layers. A comparable relationship was found when analysing the red-shifted emission of NAO (Figure 34e). Here the lateral signals peak at approximately 700 (a.u) while the septal signal reaches approximately 1300 (a.u). Thus, we must conclude that the elevated septal fluorescent signal is due to the membrane configuration and does not imply local enrichment of cardiolipin.

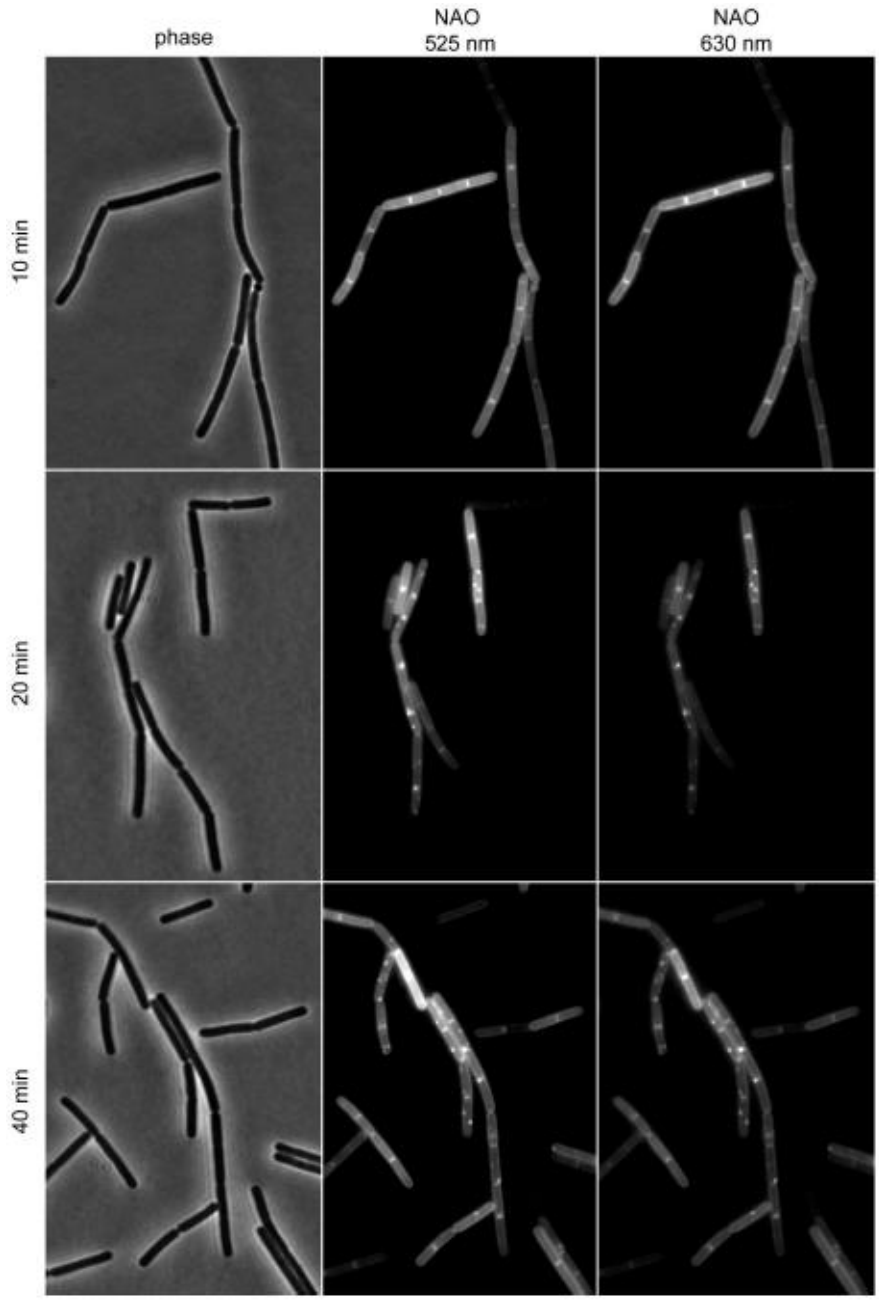

Figure 35: Phase-contrast images (left panel), and NAO fluorescent membrane stains at 525 nm (middle panel) and at 630 nm (right panels) depicting a staining time-course for logarithmic growth phase *B. subtilis* cells. For these micrographs the cells were grown in DSM medium, and stained with NAO at 20°C for a time period indicated in the left. Strain used: *B. subtilis* 168 (wild type). The data was gathered in collaboration with Henrik Strahl. (Pogmore *et al.*, 2018)

In their publication, Kawai and co-workers describe the NAO-staining being carried out at room temperature, as opposed to at growth temperature. In an attempt to reproduce their experimental conditions, we repeated the staining at 20°C for 20 min. For cells grown in LB medium, no detectable difference in the staining pattern was observed compared to the cells stained at 37°C (Figure 34b). However, when applying the same staining conditions for cells grown in DSM medium, clear foci similar to the ones reported in the original publication could now be observed (Figure 34b). The foci only appeared after 20 min incubation at 20°C (Figure 35), suggesting the domain formation is not an immediate consequence of the applied cold shock, but likely represents some so far unknown cellular process induced as a response to cold shock. Furthermore, the results clearly show the observed domains formation is medium-specific.

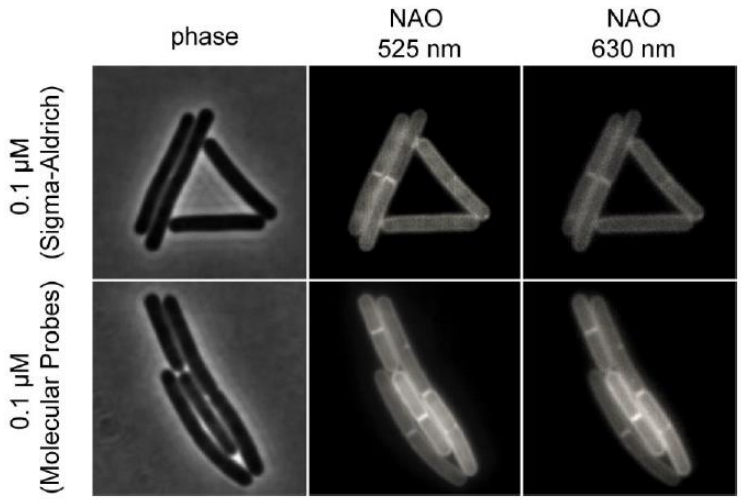

Figure 36: NAO purchased from two different companies Sigma-Aldrich and Molecular probes. Phase contrast and NAO fluorescent emission images. NAO from both companies exhibit smooth membranes. I generated all the data used in this figure. (Pogmore *et al.*, 2018)

Throughout our initial analysis of the membrane stains, we had used the NAO purchased from Sigma-Aldrich. To rule out that the lack of domains observed in LB and in the absence of cold-shock was due to the specific batch of NAO, we decided to test the compound acquired from another manufacturer. However, cells stained in LB medium at normal growth temperature also exhibited smooth membrane stains at both wavelengths for both compounds (Figure 36). Thus, we conclude that the absence of NOA foci is not due to batch-variation of the dye. After the surprising finding that NAO only detects lipid domains in DSM medium upon cold shock, we decided next to examine if the observed domains are cardiolipin specific.

5.2.2 – Determination of cardiolipin specificity of NAO in B. subtilis

In order to examine if the domains observed using NAO are clusters of cardiolipin, we made use of a *B. subtilis* strain in which the three cardiolipin synthase encoding genes *clsA*, *clsB*, and *ywiE* were deleted. This approach is made possible due to the fact that cardiolipin is not essential in *B. subtilis*. To ensure that the constructed triple deletion mutant is indeed cardiolipin-deficient, the strain's phospholipid composition was analysed using thin-layer chromatography. As shown in Figure 37a, the mutant that was deficient for all the cardiolipin synthases does not produce detectable quantities of cardiolipin. Not surprisingly, when cardiolipin synthesis capability is removed, other lipid species accumulate instead, as revealed by the more intense stains of PG and PE in the cardiolipin synthase deficient strain background.

Using the synthase deficient strain, we next tested if the NAO-staining was specific for cardiolipin in *B. subtilis*. This was conducted using the staining regime that induced visible domains, in other words cells grown in DSM medium and stained for 20 min. at 20 °C. Surprisingly, this strain also generated a NAO staining pattern with clearly visible domains that were indistinguishable from the ones observed in the wild type (Figure 37b), thus ruling out that these domains are formed by cardiolipin.

The surprising finding that the cold shock-induced domains are cardiolipin-independent prompted us to investigate what kind of membrane structure NAO was actually staining under these conditions. A possible hypothesis is that NAO stains the RIFs that cluster with MreB. In order to determine if RIFs are also induced upon cold shock, and if NAO is capable of staining them, we analysed the staining pattern in a strain deficient for the MreB-homologs (*ΔmreB, Δmbl, ΔmreBH*). However, when stained with NAO and subjected to cold shock, this strain exhibits membrane foci comparable to those observed in wild type (Figure 37b). We can therefore exclude MreB dependent RIFs as the nature of the NAO stained domains.

NAO-stained domains have recently been found in the absence of cardiolipin in *E. coli* as well (Oliver *et al.*, 2014). Here, the NAO domains were shown to be dependent on another anionic phospholipid, namely phosphatidylglycerol (PG) (Oliver *et al.*, 2014). In *B. subtilis*, PG is essential for maintaining a functional membrane and depletion of the PG synthase, PgsA, results in loss of membrane integrity (Strahl *et al.*, 2014). Instead of attempting to deplete PG, we opted to use an additional dye to determine if the NAO-stained domains are

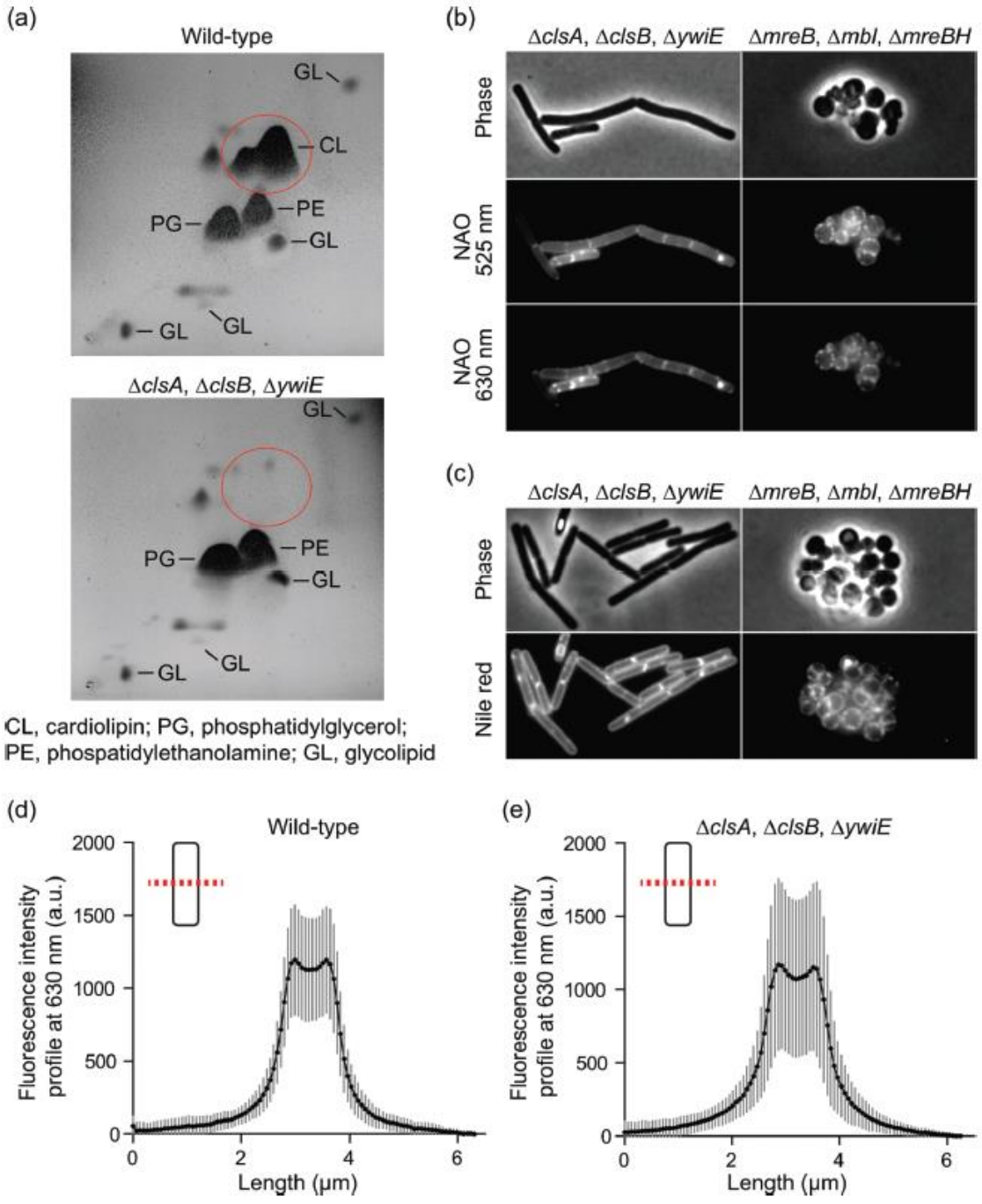

Figure 37: (a) Thin-layer chromatography of lipids extracted from *B. subtilis* wild type strain, and a strain deficient for cardiolipin synthase genes resulting in the complete absence of Cardiolipin. (b) Phase contrast and NAO fluorescence images of both the green (525 nm) and red (630 nm) wavelength of the cardiolipin synthase deficient strain and a strain deficient for MreB-homologs (Δ*mreB,* Δ*mbl,* Δ*mreBH*). Both strains exhibit readily observable NAO-stained foci in the membrane. (c) Phase contrast and Nile Red membrane stain in the cardiolipin synthase deficient strain and the strain deficient for MreB-homologs (Δ*mreB*, Δ*mbl*, Δ*mreBH*). Nile Red stains readily observable foci in both strains. (d) Average NAO fluorescent intensity profile in the red-shifted spectrum (630 nm) in the wild type strain measured perpendicular to the cell axis. Error bars represent standard deviation n=30 (e) Corresponding average NAO fluorescent intensity profile in the red-shifted spectrum (630 nm) measured for the cardiolipin synthase-deficient strain. Error bars represent standard deviation n=30. The data was obtained in collaboration with

anionic in nature. Instead of using cationic dyes such as NAO, we repeated the staining of cardiolipin synthase and MreB-deficient strains with the uncharged membrane dye Nile red, which under normal circumstances stains the membrane smoothly. As shown in Figure 37c, both strains exhibit similar domains with Nile red as those stained with NAO. These results suggest that the NAO domains formed in *B. subtilis* are unlikely to be comparable to the charge dependent domains found in *E. coli*, but rather an entirely separate cold shock-dependent phenomenon.

Finally, to determine if the postulated cardiolipin-specificity of the red-shift, which was based on *E. coli* data (Mileykovskaya and Dowhan, 2000), holds true for *B. subtilis* membranes, we measured the NAO fluorescence intensity across the membrane in both the wild type strain and the cardiolipin synthase-deficient strain. It would be expected that the signal should be higher in cardiolipin-containing membranes irrespective of domain formation. However, the two strains exhibited similar fluorescence intensities at both emission wavelengths (Figure 37d). This clearly demonstrates that NAO is not a specific stain for cardiolipin in *B. subtilis* membranes.

5.2.3 – NAO itself likely induces domains at higher concentrations

Previously, it has been postulated that in order to reliably stain polar lipid domains, higher concentrations of NAO are required than are commonly used (Oliver *et al.*, 2014). In contrast, other research groups claim that lower concentrations are needed in order to consistently stain cardiolipin domains (Mileykovskaya and Dowhan, 2009). Being a contentious subject, we decided to test if the previously observed polar-localized domains are present at higher concentrations. We tested a range of concentrations between 100 nM and 2 µM. Indeed, upon which we started observing polar and septal-localized domains forming at concentrations ~1 µM (Figure 38a). Furthermore, the cytoplasmic NAO signal increased concomitantly with concentration, suggesting a saturation of membrane association that could be toxic. To ensure that the dye was not interfering with growth at these elevated NAO concentrations we performed a MIC determination which revealed that, unlike in *E. coli*, NAO is growth-inhibitory at concentrations 1 µM and above. Worryingly, both the domain formation and inhibition of growth occurs at 1 µM, which suggests that the observed staining might be biologically meaningless and in fact induced by NAO-toxicity.

Nevertheless, we tested whether the domains observed at higher concentrations of NAO were cardiolipin specific. However, comparable domains were observed in the cardiolipin synthase-deficient strain when stained with 2 µM NAO (Figure 38b). This clearly shows that even the domains formed at growth inhibitory concentrations of NAO are not cardiolipin specific. Furthermore, we tested if these high NAO concentration domains could be localized along with the MreB-specific RIFs, but here we also found the domains in the MreB cytoskeletal deletion strain (Figure 38b). Finally, we wanted to test if the high concentration NAO domains are formed by clustering of anionic lipids. As described earlier, PG is essential in *B. subtilis*. However, the zwitterionic phospholipid phosphatidylethanolamine is not essential. It is feasible that the anionic PG and cardiolipin forms domains within the membrane by exclusion of zwitterionic PE. We therefore deleted the gene encoding the PE synthesizing enzyme *Δpsd*, pushing the membrane towards an anionic composition. If the domains are dependent on anionic exclusion from zwitterionic areas of the cells, we would expect a smooth membrane stain in the mutant. However, the

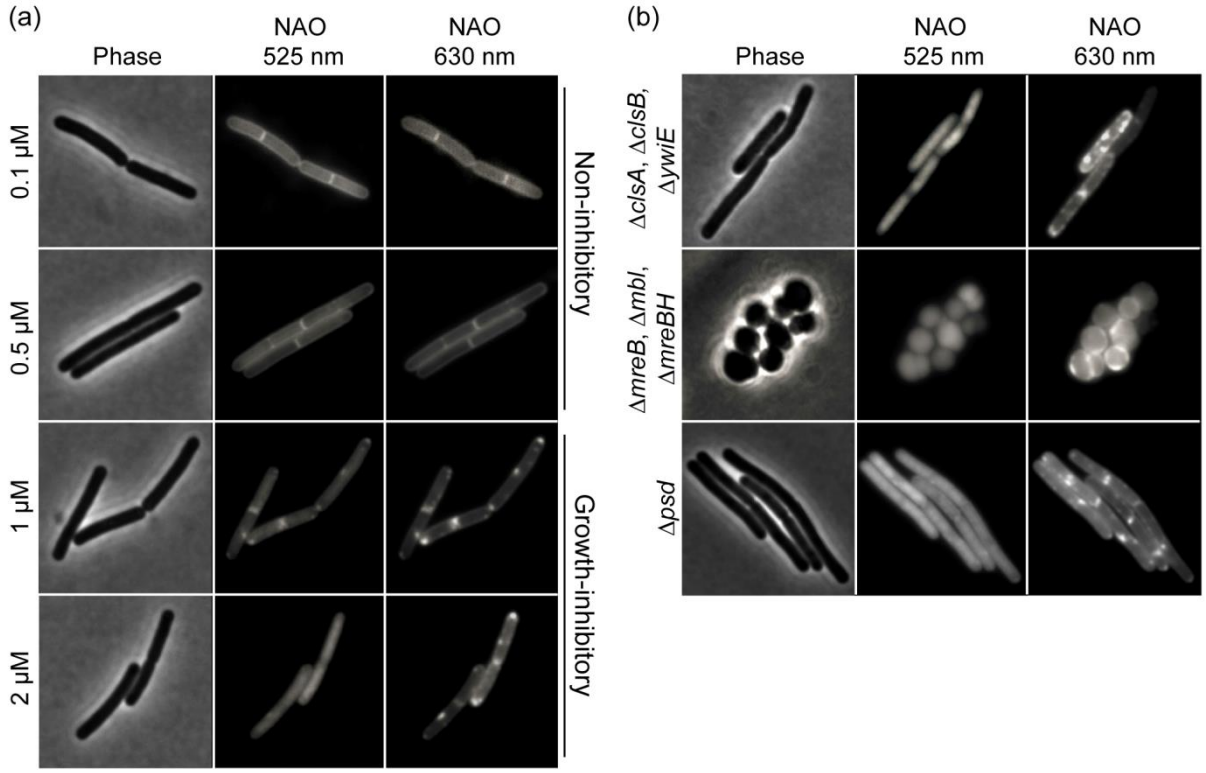

Figure 38: (a) Phase contrast and NAO fluorescent images of logarithmically growing *B. subtilis* wild type cells stained with NAO at various concentrations at 37°C for 20 minutes. Increasing concentrations of NAO induces polar and septal localized domains, but also increased green cytoplasmic signals. Note, the minimal inhibitory concentration (MIC) of NAO for *B. subtilis* is 1 µM. (b) Phase contrast and NAO fluorescent images of cells stained using 2 µM NAO. The induced domains are observed in the strains deficient for cardiolipin synthases, MreB-homologs, and the phosphatidylethanolamine synthase. I generated all the data used in this figure. (Pogmore *et al.*, 2018)

high NAO-concentration triggered domains were still observed, thus ruling out this possible explanation (Figure 38b).

In conclusion, the presented data clearly shows that, under normal growth conditions no domain that can be stained with NAO are present in *B. subtilis* membranes. Furthermore, NAO showed no specificity towards cardiolipin in this organism.

5.3 – Discussion

Cardiolipin enriched domains are arguably the most comprehensively studied and discussed type of lipid domain in *E. coli* (Mileykovskaya and Dowhan, 2009). The conserved existence of this domain in other bacteria has largely been accepted, most commonly based on microscopic evidence of NAO-stained cells. Here we show that staining specificities based on studies conducted in one organism should not be readily extrapolated to hold true for another, especially those with substantially different lipid composition, such as *B. subtilis*.

At low concentrations of NAO we did not observe any domain formation in the membrane of *B. subtilis* at our standard conditions that are designed to minimise changes in all other parameters apart from the presence and absence of the dye. In contrast, we only observed NAO-stained lipid domains in DSM medium upon extended (20 min) staining at 20°C, thus applying the cells a cold shock of 17 °C. Furthermore, the media dependency suggests that the observed domains are not an essential part of *B. subtilis* cold shock response, but rather more subtle phenomenon happening under certain specific circumstances. While speculative, the fact that the domains can be stained with both cationic NAO and neutral Nile Red and are induced under condition in which membrane fluidity is strongly reduced, suggests that these domains are characterised by increased fluidity. Due to lower lipid packing density, these areas are preferably stained by most membrane intercalating dyes. However, since these domains also emerge in the absence of MreB-cytoskeleton they appear to be distinct from the fluid lipid domains associated with the cell wall synthesis machinery (RIFs). Significantly more work is needed to appropriately characterise the composition and the biological function of this novel type if lipid domain.

The NAO stained domains forming at higher dye concentrations are, if indeed induced by NAO as seems likely, biologically irrelevant. At higher concentrations, we found that not only is NAO toxic in *B. subtilis*, but the dye had saturated the membrane and was able to

diffuse into the cytoplasm, thereby either causing toxicity by virtue of very high concentration in the membranes, or by inhibiting a critical cytoplasmic cellular process. When saturating the membrane with a probe, it is feasible that the probe itself confers changes in the packing of phospholipids. The induced changes might forcibly create domains with certain characteristics, and these are the ones in which NAO cluster. Alternatively, if the domains are biologically relevant, they might form due to high concentrations of NAO in the membrane in an attempt to contain the potential toxic compound in certain areas of the bilayer, although this hypothesis seems unlikely.

In *E. coli* it was already discovered that NAO-stained domains can form in the absence of cardiolipin, although still in an anionic dependent manner (Oliver *et al.*, 2014). It was therefore perhaps not surprising that the cardiolipin specificity of NAO is not as high as previously assumed. What is surprising, however, is the fact that the domains observed in *B. subtilis* also readily stained with neutral Nile Red and are therefore not exclusively characterised by the head group charge. Consequently, the two phenomena (polar anionic domains in *E. coli* and the cold shock induced domains in *B. subtilis*) are likely to be distinct biological processes.

Additionally, the existence of cardiolipin domains are now even being questioned in the very organism they were first discovered, *E. coli*. One research group claims that the cardiolipin domains only are visible when staining with high concentrations of NAO, where at lower concentrations a smooth membrane stain is exhibited (Oliver *et al.*, 2014). This is indeed in line with our observations. This could indicate that either cardiolipin domains simply need high concentrations of dye to penetrate the domains or, more likely, that the elevated concentrations of dye itself induces the formation of the domains. By contrast, another group claims that the NAO concentrations required for observing the cardiolipin domains should be low (Mileykovskaya and Dowhan, 2000; Mileykovskaya and Dowhan, 2009). The problem with this claim is that under the conditions stated in the publication, multiple research groups are finding it difficult to reproduce the domain staining. Indeed our own data simply cannot reproduce the claimed results. We therefore think that even in *E. coli*, there might be an underlying mechanism which remains to be fully elucidated.

Chapter 6 – Membrane Potential Dissipation-Triggered Lysis

6.1 – Introduction

In the previous chapters, we examined how the membrane composition changed upon changing environment with and without the MreB cytoskeleton, as well as explored what happened to certain proteins upon environmental challenges such as membrane depolarization in the short term. Here, we will explore what happens to the cells over longer time periods upon challenge with membrane potential dissipating compounds.

It has long been known that *B. subtilis* initiates lysis upon membrane depolarization or de-energization in general (Kaufman and Bauer, 1958). An attempt at describing the mechanism underlying the cell lysis was made in 1981 (Jolliffe *et al.*, 1981). In their paper, Jolliffe and co-authors postulated that protons, which in a normally functioning, metabolically active cell are continually pumped out of the cytoplasm and into the extracellular surroundings, diffuse away from the surface of the cell. The continuous flow of protons through the peptidoglycan layer surrounding the cell, the authors argue, would generate a stable pH gradient across the cell wall matrix. The resulting local low pH was postulated to regulate the extracellular cell wall-degrading autolysins, thereby providing necessary control over the essential but potentially hazardous cell wall turnover. In the absence of continuous proton flow upon loss of respiration or collapse of the pH gradient across the membrane, the local low pH within the cell wall matrix would rise. This, in turn, would deregulate the autolysins. The result of such dysregulation would result in unwanted digestion of the cell wall material ultimately leading to critical destabilization of the cell wall matrix and osmotic lysis (Jolliffe *et al.*, 1981). However, subsequent studies have revealed that, rather than diffusing away from the membrane surface, protons pumped out of the cell by the respiratory chain are predominately retained within a thin layer of structured water overlaying the charged membrane surface, prior to being recycled back to the cell via transporters (such as the F_1F_0 ATP synthase) (Cherepanov *et al.*, 2003). Discarding the notion that protons exported by the respiratory chain diffuse away from the cell surface in significant quantities, questions the previous model regarding the mechanism by which a collapse of proton motive force (PMF) or respiration triggers autolysis.

In this Chapter we attempt to elucidate the precise inducer of cellular lysis upon PMF dissipation, as well as the mechanisms involved. MreB is involved in the regulation of autolysins and is sensitive to PMF collapse, and is thus a good candidate to explain the

induced lysis. Additionally, MreB is known to delocalize upon membrane depolarization, and might therefore be involved in regulatory malfunctions that are conferred by the loss of membrane potential and PMF collapse. Finally, bacteriolysis is a large component of the antibacterial mode of action of membrane targeting antibiotics such as daptomycin. Therefore, the question arises whether triggered autolysis is involved in the action of membrane antibiotics. I used the proton de-coupler CCCP as the standard PMF-collapsing agent (Heytler and Prichard, 1962), although daptomycin, with the complex envelope-targeting mechanism (Muller *et al.*, 2016); gramicidin, the monovalent cation channel (Hladky and Haydon, 1972); and the human defensin LL-37, which forms transient membrane pores (Oren *et al.*, 1999) were also utilized.

6.2 – Results

6.2.1 – PMF-collapse induces lysis in B. subtilis

In order to verify that collapse of PMF actually induces cell lysis in *B. subtilis*, I decided to use the proton un-coupler CCCP (Heytler and Prichard, 1962). For this aim, I performed plate reader lysis assays in which the OD was measured every 5 min. When adding CCCP to exponentially growing *B. subtilis* 168 cells, growth was immediately arrested for

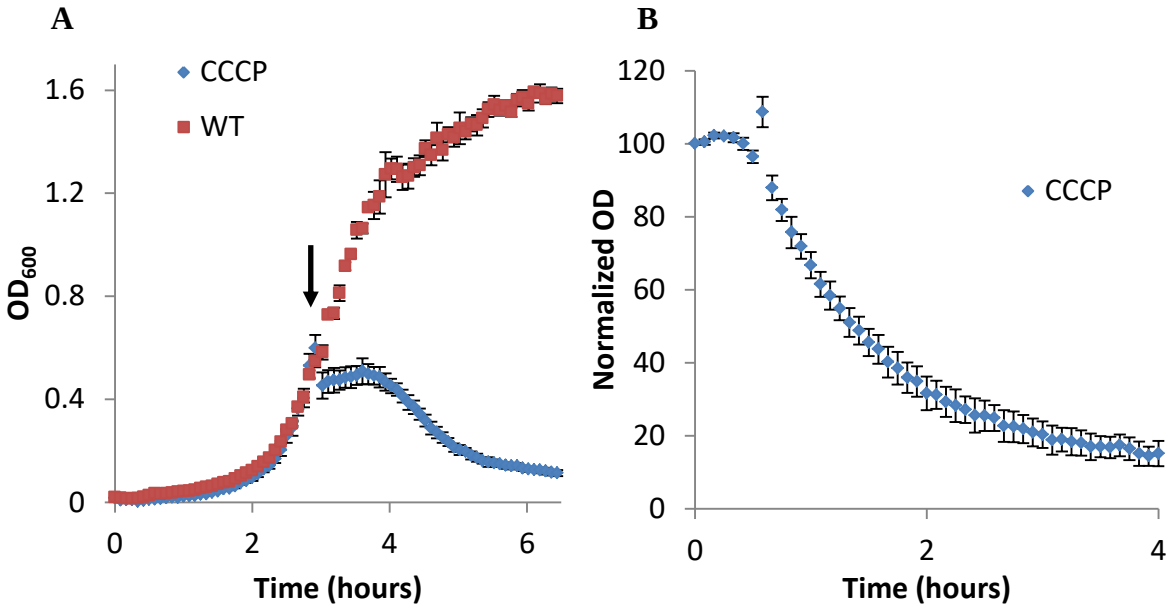

Figure 39: Growth and lysis of wild type *B. subtilis*. (A) The graph depicts the growth and lysis curves of *B. subtilis* in the presence and absence of the proton uncoupler CCCP (100uM). The time point of CCCP addition is indicated with an arrow. The cells were grown in LB medium at 37 C. (B) Graph depicting the lysis kinetics of the compound CCCP, in wild type *B. subtilis*. The normalized OD is with the initial OD upon compound addition set to 100. The strain used: *B. subtilis 168* (wild type). Error bars represent standard deviation. n=3

approximately 30 min., followed by subsequent rapid lysis that was largely completed within 3h (Figure 39A). Every lysis experiment shown in this thesis was essentially performed as shown in Figure 39. However, in order to compare the type of lysis behaviour under different growth conditions and in different strain backgrounds, the data is in the following shown normalized against the initial OD upon addition of the compound (Figure 39B).

Having shown that dissipation of PMF did indeed trigger cell lysis in our standard laboratory growth conditions; I next wanted to examine which, if any, environmental parameters influenced and/or modulated the lysis process.

6.2.2 – Temperature, growth phase, and growth speed affects lysis

We tested the lysis behaviour of our wild type at two different temperatures to determine whether lysis occurred at different velocities according to growth temperature, and to examine how the behaviour compared to the original 1981 hypothesis. According to the old hypothesis, we should experience lysis at all viable growth temperatures, as any pH gradient should be temperature independent.

When performing the CCCP-triggered lysis experiment at 37°C, we observed that the cells immediately stop growing and underwent lysis as previously described. However, when

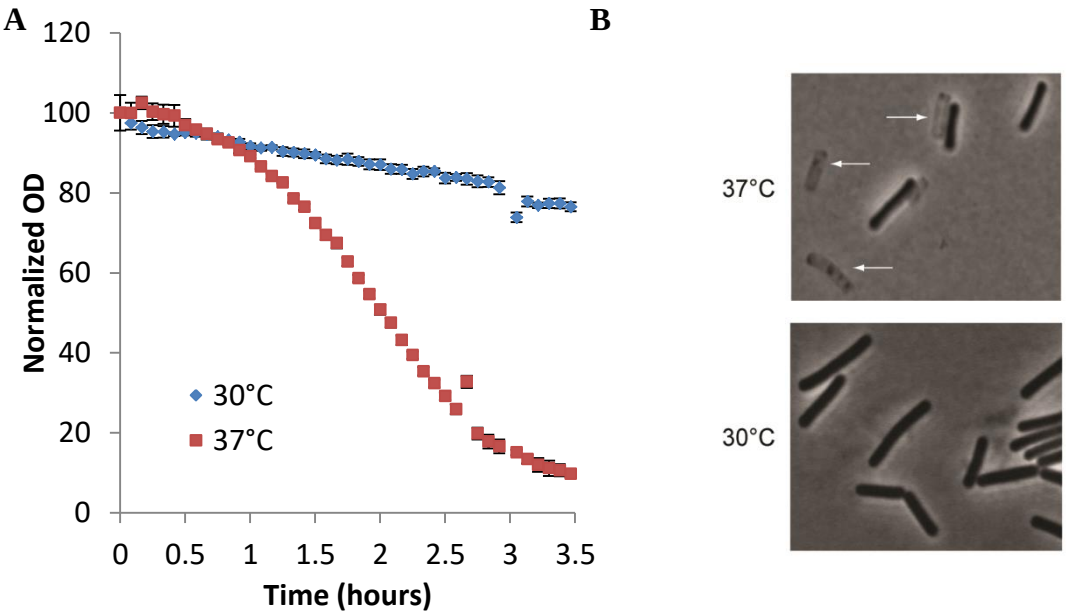

Figure 40: (A) Graph depicting the lysis kinetics of WT *B. subtilis* treated with CCCP at 37°C and 30°C. Error bars represent standard deviation. n=3. (B) Phase contrast images of cells after 2 hours of treatment with CCCP at 37°C and 30°C.

a comparable experiment was carried out at 30°C, the lysis kinetics were very different (Figure 40A). Similarly to the samples incubated at 37°C, there was the immediate halt of cell growth upon addition of CCCP to the samples incubated at 30°C. However, the 30°C samples displayed significantly slower lysis kinetics. After 3 hours, 80 % of the cells at 37°C were lysed, whereas only 15 % of the cells in the 30°C culture had lysed. In order to verify that the changes in OD indeed were reflecting cell lysis, as opposed to other parameters known to affect OD measurements such as cell volume and shape changes or precipitation, phase contrast microscopy was carried out with cells after 2 hours of CCCP treatment. As can be seen in Figure 40B, extensive cell lysis was observed in the sample incubated at 37°C, whereas at 30°C the cells are mostly intact, confirming that the reduction in OD observed upon CCCP addition indeed represents cell lysis. This surprising result entirely invalidates the old hypothesis, as the respiratory chain would function similarly at the two temperatures predicting a similar lysis pattern. This finding prompts an investigation into the actual mechanism underlying the PMF dissipation-induced lysis.

The difference in lysis kinetics observed at 37°C and 30°C might be explained by the initial growth speed of the cells. Since faster growing cells at 37°C will require a faster cell wall turnover, they presumably have more, or at least more active, autolytic enzymes acting in the cell wall. In Chapter 3 we examined the growth speeds at both temperatures and although they were fairly similar, the observed slight difference could alter the lysis kinetics. We

A

Carbon source	Doubling time (min.)
Glucose + CAA	31.3
Glycerol + CAA	43.8
Succinate + CAA	45.7
Glucose	49.2
Glycerol	55.4
Succinate	116.6

B

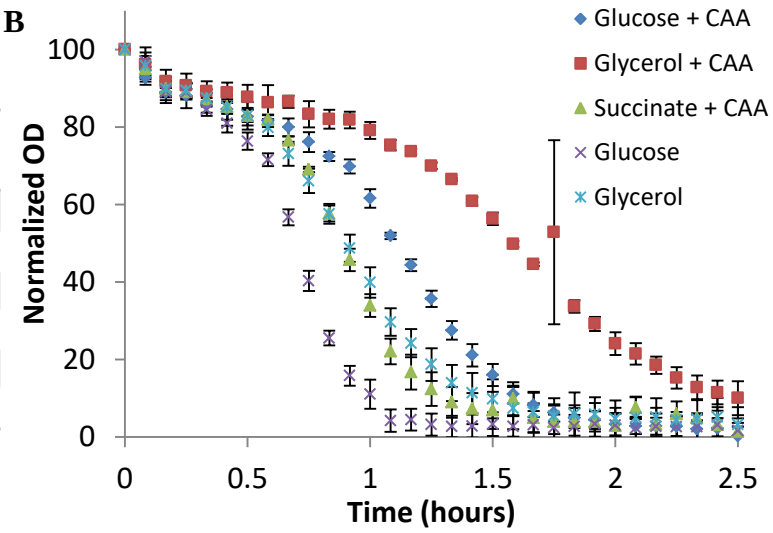

Figure 41: (A) calculated doubling times for wild type grown in SMM supplemented with different carbon sources. (B) Graph depicting the lysis kinetics of wild type grown in SMM supplemented with different carbon sources upon CCCP treatment. Error bars represent standard deviation. n=3

initially tested if the growth speed was modulating the lysis by treating our wild type cells at 37°C with CCCP at different growth speeds.

To do this, I used SMM medium supplemented with 50 µM glucose, glycerol, or succinate, respectively. Additionally, casaminoacids (CAA) were added in some of the samples to further modify the growth speed. The doubling times were determined from the slopes of the growth curves obtained (Figure 41A). As seen from the data, it is possible to substantially modify the growth speed of *B. subtilis* according to the carbohydrates and amino acids supplemented in the medium.

Next, we treated cells grown in media supporting different doubling times with CCCP in order to determine the corresponding lysis kinetics, and thus to answer the question if the lysis speed correlated with the growth speeds prior to CCCP addition. As shown in Figure 41B, the correlation is very poor. The fastest lysing samples turned out to be cells grown in glucose as a sole carbon source, which fully lysed within one hour. Cells grown in succinate supplemented with CAA, or in glycerol lysed similarly, both within 1.5 hours. In contrast, the fastest growing cells grown in glucose supplemented with CAA lysed somewhat slower, with full lysis only reached after 1.5-2 hours. The slowest lysing samples turned out to be the relatively quickly growing cells grown in glycerol supplemented with CAA. Consequently,

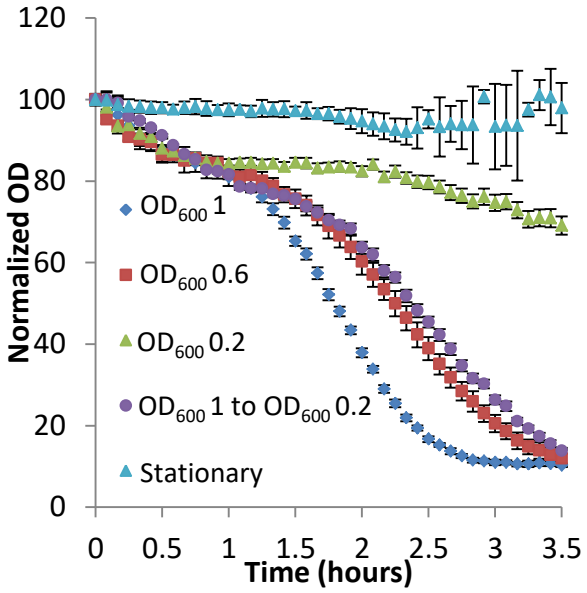

Figure 42: Graph depicting the lysis kinetics of wild type *B. subtilis* growing at 37°C treated with CCCP at ODs of 0.2, 0.6, 1, 1 diluted to OD_{600} of 0.2, and stationary phase. Error bars represent standard deviation. n=3.

there is no direct correlation between growth speed prior to CCCP addition and the kinetics of the triggered lysis.

Having discovered that the growth speed does not correlate directly with lysis speed, I decided to examine if growth phases would interfere with lysis kinetics, since this is another important parameter affecting cell wall turnover. This was tested by treating wild type cells with CCCP at different growth phases growing at 37°C (Figure 42). Surprisingly, after addition of CCCP, cells in very early exponential growth phase (OD_{600} of 0.2) exhibited a lysis phenotype that was similar to that observed for cells grown at 30°C. By contrast, cells treated in mid-exponential (OD_{600} of 0.6) and late exponential (OD_{600} of 1) phases exhibited strong lysis. Cells grown over night (stationary phase cells) prior to the treatment with CCCP did not exhibit any lysis, suggesting that non-growing cells are impervious to PMF dissipation-induced lysis. As well as the growth phase, the observed changes in lysis behaviour could be a result of the different cell densities in each population. To test this, the cells grown to an OD_{600} of 1 were diluted to an OD_{600} of 0.2, followed by addition of CCCP. The diluted cells retained the strong lysis phenotype, ruling out the possibility that the lysis is cell density dependent, rather than growth phase dependent.

Together, the findings suggest that growth-temperature, speed and phase are important parameters affecting PMF dissipation induced lysis. Additionally, the above data clearly contradicts the old lysis model, as the pH gradient in the cell wall should be retained throughout the different conditions, affecting the autolysins similarly regardless. However it is clearly observed that the induced lysis is highly modulated throughout growth and physical parameter shifts. These results made us evaluate if the lysis was in fact a coordinated response, evolved to kill compromised cells, thus saving the few cells that could survive. Thus, we tested whether various stress response proteins had any involvement in membrane potential dissipation induced lysis.

6.2.3 – Membrane depolarization induced lysis is not a programmed response

In order to examine if the induced lysis is a programmed cellular response, we used deletion strains of envelope stress σ^{ECF} (σ^{M}, σ^{V}, σ^{W}, σ^{X}, σ^{Y} and σ^{Z}). The σ^{ECF}'s have large and varied regulons that are usually activated by extracellular stresses, and are responsible for such varied processes as changes in osmolality, changes in pressure, nutrient limitation, oxidative stress, and other envelope stresses (Souza *et al.*, 2014). Additionally, we included a

ΔsigI strain, as σ^I is involved in envelope stress as well, and the deletion of the two envelope stress response proteins LiaH and PspA. If any of the corresponding stress response-regulons are involved in inducing the observed lysis, we expect the lysis phenotype to be rescued in the corresponding deletion strain. However, none of the tested sigma factor deletion strains significantly rescued the lysis phenotype (Figure 43). In some cases, such as *ΔsigI* and *ΔsigV*, the lysis kinetics were slightly altered compared to wild type cells. The results suggest that while proteins induced by ECF-sigma factors and envelope stress responses as a response to CCCP might mildly modulate the lysis process, the lysis phenomenon as such does not appear to be a cellular programme induced as part of ECF-sigma factor mediated envelope stress response.

An additional mechanism that might explain the induced lysis is prophage induction. Prophages are bacterial genomic encoded viruses which, upon activation take over the translational machinery producing vast amounts of phage particles (Hendrix, 2002). Ultimately, the escape of the phage particles causes lysis of the host cell. *B. subtilis* 168 natively contains 6 such prophages (Westers *et al.*, 2003). I wanted to test if dissipation of PMF would induce prophage activation leading to encoded lysis. To test if the observed CCCP-triggered lysis is due to prophage activation, a previously published strain called Δ6 (Westers *et al.*, 2003) that is cured for all six prophages was subjected to CCCP treatment. As

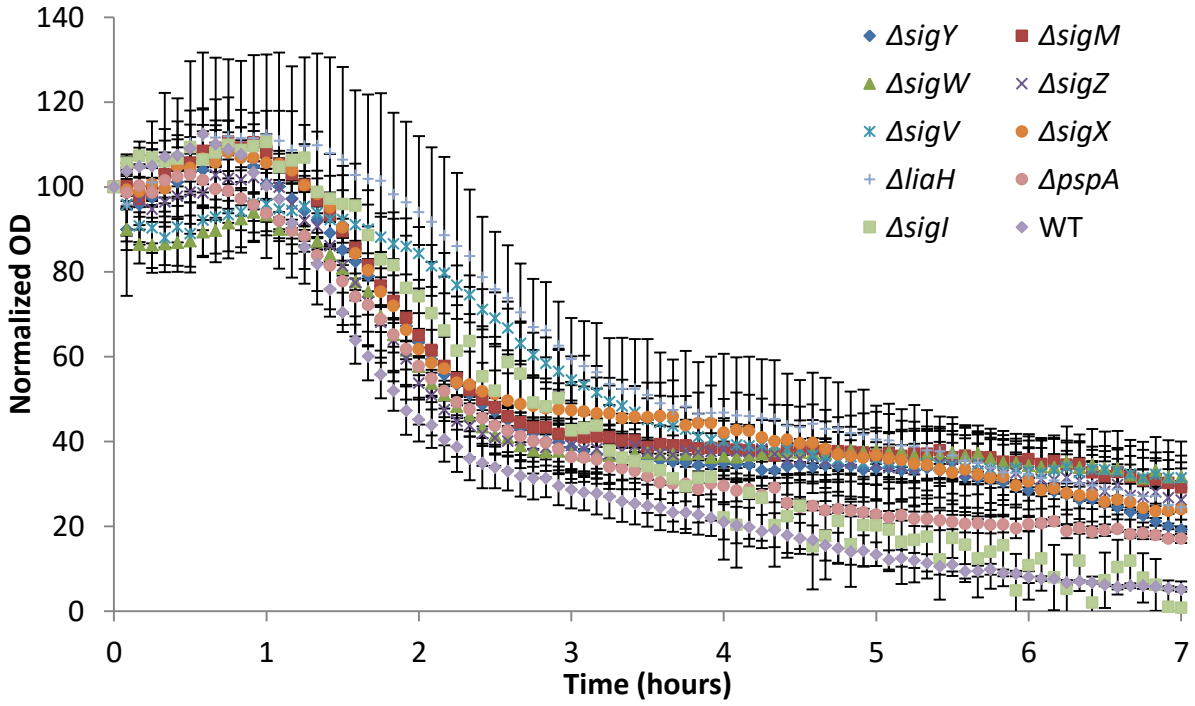

Figure 43: Graph depicting the lysis kinetics of deletion strains of the envelope stress σ^{ECF} (σ^M, σ^V, σ^W, σ^X, σ^Y and σ^Z), *ΔsigI*, *ΔliaH*, and *ΔpspA* upon treatment with CCCP. All strains are lysing. Error bars represent standard deviation. n=3

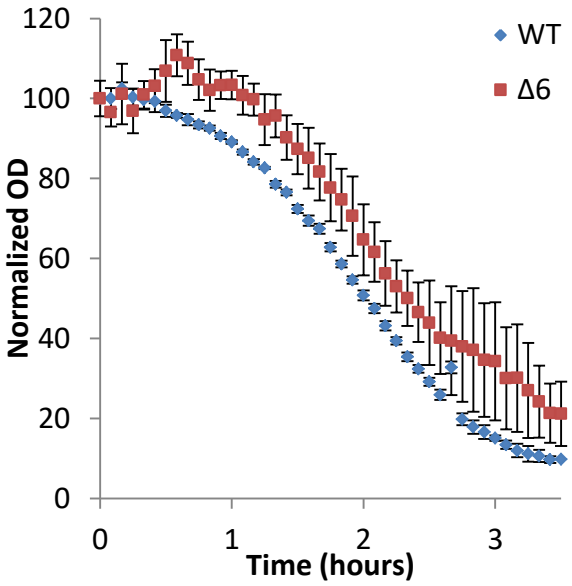

Figure 44: Graph depicting the lysis kinetics of wild type and the prophage cured *B. subtilis* strain upon treatment with CCCP. Error bars represent standard deviation. n=3

shown in Figure 44, the prophage cured strain exhibited CCCP-dependent lysis behavour that is essentially the same as that observed in the prophase-encoding wild type strain. These results clearly eliminates prophage induction as the reason why *B. subtilis* initiates lysis upon PMF collapse.

Finally, I wanted to determine whether the induction of any additional genes was requried or responsibe for the CCCP-triggred lysis. To test this, the CCCP-triggered lysis was followed in the presence of high concentrations of chloramphenicol, which inhibits translation entirely, thus exluding induction of any additional components. Chloramphenicol, which inserts itself into the peptidyl transferase site in the ribosome to inhibit peptide bond formation, is a bacteriostatic compound and will thus not cause lysis itself (Okamoto and Mizuno, 1964). In our experimental conditions, *B. subtilis* cells continue to gain OD for about 30 min. after addition of cloramphenicol (Figure 45). This is likely due to growth, and corresponds to approximately half a doubling that is presumably facilitated by proteins synthesized prior to chloramphenicol treatment. In order to allow chloramphenicol to enter the cells and to effectively abolish translation, CCCP was added 10 min. after addition of chloramphenicol. When treated with both chloramphenicol and CCCP, we observed that the lysis kinetics were effectively comparable to those for the untreated wild type cells, and were possibly even faster. Consequently, we must conclude that the cell lysis triggered by PMF-collapse is not due to induction of a gene-encoded cellular programme. Rather, all of the

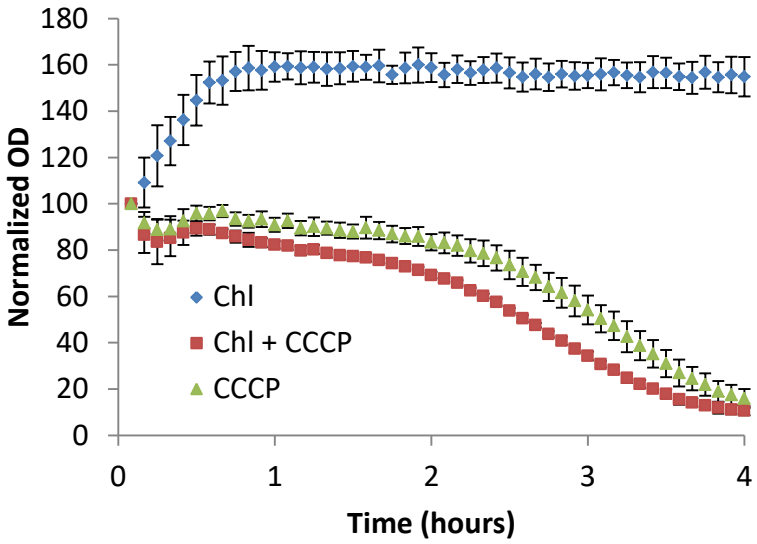

Figure 45: Graph depicting the lysis kinetics of wild type *B. subtilis* treated with chloramphenicol (Chl) (100 µg/ml), CCCP, and a combination of the two compounds. Error bars represent standard deviation. n=3

nessecray components requried for the lysis process are in place in the the cell prior to the PMF-collapse. The next step was to determine if these components indeed include cell wall lytic enzymes, as postulated by Joliffe et al (Jolliffe *et al.*, 1981).

6.2.4 – Membrane depolarization induced lysis is caused by autolysins

In order to determine if autolysins are involved in membrane depolarization induced lysis, the field of possible candidates had to be narrowed down significantly as *B. subtilis* has the impressive array of 35 individual autolysins (Smith *et al.*, 2000). Some of the best characterized autolysins in *B. subtilis* are LytC (Chen *et al.*, 2009), LytD (Margot *et al.*, 1994), LytF (H. Yamamoto *et al.*, 2003), LytE (H. Yamamoto *et al.*, 2003), and CwlO (Yamaguchi *et al.*, 2004), where the two latter are regulated by the MreB-cytoskeleton (Dominguez-Cuevas *et al.*, 2013). I first decided to examine the effect of strains carrying deletions of each individual autolysin gene on membrane depolarization induced lysis. In the case of *lytC,* the available deletion strain included the deletion of two addition genes, *lytA* and *lytB,* which are involved in secretion and regulation of LytC, respectively. The results of the lysis assay for the CCCP-treated single autolysin deletion mutants are shown in Figure 46. Immediately it can be noticed that none of the single deletion mutants rescue the lysis completely, but all of them alter the lysis kinetics to a varying degree. The *ΔlytABC, ΔlytF* and *ΔcwlO* strains lysed at slightly slower rates than the wild types strain. *ΔlytD* and *ΔlytE*

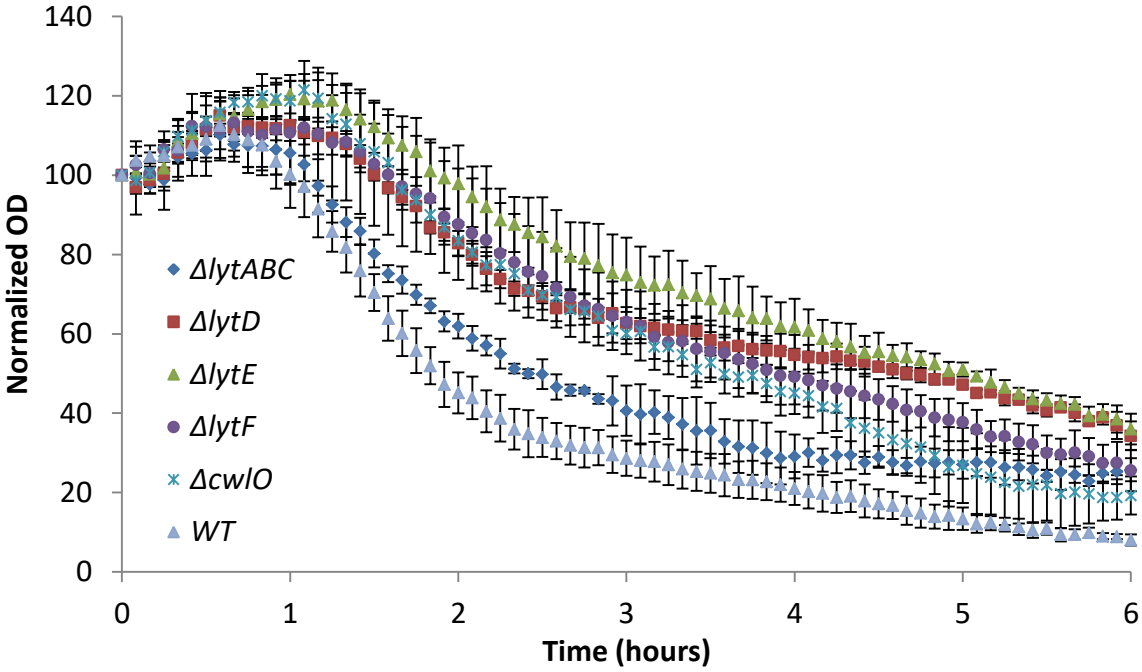

Figure 46: Graph depicting the lysis kinetics of single autolysin deletion strains upon treatment with CCCP at 37°C. Each of the mutants partially rescues the lysis but none of them are solely responsible. Error bars represent standard deviation. n=3

strains both exhibited the slowest lysis kinetics. These results clearly show that the autolysins have an effect on the CCCP-induced lysis, but none of the tested autolysins appears to be solely responsible for the phenomenon. To test if the individual autolysin deletions act additively, a strain that carried multiple deletions of the tested autolysins was constructed. The key autolysins involved in lateral cell wall synthesis, CwlO and LytE, are functionally redundant and simultaneous deletion of both genes is lethal (Bisicchia *et al.*, 2007). From our single gene deletion experiment we found that LytE appears to contribute more to autolysis than CwlO. Consequently, it was therefore decided to combine the deletion of *lytE* with deletions of *lytABC, lytD* and *lytF*, respectively. The resulting strain was thus named *ΔlytABCDEF*. The strain had clear cell separation and short length phenotypes, as it is largely unable to separate the daughter cells after a completed cell division, resulting in long filamentous growth (Figure 47A).

First, I wanted to determine if the strain had gained any further resistance towards CCCP. A MIC was therefore performed (Table 16) and it was found that the strain retained similar susceptibility to CCCP as wild type.

	CCCP (µM)
WT	12
ΔlytABCDEF	12

Table 16: MICs for WT and *ΔlytABCDEF* treated with CCCP (100-1.5 µM range). The MICs does not change for the autolytic mutant. n=3

Next, when the *ΔlytABCDEF* strain was treated with CCCP an immediate growth arrest was observed. However, in contrast to the wild type strain, no significant lysis was observed within the 3 hours testing period, or even beyond that (Figure 47B). When compared to the wild type, this represents an essentially complete rescue of the lysis phenotype. These results thus confirm that the deleted autolysins are indeed involved, and responsible for the lysis triggered by PMF-collapse.

It has long been assumed that membrane or cell wall targeting compounds are bactericidal due to the induced lysis. If this is indeed the case, we would expect that the *ΔlytABCDEF* mutant is resistant to these compounds bactericidal effect. The apparent rescue of lysis therefore prompted us to examine whether the non-lysing cells were viable or not.

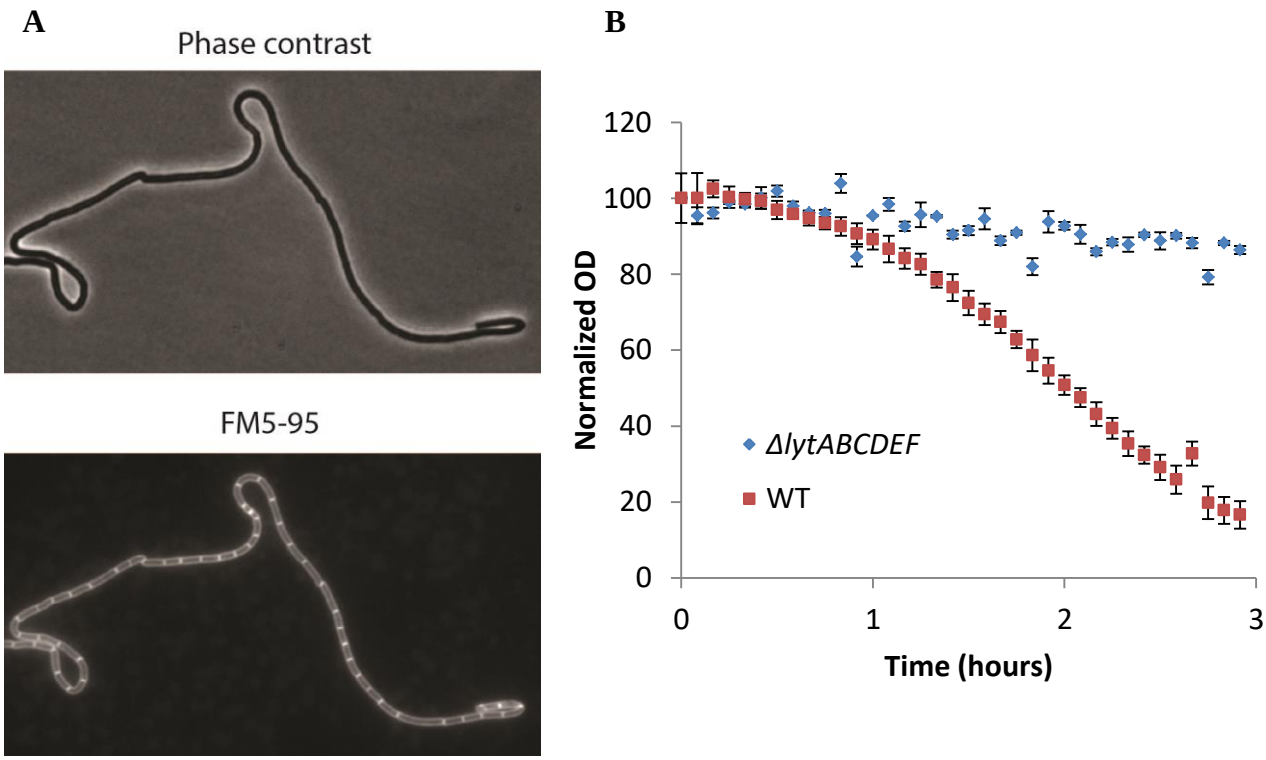

Figure 47: *ΔlytABCDEF* phenotype and lysis. (A) Phase contrast and FM5-95 membrane dye images of *ΔlytABCDEF*. The cells clearly exhibit a separation deficiency, along with growing in as shorter cells. (B) Graph depicting the lysis kinetics of wild type and *ΔlytABCDEF* treated with CCCP. Lysis is rescued entirely in the mutant. Error bars represent standard deviation. n=3

6.2.5 – The bactericidal mechanism of membrane depolarization is not solely through lysis

Having shown that deletion of the major autolysins rescued PMF dissipation induced lysis, I wanted to examine if the cells remained viable after CCCP treatment, or if the bactericidal effect was retained. In order to test whether the *ΔlytABCDEF* mutant strain rescued cell death upon PMF dissipation, the CCCP-dependent lysis experiment was repeated and samples were taken every hour for three hours for the determination of cell viability. The cells were initially diluted 1:1000 in LB medium without the compound, rapidly diluting the inhibitor concentrations below its MIC. A 1:10 dilution series was then conducted, followed by transfer nutrient agar plates as spot assay. The plates were then incubated overnight at 30°C in order to determine how many of the non-lysed cells were viable (resulting in colony formation). The untreated control sample was taken time point 0 hour as reference. The results from the cell viability assay are shown in Figure 48. When observing the results for the wild type cells, a rapid CCCP-dependent initial killing was followed by a stabilization of the viability to levels below an order of a magnitude was evident (Figure 48). When comparing this to the lysis curve shown in Figure 47, it is clear that the CCCP-dependent loss of viability precedes cell lysis, thus suggesting that bacteriolysis is not the sole determinant of CCCP's bactericidal activity. In agreement with this notion, the viability of the *ΔlytABCDEF* mutant followed a trend essentially comparable to that observed for the wild type. Consequently, we conclude that while PMF-collapse does induce autolysis, which explains its bacteriolytic properties, the cells are nevertheless dying for reasons unrelated to cell lysis.

To summarize the findings so far; it has been discovered that cell lysis upon PMF-collapse is highly conditional and dependent on environmental factors such as temperature

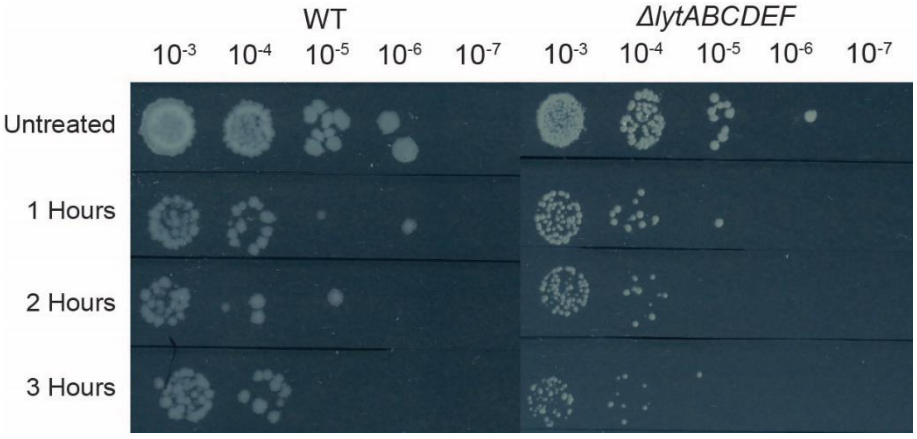

Figure 48: Cell viability assay determining the amount of CFUs for 3 hours of treatment with CCCP. Both WT and *ΔlytABCDEF* have a 10-fold reduced viability 1 hour after treatment, which is kept for the duration of the experiment. The degree of dilution from the original vial is signified as 10^{-x}.

and medium composition, while also being modulated by population-linked factors such as growth phase. Together, these findings disprove the old model, as the pH gradient on which this hypothesis relies should remain the same throughout all the stated conditions. However, the triggered lysis is autolytic at its very core and is facilitated by known autolysins responsible for cell wall turnover, which are present in actively growing cells. It therefore appears that lysis occurs when natively expressed autolytic enzymes becomes miss-regulated upon PMF-collapse. Ultimately, autolytic activity is needed for incorporation of new cell wall material, a process driven in *B. subtilis* by two distinct cellular machineries, the divisome driving cell division, and the elongasome driving cell elongation. Consequently, I decided to test if de-regulation of autolysis activity linked to these two major systems were involved in the autolysis caused by PMF-collapse.

6.2.6 – MreB and its homologues are involved in depolarization-induced autolysis

Initially we tested if cell division was involved in the PMF-collapse induced autolysis. This is because the autolysins LytD and LytF are both important for cell separation after division (Chen *et al.*, 2009). In order to test this hypothesis, we utilized strains either lacking, or deleted for, key cell division proteins. The tested strains include a mutant in which the expression of the key division scaffold protein FtsZ (Lutkenhaus and Wu, 1980) was placed under the control of an inducible promoter. Upon depletion, this strain is unable to undergo cell division, thus growing as a long filamentous cell. In addition, a Pbp2B depletion strain was tested. Pbp2B is an essential peptidoglycan synthesising enzyme of the divisome, the depletion of which results in long filamentous cells that, unlike FtsZ-depleted cell, are capable of assembling the division machinery but are incapable of driving septum formation (Gamba *et al.*, 2009). Finally, a strain deleted for *ftsA* was analysed. FtsA is an important cell division protein required for anchoring the intracellular division machinery to the membrane (Errington *et al.*, 2003). In the absence of FtsA, *B. subtilis* grows as long cells that can undergo division but only at a low frequency (Gamba *et al.*, 2009).

A

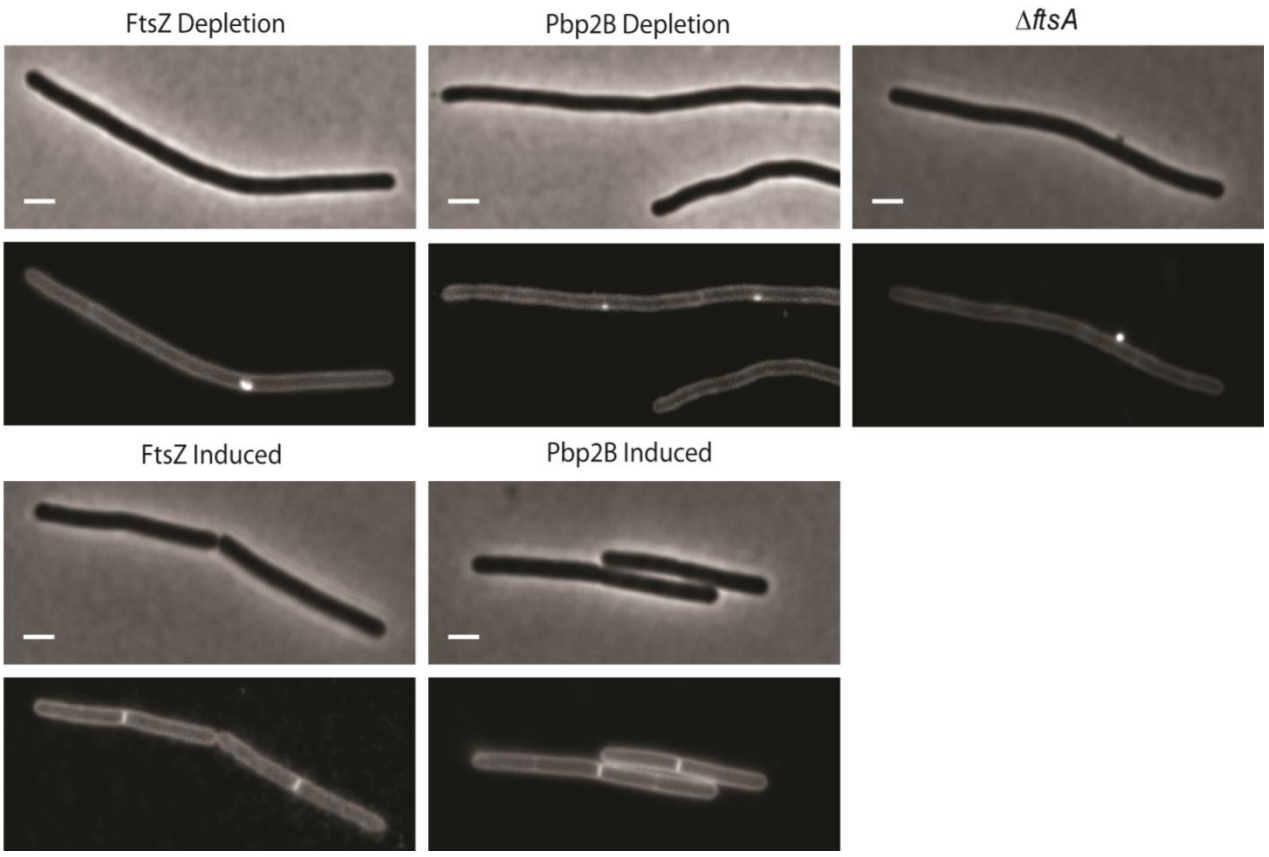

B

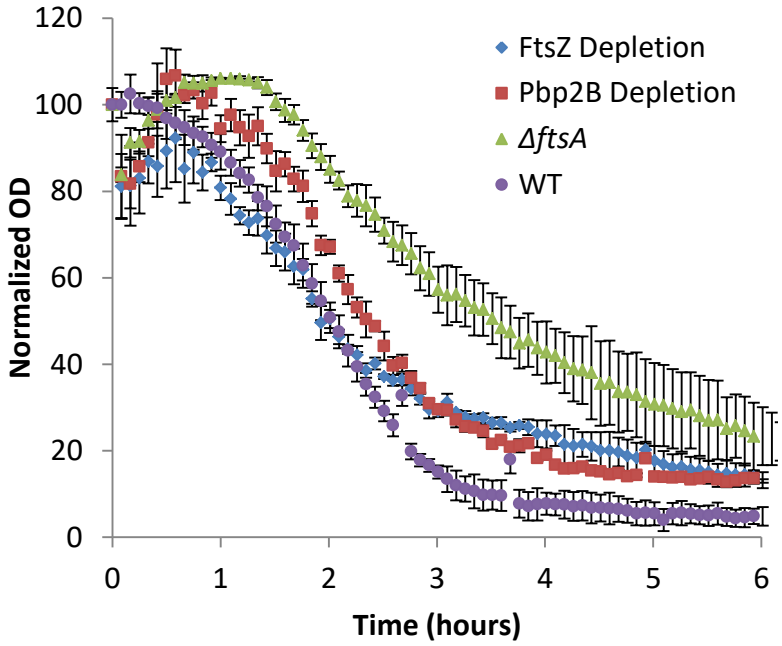

Figure 49: (A) Morphology of each strain used in the lysis assay. Note the lack of septa in the depleted strains and the *ΔftsA* strain. When inducing FtsZ and Pbp2B we again obtain the WT morphology. (Scale bar: 2 µm) : (B) CCCP lysis assay with strains without key parts of the divisome. Deleting *ftsA* or depleting for FtsZ or Pbp2B inhibits cellular division. As clearly shown, all strains lyse, thus excluding cell division as involved in the autolysis. Error bars represent standard deviation. n=3

For the depletion strains, the cells were grown over night and throughout the following day in the presence of inducers, followed by inoculation and growth in non-inducing LB medium. This ensured that the cells were robustly growing through cell elongation until the point of CCCP-treatment, but had grown long enough in the absence of an inducer to effectively abolish active cell division. The cell division phenotypes of the used strains in the presence and absence of inducers can be seen in Figure 49A, and the results of the CCCP-induced lysis experiment are shown in Figure 49B. Surprisingly, the observed CCCP-triggered lysis behaviour is essentially indistinguishable between the wild type cells and those lacking cell division. This suggests that the division process, and the proteins involved therein, is not crucial for the CCCP-triggered autolysis.

The other major uses for autolysins in growing cells is incorporation of new cell wall material through the lateral cell wall synthesis machinery (the so-called elongasome), and the poorly understood activity providing general cell wall turnover through degradation at the periphery of the cell wall matrix (Smith *et al.*, 2000; Egan and Vollmer, 2013). While the general turnover is difficult to test, the elongation machinery is well studied, providing immediate means to test its involvement in the autolytic process. Initially, it was decided to focus on single gene deletion strains for each of the three actin homologues *mreB*, *mbl*, *mreBH*, all of which are involved in elongation (Levin *et al.*, 1992; Abhayawardhane and Stewart, 1995; Carballido-Lopez *et al.*, 2006). The reason for this decision was a previous

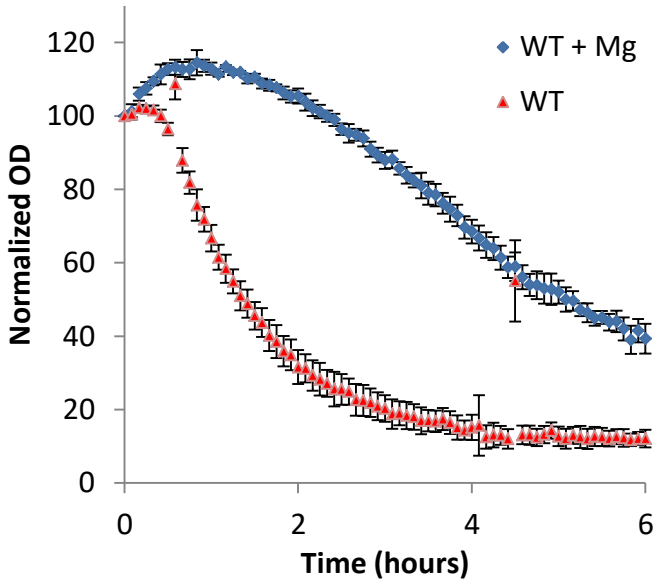

Figure 50: Graph depicting the difference in CCCP-induced lysis of *B. subtilis* wild type in standard LB medium and medium supplemented with 20 mM Mg^{2+}. Error bars represent standard deviation. n=3

study linking these important cytoskeletal proteins to regulation of autolysins (Dominguez-Cuevas *et al.*, 2013).

When deleting components of the lateral cell wall synthesis machinery, including the actin homologs, *B. subtilis* requires high concentrations of Mg^{2+} to grow (Schirner and Errington, 2009b). Consequently, in order to compare lysis between these strains and the wild type, the potential effect of Mg^{2+} on CCCP-triggered lysis needed to be examined. When *B. subtilis* wild type was treated with CCCP in the presence of 20mM $MgCl_2$, a significant reduction of lysis was observed (Figure 50). When compared to growth without supplemented $MgCl_2$, it becomes evident that lysis is clearly suppressed. Consequently, in the following experiments the lysis behaviour of strains carrying deletions of elongasome components are compared against that of the wild type cells grown in the presence of 20mM $MgCl_2$.

Intriguingly, individual deletions of the actin homologs clearly suppress the CCCP-triggered lysis (Figure 51A), thus providing a first indication that the lateral cell wall synthesis machinery might indeed be involved in the autolytic process.

As all three actin homologs partially supressed the lysis in a manner comparable to the autolysin deletions, the obvious next step was to analyse the previously constructed *ΔmreB, Δmbl, ΔmreBH* triple deletion strain (Isolate V). First I performed a MIC experiment to ensure that the strain still reacted to CCCP treatment, where it is seen that the strain is even more susceptible to the compound than wild type (Table 17). Next a lysis assay was performed using CCCP.

	CCCP (µM)
WT	12
ΔmreB, Δmbl, ΔmreBH	6

Table 17: MICs for WT and *ΔmreB, Δmbl, ΔmreBH* treated with CCCP (100-1.5 µM range). The MICs decreased for the *mre* mutant. n=3

Surprisingly, a complete rescue of lysis is observed. In this strain background the addition of CCCP induces growth arrest for about 1 hour, followed by a gradual increase in OD (Figure 51B). This was interesting since, to our knowledge, cell growth without the PMF

has never been conclusively demonstrated for any organism. Indeed, the slight increase in OD might not indicate real growth, but rather changes in the parameters underlying the OD measurement such as cell size, shape, or diffractive properties. The CCCP-triggered autolysis appeared to be based on the miss-regulation of the poorly understood regulatory pathway linking MreB-homologs to autolysis-regulation.

The absence of lysis in the triple *mre* mutant could be due to the shape change into coccoid form, or specifically due to the lack of the MreB cytoskeleton. We decided to test this by using RodA depletion and the *ΔmreC* strains. Upon depletion of RodA, the cells turn spherical due to a lack of lateral cell wall synthesis (de Pedro *et al.*, 2001), although the cells still retain the MreB cytoskeleton localized at the membrane (Strahl *et al.*, 2014). Additionally, the *ΔmreC* mutant turns into coccoid form, while retaining a membrane associated MreB-cytoskeleton (Strahl *et al.*, 2014), but abolishes the link between the cytoskeleton and the cell wall synthesis machinery (van den Ent *et al.*, 2006). The shape phenotypes of each strain are shown in Figure 52A. As with the other depletion strains, I grew the RodA depletion strain in inducing conditions overnight and the following day into logarithmic phase, followed by inoculating cells from these into non-inducing medium

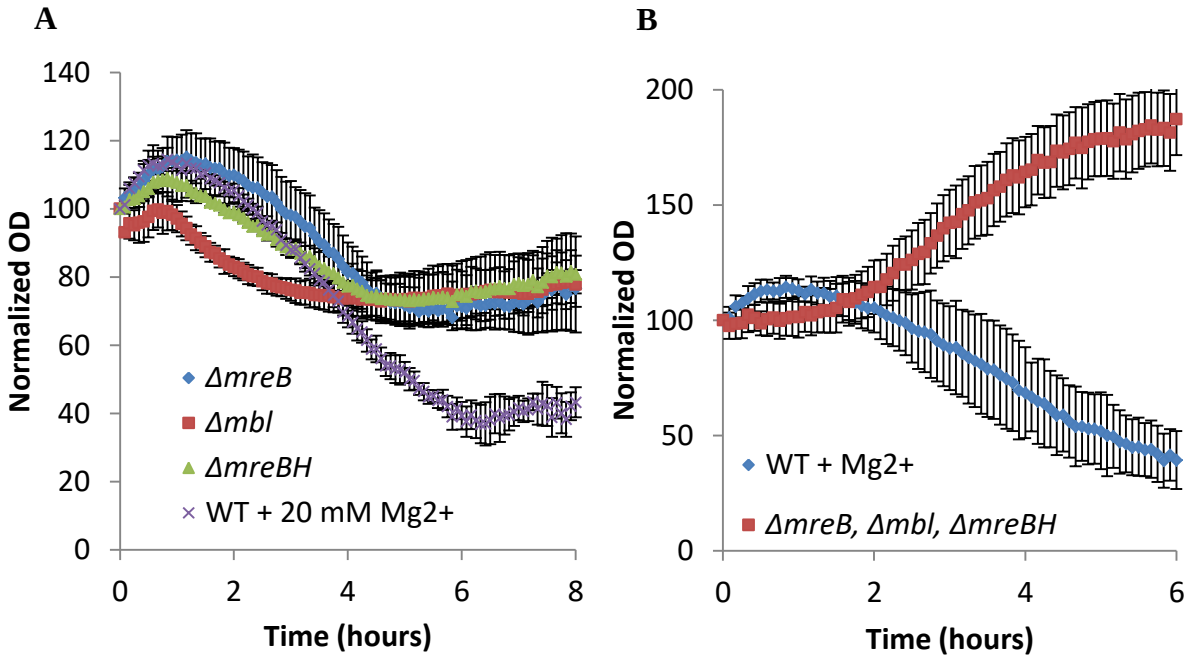

Figure 51: (A) Lysis curves of individual actin homologue deletion strains treated with CCCP. The graph shows partial rescue of lysis from all three deletion strains compared to the WT. The strains are grown with 20 mM $MgCl_2$. (B) The full MreB cytoskeletal deletion strain *ΔmreB, Δmbl, ΔmreBH* without any suppressor mutations (Isolate V) treated with the CCCP. The strain rescues lysis completely, even increases in OD when treated with CCCP. Error bars represent standard deviation. n=3

followed by growth to mid-exponential phase, before treating them with CCCP.

The lysis profiles for each of the strains when treated with CCCP are shown in Figure 52B. As discussed before, when grown with high concentrations of magnesium the autolysis if the wild type strain is partially rescued. *ΔmreC* rescues the lysis to a degree that is higher than the suppression observed in the wild type strain for magnesium only, thus suggesting that a link between the actin cytoskeleton and the elongasome might be important. In contrast, although having a slightly different lysis kinetics compared to wild type, the RodA depletion strain still lyses significantly, and to the same extent as wild type upon addition of CCCP. Consequently, the lack of lysis observed for *ΔmreB, Δmbl, ΔmreBH* is not simply due to a loss of lateral cell wall synthesis or adoption of round cell morphology, but more directly coupled to the role of MreB homologues in the lateral cell wall synthesis machinery.

Here, I have shown that CCCP-induced autolysis is rescued entirely in the absence of the MreB cytoskeleton, and excluded the potential involvement of cell division. Furthermore, I have shown that the suppression of the lysis phenotype is not a simple consequence of a general lack of lateral cell wall synthesis, but rather implies a more specific involvement of the MreB-cytoskeleton. Having found that MreB and its homologues are intimately involved

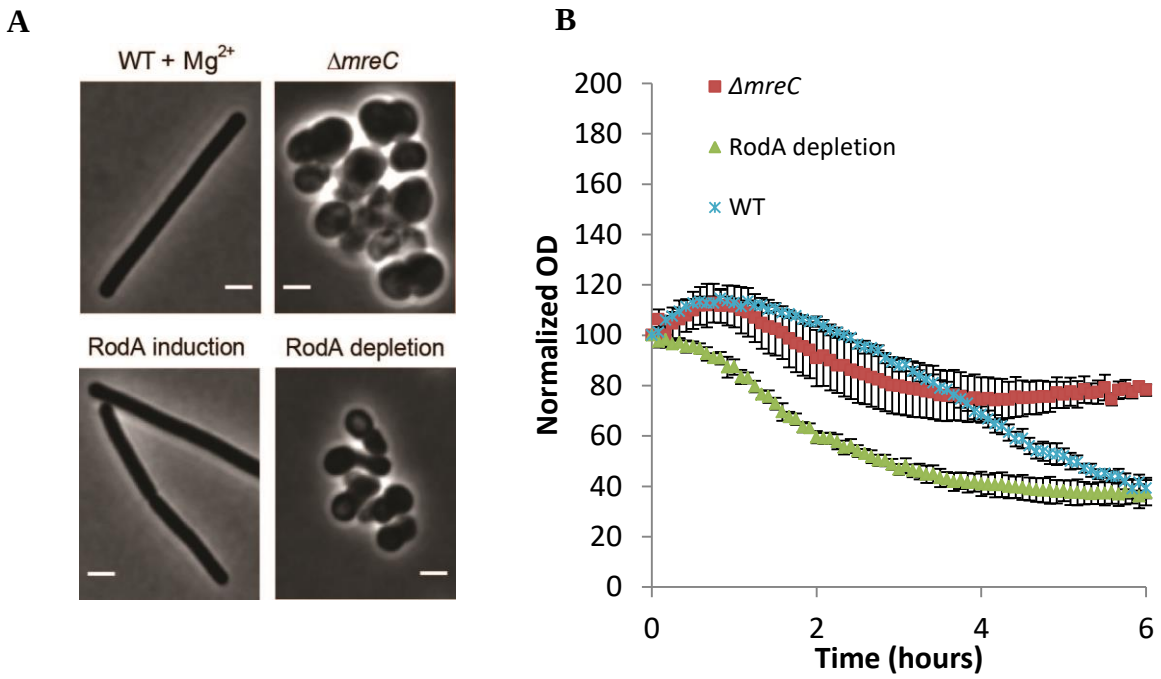

Figure 52: (A) Phase contrast images of the strains used for lateral cell wall inhibition controls for determination of autolysis. *ΔmreC,* and the depleted RodA strain all grow as cocci-like organisms. Whereas WT and the induced RodA grow in a rod-shape. Scale bar: 2µm (B) Graph depicting the lysis kinetics of the above mentioned strains when treated with CCCP. *ΔmreC* partially rescues the lysis, while the depleted RodA strain lyses comparably with wilt type. Error bars represent standard deviation. n=3

in triggered autolysis, I next wanted to examine what happens to MreB upon extended CCCP treatment to further elucidate the autolysis mechanism.

6.2.7 – PMF-collapse induced autolysis is MreB delocalization dependent

The PMF is composed of ΔpH and Δpsi. MreB is specifically sensitive to the change in charge across the membrane, meaning that the general membrane potential change upon CCCP treatment is what delocalizes MreB (Strahl and Hamoen, 2010; Strahl *et al.*, 2014). As described in the introduction, MreB shows membrane potential-dependent localization behaviours, and delocalizes immediately upon membrane depolarization. Perhaps the delocalization of MreB upon membrane potential dissipation is what triggers autolysis. However, the precise localisation of MreB was not well studied upon longer term incubation with membrane potential-dissipating compounds, and how factors such as growth phase affect this poorly understood process. I therefore wanted to examine what happens with the MreB-localization under the conditions and strain backgrounds used to study the lysis.

First I wanted to analyse the localization of each of the three actin homologues after 15-30 min. of CCCP-treatment, since this is the time window in which lysis is initiated. The experiments were performed at 37°C in LB medium, and the results are shown in Figure 53A. In untreated samples MreB localizes to discrete filaments that are membrane associated in the cylindrical part of the cell. Upon CCCP treatment, MreB mostly detaches from the membrane, resulting in a diffuse cytoplasmic signal. Occasionally, a few foci appear along the cell axis as indicated with arrows. Mbl exhibits a localization pattern essentially mimicking that of MreB. When treated with CCCP we also observed a complete delocalization of Mbl. However, in contrast to MreB, larger membrane-associated foci positioned at the cell poles and division sites are observed more frequently as shown with arrows. Finally MreBH mainly localizes to the cytoplasm with few foci appearing along the membrane. Upon treatment with CCCP, we see a clear delocalization of MreBH towards membrane foci mostly found at the poles and at septum, as highlighted with arrows. These results clearly show that each actin homologue in *B. subtilis* are either delocalized along the membrane surface, or lose membrane association upon CCCP treatment. The data confirms previous findings (Strahl and Hamoen, 2010). As the three homologues behave in a similar manner, MreB was decided as the proxy to examine general actin homologue behaviour.

To further investigate if the localization of MreB is important for induced autolysis, I tested some of the conditions under which the lysis kinetics was altered significantly. If the delocalization of MreB is important, we expect to observe clear delocalization under conditions where lysis occurs, while MreB should experience little to no delocalization when lysis is abolished. As previously shown, the lysis kinetics were significantly reduced when either treating the cells grown at 30°C or when treating the cells in the very early exponential growth phase. I therefore examined MreB's localization pattern upon CCCP treatment at low OD and at 30°C (Figure 53B). As shown previously, when grown under our standard conditions at 37°C, CCCP treatment induces detachment of MreB from the membrane with a few discrete membrane associated foci appearing. Surprisingly, when cells are grown in 30°C prior to CCCP-treatment, MreB mostly retained its membrane associated "regular" localization pattern, even in the presence of CCCP (Figure 53B middle panel). In only a few of the cells was detachment of MreB from the membrane observed (Figure 53B middle panel). Crucially, the same behaviour was observed for cells grown at 37°C but treated with CCCP at an OD_{600} of 0.2. Under these conditions the localization of MreB is largely insensitive to CCCP, although a slight increase in cytoplasmic fluorescence signal was observed (Figure 53B lower panel). Together, these results demonstrate that there is a clear correlation between the growth conditions in which CCCP triggers rapid lysis, and the corresponding membrane-potential sensitivity of MreB.

Having shown that MreB and its homologues indeed do delocalize upon membrane depolarization, and further showing that MreB delocalization, and the extent thereof, correlated with the rate of lysis for temperature- and growth stage-dependent lysis, we wanted to examine if MreB localization patterns could explain the differences in lysis observed for the *ΔmreC* deletion mutant and the RodA-depletion strain.

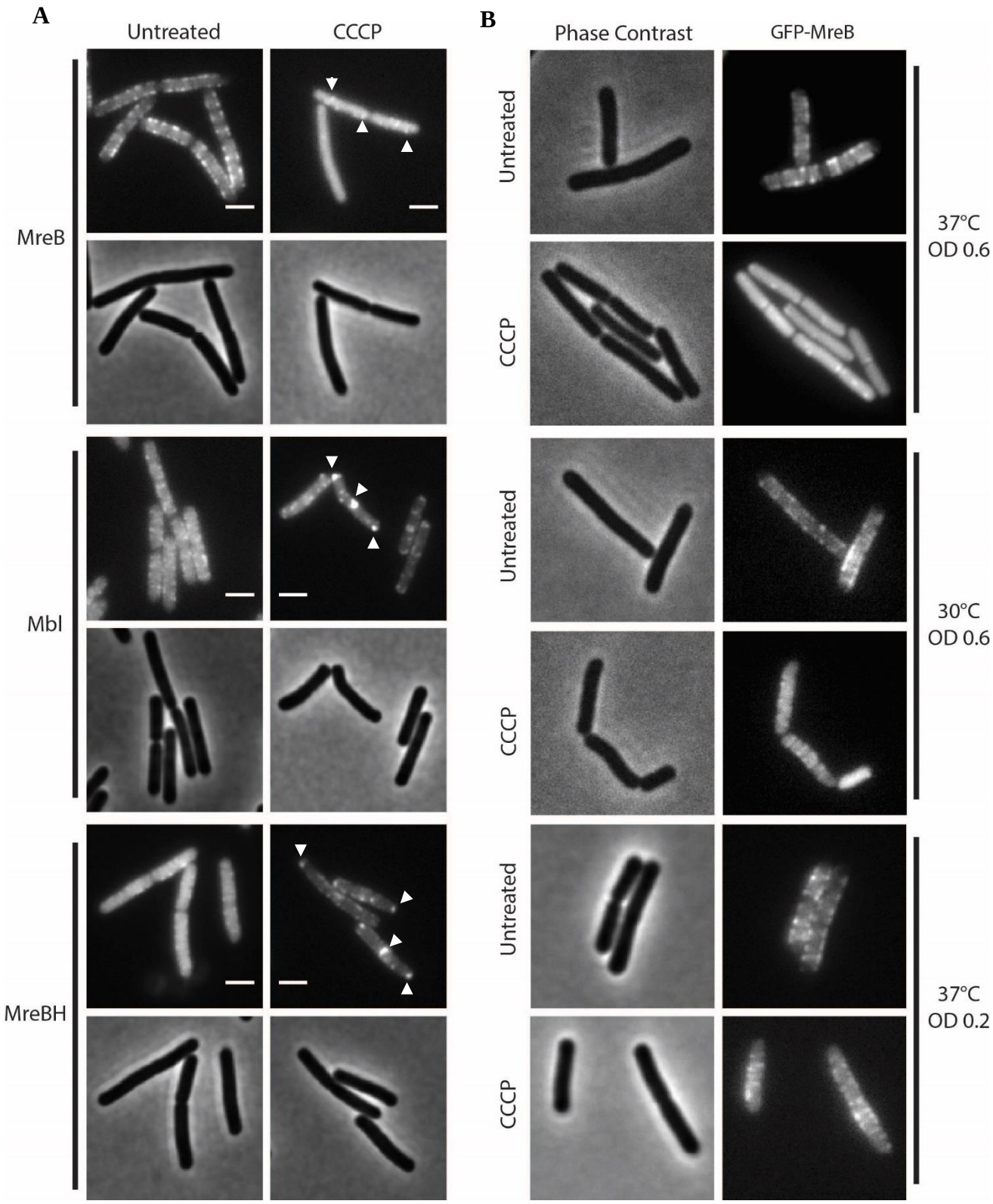

Figure 53: (A) Images showing the localization of MreB, Mbl, and MreBH untreated and about 15-30 min. after CCCP treatment. The white arrows signify foci of interest. Each of the actin homologues delocalize upon CCCP treatment. (B) Images depicting the localization of MreB before and after treatment of CCCP at 37°C at OD 0.6 and 30°C at OD 0.6, and 37°C at OD 0.2. The delocalization is not as distinct in the 30°C sample and the OD 0.2 sample.

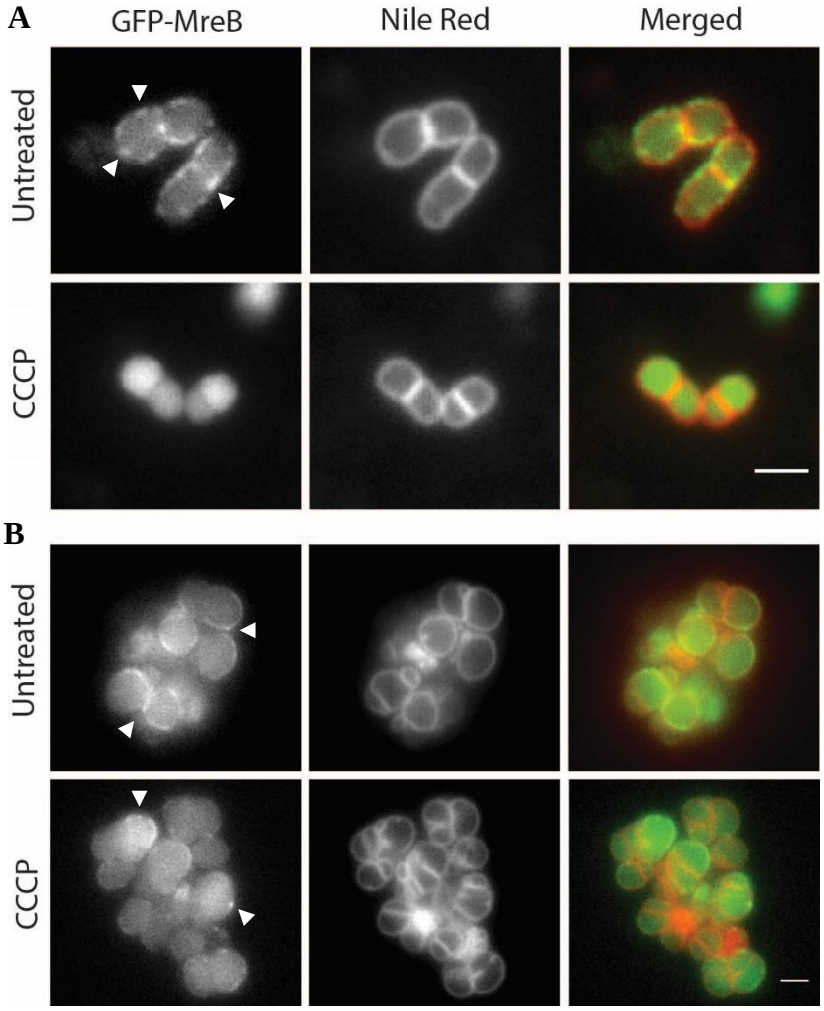

Figure 54: (A) MreB localization in the RodA-depletion strain following CCCP treatment. When untreated, MreB localizes in distinct membrane foci around the cells (white arrows). When treated with CCCP, MreB loses membrane association and localizes to the cytoplasm. (B) MreB localization in *ΔmreC* with and without CCCP treatment. Without treatment MreB localizes to both foci in the membrane (white arrows) and partially to the cytoplasm. When treated with CCCP, the localization pattern remains the same. (Scale bar: 2 µm)

To investigate this, a GFP-MreB fusion was expressed in a strain carrying a deletion of *mreC*, as well as in a strain in which RodA was under control of an inducible promoter. These strains were grown at 37°C to an OD_{600} of 0.6, followed by CCCP treatment. The results of the microscopic experiment are shown in Figure 54. In good agreement with the rapid lysis observed for RodA-depleted cells, MreB showed clear wild type-like CCCP-dependent delocalization behaviour (Figure 54A). The deletion of *mreC*, which largely rescues the lysis triggered by CCCP, also affected the delocalization of MreB. When treated with CCCP no clear difference in MreB localization pattern is observed. MreB is still found as membrane associated foci while the cytoplasmic signal remains at comparable intensity.

These data suggest that delocalization of MreB, which is conditionally triggered by dissipation of membrane potential, is the root cause for the induced autolysis process.

6.2.8 – Membrane targeting compounds generally cause lysis through a MreB delocalization mediated mechanism

Having determined that CCCP causes PMF- and membrane potential dissipation, and that the loss of these membrane gradients induces MreB delocalization dependent autolysis, the next question was: is the MreB-dependent autolysis phenomenon a specific effect of proton un-couplers or does it also have a broader role in the mode of action of membrane-targeting antibiotics that collapse the PMF and dissipate membrane potential. In order to answer this question, three compounds were selected and examined: gramicidin, daptomycin and LL-37. These molecules each target the membrane through cation specific channels, a complex mechanism including membrane perturbation and pore formation, respectively.

The behaviour of wild type upon treatment with the different compounds, including CCCP for comparison, can be found in Figure 55. Gramicidin and CCCP have fairly similar lysis kinetics, with an immediate growth arrest followed by a delay before a loss of OD due to

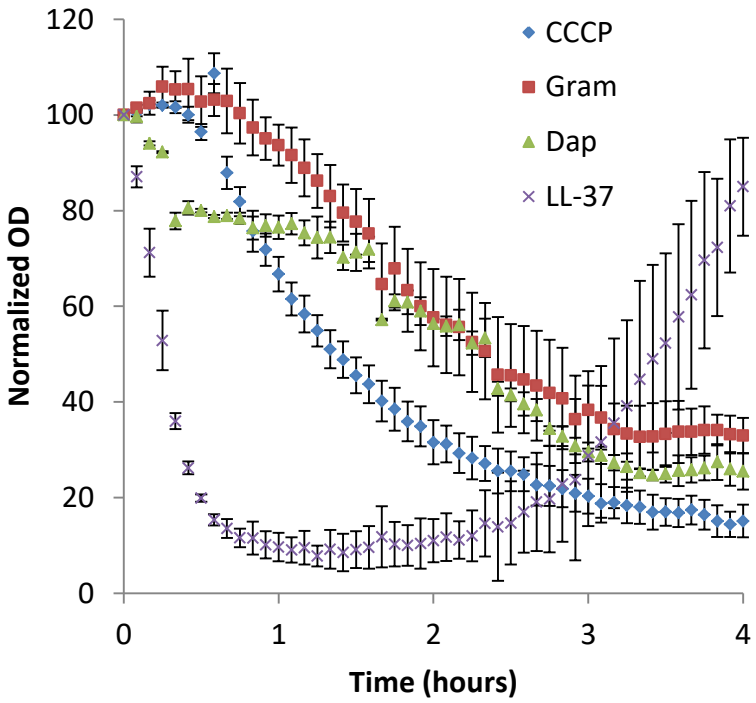

Figure 55: Graph depicting the lysis kinetics of the compounds CCCP (100 mM), Gramicidin (10 µg/ml), Daptomycin (10 µg/ml), and LL-37 (40 µg/ml) in WT *B. subtilis*. The normalized OD is with the initial OD upon compound addition set to 100. Error bars represent standard deviation. n=3

lysis. Daptomycin exhibited an initial OD reduction, followed by about an hour of stationary cell behaviour, finally culminating in lysis similar to gramicidin. Cells treated with LL-37 immediately lost OD, with only 10 % of the initial density after 30 min. of treatment. Interestingly, after approximately two hours of stationary OD measurements, the cells started to regrow. This could be explained by the compound being sequestered in the already lysed membrane fragments within solution, effectively lowering the concentration of the compound, allowing for surviving cells to continue proliferation.

	CCCP (µM)	Gramicidin (µM)	Daptomycin (µg/ml)	LL-37 (µg/ml)
WT	12	0.3 - 0.6	1.2	10
ΔlytABCDEF	12	0.3	1.2	10

Table 18: MICs for WT and *ΔlytABCDEF* treated with CCCP (100-1.5 µM range), gramicidin (10-0.15 µM range), daptomycin (50-0.8 µg/ml range), and LL-37 (40-0.15 µg/ml range). The MICs does not change for the autolytic mutant. n=3

Having shown that the compounds induce lysis in *B. subtilis*, I wanted to examine if autolysins were the cause. First, we determined the MICs of both the wild type and the *ΔlytABCDEF* strain (Table 18). We immediately observed that the deletion of several autolysins that result in a cell separation defect phenotype does not change the MICs for any of the compounds. To further establish that the principal mode of action of the compounds

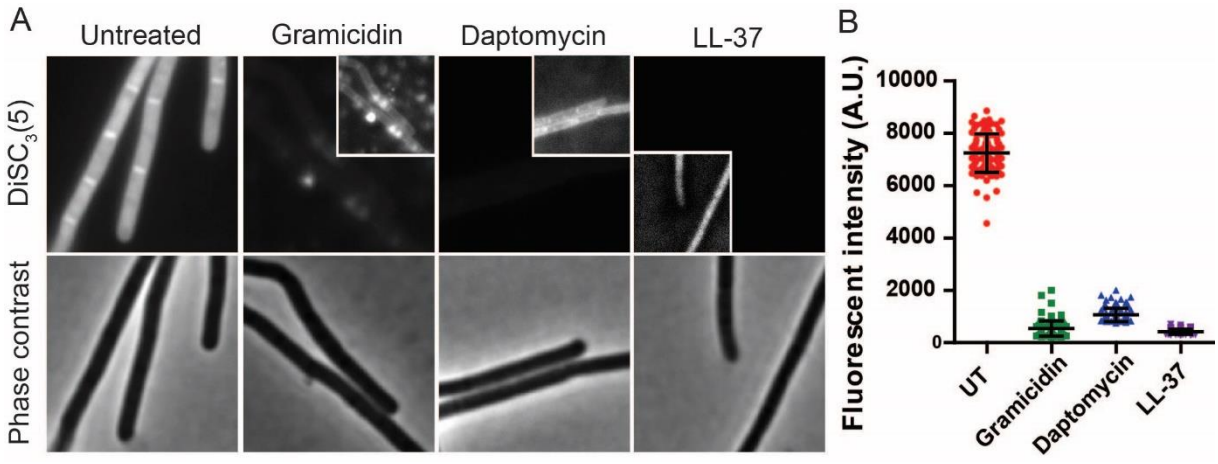

Figure 56: (A) $DiSC_3(5)$ microscopy images of *ΔlytABCDEF* untreated and treated with gramicidin, daptomycin, and LL-37. The large images in the upper panel are $DiSC_3(5)$ emission images which has similar contrast to compare intensities, while the smaller images in the corners have enhanced contrast to emphasize the cells presence. The lower panel is phase contrast images. (B) Quantification of the $DiSC_3(5)$ microscopy images. Error bars represent standard deviation. n=100

against the *ΔlytABCDEF* was membrane depolarisation, a microscopic $DiSC_3(5)$ membrane depolarization assay was carried out (Figure 56A and B).

As indicated by the high $DiSC_3(5)$ signal (Figure 56A), and quantified in (Figure 56B), the untreated *ΔlytABCDEF* cells exhibited expectedly high membrane potential levels. When treated with any of the selected compounds, a clear and essentially complete depolarisation was observed. Based on the unchanged MIC values, and the triggered membrane depolarization comparable to that observed in the wild type, we conclude that the principal mode of action of these antibacterial compounds is the same in the highly chained autolysin-deficient strain.

Next, lysis assays for the *ΔlytABCDEF* mutant were performed using the three compounds, gramicidin, daptomycin and LL-37 with the addition of CCCP for comparison (Figure 57). Upon treatment with gramicidin we see an initial drop to 80 % remaining OD which is maintained for the duration of the experiment. When comparing to wild type (Figure 55), we can report an almost complete rescue of lysis in the autolytic mutant. When treated with daptomycin, we observe that the growth continued for approximately one hour before reaching a plateau, which was maintained for the remainder of the experiment. Again, when comparing to wild type lysis, we noticed a significant rescue. Finally, when treated with LL-37, the OD oscillates between 80-110 % of initial OD, for approximately an hour before finding a plateau at about 80 % remaining OD. As with the other compounds, when

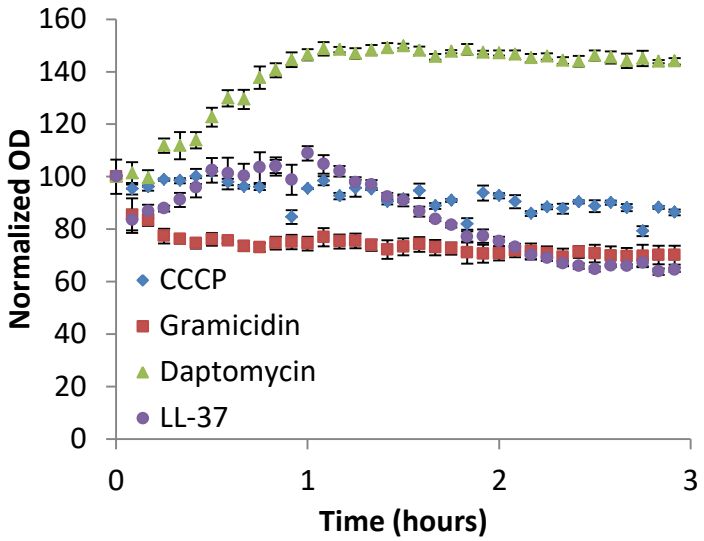

Figure 57: Graph depicting the lysis kinetics of *ΔlytABCDEF* treated with CCCP (100 mM), Gramicidin (10 µg/ml), Daptomycin (10 µg/ml), and LL-37 (40 µg/ml). Lysis is rescued for all compounds. Error bars represent standard deviation. n=3

comparing this result to that of the wild type, we observe a striking rescue of lysis.

Additionally we can see that the most effective depolarizing agent is LL-37, which was not surprising since it forms large pores in the membrane. What was surprising was the fact that even with full depolarization and loss of important metabolites, the *ΔlytABCDEF* mutant almost entirely rescued the induced lysis. Furthermore, daptomycin, which might have several modes of action, only appears to have a bacteriostatic effect on *ΔlytABCDEF*, where there appeared to even be some continued growth for a short period of time before the antimicrobial effects took place.

These results show that lysis induced by gramicidin, daptomycin and LL-37 are all autolytic in nature. I therefore wanted to examine if the compounds functioned through an MreB-dependent mechanism similar to CCCP. It was tested by treating the *mre* triple mutant with each compound. Before examining the lysis profiles of the *mreB* triple deletion, we performed the experiment on the wild type strain supplemented with magnesium to determine the baseline lysis profiles for each compound in the medium conditions required for the *mre*- mutant. The results for wild type cells with and without supplemented magnesium are found in Figure 58A and B. Here we saw that the Gramicidin-triggered lysis is supressed

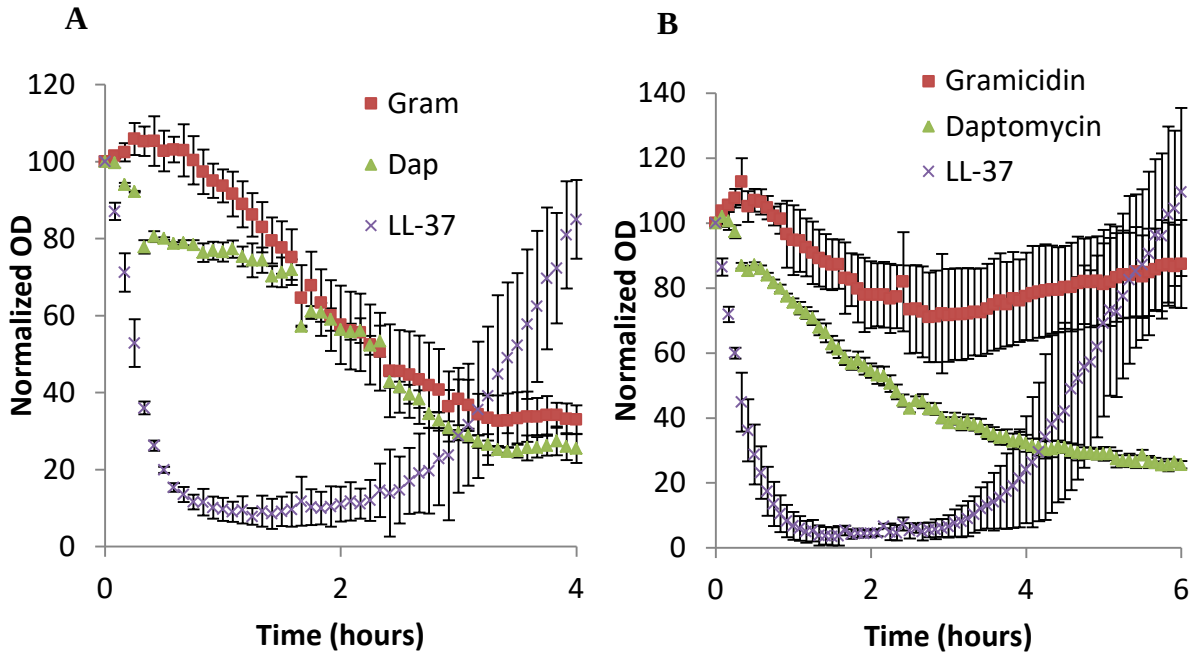

Figure 58: Comparison of bacteriolytic effects by the compounds gramicidin, daptomycin and LL-37 without and with 20 mM $MgCl^2$ supplemented in the medium (A) Graph depicting the lysis kinetics of the compounds gramicidin (10 µg/ml), daptomycin (10 µg/ml), and LL-37 (40 µg/ml) in WT *B. subtilis*. The normalized OD is with the initial OD upon compound addition set to 100. (B) Wild type grown with 20 mM $MgCl_2$, treated with the three compounds gramicidin (10 µg/ml), daptomycin (10 µg/ml) and LL-37 (40 µg/ml). The addition of magnesium partially rescues lysis for all compounds except LL-37. Error bars represent standard deviation. n=3

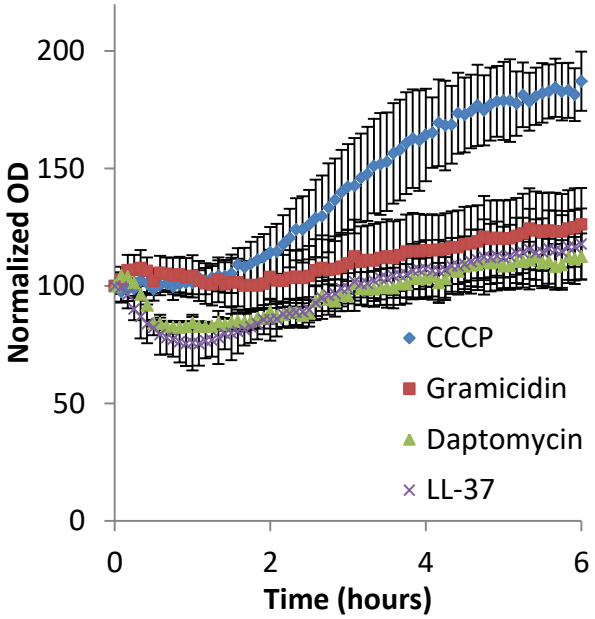

Figure 59: The full MreB cytoskeletal deletion strain *ΔmreB, Δmbl, ΔmreBH* without any suppressor mutations (Isolate V) treated with the compounds CCCP (100 mM), gramicidin (10 µg/ml), daptomycin (10 µg/ml), and LL-37 (40 µg/ml). The strain rescues lysis completely for all compounds, even increases in OD when treated with CCCP. Error bars represent standard deviation. n=3

significantly by Mg^{2+}, whereas the lytic activity of both daptomycin and LL-37 were unaffected. This might be explained by divalent cations blocking the narrow 4 Å channel, which a previous study has already shown to occur with Mn^{2+} ions (Golovanov *et al.*, 1991). Having generated a baseline from which to compare, I treated the *ΔmreB, Δmbl, ΔmreBH* triple mutant with the three compounds (CCCP is included for comparison) (Figure 59). Surprisingly, the *mre*-mutant completely rescued lysis in gramicidin and daptomycin treated cells. Even more impressively, the deletion of *mreB*-homologs entirely rescued the otherwise rapid lysis observed for the wild type when treated with LL-37. These results suggest that the MreB cytoskeleton is indeed directly involved autolysis triggered by membrane targeting antibiotics in *B. subtilis*, and appears to be a part of the general membrane targeting mechanism for multiple classes of antimicrobials.

6.3 – Discussion

We set out to understand why dissipation of PMF induces cell lysis since the existing model was based on conflicting, likely flawed assumptions. Here we show that the

mechanism underlying the lysis process involves autolytic degradation of the cell wall matrix, and is likely triggered by the membrane depolarization-dependent delocalization of MreB.

The old hypothesis was reliant on a pH gradient being formed by protons exported by the respiratory chain (Jolliffe *et al.*, 1981). Such a gradient was difficult to envisage if the later published model describing how the same protons are retained at the membrane surface is correct (Cherepanov *et al.*, 2003). Irrespectively of the presence or absence of a pH gradient over the cell wall, we show that the lysis behaviour of *B. subtilis* is much more complex, and is altered when growing at different temperatures, various growth speeds, and throughout the different growth phases. If lysis was indeed governed by a pH gradient formed by protons, we would expect similar lysis profiles regardless of circumstances, as respiratory activity is maintained in all of these conditions. The old hypothesis was correct, however, about autolysins being the effector enzymes responsible for digestion of the cell wall, although the mechanism of de-regulation was erroneous. We have instead shown a surprising correlation between the speed of autolysis and the degree of MreB delocalization, with complete membrane detachment promoting the fastest lysis. This observation does not however explain why the full MreB cytoskeleton deletion mutant entirely rescues autolysis, since a complete absence of MreB could be similar to the loss of membrane associated MreB into the cytoplasm. Perhaps, this is why osmotically protected medium is needed when creating the full MreB cytoskeleton deletion strain. When creating this triple mutant, we essentially force a similar situation to the MreB detachment scenario, where MreB has disappeared from the membrane surface resulting in unregulated autolysins. Presumably an eventual homeostasis will occur, where the secreted autolysins are all degraded by proteases or diffuse away. At this point, the elongasome will either reside as foci or will be randomly scattered across the membrane. It remains to be determined if the elongasome functions when MreB is removed, or if all growth takes place at septum. Regardless, the autolysins directed by the MreB cytoskeleton might no longer be secreted and will thus not be unregulated, allowing for non-osmotic protected growth.

We propose the following model for MreB delocalization-dependent and membrane potential dissipation-induced autolysis in *B. subtilis* (Figure 60). In polarized cells, the cell wall synthesis machinery is associated with the MreB cytoskeleton (green balls). In order to insert newly synthesized peptidoglycan, the old crosslinks have to be opened, an activity performed by the autolysins (orange balls). The essential and careful regulation of the autolysins is mediated by the MreB cytoskeleton through a process that is currently inferred

(Dominguez-Cuevas *et al.*, 2013) but poorly understood. This system upholds the fragile balance of cell wall homeostasis, constantly opening and inserting new material in order for the organism to grow unhindered. When the membrane potential is dissipated, MreB delocalizes into foci, presumably bringing the cell wall synthesis machinery along as elucidated by PBP1 localization analysis (Y. Kawai *et al.*, 2009). The autolysins, which were secreted to the extracellular space, loose the tight association with the proteins controlling their potentially destructive autolytic activity, thus causing runaway degradation of the cell wall that ultimately leads to cell lysis. Alternatively, upon membrane depolarization, MreB detaches entirely from the membrane, leaving the cell wall synthesis machinery un-guided. The resulting mis-regulation between autolysis and insertion of new peptidoglycan eventually results in cell lysis.

In good agreement with our model, a previous study from our laboratory found that the synthetic lytic cyclic hexapeptide cWFW causes MreB and Mbl delocalization, but crucially not membrane depolarization (Scheinpflug *et al.*, 2017). The induced lysis thus appears to be initiated entirely by the delocalization of the actin homologues (Scheinpflug *et al.*, 2017). Another study from our lab showed that when inducing a type 1 toxin BsrG, *B. subtilis* cells undergo autolysis in a manner similar to when treated with CCCP. Crucially, the induction of BsrG does not cause membrane depolarization, but does cause significant delocalization of MreB (Jahn *et al.*, 2015). Furthermore, it was found that amongst the actin homologues in *B. subtilis*, only MreB was delocalized, and deleting the gene allowed for full suppression of the lytic phenotype (Jahn *et al.*, 2015). These data fully support our model.

Finally, we discovered that membrane depolarization induced autolysis is not just a curiosity of CCCP treatment. Instead it appears to be a rather major, and so far overlooked, component of the mode of action of a multitude of membrane targeting antibiotics. These include molecules such as ion-channels, pore-forming compounds, and the more intricate membrane targeting compounds such as daptomycin. Additionally, a study into the mode of action of daptomycin found that mutations in MreB conferred resistance (Hachmann *et al.*, 2011), implying that the MreB-triggered autolytic process can have broader relevance, and is therefore a prime target for further and more detailed studies.

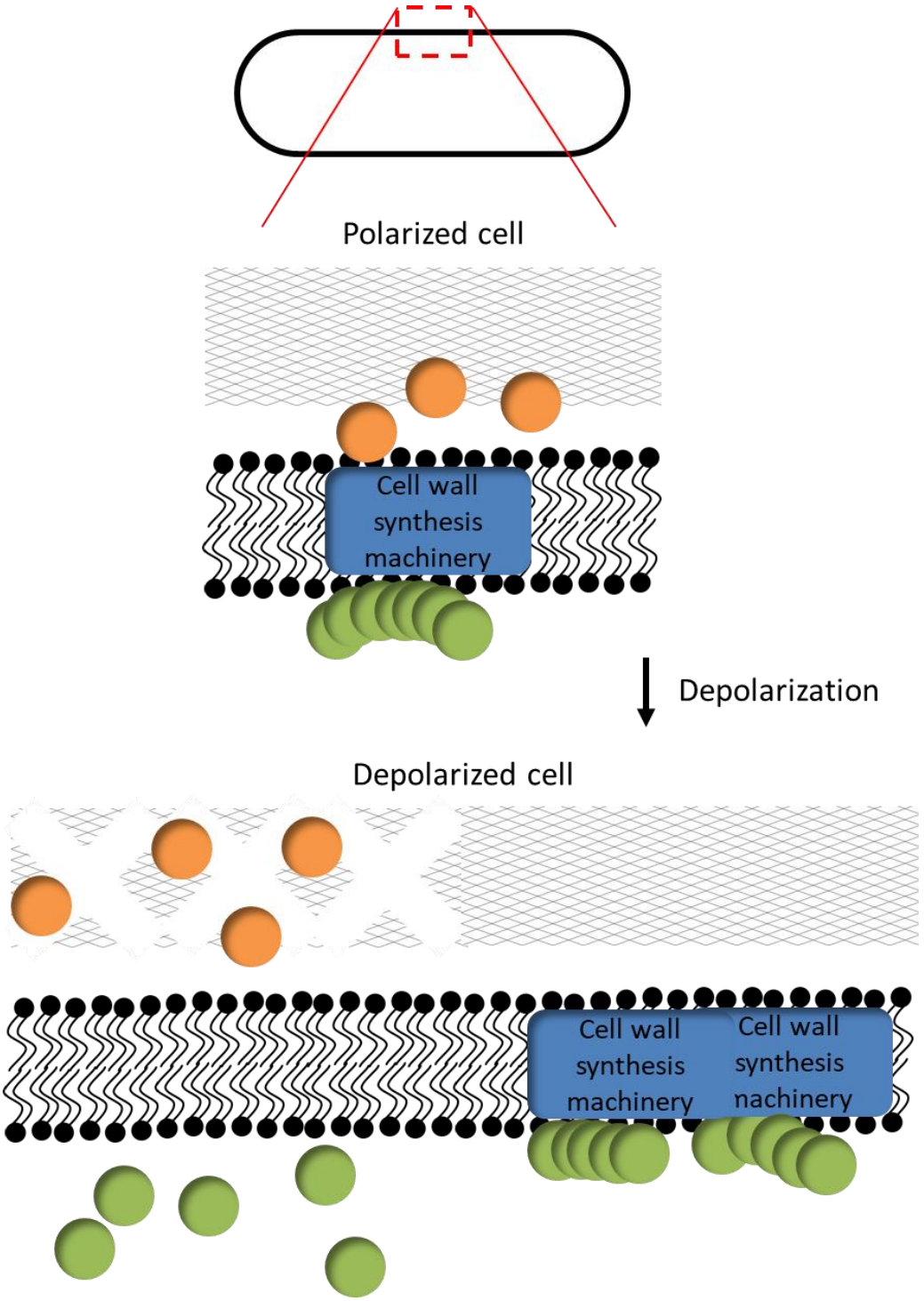

Figure 60: Schematic of our model for MreB delocalization induced autolysis. In a polarized cell MreB (green balls) directs the cell wall synthesis machinery for lateral insertion of newly synthesized peptidoglycan. Autolysins (orange balls) are directed and regulated through a MreB cytoskeleton dependent manner. This couples the degradation and synthesis of peptidoglycan. When the cells get depolarized MreB delocalizes to a few foci within the membrane presumably bringing the rest of the elongasome, or detaches from the membrane entirely. This leaves the already secreted autolysins without their regulators allowing for constitutive activation. The cell wall is degraded uncontrollably without the synthesis machinery in place to insert new material, eventually causing cellular lysis.

Chapter 7 – Mode of Action Determination of Vancoresmycin

7.1 – Introduction

During my PhD studies, I was asked to assist in determining the mode of action of the antimicrobial compound vancoresmycin, as early experiments suggested that it was targeting the bacterial cell membrane. The results became part of a collaborative publication together with the group of Jeff Errington and Demuris Ltd., in which Dr. Bernhard Kepplinger expressed an impressive 141 kbp gene cluster encoding the vancoresmycin synthesis pathway within the heterologous host *Streptomyces coelicolor* M1152, while I performed experiments aiming towards the elucidation of the antimicrobial mode of action (Kepplinger *et al.*, 2018). The compound is a structurally unique tetramic acid containing a polyketide natural product antibiotic, and was originally isolated from the Actinomycete *Amycolatopsis* sp. ST 101170 (Hopmann *et al.*, 2002). Vancoresmycin exhibits MICs in the sub-µg/ml range towards a wide range of Gram positive pathogens such as methicillin-resistant *S. aureus* and vancomycin resistant *Enterococcus* spp. (VRE) (Hopmann *et al.*, 2002).

Previous attempts to elucidate the mode of action of vancoresmycin involved attempting to generate resistant suppressor mutants in *Streptococcus pneumoniae.* When exposing the cells to low concentrations of the compound a low frequency ($2 \cdot 10^{-7}$) of only marginally resistant strains (MICs increased from 0.4 µg/ml to 0.5 µg/ml) were obtained (Becker *et al.*, 2009). It was found through transcription analysis that the differentially expressed genes were all encoding proteins dependent or associated with cytoplasmic membrane activity (Mascher *et al.*, 2003; Becker *et al.*, 2009). Furthermore, initial studies conducted by Bernhard Kepplinger showed that LiaS was up-regulated upon treatment of *B. subtilis* with vancoresmycin, suggesting cell envelope as the principal antimicrobial target. While the Lia-response is commonly observed as part of the cellular response towards antibiotics that inhibit membrane-anchored steps of cell wall biosynthesis (Mascher *et al.*, 2004), additional tests using wall less L-forms showed that the compound does not target the peptidoglycan synthesis (Kepplinger *et al.*, 2018). This directed our focus towards the remaining part of the cell envelope, the cytoplasmic membrane.

I analysed the mode of action of vancoresmycin against *B. subtilis* through a combination of microscopy, spectroscopy, and examination of the ability of the cells to carry out oxidative phosphorylation. Furthermore, I developed an assay combining two fluorescent

dyes to determine cell polarization and membrane integrity at single cell resolution. All the results shown in this chapter were generated by me.

7.2 – Results

7.2.1 – Vancoresmycin induces lysis in B. subtilis

Initially we wanted to test the functional concentration range of vancoresmycin in *B. subtilis*. To test this, we performed a lysis assay essentially as described earlier in the thesis. However, instead of growing the cells to middle exponential phase, the cells were treated at the lower cell density of OD_{600} of 0.2. This was to maintain same cell density throughout the different experiments, and guided by the optimal OD-range for the membrane depolarization assays. As shown in Figure 61, the functional range of vancoresmycin in *B. subtilis* ranges from 50 ng/ml, where we observe the first inhibition of growth, to 200 ng/ml where the cells are rapidly lysed after the addition of vancoresmycin (Figure 61). The compound works in a dose dependent manner with a relatively short change in concentration resulting in a shift

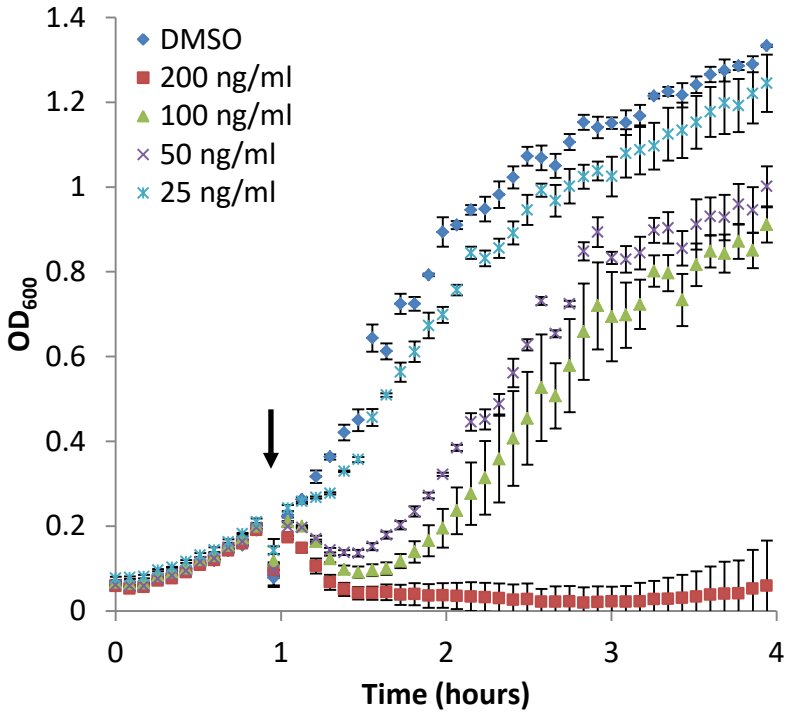

Figure 61: Vancoresmycin concentration dependent lysis of *B. subtilis*. The first concentration influencing the growht of *B. subtilis* is 50 ng/ml, which induces a drop of OD followed by growth at similar speed to untreated cells. The first inhibitory concentration is at 200 ng/ml. Error bars represent standard deviation. n=3 (Kepplinger *et al.*, 2018)

from non-inhibitory to fully bacteriolytic activity. Having found the functional concentration of vancoresmycin, we next wanted to examine if the compound interferes with the membrane permeability barrier, and whether it does so by membrane depolarization or a larger scale membrane permeabilization through pore formation.

7.2.2 – Vancoresmycin dissipates membrane potential

In order to quantitatively determine if vancoresmycin dissipates membrane potential, I performed a calibrated $DiSC_3(5)$ assay that not only resolves if vancoresmycin can influence cell membrane potential levels, but also provides an estimate of the degree of depolarisation caused. In this assay, valinomycin is used to calibrate the $DiSC_3(5)$ signal according to a set voltage across the membrane. Using the Nernst equation, which describes electrical equilibrium potential across the membrane according to compound concentrations on either side, we can calculate the medium K^+ concentrations that lead to a given level of membrane potential upon addition of valinomycin (Te Winkel *et al.*, 2016). Based on the published

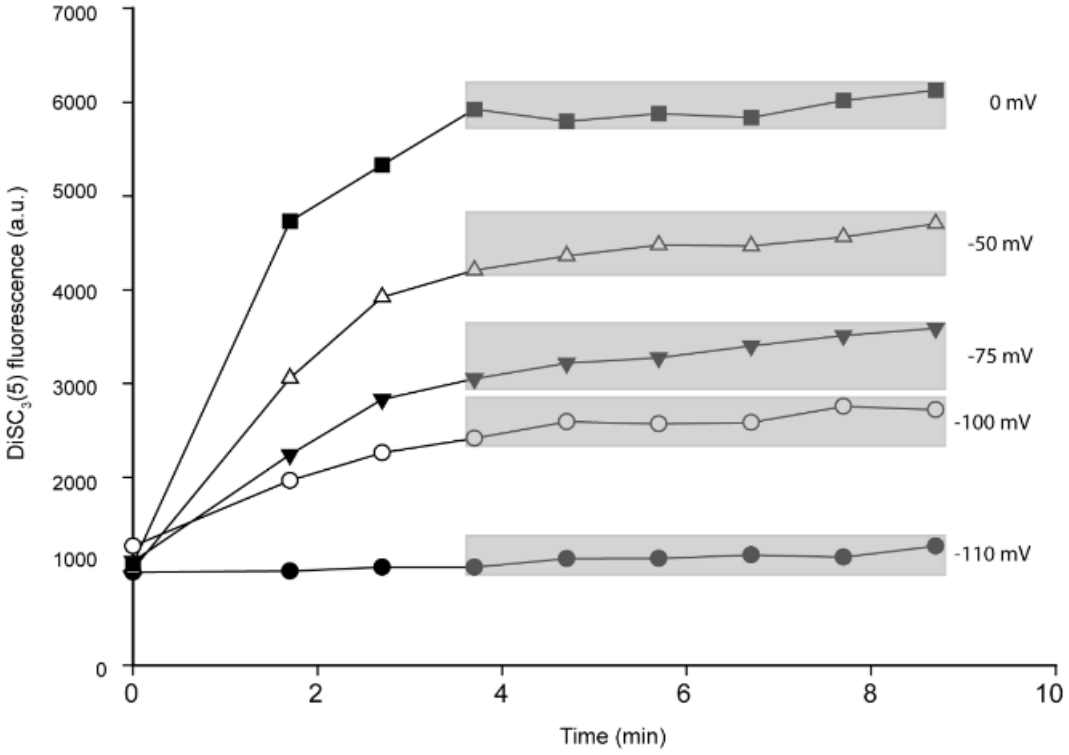

Figure 62: $DiSC_3(5)$ membrane potential calibration using valinomycin and K^+. Fluorescence intensity of $DiSC_3(5)$ in *B. subtilis* cell suspensions in which the membrane potential levels are clamped to predefined values, using a combination of varying medium K^+ concentrations and the addition of K^+ carrier valinomycin. The addition of valinomycin at time point 0 dissipates the membrane potential to values which are determined by the varying K^+ concentration within. The grey ranges represent the 95% confidence interval of the mean fluorescence values obtained from triplicate measurements. (Kepplinger *et al.*, 2018)

intracellular concentration of K^+ in *B. subtilis* of about 300 mM (Whatmore *et al.*, 1990), we can set membrane potential to 0 mV (no gradient) using a medium supplemented with the same concentration of K^+. In contrast, adding no K^+ to the medium and relying on approximately 3 mM provided by the rich medium components, a voltage across the membrane of -110 mV can be achieved. Trans-membrane voltage levels between these extremes can be transiently achieved by medium K+ concentrations calculated by Nernst equation. After addition of valinomycin that allows for K^+ to traverse the membrane and establish the equilibrium potential, I waited until the $DiSC_3(5)$ signal equilibrated (Figure 62). The last six values obtained are shown with grey boxes and were used to calculate the 95% confidence intervals used in following experiments as calibration of the $DiSC_3(5)$ signal.

A $DiSC_3(5)$ assay was now performed to determine if vancoresmycin depolarized the membrane, and if so, to what extent. Vancoresmycin concentrations of both lethal and sub-lethal levels were included, as judged by the data shown in Figure 61. Surprisingly, the cells do not exhibit full depolarization from any of the concentrations examined (Figure 63). Instead the depolarization is concentration-dependent, gradual and incomplete. While this result does support the notion that vancoresmycin inhibits *B. subtilis* cells by causing membrane depolarisation, it is inconsistent with pore formation and does not explain the observed rapid loss of OD.

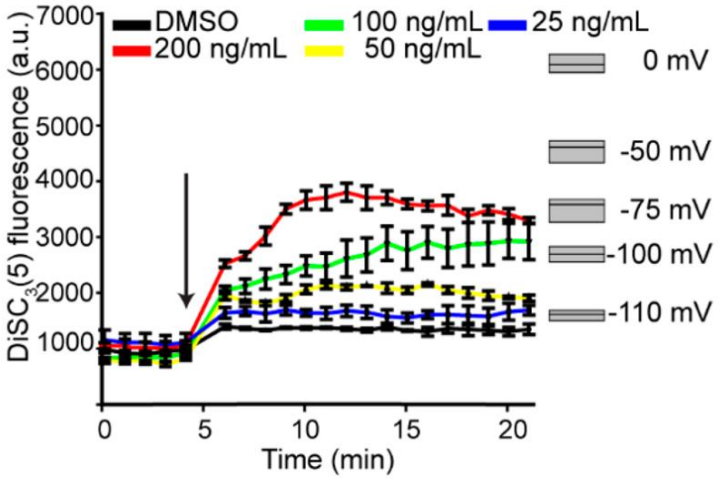

Figure 63: Dissipation of membrane potential triggered by vancoresmycin. *B. subtilis* membrane potential levels were quantified following addition of different levels of vancoresmycin using $DiSC_3(5)$. The time point of antibiotic addition is indicated with an arrow. The calibration depicted to the right represents the mean and the 95% confidence interval of DiSC3(5) fluorescence in cells with predefined membrane potential levels. Error bars represent standard deviation. n=3 (Kepplinger *et al.*, 2018)

One possibility to explain the partial depolarisation observed with the DiSC3(5)-assay is a significant cell-to-cell heterogeneity, with a fraction of cells fully depolarized, and another fraction remaining fully energized. This scenario would result in erroneous interpretations of the DiSC3(5)-assay results and would exclude pore-formation as a potential mechanism of action. To address this question in the context of vancoresmycin, and to also provide an assay that will unambiguously distinguish between more subtle cell depolarisation and physical, indiscriminate membrane permeabilization, I developed a single cell assay combining two reporters $DiSC_3(5)$ and Sytox Green. In this assay, the voltage-dependent cellular accumulation of $DiSC_3(5)$ that is used to monitor membrane potential was combined with the membrane permeability indicator Sytox green. Sytox green is a large high-affinity nucleic acid staining dye, which accumulates within the cytoplasm when the membrane is perforated. The fluorescence intensity for both dyes is quantified immediately after treatment with the selected compound, and plotted against each other to determine which cells were depolarized and those that, in addition to being depolarized, had been permeabilized. Gramicidin, a compound that forms small channels specific for monovalent cations was included as a positive control for membrane depolarization without pore formation; whereas nisin was included as a pore forming compound. DMSO, which was used as the solvent for both gramicidin and vancoresmycin, was included as a negative control.

When treating the cells with DMSO only, we observed strong $DiSC_3(5)$ signals while the Sytox Green intensities remained extremely low, indicating the cells, as expected, were well energized and there were no perforations in the membrane (Figure 64A). When treating with gramicidin, the $DiSC_3(5)$ intensity reduced significantly while the Sytox Green intensity remained low, clearly showing depolarized cells with otherwise intact membranes. The nisin treated cells exhibited similarly low intensities of $DiSC_3(5)$ while the Sytox Green intensity had increased significantly, clearly showing that the cells were depolarized through pore formation. Vancoresmycin induced $DiSC_3(5)$ intensities that were between DMSO and gramicidin treated cells, while Sytox Green intensities were low, suggesting incomplete non-pore forming depolarization.

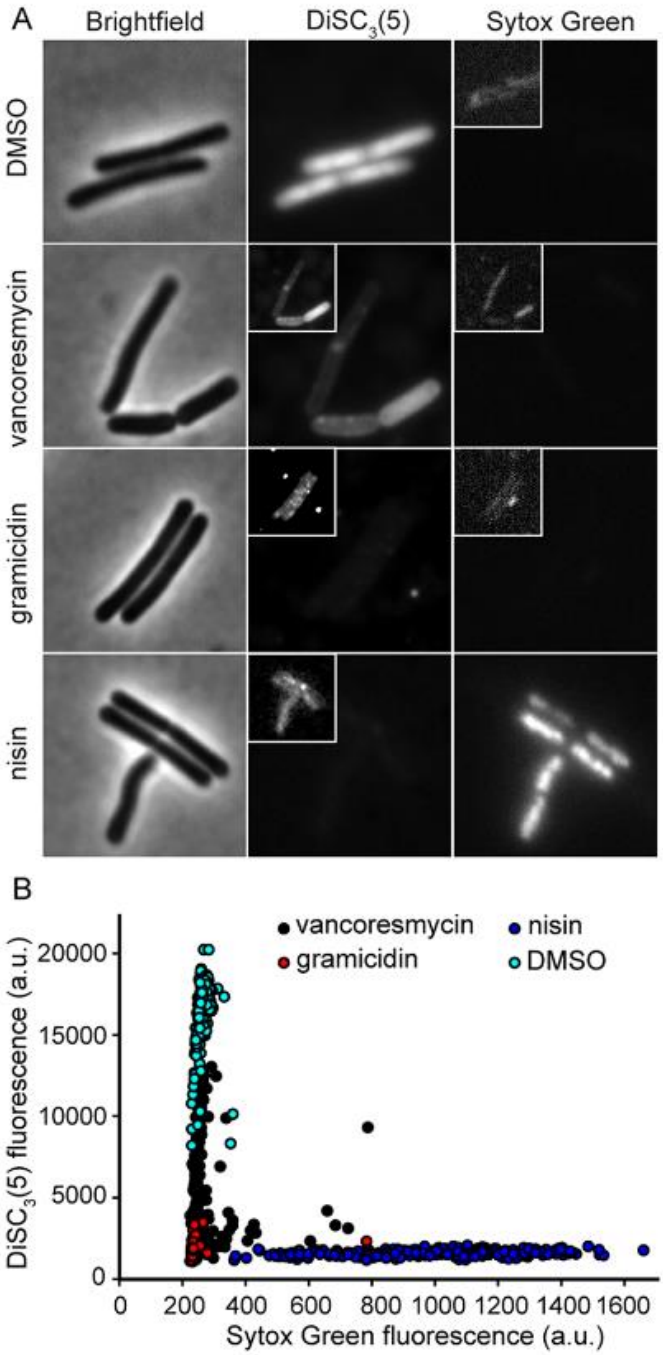

Figure 64: Single cell measurements of membrane potential and permeability. (A) Phase contrast and fluorescent images of *B. subtilis* cells stained with $DiSC_3(5)$ and the membrane impermeable Sytox Green. The large images depict the cells with identical contrast settings, while the smaller images are optimized to reveal cells with low signal intensity. The used concentrations of compounds are 100 ng/ml (vancoresmycin), 5 µg/ml (gramicidin), 10 µM (nisin). Incubation of 1 min. (B) Quantified $DiSC_3(5)$ and Sytox Green signal intensities for cells treated with vancoresmycin, gramicidin, nisin and DMSO. n=112. (Kepplinger *et al.*, 2018)

To gain more quantitative insights into the membrane activity of vancoresmycin, I quantified the cellular intensities for 112 cells picked randomly from the phase contrast images (Figure 64B). DMSO treated cells on average show a high $DiSC_3(5)$ intensity with variations from about 8.000 to 21.000 a.u. whereas the Sytox Green signal was relatively low and stable at about 220 a.u.. Gramicidin treated cells exhibited $DiSC_3(5)$ intensities between 500 and 4.000 a.u., and Sytox Green intensities at about 220 a.u. as well. This corresponds well to the expected scenario of de-energized cells with intact membranes. Nisin treated cells exhibited $DiSC_3(5)$ intensities below 2.000 a.u., and Sytox Green intensities between 250 and 1.700 a.u.. This clearly shows a majority of depolarized cells with a perforated membrane. Finally, vancoresmycin treated cells exhibited $DiSC_3(5)$ intensities between 13.000 and 2.000 a.u, and Sytox Green intensities between 220 and 800 a.u., although the majority of the cells are at low intensity end of this spectrum. These results are consistent with cells that have partially depolarized membranes, and where only a small minority of cells show signs of membrane permeabilization. These results are in good agreement with the data shown in Figure 63, and suggest that vancoresmycin indeed triggers partial, although very heterogeneous, membrane depolarisation in the active concentration range. Critically, both the partial membrane depolarisation and the lack of Sytox Green signal rules out pore formation as the principal mechanism of action.

In order to examine the redox potential of the cell, which is directly linked to the activity of the electron transport chain, the commercially available kit alamarBlue was used. This method relies on redox, and thus respiration-dependent conversion of the colourless compound resazurin into the fluorescent resorufin. Again, as the solvent used for dissolving vancoresmycin, DMSO was included as a negative control. Oxygen-depleted and heat inactivated cells were included as positive controls. The effect of vancomycin was tested at concentrations of 100 ng/ml, 200 ng/ml, and 400 ng/ml. All samples incubated for 60 min. The DMSO treated cells reached a fluorescence intensity of about 95.000 a.u. (Figure 65). The oxygen depleted cells, which were purged with argon for 45 min. prior to addition of resazurin, exhibited an expected decrease in the fluorescence intensity of about 55.000 a.u., showing that although the cells were oxygen depleted, they still exhibited a reducing cytoplasmic environment. As expected, the heat inactivated cells supported only a very low level of resazurin conversion. The vancoresmycin treated cells exhibited a concentration dependent decrease in resazurin conversion, indeed indicating that electron transport chain is likely to be inhibited by the compound. However, this is not necessarily a direct effect

because respiration and membrane potential are intricately connected in *B. subtilis*. Not only is respiration required for building up the membrane potential but, conversely, high respiratory activity requires membrane potential (Schirawski and Unden, 1998). Consequently, it remains speculative if the observed reduction in respiratory chain activity is a cause or a consequence of the loss of membrane potential.

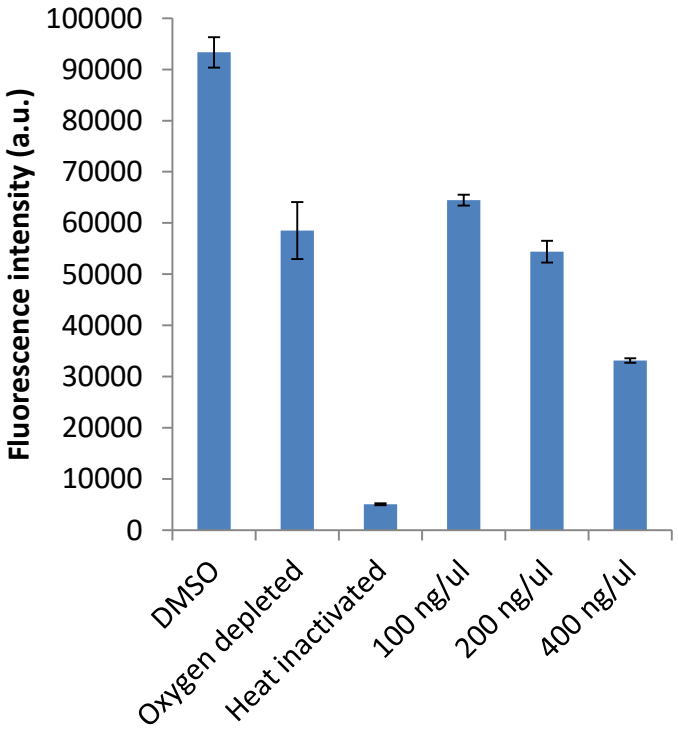

Figure 65: Concentration dependent inhibition of *B. subtilis* respiratory chain activity by vancoresmycin. The graph depicts the relative respiration levels of untreated *B. subtilis* cells, and cells incubated with 100 ng/mL, 200 ng/mL and 400 ng/mL vancoresmycin. Heat inactivated cells and cells depleted for the terminal electron acceptor O^2 were measured in parallel as positive controls. Error bars represent standard deviation. n=3

7.3 – Discussion

The data presented suggest that vancoresmycin is indeed a membrane targeting compound, which dissipates membrane potential at least as part of its antibacterial mode of action. The mechanism through which the compound depolarizes the membrane is thus far unknown, but our data clearly demonstrates that there is no pore formation associated with the membrane depolarization *in vivo*. Rather, we believe that vancoresmycin functions through a more subtle membrane perturbation mechanism, or through ion carrier activity. More detailed studies are required in order to elucidate the specific interaction between vancoresmycin and

the membrane, and its consequences on trans-membrane voltage. Additionally, we found that vancoresmycin inhibits the electron transport chain in a concentration dependent manner. Consequently, we cannot rule out the possibility that vancoresmycin does not directly act on bacterial membranes but rather inhibits a specific component of the respiratory chain. However, the fact that respiration and membrane potential are intimately connected in *B. subtilis* makes it difficult to prove the direction of causality. The fact that vancoresmycin retains a strong antibacterial activity against Enterococci and Streptococci (Kepplinger *et al.*, 2018), both of which are without the classical TCA and respiratory chain under standard laboratory conditions (Y. Yamamoto *et al.*, 2005; Yuehua *et al.*, 2016), suggest that the most likely explanation is that vancoresmycin depolarizes the membrane, which in turn inhibits respiration as a secondary effect.

To further elucidate the exact mechanism through which vancoresmycin functions, multiple avenues could be explored. First, we could examine if lysis still occurs in the *ΔlytABCDEF* strain in which the major autolysins are deleted. As discovered in Chapter 6, depolarization induced lysis is indeed autolysis. If the lysis caused by vancoresmycin is rescued in the mutant strain, the bacteriolytic activity of vancoresmycin could also be attributed to autolysis. Additionally, it would be interesting to examine the ion conductivity of the membrane upon treatment with vancoresmycin using the already well-established method of black lipid membranes (Tien and Diana, 1967), in which electrodes are utilized to determine ion movement across membranes. When comparing to treatment with other compounds with known membrane mode of action, we could possibly be able to determine the specific mode of action for vancoresmycin. Finally, using Molecular Dynamics, a model could be generated that attempts to predict the structure vancoresmycin forms within the membrane, further elucidating its effects.

Chapter 8 – Concluding Remarks and Future Directions

The focus of the research presented in this thesis has been the remarkably complex and intricate interplay between bacterial cytoplasmic membrane and the MreB cytoskeleton. Three main avenues were studied: the mechanisms of MreB-dependent adaptation of membrane fatty acid composition and fluidity; the effects of the dissipation of membrane potential, as well as the accompanied changes in membrane fluidity and delocalization of peripheral membrane proteins including MreB; and finally, membrane potential dissipation induced autolysis.

In Chapter 3 membrane fatty acid composition and fluidity changes were examined upon deletion of MreB and its homologues. Prior to this project, a previous publication from our laboratory had already suggested that the composition of fatty acids changed when *mreB* and its homologues were deleted (Strahl *et al.*, 2014). Here, the altered membrane fatty acid composition was shown in previously constructed deletions strains that all share a common parent strain, 168ED. However, this strain background carries a mutation rendering a major cell envelope regulatory two component system WalRK constitutively active (Dominguez-Cuevas *et al.*, 2012). Due to its role in envelope homeostasis, it was suspected that the constitutive activation of the corresponding extensive regulon could have influenced the observed changes in lipid composition. Furthermore, the presence or absence of additional suppressor mutations that might have occurred upon construction of the *mre*-strains was unknown. For these reasons, reconstruction of the strains in a strain background with a functional WalRK-system was conducted. The strains, which included a single deletion of *mreC* and 4 independently constructed strains carrying deletion of all three *mreB*-homologs, were then sent for genome sequencing to analyse any potentially emerging suppressor mutations . The genome analysis revealed that while deletion of *mreC* had not prompted the emergence of suppressor mutations, three of the four *mreB* triple deletion strains carried extensive suppressor mutations. None of the observed suppressors appeared more than once, with the exception for a large duplicated stretch of the genome containing important genes involved in division and peptidoglycan synthesis that emerged twice through independent duplication events. These suppressor mutations turned out to be non-essential for survival without the MreB-cytoskeleton, but nevertheless appeared to correlate with faster growth. When comparing the *mreB*-triple deletion strain without suppressor mutations against one containing the most, it was found that deletion of *mreB* and its homologues does indeed alter the fatty acid composition significantly towards longer anteiso fatty acid species.

Surprisingly, it was found that the drastically altered fatty acid composition was in no clear way reflected in the accompanied measurement of membrane fluidity. It was found that the MreB cytoskeleton deletion strain with the most suppressor mutations (KS60) exhibited the least fatty acid changes compared to the strain without suppressor mutations (isolate V), but that the fluidity of KS60 deviated more from the wild type than isolate V. Consequently, it appears that the absence of MreB-homologs indeed affects the membrane homeostasis, but in a non-trivial way. Our findings are consistent with a model in which the presence or absence of the MreB-cytoskeleton directly influences the way a given fatty acid composition translates to a corresponding level of membrane fluidity. In the absence of this factor, the cells appear to correct the mismatch between composition and fluidity by accumulating suppressor mutations that restore the fatty acid composition, rather than fluidity, towards a membrane state found in the wild type.

A component of the membrane that was not examined in this study, but which has high potential to influence the membrane fluidity, is the lipid head group composition (Bernal *et al.*, 2007b). In order to better understand the role of the MreB cytoskeleton in membrane homeostasis, an analysis of the lipid head group composition should be performed in future studies. This current information gap might assist in explaining the discrepancies observed between fatty acid composition and fluidity in the MreB deletion mutants.

The current prevailing model of membrane homeostasis builds on the basic premise that cells maintain stable levels of membrane fluidity in changing environmental conditions through the adaptation of lipid fatty acid composition (Ernst *et al.*, 2016). Conversely, membrane fluidity is seen solely as a function of its lipid composition. Our observations that the MreB-cytoskeleton has a significant contribution to membrane fluidity, together with the surprising finding that the membrane fluidity-levels observed in live cells at different temperatures are remarkably different, somewhat questions the validity of this currently simplistic model.

Furthermore, in the context of growth speed adaptations, the duplicated genes are interesting, as these might explain why the strain is able to grow and divide much faster than the strain lacking the duplication. Genes of immediate interest would be the *fts* genes responsible for division, the *ylm*-operon that includes the important division proteins SepF and DivIVA, and the *mur* genes responsible for peptidoglycan synthesis. Together, these genes might explain the decreased doubling time. They are also good candidates to explain

the fluidity alterations due to their proximity to the membrane, and the components thereof. Perhaps the increased amounts of FtsAZ are needed to properly carry out division in the wider spherical cells. This might explain why septum initiation in the MreB triple deletion strain was occasionally only located over one side of the cell rather than the entire circumference, since too few division proteins are present to form a complete, correct, Z-ring. Additionally, the reason for the duplicated cell wall precursor genes could be to support growth solely from septa as seen in *Streptococcus* (Higgins and Shockman, 1970), or through septal and dispersed cell wall insertion as seen in *Lactococcus lactis* (Perez-Nunez *et al.*, 2011). To test which duplicated gene operon or snp is responsible for the increased growth speed, each individual operon and snp could be transferred (or recreated alone) into our suppressor free triple *mreB* deletion strain and subjected to growth assays.

Finally, it would be interesting to explore how *B. subtilis* inserts new peptidoglycan when growing in these mutants, as the lateral cytoskeleton has been deleted. The growth could occur through two different mechanisms. The first being growth from septum, like that seen in many cocci bacteria (Higgins and Shockman, 1970; Zapun *et al.*, 2008). The second would still have a functioning elongasome, albeit in an undirected manner that allows for peptidoglycan insertion in whatever location the cell wall synthesis machinery resided upon the deletion of MreB. This could be studied using a fluorescent version of vancomycin that binds to exposed D-ala-D-ala (Tiyanont *et al.*, 2006), or by using the antibiotic-free fluorescently labelled D-amino acids (FDAAs) that allow *in situ* labelling of nascent peptidoglycan (Kuru *et al.*, 2015; Hsu *et al.*, 2017), thus revealing insertion sites. Both are already well-established methods in *B. subtilis*.

In Chapter 4, membrane potential dependent fluidity changes and subsequent protein delocalization was explored. At the onset of the project it was known that multiple peripheral membrane proteins – including MinD, FtsA, and MreB – delocalize upon membrane depolarization (Strahl and Hamoen, 2010). The mechanism through which this delocalization occurs is not understood but, in case of MinD and FtsA, appears to be a property of their membrane binding amphipathic helix (Strahl and Hamoen, 2010)(Unpublished observations). Preliminary experiments from our own laboratory, which were confirmed in this study, indicated that upon membrane depolarization the fluidity of the membrane was significantly reduced, thus providing a prime candidate for a mechanism to explain the membrane-potential dependency of amphipathic helices. To study why the membrane fluidity changed upon depolarization, three hypotheses were formulated.

The first hypothesis involved cardiolipin enriched membrane domains, and how these could potentially be influenced by membrane depolarization, thereby affecting the overall membrane fluidity. The postulated cardiolipin domains are localized to the same cellular areas as MinD and FtsA (F. Kawai *et al.*, 2004). Consequently, dispersal or delocalization of cardiolipin-domains through membrane depolarization could plausibly cause a concomitant loss of localisation of any associated proteins as well. In the course of this thesis, it was discovered that the tool used to detect these lipid domains (the membrane dye NAO) is not as specific for cardiolipin as assumed, and that the observed domains were in fact a consequence of the staining procedure rather than something that *B. subtilis* cells natively feature (Chapter 5) (Pogmore *et al.*, 2018). Consequently, the very existence of cardiolipin enriched domains in *B. subtilis* was questioned and the associated hypothesis was thus discarded.

The second hypothesis addressed the possibility that the observed fluidity reduction upon membrane depolarization could be caused by the simultaneous delocalization of MreB. MreB co-localizes with lipid domains characterized by high membrane fluidity, and upon membrane depolarization, both structures delocalize (Strahl and Hamoen, 2010). Consequently, the observed change in overall membrane fluidity could be caused by local changes affecting these lipid domains. However, it turned out that the fluidity changes upon membrane depolarization still occurred in the complete *mre*-cytoskeleton deletion mutant (*ΔmreB*, *Δmbl*, *ΔmreBH*). Additionally, it was found that MinD and FtsA delocalized in a *ΔmreC* strain, in which MreB remains localized upon membrane depolarization. Together, these results revealed that the fluidity changes and protein delocalization upon membrane depolarization occurs independent of MreB, prompting the rejection of this hypothesis as well.

Finally, the third hypothesis involved the phenomenon termed electrostriction. This physical effect occurs when two compartments (such the cytoplasm and the extracellular environment) are separated by a flexible insulator (such as the cell membrane) and an electrical field (such as the trans-membrane potential) is present across the insulator. Under these conditions, the electrical field exerts a compressing force upon the insulator, which is dependent on the strength of the field and the thickness of the insulator. Given the relatively high level of membrane potential in living cells and the thin lipid bilayer acting as an the insulator, this force can reach significant values in biological systems (Heimburg, 2012). More fluid membranes adopt a characteristically thinner configuration due the higher degree of fatty acid disorder. Consequently, a dissipation of an electrical field across the membrane,

which normally promotes the thinner, more fluid configuration, allows the membrane to relax into a thicker, less fluid configuration (Heimburg, 2012).

To examine if this physical effect was indeed responsible for the observed membrane rigidification upon depolarization (and the associated protein delocalization), we chose to analyse if comparable effects occur when another membrane-compressive force, the turgor pressure, was modulated. It was found that changes in turgor alone are not sufficient to change membrane fluidity significantly, or to cause delocalization FtsA, although slight localization alterations occurred for MinD. Nevertheless, the observed membrane rigidification upon depolarization, and electrostriction as a potential underlying mechanism, still remain the best explanation for how MinD and FtsA delocalizes upon membrane depolarization. To study this phenomenon further, a collaboration with Dr. Ulrich Zachariae (Dundee University) has been established with the aim to use molecular dynamics simulations to characterize the changes in the lipid bilayer caused by collapse of trans-membrane potential. This approach should allow verification of the hypothesis that changes in eletrostrictive forces underlay the membrane rigidification observed upon depolarization.

In Chapter 6 the mechanism for membrane potential dissipation induced lysis was examined. At the onset of the project, a hypothesis that attempts to describe the phenomenon already existed (Jolliffe *et al.*, 1981). This was based on the fact that in well energized cells the respiratory chain continuously pumps protons out into the extracellular environment. These protons were assumed to diffuse away from the membrane surface and enter the surrounding cell wall matrix, resulting in a pH gradient across the cell wall. Such a pH gradient would, in turn, modulate the activity of autolytic enzymes present within the cell wall. When the proton motive force becomes dissipated, the hypothesis proposes that the pH gradient would also dissipate, thereby activating autolysins and, consequently, causing degradation of the cell wall and cell lysis (Jolliffe *et al.*, 1981). However, it was later discovered that the protons pumped out of the cell by the respiratory chain are predominately retained in a boundary layer close to the membrane surface, thus never entering the cell wall mesh (Cherepanov *et al.*, 2003). This finding directly invalidates the basic premise of the pH-dependent autolysis-hypothesis. In this thesis, it was confirmed that lysis triggered by collapse of PMF is indeed based on autolysis. Furthermore, the autolytic process was shown to be highly dependent on environmental conditions, such as medium, growth phase, and growth temperature. No cellular programming appeared to be induced as a response to PMF collapse. Having confirmed that autolysis is the mechanism through which lysis occurs, MreB and its

homologues were examined since they are the regulators of the major autolysins in *B. subtilis* (Dominguez-Cuevas *et al.*, 2013). Using a *mreB* triple deletion strain (*ΔmreB, Δmbl, ΔmreBH*), it was shown that PMF-collapse induced autolysis was rescued in the absence of the lateral cytoskeleton, suggesting that the induced autolysis was caused by disturbance in the poorly understood regulatory network that connects the intracellular MreB-cytoskeleton to the extracellular autolysins. As mentioned earlier, dissipation of membrane potential triggers delocalization of MreB-homologs (Strahl and Hamoen, 2010). Upon examining MreB localization patterns in wild type *B. subtilis* during conditions with different lysis kinetics, it was discovered that the lysis showed a remarkably strong correlation with the degree of MreB delocalization. These results suggest that the mechanism through which membrane depolarization-induced autolysis occurs is via MreB delocalization-dependent miss-regulation of already secreted autolysins. Finally, we showed that this observed autolytic process explains the bacteriolytic activity of membrane active antimicrobials such as daptomycin and host-defence peptide LL-37.

Future work is needed to examine this new model in more detail. This includes examining other organisms to determine if the proposed mode of action is specific to *B. subtilis*. For example, initial experiments could examine bacterial species evolutionarily close to *B. subtilis*. If the close relative of *B. subtilis* exhibit similar autolysis, Gram-positive species more distantly related should be included to reveal precisely how widespread this mechanism actually is. Furthermore, an examination of cocci bacteria would be interesting since they do not encode *mreB*, and so must presumably have evolved different mechanisms. Finally, testing a range of Gram negatives would be interesting, as experiments using CCCP treated *E. coli* revealed a bacteriostatic, rather than lytic, effect (Ghoul *et al.*, 1989). Finally, further studies into the mechanism through which MreB delocalizes, and the pathway leading to miss-regulation of autolytic enzymes should be undertaken.

In Chapter 7 the antibacterial mode of action for the natural product compound vancoresmycin was determined. At the onset of the project, previous attempts to elucidate the mode of action had involved the generation of resistant mutants in *Streptococcus pneumoniae*. Only marginally resistant strains were obtained at low frequency (Becker *et al.*, 2009). It was also published that the genes that become differentially expressed upon vancoresmycin treatment were all encoding proteins dependent or associated with cytoplasmic membrane activity (Mascher *et al.*, 2003; Becker *et al.*, 2009). Initial screens conducted by our collaborator Demuris \Ltd. had shown that the Lia-regulon was up-regulated upon treatment

with vancoresmycin, thus suggesting cell envelope stress. However, inhibition of cell wall synthesis as potential mechanism was ruled out (Kepplinger *et al.*, 2018). This left the cytoplasmic membrane as the most likely molecular target. Using a combination of microscopy and spectroscopy, hereunder a newly developed combinational microscopic assay, it was discovered that vancoresmycin indeed targets the cell membrane, where it triggers dissipation of membrane potential through a mechanism that does not involve pore formation. Furthermore, it was discovered that cellular respiration was also inhibited upon compound treatment. The gathered data suggest a non-pore forming membrane perturbation mechanism that dissipates the membrane potential, resulting in the inhibition of cellular respiration and, ultimately, cell lysis.

To further elucidate the mode of action of vancoresmycin, the major autolysin deletion strain (*ΔlytABCDEF*) could be used to determine, as appears likely, if vancoresmycin induces lysis through the same autolytic mechanism as proposed in Chapter 6. Another avenue of research could be an ion conductivity assay using the established black lipid membrane system (Tien and Diana, 1967). Using this method, it would be possible to directly measure the effects on ion conductibility that vancoresmycin induces upon membrane association. Additionally, Molecular Dynamics could be used to gain insight into the interactions between the compound and the membrane.

References

Abhayawardhane, Y. and Stewart, G. C. (1995) 'Bacillus subtilis possesses a second determinant with extensive sequence similarity to the Escherichia coli mreB morphogene', *J Bacteriol*, 177(3), pp. 765-73.

Aguilar, P. S., Cronan, J. E., Jr. and de Mendoza, D. (1998) 'A Bacillus subtilis gene induced by cold shock encodes a membrane phospholipid desaturase', *J Bacteriol*, 180(8), pp. 2194-200.

Aguilar, P. S., Hernandez-Arriaga, A. M., Cybulski, L. E., Erazo, A. C. and de Mendoza, D. (2001) 'Molecular basis of thermosensing: a two-component signal transduction thermometer in Bacillus subtilis', *EMBO J*, 20(7), pp. 1681-91.

Allen, N. E., Hobbs, J. N. and Alborn, W. E., Jr. (1987) 'Inhibition of peptidoglycan biosynthesis in gram-positive bacteria by LY146032', *Antimicrob Agents Chemother*, 31(7), pp. 1093-9.

Andersen, O. S. and Koeppe, R. E., 2nd (2007) 'Bilayer thickness and membrane protein function: an energetic perspective', *Annu Rev Biophys Biomol Struct*, 36, pp. 107-30.

Anderson, J. S., Matsuhashi, M., Haskin, M. A. and Strominger, J. L. (1965) 'Lipid-Phosphoacetylmuramyl-Pentapeptide and Lipid-Phosphodisaccharide-Pentapeptide: Presumed Membrane Transport Intermediates in Cell Wall Synthesis', *Proc Natl Acad Sci U S A*, 53, pp. 881-9.

Asai, K., Ootsuji, T., Obata, K., Matsumoto, T., Fujita, Y. and Sadaie, Y. (2007) 'Regulatory role of RsgI in sigI expression in Bacillus subtilis', *Microbiology*, 153(Pt 1), pp. 92-101.

Asai, K., Yamaguchi, H., Kang, C. M., Yoshida, K., Fujita, Y. and Sadaie, Y. (2003) 'DNA microarray analysis of Bacillus subtilis sigma factors of extracytoplasmic function family', *FEMS Microbiol Lett*, 220(1), pp. 155-60.

Au, N., Kuester-Schoeck, E., Mandava, V., Bothwell, L. E., Canny, S. P., Chachu, K., Colavito, S. A., Fuller, S. N., Groban, E. S., Hensley, L. A., O'Brien, T. C., Shah, A., Tierney, J. T., Tomm, L. L., O'Gara, T. M., Goranov, A. I., Grossman, A. D. and Lovett, C. M. (2005) 'Genetic composition of the Bacillus subtilis SOS system', *J Bacteriol*, 187(22), pp. 7655-66.

Bach, J. N., Albrecht, N. and Bramkamp, M. (2014) 'Imaging DivIVA dynamics using photo-convertible and activatable fluorophores in Bacillus subtilis', *Front Microbiol*, 5, p. 59.

Bach, J. N. and Bramkamp, M. (2013) 'Flotillins functionally organize the bacterial membrane', *Mol Microbiol*, 88(6), pp. 1205-17.

Balaji, B., O'Connor, K., Lucas, J. R., Anderson, J. M. and Csonka, L. N. (2005) 'Timing of induction of osmotically controlled genes in Salmonella enterica Serovar Typhimurium, determined with quantitative real-time reverse transcription-PCR', *Appl Environ Microbiol*, 71(12), pp. 8273-83.

Barbe, V., Cruveiller, S., Kunst, F., Lenoble, P., Meurice, G., Sekowska, A., Vallenet, D., Wang, T., Moszer, I., Medigue, C. and Danchin, A. (2009) 'From a consortium sequence to a unified sequence: the Bacillus subtilis 168 reference genome a decade later', *Microbiology*, 155(Pt 6), pp. 1758-75.

Barreteau, H., Kovac, A., Boniface, A., Sova, M., Gobec, S. and Blanot, D. (2008) 'Cytoplasmic steps of peptidoglycan biosynthesis', *FEMS Microbiol Rev*, 32(2), pp. 168-207.

Barrett, D., Wang, T. S., Yuan, Y., Zhang, Y., Kahne, D. and Walker, S. (2007) 'Analysis of glycan polymers produced by peptidoglycan glycosyltransferases', *J Biol Chem*, 282(44), pp. 31964-71.

Beall, B. and Lutkenhaus, J. (1991) 'FtsZ in Bacillus subtilis is required for vegetative septation and for asymmetric septation during sporulation', *Genes Dev*, 5(3), pp. 447-55.

Becker, P., Hakenbeck, R. and Henrich, B. (2009) 'An ABC transporter of Streptococcus pneumoniae involved in susceptibility to vancoresmycin and bacitracin', *Antimicrob Agents Chemother*, 53(5), pp. 2034-41.
Belas, R. (2014) 'Biofilms, flagella, and mechanosensing of surfaces by bacteria', *Trends Microbiol*, 22(9), pp. 517-27.
Bendezu, F. O. and de Boer, P. A. (2008) 'Conditional lethality, division defects, membrane involution, and endocytosis in mre and mrd shape mutants of Escherichia coli', *J Bacteriol*, 190(5), pp. 1792-811.
Bernal, P., Munoz-Rojas, J., Hurtado, A., Ramos, J. L. and Segura, A. (2007a) 'A Pseudomonas putida cardiolipin synthesis mutant exhibits increased sensitivity to drugs related to transport functionality', *Environ Microbiol*, 9(5), pp. 1135-45.
Bernal, P., Segura, A. and Ramos, J. L. (2007b) 'Compensatory role of the cis-trans-isomerase and cardiolipin synthase in the membrane fluidity of Pseudomonas putida DOT-T1E', *Environ Microbiol*, 9(7), pp. 1658-64.
Bigay, J. and Antonny, B. (2012) 'Curvature, lipid packing, and electrostatics of membrane organelles: defining cellular territories in determining specificity', *Dev Cell*, 23(5), pp. 886-95.
Bisicchia, P., Noone, D., Lioliou, E., Howell, A., Quigley, S., Jensen, T., Jarmer, H. and Devine, K. M. (2007) 'The essential YycFG two-component system controls cell wall metabolism in Bacillus subtilis', *Mol Microbiol*, 65(1), pp. 180-200.
Bisson-Filho, A. W., Hsu, Y. P., Squyres, G. R., Kuru, E., Wu, F., Jukes, C., Sun, Y., Dekker, C., Holden, S., VanNieuwenhze, M. S., Brun, Y. V. and Garner, E. C. (2017) 'Treadmilling by FtsZ filaments drives peptidoglycan synthesis and bacterial cell division', *Science*, 355(6326), pp. 739-743.
Bligh, E. G. and Dyer, W. J. (1959) 'A rapid method of total lipid extraction and purification', *Can J Biochem Physiol*, 37(8), pp. 911-7.
Bouhss, A., Trunkfield, A. E., Bugg, T. D. and Mengin-Lecreulx, D. (2008) 'The biosynthesis of peptidoglycan lipid-linked intermediates', *FEMS Microbiol Rev*, 32(2), pp. 208-33.
Boylan, S. A., Thomas, M. D. and Price, C. W. (1991) 'Genetic method to identify regulons controlled by nonessential elements: isolation of a gene dependent on alternate transcription factor sigma B of Bacillus subtilis', *J Bacteriol*, 173(24), pp. 7856-66.
Boylen, C. W. and Ensign, J. C. (1968) 'Ratio of teichoic acid and peptidoglycan in cell walls of Bacillus subtilis following spire germination and during vegetative growth', *J Bacteriol*, 96(2), pp. 421-7.
Bramkamp, M., Emmins, R., Weston, L., Donovan, C., Daniel, R. A. and Errington, J. (2008) 'A novel component of the division-site selection system of Bacillus subtilis and a new mode of action for the division inhibitor MinCD', *Mol Microbiol*, 70(6), pp. 1556-69.
Branda, S. S., Gonzalez-Pastor, J. E., Ben-Yehuda, S., Losick, R. and Kolter, R. (2001) 'Fruiting body formation by Bacillus subtilis', *Proc Natl Acad Sci U S A*, 98(20), pp. 11621-6.
Breukink, E., van Heusden, H. E., Vollmerhaus, P. J., Swiezewska, E., Brunner, L., Walker, S., Heck, A. J. and de Kruijff, B. (2003) 'Lipid II is an intrinsic component of the pore induced by nisin in bacterial membranes', *J Biol Chem*, 278(22), pp. 19898-903.
Brooks, N. J. (2014) 'Pressure effects on lipids and bio-membrane assemblies', *IUCrJ*, 1(Pt 6), pp. 470-7.
Burkholder, P. R. and Giles, N. H., Jr. (1947) 'Induced biochemical mutations in Bacillus subtilis', *Am J Bot*, 34(6), pp. 345-8.
Cao, M., Bernat, B. A., Wang, Z., Armstrong, R. N. and Helmann, J. D. (2001) 'FosB, a cysteine-dependent fosfomycin resistance protein under the control of sigma(W), an extracytoplasmic-function sigma factor in Bacillus subtilis', *J Bacteriol*, 183(7), pp. 2380-3.

Cao, M., Kobel, P. A., Morshedi, M. M., Wu, M. F., Paddon, C. and Helmann, J. D. (2002) 'Defining the Bacillus subtilis sigma(W) regulon: a comparative analysis of promoter consensus search, run-off transcription/macroarray analysis (ROMA), and transcriptional profiling approaches', *J Mol Biol*, 316(3), pp. 443-57.
Cao, M., Moore, C. M. and Helmann, J. D. (2005) 'Bacillus subtilis paraquat resistance is directed by sigmaM, an extracytoplasmic function sigma factor, and is conferred by YqjL and BcrC', *J Bacteriol*, 187(9), pp. 2948-56.
Cao, M., Salzberg, L., Tsai, C. S., Mascher, T., Bonilla, C., Wang, T., Ye, R. W., Marquez-Magana, L. and Helmann, J. D. (2003) 'Regulation of the Bacillus subtilis extracytoplasmic function protein sigma(Y) and its target promoters', *J Bacteriol*, 185(16), pp. 4883-90.
Carballido-Lopez, R., Formstone, A., Li, Y., Ehrlich, S. D., Noirot, P. and Errington, J. (2006) 'Actin homolog MreBH governs cell morphogenesis by localization of the cell wall hydrolase LytE', *Dev Cell*, 11(3), pp. 399-409.
Cayley, S. and Record, M. T., Jr. (2003) 'Roles of cytoplasmic osmolytes, water, and crowding in the response of Escherichia coli to osmotic stress: biophysical basis of osmoprotection by glycine betaine', *Biochemistry*, 42(43), pp. 12596-609.
Chen, R., Guttenplan, S. B., Blair, K. M. and Kearns, D. B. (2009) 'Role of the sigmaD-dependent autolysins in Bacillus subtilis population heterogeneity', *J Bacteriol*, 191(18), pp. 5775-84.
Cheng, Y. Q. (2006) 'Deciphering the biosynthetic codes for the potent anti-SARS-CoV cyclodepsipeptide valinomycin in Streptomyces tsusimaensis ATCC 15141', *Chembiochem*, 7(3), pp. 471-7.
Cherepanov, D. A., Feniouk, B. A., Junge, W. and Mulkidjanian, A. Y. (2003) 'Low dielectric permittivity of water at the membrane interface: effect on the energy coupling mechanism in biological membranes', *Biophys J*, 85(2), pp. 1307-16.
Cocucci, E., Kim, J. Y., Bai, Y. and Pabla, N. (2017) 'Role of Passive Diffusion, Transporters, and Membrane Trafficking-Mediated Processes in Cellular Drug Transport', *Clin Pharmacol Ther*, 101(1), pp. 121-129.
Commichau, F. M., Wacker, I., Schleider, J., Blencke, H. M., Reif, I., Tripal, P. and Stulke, J. (2007) 'Characterization of Bacillus subtilis mutants with carbon source-independent glutamate biosynthesis', *J Mol Microbiol Biotechnol*, 12(1-2), pp. 106-13.
Courtney, C. R., Cozy, L. M. and Kearns, D. B. (2012) 'Molecular characterization of the flagellar hook in Bacillus subtilis', *J Bacteriol*, 194(17), pp. 4619-29.
Cunarro, J. and Weiner, M. W. (1975) 'Mechanism of action of agents which uncouple oxidative phosphorylation: direct correlation between proton-carrying and respiratory-releasing properties using rat liver mitochondria', *Biochim Biophys Acta*, 387(2), pp. 234-40.
Cybulski, L. E., Martin, M., Mansilla, M. C., Fernandez, A. and de Mendoza, D. (2010) 'Membrane thickness cue for cold sensing in a bacterium', *Curr Biol*, 20(17), pp. 1539-44.
D'Elia, M. A., Millar, K. E., Beveridge, T. J. and Brown, E. D. (2006) 'Wall teichoic acid polymers are dispensable for cell viability in Bacillus subtilis', *J Bacteriol*, 188(23), pp. 8313-6.
Daniel, R. A., Williams, A. M. and Errington, J. (1996) 'A complex four-gene operon containing essential cell division gene pbpB in Bacillus subtilis', *J Bacteriol*, 178(8), pp. 2343-50.
Daniels, C. J., Bole, D. G., Quay, S. C. and Oxender, D. L. (1981) 'Role for membrane potential in the secretion of protein into the periplasm of Escherichia coli', *Proc Natl Acad Sci U S A*, 78(9), pp. 5396-400.
de Pedro, M. A., Donachie, W. D., Holtje, J. V. and Schwarz, H. (2001) 'Constitutive septal murein synthesis in Escherichia coli with impaired activity of the morphogenetic proteins RodA and penicillin-binding protein 2', *J Bacteriol*, 183(14), pp. 4115-26.

Debono, M., Barnhart, M., Carrell, C. B., Hoffmann, J. A., Occolowitz, J. L., Abbott, B. J., Fukuda, D. S., Hamill, R. L., Biemann, K. and Herlihy, W. C. (1987) 'A21978C, a complex of new acidic peptide antibiotics: isolation, chemistry, and mass spectral structure elucidation', *J Antibiot (Tokyo)*, 40(6), pp. 761-77.
Defeu Soufo, H. J. and Graumann, P. L. (2005) 'Bacillus subtilis actin-like protein MreB influences the positioning of the replication machinery and requires membrane proteins MreC/D and other actin-like proteins for proper localization', *BMC Cell Biol*, 6(1), p. 10.
Dempwolff, F., Moller, H. M. and Graumann, P. L. (2012a) 'Synthetic motility and cell shape defects associated with deletions of flotillin/reggie paralogs in Bacillus subtilis and interplay of these proteins with NfeD proteins', *J Bacteriol*, 194(17), pp. 4652-61.
Dempwolff, F., Wischhusen, H. M., Specht, M. and Graumann, P. L. (2012b) 'The deletion of bacterial dynamin and flotillin genes results in pleiotrophic effects on cell division, cell growth and in cell shape maintenance', *BMC Microbiol*, 12, p. 298.
den Blaauwen, T., Hamoen, L. W. and Levin, P. A. (2017) 'The divisome at 25: the road ahead', *Curr Opin Microbiol*, 36, pp. 85-94.
Dinnbier, U., Limpinsel, E., Schmid, R. and Bakker, E. P. (1988) 'Transient accumulation of potassium glutamate and its replacement by trehalose during adaptation of growing cells of Escherichia coli K-12 to elevated sodium chloride concentrations', *Arch Microbiol*, 150(4), pp. 348-57.
Diskowski, M., Mehdipour, A. R., Wunnicke, D., Mills, D. J., Mikusevic, V., Barland, N., Hoffmann, J., Morgner, N., Steinhoff, H. J., Hummer, G., Vonck, J. and Hanelt, I. (2017) 'Helical jackknives control the gates of the double-pore K(+) uptake system KtrAB', *Elife*, 6.
Doi, M., Wachi, M., Ishino, F., Tomioka, S., Ito, M., Sakagami, Y., Suzuki, A. and Matsuhashi, M. (1988) 'Determinations of the DNA sequence of the mreB gene and of the gene products of the mre region that function in formation of the rod shape of Escherichia coli cells', *J Bacteriol*, 170(10), pp. 4619-24.
Dominguez-Cuevas, P., Mercier, R., Leaver, M., Kawai, Y. and Errington, J. (2012) 'The rod to L-form transition of Bacillus subtilis is limited by a requirement for the protoplast to escape from the cell wall sacculus', *Mol Microbiol*, 83(1), pp. 52-66.
Dominguez-Cuevas, P., Porcelli, I., Daniel, R. A. and Errington, J. (2013) 'Differentiated roles for MreB-actin isologues and autolytic enzymes in Bacillus subtilis morphogenesis', *Mol Microbiol*, 89(6), pp. 1084-98.
Dominguez-Escobar, J., Chastanet, A., Crevenna, A. H., Fromion, V., Wedlich-Soldner, R. and Carballido-Lopez, R. (2011) 'Processive movement of MreB-associated cell wall biosynthetic complexes in bacteria', *Science*, 333(6039), pp. 225-8.
Donovan, C. and Bramkamp, M. (2009) 'Characterization and subcellular localization of a bacterial flotillin homologue', *Microbiology*, 155(Pt 6), pp. 1786-99.
Dramsi, S., Magnet, S., Davison, S. and Arthur, M. (2008) 'Covalent attachment of proteins to peptidoglycan', *FEMS Microbiol Rev*, 32(2), pp. 307-20.
Duax, W. L., Griffin, J. F., Langs, D. A., Smith, G. D., Grochulski, P., Pletnev, V. and Ivanov, V. (1996) 'Molecular structure and mechanisms of action of cyclic and linear ion transport antibiotics', *Biopolymers*, 40(1), pp. 141-55.
Dubrac, S. and Msadek, T. (2008) 'Tearing down the wall: peptidoglycan metabolism and the WalK/WalR (YycG/YycF) essential two-component system', *Adv Exp Med Biol*, 631, pp. 214-28.
Duman, R., Ishikawa, S., Celik, I., Strahl, H., Ogasawara, N., Troc, P., Lowe, J. and Hamoen, L. W. (2013) 'Structural and genetic analyses reveal the protein SepF as a new membrane anchor for the Z ring', *Proc Natl Acad Sci U S A*, 110(48), pp. E4601-10.

Edwards, D. H. and Errington, J. (1997) 'The Bacillus subtilis DivIVA protein targets to the division septum and controls the site specificity of cell division', *Mol Microbiol*, 24(5), pp. 905-15.
Egan, A. J. and Vollmer, W. (2013) 'The physiology of bacterial cell division', *Ann N Y Acad Sci*, 1277, pp. 8-28.
El Khoury, M., Swain, J., Sautrey, G., Zimmermann, L., Van Der Smissen, P., Decout, J. L. and Mingeot-Leclercq, M. P. (2017) 'Targeting Bacterial Cardiolipin Enriched Microdomains: An Antimicrobial Strategy Used by Amphiphilic Aminoglycoside Antibiotics', *Sci Rep*, 7(1), p. 10697.
Emami, K., Guyet, A., Kawai, Y., Devi, J., Wu, L. J., Allenby, N., Daniel, R. A. and Errington, J. (2017) 'RodA as the missing glycosyltransferase in Bacillus subtilis and antibiotic discovery for the peptidoglycan polymerase pathway', *Nat Microbiol*, 2, p. 16253.
Epand, R. M., Walker, C., Epand, R. F. and Magarvey, N. A. (2016) 'Molecular mechanisms of membrane targeting antibiotics', *Biochim Biophys Acta*, 1858(5), pp. 980-7.
Ernst, R., Ejsing, C. S. and Antonny, B. (2016) 'Homeoviscous Adaptation and the Regulation of Membrane Lipids', *J Mol Biol*, 428(24 Pt A), pp. 4776-4791.
Errington, J. (2015) 'Bacterial morphogenesis and the enigmatic MreB helix', *Nat Rev Microbiol*, 13(4), pp. 241-8.
Errington, J. (2017) 'Cell wall-deficient, L-form bacteria in the 21st century: a personal perspective', *Biochem Soc Trans*, 45(2), pp. 287-295.
Errington, J., Daniel, R. A. and Scheffers, D. J. (2003) 'Cytokinesis in bacteria', *Microbiol Mol Biol Rev*, 67(1), pp. 52-65, table of contents.
Errington, J. and Wu, L. J. (2017) 'Cell Cycle Machinery in Bacillus subtilis', *Subcell Biochem*, 84, pp. 67-101.
Fajardo, V. A., McMeekin, L. and LeBlanc, P. J. (2011) 'Influence of phospholipid species on membrane fluidity: a meta-analysis for a novel phospholipid fluidity index', *J Membr Biol*, 244(2), pp. 97-103.
Favini-Stabile, S., Contreras-Martel, C., Thielens, N. and Dessen, A. (2013) 'MreB and MurG as scaffolds for the cytoplasmic steps of peptidoglycan biosynthesis', *Environ Microbiol*, 15(12), pp. 3218-28.
Formstone, A., Carballido-Lopez, R., Noirot, P., Errington, J. and Scheffers, D. J. (2008) 'Localization and interactions of teichoic acid synthetic enzymes in Bacillus subtilis', *J Bacteriol*, 190(5), pp. 1812-21.
Frolov, V. A., Shnyrova, A. V. and Zimmerberg, J. (2011) 'Lipid polymorphisms and membrane shape', *Cold Spring Harb Perspect Biol*, 3(11), p. a004747.
Gamba, P., Veening, J. W., Saunders, N. J., Hamoen, L. W. and Daniel, R. A. (2009) 'Two-step assembly dynamics of the Bacillus subtilis divisome', *J Bacteriol*, 191(13), pp. 4186-94.
Ganchev, D. N., Hasper, H. E., Breukink, E. and de Kruijff, B. (2006) 'Size and orientation of the lipid II headgroup as revealed by AFM imaging', *Biochemistry*, 45(19), pp. 6195-202.
Garner, E. C., Bernard, R., Wang, W., Zhuang, X., Rudner, D. Z. and Mitchison, T. (2011) 'Coupled, circumferential motions of the cell wall synthesis machinery and MreB filaments in B. subtilis', *Science*, 333(6039), pp. 222-5.
Gerbino, E., Carasi, P., Mobili, P., Serradell, M. A. and Gomez-Zavaglia, A. (2015) 'Role of S-layer proteins in bacteria', *World J Microbiol Biotechnol*, 31(12), pp. 1877-87.
Ghoul, M., Pommepuy, M., Moillo-Batt, A. and Cormier, M. (1989) 'Effect of carbonyl cyanide m-chlorophenylhydrazone on Escherichia coli halotolerance', *Appl Environ Microbiol*, 55(4), pp. 1040-3.
Gilbert, R. J., Dalla Serra, M., Froelich, C. J., Wallace, M. I. and Anderluh, G. (2014) 'Membrane pore formation at protein-lipid interfaces', *Trends Biochem Sci*, 39(11), pp. 510-6.

Golovanov, A. P., Barsukov, I. L., Arseniev, A. S., Bystrov, V. F., Sukhanov, S. V. and Barsukov, L. I. (1991) 'The divalent cation-binding sites of gramicidin A transmembrane ion-channel', *Biopolymers*, 31(4), pp. 425-34.
Gregory, J. A., Becker, E. C. and Pogliano, K. (2008) 'Bacillus subtilis MinC destabilizes FtsZ-rings at new cell poles and contributes to the timing of cell division', *Genes Dev*, 22(24), pp. 3475-88.
Gruber, T. M. and Gross, C. A. (2003) 'Multiple sigma subunits and the partitioning of bacterial transcription space', *Annu Rev Microbiol*, 57, pp. 441-66.
Gruszecki, W. I. and Strzalka, K. (2005) 'Carotenoids as modulators of lipid membrane physical properties', *Biochim Biophys Acta*, 1740(2), pp. 108-15.
Gudmundsson, G. H., Agerberth, B., Odeberg, J., Bergman, T., Olsson, B. and Salcedo, R. (1996) 'The human gene FALL39 and processing of the cathelin precursor to the antibacterial peptide LL-37 in granulocytes', *Eur J Biochem*, 238(2), pp. 325-32.
Guffanti, A. A., Clejan, S., Falk, L. H., Hicks, D. B. and Krulwich, T. A. (1987) 'Isolation and characterization of uncoupler-resistant mutants of Bacillus subtilis', *J Bacteriol*, 169(10), pp. 4469-78.
Gundlach, J., Commichau, F. M. and Stulke, J. (2018) 'Perspective of ions and messengers: an intricate link between potassium, glutamate, and cyclic di-AMP', *Curr Genet*, 64(1), pp. 191-195.
Gundogdu, M. E., Kawai, Y., Pavlendova, N., Ogasawara, N., Errington, J., Scheffers, D. J. and Hamoen, L. W. (2011) 'Large ring polymers align FtsZ polymers for normal septum formation', *EMBO J*, 30(3), pp. 617-26.
Guo, W., Kurze, V., Huber, T., Afdhal, N. H., Beyer, K. and Hamilton, J. A. (2002) 'A solid-state NMR study of phospholipid-cholesterol interactions: sphingomyelin-cholesterol binary systems', *Biophys J*, 83(3), pp. 1465-78.
Gurtovenko, A. A. and Anwar, J. (2007) 'Modulating the structure and properties of cell membranes: the molecular mechanism of action of dimethyl sulfoxide', *J Phys Chem B*, 111(35), pp. 10453-60.
Hachmann, A. B., Angert, E. R. and Helmann, J. D. (2009) 'Genetic analysis of factors affecting susceptibility of Bacillus subtilis to daptomycin', *Antimicrob Agents Chemother*, 53(4), pp. 1598-609.
Hachmann, A. B., Sevim, E., Gaballa, A., Popham, D. L., Antelmann, H. and Helmann, J. D. (2011) 'Reduction in membrane phosphatidylglycerol content leads to daptomycin resistance in Bacillus subtilis', *Antimicrob Agents Chemother*, 55(9), pp. 4326-37.
Haest, C. W., de Gier, J., den Kamp, J. O., Bartels, P. and van Deenen, L. L. (1972) 'Chages in permeability of Staphylococcus aureus and derived liposomes with varying lipid composition', *Biochim Biophys Acta*, 255(3), pp. 720-33.
Hamaide, F., Kushner, D. J. and Sprott, G. D. (1983) 'Proton motive force and Na+/H+ antiport in a moderate halophile', *J Bacteriol*, 156(2), pp. 537-44.
Harry, E. J., Rodwell, J. and Wake, R. G. (1999) 'Co-ordinating DNA replication with cell division in bacteria: a link between the early stages of a round of replication and mid-cell Z ring assembly', *Mol Microbiol*, 33(1), pp. 33-40.
Haugland, R. P., Spence, M. T. Z. and Johnson, I. D. (1996) *Handbook of fluorescent probes and research chemicals*. 6th edn. Eugene, OR, USA (4849 Pitchford Ave., Eugene 97402): Molecular Probes.
Hazel, J. R. and Williams, E. E. (1990) 'The role of alterations in membrane lipid composition in enabling physiological adaptation of organisms to their physical environment', *Prog Lipid Res*, 29(3), pp. 167-227.
Heefner, D. L. (1982) 'Transport of H+, K+, Na+ and Ca++ in Streptococcus', *Mol Cell Biochem*, 44(2), pp. 81-106.

Heimburg, T. (2012) 'The capacitance and electromechanical coupling of lipid membranes close to transitions: the effect of electrostriction', *Biophys J*, 103(5), pp. 918-29.
Hendrix, R. W. (2002) 'Bacteriophages: evolution of the majority', *Theor Popul Biol*, 61(4), pp. 471-80.
Heytler, P. G. and Prichard, W. W. (1962) 'A new class of uncoupling agents--carbonyl cyanide phenylhydrazones', *Biochem Biophys Res Commun*, 7, pp. 272-5.
Higashi, Y., Strominger, J. L. and Sweeley, C. C. (1967) 'Structure of a lipid intermediate in cell wall peptidoglycan synthesis: a derivative of a C55 isoprenoid alcohol', *Proc Natl Acad Sci U S A*, 57(6), pp. 1878-84.
Higgins, M. L. and Shockman, G. D. (1970) 'Model for cell wall growth of Streptococcus faecalis', *J Bacteriol*, 101(2), pp. 643-8.
Hladky, S. B. and Haydon, D. A. (1972) 'Ion transfer across lipid membranes in the presence of gramicidin A. I. Studies of the unit conductance channel', *Biochim Biophys Acta*, 274(2), pp. 294-312.
Ho, T. D. and Ellermeier, C. D. (2012) 'Extra cytoplasmic function sigma factor activation', *Curr Opin Microbiol*, 15(2), pp. 182-8.
Ho, T. D., Hastie, J. L., Intile, P. J. and Ellermeier, C. D. (2011) 'The Bacillus subtilis extracytoplasmic function sigma factor sigma(V) is induced by lysozyme and provides resistance to lysozyme', *J Bacteriol*, 193(22), pp. 6215-22.
Holtmann, G., Bakker, E. P., Uozumi, N. and Bremer, E. (2003) 'KtrAB and KtrCD: two K+ uptake systems in Bacillus subtilis and their role in adaptation to hypertonicity', *J Bacteriol*, 185(4), pp. 1289-98.
Hooke, R. (1665) 'Micrographia: or some Physiological Descriptions of Minute Bodies made by Magnifying Glasses with Observations and Inquiries thereupon', *Martyn and Ja. Allestry, Printers to the Royal Society, London*.
Hopmann, C., Kurz, M., Brönstrup, M., Wink, J. and LeBeller, D. (2002) 'Isolation and structure elucidation of vancoresmycin—a new antibiotic from Amycolatopsis sp. ST 101170', *Tetrahedron Letters*, 43(3), pp. 435-438.
Hosoi, S., Mochizuki, N., Hayashi, S. and Kasai, M. (1980) 'Control of membrane potential by external H+ concentration in Bacillus subtilis as determined by an ion-selective electrode', *Biochim Biophys Acta*, 600(3), pp. 844-52.
Hsu, Y. P., Rittichier, J., Kuru, E., Yablonowski, J., Pasciak, E., Tekkam, S., Hall, E., Murphy, B., Lee, T. K., Garner, E. C., Huang, K. C., Brun, Y. V. and VanNieuwenhze, M. S. (2017) 'Full color palette of fluorescent d-amino acids for in situ labeling of bacterial cell walls', *Chem Sci*, 8(9), pp. 6313-6321.
Huang, W. Z., Wang, J. J., Chen, H. J., Chen, J. T. and Shaw, G. C. (2013) 'The heat-inducible essential response regulator WalR positively regulates transcription of sigI, mreBH and lytE in Bacillus subtilis under heat stress', *Res Microbiol*, 164(10), pp. 998-1008.
Huang, X., Decatur, A., Sorokin, A. and Helmann, J. D. (1997) 'The Bacillus subtilis sigma(X) protein is an extracytoplasmic function sigma factor contributing to survival at high temperature', *J Bacteriol*, 179(9), pp. 2915-21.
Huang, X. and Helmann, J. D. (1998) 'Identification of target promoters for the Bacillus subtilis sigma X factor using a consensus-directed search', *J Mol Biol*, 279(1), pp. 165-73.
Huber, F. M., Pieper, R. L. and Tietz, A. J. (1988) 'The formation of daptomycin by supplying decanoic acid to Streptomyces roseosporus cultures producing the antibiotic complex A21978C', *Journal of Biotechnology*, 7(4), pp. 283-292.
Ikeda, M., Wachi, M., Jung, H. K., Ishino, F. and Matsuhashi, M. (1991) 'The Escherichia coli mraY gene encoding UDP-N-acetylmuramoyl-pentapeptide: undecaprenyl-phosphate phospho-N-acetylmuramoyl-pentapeptide transferase', *J Bacteriol*, 173(3), pp. 1021-6.

Ipsen, J. H., Karlstrom, G., Mouritsen, O. G., Wennerstrom, H. and Zuckermann, M. J. (1987) 'Phase equilibria in the phosphatidylcholine-cholesterol system', *Biochim Biophys Acta*, 905(1), pp. 162-72.
Ishikawa, S., Hara, Y., Ohnishi, R. and Sekiguchi, J. (1998) 'Regulation of a new cell wall hydrolase gene, cwlF, which affects cell separation in Bacillus subtilis', *J Bacteriol*, 180(9), pp. 2549-55.
Ishikawa, S., Kawai, Y., Hiramatsu, K., Kuwano, M. and Ogasawara, N. (2006) 'A new FtsZ-interacting protein, YlmF, complements the activity of FtsA during progression of cell division in Bacillus subtilis', *Mol Microbiol*, 60(6), pp. 1364-80.
Israelachvili, J. N. (2011) *Intermolecular and surface forces*. 3rd edn. Burlington, MA: Academic Press.
Jaenicke, R. (2005) 'Abundance of cellular material and proteins in the atmosphere', *Science*, 308(5718), p. 73.
Jahn, N., Brantl, S. and Strahl, H. (2015) 'Against the mainstream: the membrane-associated type I toxin BsrG from Bacillus subtilis interferes with cell envelope biosynthesis without increasing membrane permeability', *Mol Microbiol*, 98(4), pp. 651-66.
Jay, A. G. and Hamilton, J. A. (2017) 'Disorder Amidst Membrane Order: Standardizing Laurdan Generalized Polarization and Membrane Fluidity Terms', *J Fluoresc*, 27(1), pp. 243-249.
Jia, Z., O'Mara, M. L., Zuegg, J., Cooper, M. A. and Mark, A. E. (2011) 'The effect of environment on the recognition and binding of vancomycin to native and resistant forms of lipid II', *Biophys J*, 101(11), pp. 2684-92.
Jolliffe, L. K., Doyle, R. J. and Streips, U. N. (1981) 'The energized membrane and cellular autolysis in Bacillus subtilis', *Cell*, 25(3), pp. 753-63.
Jung, D., Rozek, A., Okon, M. and Hancock, R. E. (2004) 'Structural transitions as determinants of the action of the calcium-dependent antibiotic daptomycin', *Chem Biol*, 11(7), pp. 949-57.
Kaiser, R. D. and London, E. (1998) 'Location of diphenylhexatriene (DPH) and its derivatives within membranes: comparison of different fluorescence quenching analyses of membrane depth', *Biochemistry*, 37(22), pp. 8180-90.
Kasahara, J., Kiriyama, Y., Miyashita, M., Kondo, T., Yamada, T., Yazawa, K., Yoshikawa, R. and Yamamoto, H. (2016) 'Teichoic acid polymers affect expression and localization of dl-endopeptidase LytE required for lateral cell wall hydrolysis in Bacillus subtilis', *J Bacteriol*.
Kaufman, W. and Bauer, K. (1958) 'Some studies of the mechanism of the anaerobic autolysis of *Bacillus subtilis*', *J. Gen. Microbial.*, 78(xi).
Kawai, F., Shoda, M., Harashima, R., Sadaie, Y., Hara, H. and Matsumoto, K. (2004) 'Cardiolipin domains in Bacillus subtilis marburg membranes', *J Bacteriol*, 186(5), pp. 1475-83.
Kawai, Y., Daniel, R. A. and Errington, J. (2009) 'Regulation of cell wall morphogenesis in Bacillus subtilis by recruitment of PBP1 to the MreB helix', *Mol Microbiol*, 71(5), pp. 1131-44.
Kelkar, D. A. and Chattopadhyay, A. (2007) 'The gramicidin ion channel: a model membrane protein', *Biochim Biophys Acta*, 1768(9), pp. 2011-25.
Kepplinger, B., Morton-Laing, S., Seistrup, K. H., Marrs, E. C. L., Hopkins, A. P., Perry, J. D., Strahl, H., Hall, M. J., Errington, J. and Allenby, N. E. E. (2018) 'Mode of Action and Heterologous Expression of the Natural Product Antibiotic Vancoresmycin', *ACS Chem Biol*, 13(1), pp. 207-214.
Kingston, A. W., Subramanian, C., Rock, C. O. and Helmann, J. D. (2011) 'A sigmaW-dependent stress response in Bacillus subtilis that reduces membrane fluidity', *Mol Microbiol*, 81(1), pp. 69-79.

Kiriyama, Y., Yazawa, K., Tanaka, T., Yoshikawa, R., Yamane, H., Hashimoto, M., Sekiguchi, J. and Yamamoto, H. (2014) 'Localization and expression of the Bacillus subtilis DL-endopeptidase LytF are influenced by mutations in LTA synthases and glycolipid anchor synthetic enzymes', *Microbiology*, 160(Pt 12), pp. 2639-2649.
Klymchenko, A. S. and Kreder, R. (2014) 'Fluorescent probes for lipid rafts: from model membranes to living cells', *Chem Biol*, 21(1), pp. 97-113.
Koo, B. M., Kritikos, G., Farelli, J. D., Todor, H., Tong, K., Kimsey, H., Wapinski, I., Galardini, M., Cabal, A., Peters, J. M., Hachmann, A. B., Rudner, D. Z., Allen, K. N., Typas, A. and Gross, C. A. (2017) 'Construction and Analysis of Two Genome-Scale Deletion Libraries for Bacillus subtilis', *Cell Syst*, 4(3), pp. 291-305 e7.
Koppelman, C. M., Den Blaauwen, T., Duursma, M. C., Heeren, R. M. and Nanninga, N. (2001) 'Escherichia coli minicell membranes are enriched in cardiolipin', *J Bacteriol*, 183(20), pp. 6144-7.
Kroten, M. A., Bartoszewicz, M. and Swiecicka, I. (2010) 'Cereulide and valinomycin, two important natural dodecadepsipeptides with ionophoretic activities', *Pol J Microbiol*, 59(1), pp. 3-10.
Kunst, F., Ogasawara, N., Moszer, I., Albertini, A. M., Alloni, G., Azevedo, V., Bertero, M. G., Bessieres, P., Bolotin, A., Borchert, S., Borriss, R., Boursier, L., Brans, A., Braun, M., Brignell, S. C., Bron, S., Brouillet, S., Bruschi, C. V., Caldwell, B., Capuano, V., Carter, N. M., Choi, S. K., Cordani, J. J., Connerton, I. F., Cummings, N. J., Daniel, R. A., Denziot, F., Devine, K. M., Dusterhoft, A., Ehrlich, S. D., Emmerson, P. T., Entian, K. D., Errington, J., Fabret, C., Ferrari, E., Foulger, D., Fritz, C., Fujita, M., Fujita, Y., Fuma, S., Galizzi, A., Galleron, N., Ghim, S. Y., Glaser, P., Goffeau, A., Golightly, E. J., Grandi, G., Guiseppi, G., Guy, B. J., Haga, K., Haiech, J., Harwood, C. R., Henaut, A., Hilbert, H., Holsappel, S., Hosono, S., Hullo, M. F., Itaya, M., Jones, L., Joris, B., Karamata, D., Kasahara, Y., Klaerr-Blanchard, M., Klein, C., Kobayashi, Y., Koetter, P., Koningstein, G., Krogh, S., Kumano, M., Kurita, K., Lapidus, A., Lardinois, S., Lauber, J., Lazarevic, V., Lee, S. M., Levine, A., Liu, H., Masuda, S., Mauel, C., Medigue, C., Medina, N., Mellado, R. P., Mizuno, M., Moestl, D., Nakai, S., Noback, M., Noone, D., O'Reilly, M., Ogawa, K., Ogiwara, A., Oudega, B., Park, S. H., Parro, V., Pohl, T. M., Portelle, D., Porwollik, S., Prescott, A. M., Presecan, E., Pujic, P., Purnelle, B., et al. (1997) 'The complete genome sequence of the gram-positive bacterium Bacillus subtilis', *Nature*, 390(6657), pp. 249-56.
Kuroda, A. and Sekiguchi, J. (1991) 'Molecular cloning and sequencing of a major Bacillus subtilis autolysin gene', *J Bacteriol*, 173(22), pp. 7304-12.
Kuru, E., Tekkam, S., Hall, E., Brun, Y. V. and Van Nieuwenhze, M. S. (2015) 'Synthesis of fluorescent D-amino acids and their use for probing peptidoglycan synthesis and bacterial growth in situ', *Nat Protoc*, 10(1), pp. 33-52.
Lages, M. C., Beilharz, K., Morales Angeles, D., Veening, J. W. and Scheffers, D. J. (2013) 'The localization of key Bacillus subtilis penicillin binding proteins during cell growth is determined by substrate availability', *Environ Microbiol*, 15(12), pp. 3272-81.
Lazarevic, V., Margot, P., Soldo, B. and Karamata, D. (1992) 'Sequencing and analysis of the Bacillus subtilis lytRABC divergon: a regulatory unit encompassing the structural genes of the N-acetylmuramoyl-L-alanine amidase and its modifier', *J Gen Microbiol*, 138(9), pp. 1949-61.
Leaver, M., Dominguez-Cuevas, P., Coxhead, J. M., Daniel, R. A. and Errington, J. (2009) 'Life without a wall or division machine in Bacillus subtilis', *Nature*, 457(7231), pp. 849-53.
Leaver, M. and Errington, J. (2005) 'Roles for MreC and MreD proteins in helical growth of the cylindrical cell wall in Bacillus subtilis', *Mol Microbiol*, 57(5), pp. 1196-209.
Leewenhoeck, A. (1677) 'Observation, communicated to the publisher by Mr. Antony van Leewenhoeck, in a Dutch letter of the 9 Octob. 1676 here English'd: concerning little animals

by him observed in rain-well-sea and snow water; as also in water wherein pepper had lain infused.', *Phil. Trans.*, 12, pp. 821–831.
Lehninger, A. L., Nelson, D. L. and Cox, M. M. (2013) *Lehninger principles of biochemistry*. 6th edn (1 vols). New York: W.H. Freeman.
Lenarcic, R., Halbedel, S., Visser, L., Shaw, M., Wu, L. J., Errington, J., Marenduzzo, D. and Hamoen, L. W. (2009) 'Localisation of DivIVA by targeting to negatively curved membranes', *EMBO J*, 28(15), pp. 2272-82.
Levin, P. A., Margolis, P. S., Setlow, P., Losick, R. and Sun, D. (1992) 'Identification of Bacillus subtilis genes for septum placement and shape determination', *J Bacteriol*, 174(21), pp. 6717-28.
Lingwood, D. and Simons, K. (2010) 'Lipid rafts as a membrane-organizing principle', *Science*, 327(5961), pp. 46-50.
Lobasso, S., Saponetti, M. S., Polidoro, F., Lopalco, P., Urbanija, J., Kralj-Iglic, V. and Corcelli, A. (2009) 'Archaebacterial lipid membranes as models to study the interaction of 10-N-nonyl acridine orange with phospholipids', *Chem Phys Lipids*, 157(1), pp. 12-20.
Lodish, H. F. (2000) *Molecular cell biology*. 4th edn. New York: W.H. Freeman.
Lopez-Montero, I., Arriaga, L. R., Monroy, F., Rivas, G., Tarazona, P. and Velez, M. (2008) 'High fluidity and soft elasticity of the inner membrane of Escherichia coli revealed by the surface rheology of model Langmuir monolayers', *Langmuir*, 24(8), pp. 4065-76.
Lopez, C. S., Heras, H., Ruzal, S. M., Sanchez-Rivas, C. and Rivas, E. A. (1998) 'Variations of the envelope composition of Bacillus subtilis during growth in hyperosmotic medium', *Curr Microbiol*, 36(1), pp. 55-61.
Lopez, D. and Kolter, R. (2010a) 'Extracellular signals that define distinct and coexisting cell fates in Bacillus subtilis', *FEMS Microbiol Rev*, 34(2), pp. 134-49.
Lopez, D. and Kolter, R. (2010b) 'Functional microdomains in bacterial membranes', *Genes Dev*, 24(17), pp. 1893-902.
Luo, Y. and Helmann, J. D. (2012) 'Analysis of the role of Bacillus subtilis sigma(M) in beta-lactam resistance reveals an essential role for c-di-AMP in peptidoglycan homeostasis', *Mol Microbiol*, 83(3), pp. 623-39.
Lutkenhaus, J. F. and Wu, H. C. (1980) 'Determination of transcriptional units and gene products from the ftsA region of Escherichia coli', *J Bacteriol*, 143(3), pp. 1281-8.
Luzzati, V. and Reiss-Husson, F. (1966) 'Structure of the Cubic Phase of Lipid-Water Systems', *Nature*, 210, p. 1351.
Macgregor, R. B. and Weber, G. (1981) 'FLUOROPHORES IN POLAR MEDIA: SPECTRAL EFFECTS OF THE LANGEVIN DISTRIBUTION OF ELECTROSTATIC INTERACTIONS', *Annals of the New York Academy of Sciences*, 366(1), pp. 140-154.
Maloney, E., Madiraju, S. C., Rajagopalan, M. and Madiraju, M. (2011) 'Localization of acidic phospholipid cardiolipin and DnaA in mycobacteria', *Tuberculosis (Edinb)*, 91 Suppl 1, pp. S150-5.
Margot, P., Mauel, C. and Karamata, D. (1994) 'The gene of the N-acetylglucosaminidase, a Bacillus subtilis 168 cell wall hydrolase not involved in vegetative cell autolysis', *Mol Microbiol*, 12(4), pp. 535-45.
Margot, P., Pagni, M. and Karamata, D. (1999) 'Bacillus subtilis 168 gene lytF encodes a gamma-D-glutamate-meso-diaminopimelate muropeptidase expressed by the alternative vegetative sigma factor, sigmaD', *Microbiology*, 145 (Pt 1), pp. 57-65.
Margot, P., Wahlen, M., Gholamhoseinian, A., Piggot, P. and Karamata, D. (1998) 'The lytE gene of Bacillus subtilis 168 encodes a cell wall hydrolase', *J Bacteriol*, 180(3), pp. 749-52.
Marston, A. L., Thomaides, H. B., Edwards, D. H., Sharpe, M. E. and Errington, J. (1998) 'Polar localization of the MinD protein of Bacillus subtilis and its role in selection of the mid-cell division site', *Genes Dev*, 12(21), pp. 3419-30.

Martinez, J. L. (2014) 'General principles of antibiotic resistance in bacteria', *Drug Discov Today Technol*, 11, pp. 33-9.
Mascher, T., Zahner, D., Merai, M., Balmelle, N., de Saizieu, A. B. and Hakenbeck, R. (2003) 'The Streptococcus pneumoniae cia regulon: CiaR target sites and transcription profile analysis', *J Bacteriol*, 185(1), pp. 60-70.
Mascher, T., Zimmer, S. L., Smith, T. A. and Helmann, J. D. (2004) 'Antibiotic-inducible promoter regulated by the cell envelope stress-sensing two-component system LiaRS of Bacillus subtilis', *Antimicrob Agents Chemother*, 48(8), pp. 2888-96.
Matsumoto, K., Kusaka, J., Nishibori, A. and Hara, H. (2006) 'Lipid domains in bacterial membranes', *Mol Microbiol*, 61(5), pp. 1110-7.
Mattick, A. T. and Hirsch, A. (1947) 'Further observations on an inhibitory substance (nisin) from lactic streptococci', *Lancet*, 2(6462), pp. 5-8.
Mazor, S., Regev, T., Mileykovskaya, E., Margolin, W., Dowhan, W. and Fishov, I. (2008) 'Mutual effects of MinD-membrane interaction: I. Changes in the membrane properties induced by MinD binding', *Biochim Biophys Acta*, 1778(11), pp. 2496-504.
McBain, J. W. (1913) 'Discussion', *Transactions of the Faraday Society*, 9(0), p. 99.
McKersie, B. D. and Thompson, J. E. (1977) 'Lipid crystallization in senescent membranes from cotyledons', *Plant Physiol*, 59(5), pp. 803-7.
Medini, D., Donati, C., Tettelin, H., Masignani, V. and Rappuoli, R. (2005) 'The microbial pan-genome', *Curr Opin Genet Dev*, 15(6), pp. 589-94.
Mekjian, K. R., Bryan, E. M., Beall, B. W. and Moran, C. P., Jr. (1999) 'Regulation of hexuronate utilization in Bacillus subtilis', *J Bacteriol*, 181(2), pp. 426-33.
Mesquita, R. M., Melo, E., Thompson, T. E. and Vaz, W. L. (2000) 'Partitioning of amphiphiles between coexisting ordered and disordered phases in two-phase lipid bilayer membranes', *Biophys J*, 78(6), pp. 3019-25.
Meury, J. and Kepes, A. (1981) 'The regulation of potassium fluxes for the adjustment and maintenance of potassium levels in Escherichia coli', *Eur J Biochem*, 119(1), pp. 165-70.
Meury, J., Robin, A. and Monnier-Champeix, P. (1985) 'Turgor-controlled K+ fluxes and their pathways in Escherichia coli', *Eur J Biochem*, 151(3), pp. 613-9.
Michod, R. E., Wojciechowski, M. F. and Hoelzer, M. A. (1988) 'DNA repair and the evolution of transformation in the bacterium Bacillus subtilis', *Genetics*, 118(1), pp. 31-9.
Mielich-Suss, B., Schneider, J. and Lopez, D. (2013) 'Overproduction of flotillin influences cell differentiation and shape in Bacillus subtilis', *MBio*, 4(6), pp. e00719-13.
Mileykovskaya, E. and Dowhan, W. (2000) 'Visualization of phospholipid domains in Escherichia coli by using the cardiolipin-specific fluorescent dye 10-N-nonyl acridine orange', *J Bacteriol*, 182(4), pp. 1172-5.
Mileykovskaya, E. and Dowhan, W. (2005) 'Role of membrane lipids in bacterial division-site selection', *Curr Opin Microbiol*, 8(2), pp. 135-42.
Mileykovskaya, E. and Dowhan, W. (2009) 'Cardiolipin membrane domains in prokaryotes and eukaryotes', *Biochim Biophys Acta*, 1788(10), pp. 2084-91.
Mileykovskaya, E., Fishov, I., Fu, X., Corbin, B. D., Margolin, W. and Dowhan, W. (2003) 'Effects of phospholipid composition on MinD-membrane interactions in vitro and in vivo', *J Biol Chem*, 278(25), pp. 22193-8.
Mitchell, P. (1961) 'Coupling of phosphorylation to electron and hydrogen transfer by a chemi-osmotic type of mechanism', *Nature*, 191, pp. 144-8.
Mohammadi, T., van Dam, V., Sijbrandi, R., Vernet, T., Zapun, A., Bouhss, A., Diepeveen-de Bruin, M., Nguyen-Disteche, M., de Kruijff, B. and Breukink, E. (2011) 'Identification of FtsW as a transporter of lipid-linked cell wall precursors across the membrane', *EMBO J*, 30(8), pp. 1425-32.

Monahan, L. G., Liew, A. T., Bottomley, A. L. and Harry, E. J. (2014) 'Division site positioning in bacteria: one size does not fit all', *Front Microbiol*, 5, p. 19.
Muller, A., Wenzel, M., Strahl, H., Grein, F., Saaki, T. N., Kohl, B., Siersma, T., Bandow, J. E., Sahl, H. G., Schneider, T. and Hamoen, L. W. (2016) 'Daptomycin inhibits cell envelope synthesis by interfering with fluid membrane microdomains', *Proc Natl Acad Sci U S A*.
Nath, S. and Villadsen, J. (2015) 'Oxidative phosphorylation revisited', *Biotechnol Bioeng*, 112(3), pp. 429-37.
Neuhaus, F. C. and Baddiley, J. (2003) 'A continuum of anionic charge: structures and functions of D-alanyl-teichoic acids in gram-positive bacteria', *Microbiol Mol Biol Rev*, 67(4), pp. 686-723.
Nicolas, P., Mader, U., Dervyn, E., Rochat, T., Leduc, A., Pigeonneau, N., Bidnenko, E., Marchadier, E., Hoebeke, M., Aymerich, S., Becher, D., Bisicchia, P., Botella, E., Delumeau, O., Doherty, G., Denham, E. L., Fogg, M. J., Fromion, V., Goelzer, A., Hansen, A., Hartig, E., Harwood, C. R., Homuth, G., Jarmer, H., Jules, M., Klipp, E., Le Chat, L., Lecointe, F., Lewis, P., Liebermeister, W., March, A., Mars, R. A., Nannapaneni, P., Noone, D., Pohl, S., Rinn, B., Rugheimer, F., Sappa, P. K., Samson, F., Schaffer, M., Schwikowski, B., Steil, L., Stulke, J., Wiegert, T., Devine, K. M., Wilkinson, A. J., van Dijl, J. M., Hecker, M., Volker, U., Bessieres, P. and Noirot, P. (2012) 'Condition-dependent transcriptome reveals high-level regulatory architecture in Bacillus subtilis', *Science*, 335(6072), pp. 1103-6.
Noone, D., Salzberg, L. I., Botella, E., Basell, K., Becher, D., Antelmann, H. and Devine, K. M. (2014) 'A highly unstable transcript makes CwlO D,L-endopeptidase expression responsive to growth conditions in Bacillus subtilis', *J Bacteriol*, 196(2), pp. 237-47.
O'Shea, P. (2003) 'Intermolecular interactions with/within cell membranes and the trinity of membrane potentials: kinetics and imaging', *Biochem Soc Trans*, 31(Pt 5), pp. 990-6.
Ohnishi, R., Ishikawa, S. and Sekiguchi, J. (1999) 'Peptidoglycan hydrolase LytF plays a role in cell separation with CwlF during vegetative growth of Bacillus subtilis', *J Bacteriol*, 181(10), pp. 3178-84.
Okamoto, S. and Mizuno, D. (1964) 'Mechanism of Chloramphenicol and Tetracycline Resistance in Escherichia Coli', *J Gen Microbiol*, 35, pp. 125-33.
Oliver, P. M., Crooks, J. A., Leidl, M., Yoon, E. J., Saghatelian, A. and Weibel, D. B. (2014) 'Localization of anionic phospholipids in Escherichia coli cells', *J Bacteriol*, 196(19), pp. 3386-98.
Oliynyk, V., Jager, M., Heimburg, T., Buckin, V. and Kaatze, U. (2008) 'Lipid membrane domain formation and alamethicin aggregation studied by calorimetry, sound velocity measurements, and atomic force microscopy', *Biophys Chem*, 134(3), pp. 168-77.
Oren, Z., Lerman, J. C., Gudmundsson, G. H., Agerberth, B. and Shai, Y. (1999) 'Structure and organization of the human antimicrobial peptide LL-37 in phospholipid membranes: relevance to the molecular basis for its non-cell-selective activity', *Biochem J*, 341 (Pt 3), pp. 501-13.
Osawa, M. and Erickson, H. P. (2018) 'Turgor Pressure and Possible Constriction Mechanisms in Bacterial Division', *Front Microbiol*, 9, p. 111.
Oswald, F., Varadarajan, A., Lill, H., Peterman, E. J. and Bollen, Y. J. (2016) 'MreB-Dependent Organization of the E. coli Cytoplasmic Membrane Controls Membrane Protein Diffusion', *Biophys J*, 110(5), pp. 1139-49.
Paget, M. S. and Helmann, J. D. (2003) 'The sigma70 family of sigma factors', *Genome Biol*, 4(1), p. 203.
Parsons, J. B. and Rock, C. O. (2013) 'Bacterial lipids: metabolism and membrane homeostasis', *Prog Lipid Res*, 52(3), pp. 249-76.
Perez-Nunez, D., Briandet, R., David, B., Gautier, C., Renault, P., Hallet, B., Hols, P., Carballido-Lopez, R. and Guedon, E. (2011) 'A new morphogenesis pathway in bacteria:

unbalanced activity of cell wall synthesis machineries leads to coccus-to-rod transition and filamentation in ovococci', *Mol Microbiol*, 79(3), pp. 759-71.
Pogliano, J., Pogliano, N. and Silverman, J. A. (2012) 'Daptomycin-mediated reorganization of membrane architecture causes mislocalization of essential cell division proteins', *J Bacteriol*, 194(17), pp. 4494-504.
Pogmore, A. R., Seistrup, K. H. and Strahl, H. (2018) 'The Gram-positive model organism Bacillus subtilis does not form microscopically detectable cardiolipin-specific lipid domains', *Microbiology*, 164(4), pp. 475-482.
Poyry, S. and Vattulainen, I. (2016) 'Role of charged lipids in membrane structures - Insight given by simulations', *Biochim Biophys Acta*, 1858(10), pp. 2322-2333.
Quinn, P. J. (2012) 'Lipid-lipid interactions in bilayer membranes: married couples and casual liaisons', *Prog Lipid Res*, 51(3), pp. 179-98.
Ramamurthi, K. S. and Losick, R. (2009) 'Negative membrane curvature as a cue for subcellular localization of a bacterial protein', *Proc Natl Acad Sci U S A*, 106(32), pp. 13541-5.
Ramaniuk, O., Prevorovsky, M., Pospisil, J., Vitovska, D., Kofronova, O., Benada, O., Schwarz, M., Sanderova, H., Hnilicova, J. and Krasny, L. (2018) 'sigma(I) from Bacillus subtilis: Impact on Gene Expression and Characterization of sigma(I)-dependent Transcription that Requires New Types of Promoters with Extended -35 and -10 Elements', *J Bacteriol*.
Rashid, M. H., Mori, M. and Sekiguchi, J. (1995) 'Glucosaminidase of Bacillus subtilis: cloning, regulation, primary structure and biochemical characterization', *Microbiology*, 141 (Pt 10), pp. 2391-404.
Renner, L. D. and Weibel, D. B. (2011) 'Cardiolipin microdomains localize to negatively curved regions of Escherichia coli membranes', *Proc Natl Acad Sci U S A*, 108(15), pp. 6264-9.
Reyes, J. and Latorre, R. (1979) 'Effect of the anesthetics benzyl alcohol and chloroform on bilayers made from monolayers', *Biophys J*, 28(2), pp. 259-79.
Rico, A. I., Krupka, M. and Vicente, M. (2013) 'In the beginning, Escherichia coli assembled the proto-ring: an initial phase of division', *J Biol Chem*, 288(29), pp. 20830-6.
Rojas, E. R. and Huang, K. C. (2018) 'Regulation of microbial growth by turgor pressure', *Curr Opin Microbiol*, 42, pp. 62-70.
Romantsov, T., Battle, A. R., Hendel, J. L., Martinac, B. and Wood, J. M. (2010) 'Protein localization in Escherichia coli cells: comparison of the cytoplasmic membrane proteins ProP, LacY, ProW, AqpZ, MscS, and MscL', *J Bacteriol*, 192(4), pp. 912-24.
Ros, U. and Garcia-Saez, A. J. (2015) 'More Than a Pore: The Interplay of Pore-Forming Proteins and Lipid Membranes', *J Membr Biol*, 248(3), pp. 545-61.
Rosch, J. W., Hsu, F. F. and Caparon, M. G. (2007) 'Anionic lipids enriched at the ExPortal of Streptococcus pyogenes', *J Bacteriol*, 189(3), pp. 801-6.
Ryter, A. (1965) '[Morphologic Study of the Sporulation of Bacillus Subtilis]', *Ann Inst Pasteur (Paris)*, 108, pp. 40-60.
Saenz, J. P., Grosser, D., Bradley, A. S., Lagny, T. J., Lavrynenko, O., Broda, M. and Simons, K. (2015) 'Hopanoids as functional analogues of cholesterol in bacterial membranes', *Proc Natl Acad Sci U S A*, 112(38), pp. 11971-6.
Saenz, J. P., Sezgin, E., Schwille, P. and Simons, K. (2012) 'Functional convergence of hopanoids and sterols in membrane ordering', *Proc Natl Acad Sci U S A*, 109(35), pp. 14236-40.
Saita, E., Albanesi, D. and de Mendoza, D. (2016) 'Sensing membrane thickness: Lessons learned from cold stress', *Biochim Biophys Acta*, 1861(8 Pt B), pp. 837-846.

Salje, J., van den Ent, F., de Boer, P. and Lowe, J. (2011) 'Direct membrane binding by bacterial actin MreB', *Mol Cell*, 43(3), pp. 478-87.
Salzberg, L. I. and Helmann, J. D. (2008) 'Phenotypic and transcriptomic characterization of Bacillus subtilis mutants with grossly altered membrane composition', *J Bacteriol*, 190(23), pp. 7797-807.
Salzberg, L. I., Powell, L., Hokamp, K., Botella, E., Noone, D. and Devine, K. M. (2013) 'The WalRK (YycFG) and sigma(I) RsgI regulators cooperate to control CwlO and LytE expression in exponentially growing and stressed Bacillus subtilis cells', *Mol Microbiol*, 87(1), pp. 180-95.
Sanchez, M., Valencia, A., Ferrandiz, M. J., Sander, C. and Vicente, M. (1994) 'Correlation between the structure and biochemical activities of FtsA, an essential cell division protein of the actin family', *EMBO J*, 13(20), pp. 4919-25.
Sarges, R. and Witkop, B. (1965) 'Gramicidin A. V. The Structure of Valine- and Isoleucine-Gramicidin A', *J Am Chem Soc*, 87, pp. 2011-20.
Sauvage, E., Kerff, F., Terrak, M., Ayala, J. A. and Charlier, P. (2008) 'The penicillin-binding proteins: structure and role in peptidoglycan biosynthesis', *FEMS Microbiol Rev*, 32(2), pp. 234-58.
Schaffer, C. and Messner, P. (2005) 'The structure of secondary cell wall polymers: how Gram-positive bacteria stick their cell walls together', *Microbiology*, 151(Pt 3), pp. 643-51.
Scheinpflug, K., Wenzel, M., Krylova, O., Bandow, J. E., Dathe, M. and Strahl, H. (2017) 'Antimicrobial peptide cWFW kills by combining lipid phase separation with autolysis', *Sci Rep*, 7, p. 44332.
Schindelin, J., Arganda-Carreras, I., Frise, E., Kaynig, V., Longair, M., Pietzsch, T., Preibisch, S., Rueden, C., Saalfeld, S., Schmid, B., Tinevez, J. Y., White, D. J., Hartenstein, V., Eliceiri, K., Tomancak, P. and Cardona, A. (2012) 'Fiji: an open-source platform for biological-image analysis', *Nat Methods*, 9(7), pp. 676-82.
Schirawski, J. and Unden, G. (1998) 'Menaquinone-dependent succinate dehydrogenase of bacteria catalyzes reversed electron transport driven by the proton potential', *Eur J Biochem*, 257(1), pp. 210-5.
Schirner, K. and Errington, J. (2009a) 'The cell wall regulator {sigma}I specifically suppresses the lethal phenotype of mbl mutants in Bacillus subtilis', *J Bacteriol*, 191(5), pp. 1404-13.
Schirner, K. and Errington, J. (2009b) 'Influence of heterologous MreB proteins on cell morphology of Bacillus subtilis', *Microbiology*, 155(Pt 11), pp. 3611-21.
Schirner, K., Marles-Wright, J., Lewis, R. J. and Errington, J. (2009) 'Distinct and essential morphogenic functions for wall- and lipo-teichoic acids in Bacillus subtilis', *EMBO J*, 28(7), pp. 830-42.
Seddon, J. M., Kaye, R. D. and Marsh, D. (1983) 'Induction of the lamellar-inverted hexagonal phase transition in cardiolipin by protons and monovalent cations', *Biochimica et Biophysica Acta (BBA) - Biomembranes*, 734(2), pp. 347-352.
Seu, K. J., Cambrea, L. R., Everly, R. M. and Hovis, J. S. (2006) 'Influence of lipid chemistry on membrane fluidity: tail and headgroup interactions', *Biophys J*, 91(10), pp. 3727-35.
Severina, E., Severin, A. and Tomasz, A. (1998) 'Antibacterial efficacy of nisin against multidrug-resistant Gram-positive pathogens', *J Antimicrob Chemother*, 41(3), pp. 341-7.
Simons, K. and Ikonen, E. (1997) 'Functional rafts in cell membranes', *Nature*, 387(6633), pp. 569-72.
Singer, S. J. and Nicolson, G. L. (1972) 'The fluid mosaic model of the structure of cell membranes', *Science*, 175(4023), pp. 720-31.
Smith, T. J., Blackman, S. A. and Foster, S. J. (2000) 'Autolysins of Bacillus subtilis: multiple enzymes with multiple functions', *Microbiology*, 146 (Pt 2), pp. 249-62.

Souza, B. M., Castro, T. L., Carvalho, R. D., Seyffert, N., Silva, A., Miyoshi, A. and Azevedo, V. (2014) 'sigma(ECF) factors of gram-positive bacteria: a focus on Bacillus subtilis and the CMNR group', *Virulence*, 5(5), pp. 587-600.
Spanova, M., Zweytick, D., Lohner, K., Klug, L., Leitner, E., Hermetter, A. and Daum, G. (2012) 'Influence of squalene on lipid particle/droplet and membrane organization in the yeast Saccharomyces cerevisiae', *Biochim Biophys Acta*, 1821(4), pp. 647-53.
Sperber, A. M. and Herman, J. K. (2017) 'Metabolism Shapes the Cell', *J Bacteriol*, 199(11).
Strahl, H., Burmann, F. and Hamoen, L. W. (2014) 'The actin homologue MreB organizes the bacterial cell membrane', *Nat Commun*, 5, p. 3442.
Strahl, H. and Errington, J. (2017) 'Bacterial Membranes: Structure, Domains, and Function', *Annu Rev Microbiol*, 71, pp. 519-538.
Strahl, H. and Hamoen, L. W. (2010) 'Membrane potential is important for bacterial cell division', *Proc Natl Acad Sci U S A*, 107(27), pp. 12281-6.
'Structural chemistry' (1990). Deerfield Beach, FL: VCH, p. v.
Tam, N. K., Uyen, N. Q., Hong, H. A., Duc le, H., Hoa, T. T., Serra, C. R., Henriques, A. O. and Cutting, S. M. (2006) 'The intestinal life cycle of Bacillus subtilis and close relatives', *J Bacteriol*, 188(7), pp. 2692-700.
Te Winkel, J. D., Gray, D. A., Seistrup, K. H., Hamoen, L. W. and Strahl, H. (2016) 'Analysis of Antimicrobial-Triggered Membrane Depolarization Using Voltage Sensitive Dyes', *Front Cell Dev Biol*, 4, p. 29.
Thackray, P. D. and Moir, A. (2003) 'SigM, an extracytoplasmic function sigma factor of Bacillus subtilis, is activated in response to cell wall antibiotics, ethanol, heat, acid, and superoxide stress', *J Bacteriol*, 185(12), pp. 3491-8.
Tien, H. T. and Diana, A. L. (1967) 'Black lipid membranes in aqueous media: the effect of salts on electrical properties', *J Colloid Interface Sci*, 24(3), pp. 287-96.
Tindall, B. J., Sikorski, J., Smibert, R. A. and Krieg, N. R. (2007) 'Phenotypic Characterization and the Principles of Comparative Systematics', in *Methods for General and Molecular Microbiology, Third Edition*. American Society of Microbiology.
Tiyanont, K., Doan, T., Lazarus, M. B., Fang, X., Rudner, D. Z. and Walker, S. (2006) 'Imaging peptidoglycan biosynthesis in Bacillus subtilis with fluorescent antibiotics', *Proc Natl Acad Sci U S A*, 103(29), pp. 11033-8.
Togawa, N., Juge, N., Miyaji, T., Hiasa, M., Omote, H. and Moriyama, Y. (2015) 'Wide expression of type I Na+-phosphate cotransporter 3 (NPT3/SLC17A2), a membrane potential-driven organic anion transporter', *Am J Physiol Cell Physiol*, 309(2), pp. C71-80.
Tong, Z., Ni, L. and Ling, J. (2014) 'Antibacterial peptide nisin: a potential role in the inhibition of oral pathogenic bacteria', *Peptides*, 60, pp. 32-40.
Tran, T. T., Panesso, D., Mishra, N. N., Mileykovskaya, E., Guan, Z., Munita, J. M., Reyes, J., Diaz, L., Weinstock, G. M., Murray, B. E., Shamoo, Y., Dowhan, W., Bayer, A. S. and Arias, C. A. (2013) 'Daptomycin-resistant Enterococcus faecalis diverts the antibiotic molecule from the division septum and remodels cell membrane phospholipids', *MBio*, 4(4).
Trip, E. N., Veening, J. W., Stewart, E. J., Errington, J. and Scheffers, D. J. (2013) 'Balanced transcription of cell division genes in Bacillus subtilis as revealed by single cell analysis', *Environ Microbiol*, 15(12), pp. 3196-209.
Tseng, C. L., Chen, J. T., Lin, J. H., Huang, W. Z. and Shaw, G. C. (2011) 'Genetic evidence for involvement of the alternative sigma factor SigI in controlling expression of the cell wall hydrolase gene lytE and contribution of LytE to heat survival of Bacillus subtilis', *Arch Microbiol*, 193(9), pp. 677-85.
Tseng, C. L. and Shaw, G. C. (2008) 'Genetic evidence for the actin homolog gene mreBH and the bacitracin resistance gene bcrC as targets of the alternative sigma factor SigI of Bacillus subtilis', *J Bacteriol*, 190(5), pp. 1561-7.

Typas, A., Banzhaf, M., Gross, C. A. and Vollmer, W. (2012) 'From the regulation of peptidoglycan synthesis to bacterial growth and morphology', *Nat Rev Microbiol*, 10(2), pp. 123-36.
Urry, D. W., Goodall, M. C., Glickson, J. D. and Mayers, D. F. (1971) 'The gramicidin A transmembrane channel: characteristics of head-to-head dimerized (L,D) helices', *Proc Natl Acad Sci U S A*, 68(8), pp. 1907-11.
Ursell, T. S., Nguyen, J., Monds, R. D., Colavin, A., Billings, G., Ouzounov, N., Gitai, Z., Shaevitz, J. W. and Huang, K. C. (2014) 'Rod-like bacterial shape is maintained by feedback between cell curvature and cytoskeletal localization', *Proc Natl Acad Sci U S A*, 111(11), pp. E1025-34.
van den Ent, F., Izore, T., Bharat, T. A., Johnson, C. M. and Lowe, J. (2014) 'Bacterial actin MreB forms antiparallel double filaments', *Elife*, 3, p. e02634.
van den Ent, F., Leaver, M., Bendezu, F., Errington, J., de Boer, P. and Lowe, J. (2006) 'Dimeric structure of the cell shape protein MreC and its functional implications', *Mol Microbiol*, 62(6), pp. 1631-42.
van Ginkel, G., van Langen, H. and Levine, Y. K. (1989) 'The membrane fluidity concept revisited by polarized fluorescence spectroscopy on different model membranes containing unsaturated lipids and sterols', *Biochimie*, 71(1), pp. 23-32.
van Heijenoort, Y., Gomez, M., Derrien, M., Ayala, J. and van Heijenoort, J. (1992) 'Membrane intermediates in the peptidoglycan metabolism of Escherichia coli: possible roles of PBP 1b and PBP 3', *J Bacteriol*, 174(11), pp. 3549-57.
Vanounou, S., Pines, D., Pines, E., Parola, A. H. and Fishov, I. (2002) 'Coexistence of domains with distinct order and polarity in fluid bacterial membranes', *Photochem Photobiol*, 76(1), pp. 1-11.
Vollmer, W., Blanot, D. and de Pedro, M. A. (2008) 'Peptidoglycan structure and architecture', *FEMS Microbiol Rev*, 32(2), pp. 149-67.
Vollmer, W. and Seligman, S. J. (2010) 'Architecture of peptidoglycan: more data and more models', *Trends Microbiol*, 18(2), pp. 59-66.
Weber, M. E., Schlesinger, P. H. and Gokel, G. W. (2005) 'Dynamic assessment of bilayer thickness by varying phospholipid and hydraphile synthetic channel chain lengths', *J Am Chem Soc*, 127(2), pp. 636-42.
Westers, H., Dorenbos, R., van Dijl, J. M., Kabel, J., Flanagan, T., Devine, K. M., Jude, F., Seror, S. J., Beekman, A. C., Darmon, E., Eschevins, C., de Jong, A., Bron, S., Kuipers, O. P., Albertini, A. M., Antelmann, H., Hecker, M., Zamboni, N., Sauer, U., Bruand, C., Ehrlich, D. S., Alonso, J. C., Salas, M. and Quax, W. J. (2003) 'Genome engineering reveals large dispensable regions in Bacillus subtilis', *Mol Biol Evol*, 20(12), pp. 2076-90.
Whatmore, A. M., Chudek, J. A. and Reed, R. H. (1990) 'The effects of osmotic upshock on the intracellular solute pools of Bacillus subtilis', *J Gen Microbiol*, 136(12), pp. 2527-35.
White, S. W., Zheng, J., Zhang, Y. M. and Rock (2005) 'The structural biology of type II fatty acid biosynthesis', *Annu Rev Biochem*, 74, pp. 791-831.
Woese, C. R., Magrum, L. J. and Fox, G. E. (1978) 'Archaebacteria', *J Mol Evol*, 11(3), pp. 245-51.
Wood, J. M. (1999) 'Osmosensing by bacteria: signals and membrane-based sensors', *Microbiol Mol Biol Rev*, 63(1), pp. 230-62.
Yamaguchi, H., Furuhata, K., Fukushima, T., Yamamoto, H. and Sekiguchi, J. (2004) 'Characterization of a new Bacillus subtilis peptidoglycan hydrolase gene, yvcE (named cwlO), and the enzymatic properties of its encoded protein', *J Biosci Bioeng*, 98(3), pp. 174-81.

Yamamoto, H., Kurosawa, S. and Sekiguchi, J. (2003) 'Localization of the vegetative cell wall hydrolases LytC, LytE, and LytF on the Bacillus subtilis cell surface and stability of these enzymes to cell wall-bound or extracellular proteases', *J Bacteriol*, 185(22), pp. 6666-77.
Yamamoto, Y., Poyart, C., Trieu-Cuot, P., Lamberet, G., Gruss, A. and Gaudu, P. (2005) 'Respiration metabolism of Group B Streptococcus is activated by environmental haem and quinone and contributes to virulence', *Mol Microbiol*, 56(2), pp. 525-34.
Yan, N. (2013) 'Structural investigation of the proton-coupled secondary transporters', *Curr Opin Struct Biol*, 23(4), pp. 483-91.
Yuehua, J., Lanwei, Z., Fei, L., Huaxi, Y. and Xue, H. (2016) 'Complete genome sequence of Enterococcus faecalis LD33, a bacteriocin-producing strain', *J Biotechnol*, 227, pp. 79-80.
Zaprasis, A., Bleisteiner, M., Kerres, A., Hoffmann, T. and Bremer, E. (2015) 'Uptake of amino acids and their metabolic conversion into the compatible solute proline confers osmoprotection to Bacillus subtilis', *Appl Environ Microbiol*, 81(1), pp. 250-9.
Zapun, A., Vernet, T. and Pinho, M. G. (2008) 'The different shapes of cocci', *FEMS Microbiol Rev*, 32(2), pp. 345-60.
Zeigler, D. R., Pragai, Z., Rodriguez, S., Chevreux, B., Muffler, A., Albert, T., Bai, R., Wyss, M. and Perkins, J. B. (2008) 'The origins of 168, W23, and other Bacillus subtilis legacy strains', *J Bacteriol*, 190(21), pp. 6983-95.
Zenz, K. I., Neve, H., Geis, A. and Heller, K. J. (1998) 'Bacillus subtilis develops competence for uptake of plasmid DNA when growing in milk products', *Syst Appl Microbiol*, 21(1), pp. 28-32.
Zhang, Y. M. and Rock, C. O. (2008) 'Membrane lipid homeostasis in bacteria', *Nat Rev Microbiol*, 6(3), pp. 222-33.
Zuber, U., Drzewiecki, K. and Hecker, M. (2001) 'Putative sigma factor SigI (YkoZ) of Bacillus subtilis is induced by heat shock', *J Bacteriol*, 183(4), pp. 1472-5.